Characterisation of molten filled hard gelatin capsules.

Chatham, Sarah Marianna

CHARACTERISATION OF MOLTEN FILLED HARD GELATIN CAPSULES

by

Sarah Marianna Chatham

Thesis submitted for the degree of Doctor of Philosophy in the University of London

Chelsea Department of Pharmacy
King's College
UNIVERSITY OF LONDON

August 1985

ABSTRACT

A study has been undertaken of the influence of thermal history on the physical and dissolution properties of the polymer, polyethylene glycol (PEG) 4000 alone and its dispersions with trimethoprim. Of particular interest were thermal profiles which might be experienced during the manufacture of molten filled hard gelatin capsules.

The effect of thermal history on the morphology of PEG 4000 was established by DSC and X-ray diffraction studies. The previous thermal treatment was found to influence both the degree of crystallinity and the crystal form, i.e. the relative proportions of extended and folded chain crystals. Addition of a wide range of concentrations of up to 50% w/w of trimethoprim did not particularly influence the crystallisation of the polymer. Conversely, the crystallisation of the drug was found to be inhibited in the presence of the polymer. However, no solid solution or eutectic formation could be detected, and the phase diagrams obtained were of the monotectic type for solid dispersions prepared under all conditions investigated. Studies on the effects of ageing on these systems were also undertaken.

Further investigations of PEG 4000 and its dispersions were performed by dielectric spectroscopy, which has not previously been applied to pharmaceutical systems. This method allowed their structure and behaviour to be characterised with greater definition over a range of temperatures and during temperature cycling, in both the liquid and solid and thus offers potential advantages over many previously utilised techniques.

Dissolution studies revealed that the dissolution rate of the polymer was influenced by its degree of crystallinity, and that as this increased on ageing,

so the speed of dissolution decreased. The mechanism of enhanced drug release is complex, but the formation of an amorphous form of the drug and microenvironmental solubilisation appear to be implicated.

For my parents

ACKNOWLEDGEMENTS

I would like to thank my supervisor, Prof. J. M. Newton, for his guidance and encouragement throughout these studies. Thanks are also due to my industrial supervisor, Dr. S. E. Walker for his interest and support, and to Hoechst and SERC for sponsoring this CASE award.

I am deeply indebted to the Dielectrics Group at Chelsea College for the use of their facilities and for their considerable assistance, in particular Dr. L. A. Dissado, Prof. R. M. Hill and Dr. C. Pickup. Further thanks go to Mr. G. Ingram of the Geology department, Chelsea College for his aid with the X-ray diffraction studies; to Mr. M. Wineberg for the SEM photographs and to the technical staff of the Pharmacy department, especially Mr. S. Ingham and Mr. M. Harris. I would also like to thank Mary Newton for typing this thesis.

Finally, thanks are definitely due to my husband, Graham, for putting up with me during the writing of this thesis and to all my family and friends for their support.

CONTENTS

Contents Page

Contents Page

Contents Page

LIST OF FIGURES

List of Figures — Page

Chapter 3

List of Figures

List of Figures — Page

Chapter 4

List of Figures — Page

List of Figures

List of Figures — Page

List of Figures

LIST OF TABLES

List of Tables

List of Tables

LIST OF PLATES

SYMBOLS

A	Area of electrodes
A'	Hill dielectric constant
C	Capacitance
C_b	Capacitance associated with bulk response
C_s	Capacitance associated with surface of barrier response
C_∞	Capacitance of all elements which respond instantaneously at the measuring frequency
$C_{\infty TOTAL}$	Sum of all C_∞s'
$C_{(0)}$	Magnitude of loss peak
$C_{(0)1}$	Magnitude of loss peak associated with barrier response
$C_{(0)2}$	Magnitude of loss peak associated with bulk response
C_∞'	Capacitance at infinite time after start
C_t	Capacitance at time, t after start
C_0	Capacitance at t = 0
C^*	Bulk concentration of drug in dissolution medium
C^*_s	Concentration of drug in the thin saturated liquid film/boundary layer adjacent to the solid surface
D	Diffusion coefficient
E	Electric field
E_0	Amplitude of electric field
F	Frequency
$F(\omega/\omega_c)$	Dielectric shape function
${}_1F_1(; ;)$	Confluent hypergeometric function

Symbols

$_2F_1(; ; ;)$	Gaussian hypergeometric function
G	Conductance
G_b	Conductance associated with bulk response in liquid
G_{02}	Conductance associated with bulk response in solid
G/ω	Dielectric loss
H	Dissolution rate per unit area
I	Intensity of X-ray diffraction peak
I_0	Intensity of strongest X-ray diffraction peak
J	Current
K	Temperature in Kelvin
M_n	Number average molecular weight
M_w	Weight average molecular weight
N_s	Number density of occupied sites
O_a	X-ray diffraction intensity of amorphous phase of sample
O_c	X-ray diffraction intensity of crystalline phase of sample
P	Polarisation
P_o	Amplitude of polarisation
R	Electrical resistance
S	Surface area of drug
T	Temperature
T_p	DSC peak melting temperature
X_d	Relative dissolution rate of trimethoprim

Symbols

X_p	Relative dissolution rate of PEG 4000
a	Constant
a'	Constant
b	Constant
d	Distance between planes of atoms
d'	Distance between electrodes
e	Separation and density of hopping sites
g	Positive gauche conformation
$\overline{g}$	Negative gauche conformation
g(y)	Probability density of cluster structures
h	Diffusion layer thickness
i	Imaginary component of a complex mathematical function
k	Constant
k_d	Proportionality constant related to the diffusion coefficient of the solute and the thickness of the diffusion layer
k_r	Avrami rate constant
k_x	Constant accounting for relative X-ray scattering intensity of crystalline and amorphous phases
m	Dissado-Hill shape parameter
n	Dissado-Hill shape parameter
n_x	Order of reflection of X-rays
n_a	Avrami exponent
n_c	Number of chain folds per PEG molecule in lamella

Symbols

p	Dissado-Hill shape parameter
s	Hill shape parameter
t	Time
t'	Time after start
t_c	Crystallisation time
$t_{\frac{1}{2}c}$	Half time of crystallisation
t_m	Melting time
$t_{\frac{1}{2}m}$	Half time of melting
Γ	Solution to integral in terms of gamma function
Δ	Unspecified activation energy
Δ_C	Activation energy associated with loss peak magnitude
Δ_G	Activation energy associated with conductance
$\Delta_{\omega p}$	Activation energy associated with loss peak frequency
ΔH	Change in enthalpy
ΔH_c	Enthalpy of crystallisation
ΔH_f	Enthalpy of fusion
ΔH_{f^*}	Enthalpy of fusion of perfectly crystalline polymer
ΔH_{f1}	Enthalpy of fusion on melting initially
ΔH_{f2}	Enthalpy of fusion on subsequent remelting
Φ	General polarisation response function
$\Psi(\ )$	Cook, Watt and Williams dielectric decay function

Symbols

Ω	Ohms
Ω^{-1}	Reciprocal ohms (mhos)
α	Dielectric relaxation process in a polymer (High temperature)
α_c	Dielectric relaxation process arising from crystalline regions in a polymer
α'	Cole and Cole dielectric empirical shape parameter
β	Dielectric relaxation process in a polymer (Lower temperature than α)
β_a	Dielectric relaxation process arising from amorphous regions in a polymer
β'	Davidson and Cole empirical shape parameter
γ	Dielectric relaxation process in a polymer (Lower temperature than β)
γ'	Cook, Watt and Williams empirical shape parameter
δ	Delta function electric field
$\tan \delta$	Dielectric loss tangent
ϵ_o	Dielectric permittivity
ϵ_∞	Dielectric permittivity of elements which respond instantaneously at the frequencies
η	Viscosity
θ	Angle of incidence of X-rays
λ	Wavelength of X-rays
ν	Wavelength
ρ	Density
τ	Characteristic Debye relaxation time

Symbols

τ_∞	Characteristic Debye relaxation time at zero frequency
$\chi(\omega)$	Dielectric susceptibility function
$\chi'(\omega)$	Real component of dielectric susceptibility function
$\chi''(\omega)$	Imaginary component of dielectric susceptibility function
$\chi(0)$	Magnitude of real part of dielectric susceptibility at zero frequency
$\chi_{LFD}(\omega)$	Dielectric susceptibility function for low frequency dispersion
ω	Angular frequency
ω_p	Loss peak frequency
ω_{p1}	Loss peak frequency associated with barrier dielectric response
ω_{p2}	Loss peak frequency associated with bulk dielectric response

CHAPTER 1

CHAPTER 1 Introduction

1.1 Background and definition of solid dispersions

The rate determining step in the absorption process for drugs of slow or poor solubility is generally the dissolution rate of such drugs in the gastro-intestinal fluids rather than their speed of diffusion across the gut wall. From the Noyes-Whitney equation which describes dissolution (Martin et al, 1969):

$$\frac{dC^*}{dt} = k_d S (C_s^* - C^*) \qquad \ldots 1.1.$$

where $\frac{dC^*}{dt}$ is the dissolution rate of the drug

S is the surface area of the drug

$C_s^* - C^*$ is the concentration gradient, where C_s^* is the concentration of drug in the thin saturated liquid film/boundary layer adjacent to the solid surface and C^* is the bulk concentration of the drug in the dissolution medium

k_d is the proportionality constant related to the diffusion coefficient of the solute and the thickness of the diffusion layer

it can be seen that one of the factors which controls the dissolution rate of the drug is its surface area. Hence one possible method of improving the dissolution rate would be to reduce the drug's particle size thus giving an increased surface area. Methods by which particle size reduction has been achieved include conventional milling and fluid energy micronisation (Carter, 1972), controlled precipitation involving a change of solvent or temperature (Scheikh et al, 1966), application of ultrasonic waves (Skauern, 1967) and spray drying (Kornblum and Hirschom, 1970). However, particle size reduction by these techniques may not give a faster dissolution rate

due to subsequent agglomeration and aggregation of the resultant fine particles which arises from their increased surface energy. This was noted by Lin et al (1968) who found that the in vitro dissolution rate of micronised griseofulvin was slower than that of drug samples with a larger particle size. Another disadvantage of fine powders of poorly soluble drugs is their poor wettability and particles must be wetted as the first step of their dissolution in water.

Alternative techniques of particle size reduction have included administering liquid solutions or water soluble salts which upon dilution with gastric fluids precipitate the drug itself in the form of ultrafine particles (Levy, 1963a). Often, however, these methods are not possible in practice.

Sekiguchi and Obi (1961) proposed that poorly soluble drugs should be formulated as solid dispersions with water soluble carriers as a means of achieving particle size reduction. Also, since the dissolution of a component from a surface is affected by the second component in a multiple component system (Higuchi, 1967), selection of a hydrophilic carrier should result in a fast release of drug from the matrix. A solid dispersion is defined as a dispersion of one or more active ingredients in an inert carrier or matrix in the solid state prepared by melting, solvent (coprecipitate) or melting-solvent methods (Chiou and Riegelman, 1971). This does not include dispersion of active ingredients in solid diluents by traditional mechanical mixing. A wide variety of materials has been investigated for suitability as carriers and a summary is given in Table 1.1. One of the most frequently used classes of carrier are the hydrophilic polyethylene glycols (PEGS), which have even been advocated as universal carriers for solid dispersion formulations because of their non-toxicity and compatability with most drugs (Chiou and Riegelman, 1971), and it is this polymer which is studied in the work presented here.

Table 1.1. Examples of materials investigated as carriers for solid dispersions

Carrier	Workers
Polyethylene glycols	Chiou and Riegelman (1971)
Urea	Sekiguchi and Obi (1961)
Deoxycholic acid	Malone et al (1966)
Silicon dioxide	Kim et al (1985)
Urethran	Maulding (1978)
Polyvinyl pyrrolidone	Tachibana and Nakamura (1965)
Polyoxyethylene 40 stearate	Kaur et al (1980a and 1980b) .
Renex 650 (polyoxyethylene-nonylphenylether)	Ford and Rubinstein (1978a)
Cetomacrogol 1000	Hoelgaard and Møller (1975b)
Methylcellulose	Kassem et al (1978)
Pentaerythritol	Chiou and Riegelman (1969)
Pentaerythritol acetate	Chiou and Riegelman (1969)
Poloxamer 188	Reddy et al (1976)
Acrylic copolymer	Larson and Banker (1976)
Succinic acid	Goldberg et al (1966)
Citric acid	Chiou and Riegelman (1969)
Mannitol	McGinity et al (1975)
Sorbitol	Ghanem et al (1980)
Glucose	Ghanem et al (1980)
Maltose	Ghanem et al (1980)
Dextrose	McGinity et al (1975)
Galactose	Allen et al (1977)
Sucrose	Allen et al (1977)
Xylitol	Sirenius et al (1979)

1.2. Classification of solid dispersion systems

Solid dispersions may exist in a number of different physical forms dependent on both the inherent properties of the constituent materials and the conditions of manufacture. Chiou and Riegelman (1971) proposed a classification of binary pharmaceutical systems into six groups which are outlined below. It should be noted that many of the theories they put forward are drawn from the disciplines of geology and metallurgy and therefore may be of limited applicability to pharmaceutical systems. This is because the properties and behaviour of pharmaceutical materials, which tend to be relatively large organic molecules are often very different to those of metals and small inorganic molecules.

1.2.1. Eutectic mixtures

Eutectics are two phase systems where the two components are miscible in all proportions in the liquid state but are totally immiscible in the solid state (Reisman, 1970). On cooling from the melt, at a particular composition known as the eutectic composition, the two components crystallise simultaneously from the melt to give an intimately blended physical mixture. This eutectic has a unique melting point, which is lower than that of either of the two constituents and the melting points of each component in excess of the eutectic composition are depressed with respect to the pure materials. This can be represented by the phase diagram shown in Fig. 1.1. Generally, the eutectic of a poorly soluble drug shows an increased dissolution rate relative to that of the pure drug and a number of explanations of this enhancement have been postulated. These include a reduction in the particle size of the drug (Sekiguchi and Obi, 1961), an increase in drug solubility (Martin et al, 1969), solubilisation of the drug by the carrier (Goldberg

Fig. 1.1. Typical phase diagram of a binary eutectic system

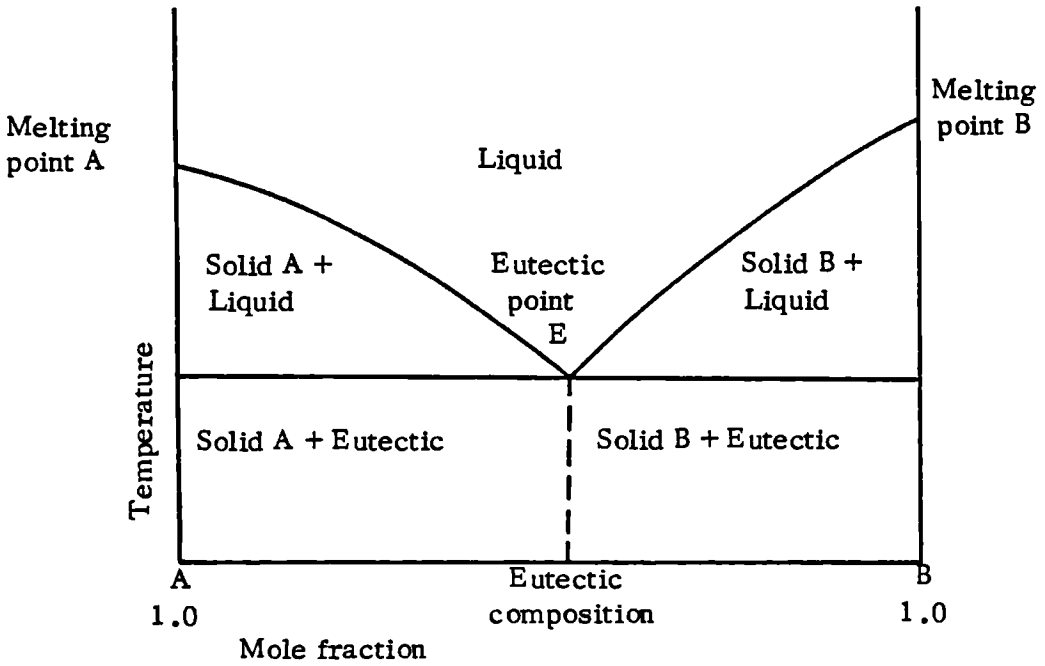

1966), absence of aggregation and agglomeration (Chiou and Riegelman, 1971), improved wettability and dispersibility (Sekiguchi and Obi, 1961) and crystallisation of a more soluble, metastable polymorph (Chiou and Riegelman, 1971). These possible mechanisms of dissolution enhancement will be discussed in greater depth in Chapter 5.

1.2.2. Solid solutions

Solid solutions also known as mixed crystals, are homogeneous, one phase systems made up of solid solute dissolved in solid solvent, which should theoretically provide a faster dissolution rate than eutectic systems since the particle size is reduced to a molecular level, thus providing the maximum surface area for dissolution (Goldberg et al, 1965). They can be subdivided according to the extent of miscibility of the two components into discontinuous and continuous solid solutions. In the latter case, the two components are miscible in all proportions in the solid state. Sodium bromide and silver bromide form this type of solid solution (Tsuji et al, 1969), but no pharmaceutical system has been shown to be able to crystallise in this manner. With discontinuous solid solutions, the two components show only partial miscibility with each other which can be represented by the phase diagram in Fig. 1.2. It has been postulated that some degree of solid state miscibility exists in most two component systems (Chiou and Riegelman, 1971) but in many cases this degree of solubility is considered to be negligible.

An alternative method of classifying solid solutions is according to their crystalline structure into substitutional, where one solute molecule substitutes for a solvent molecule in the crystal lattice of the solid solvent (Fig. 1.3.) and interstitial, where the solute molecule occupies the interstitial space of the solvent lattice (Fig. 1.4.). For substitutional solid

Fig. 1.2. Typical phase diagram of a discontinuous solid solution of a binary system

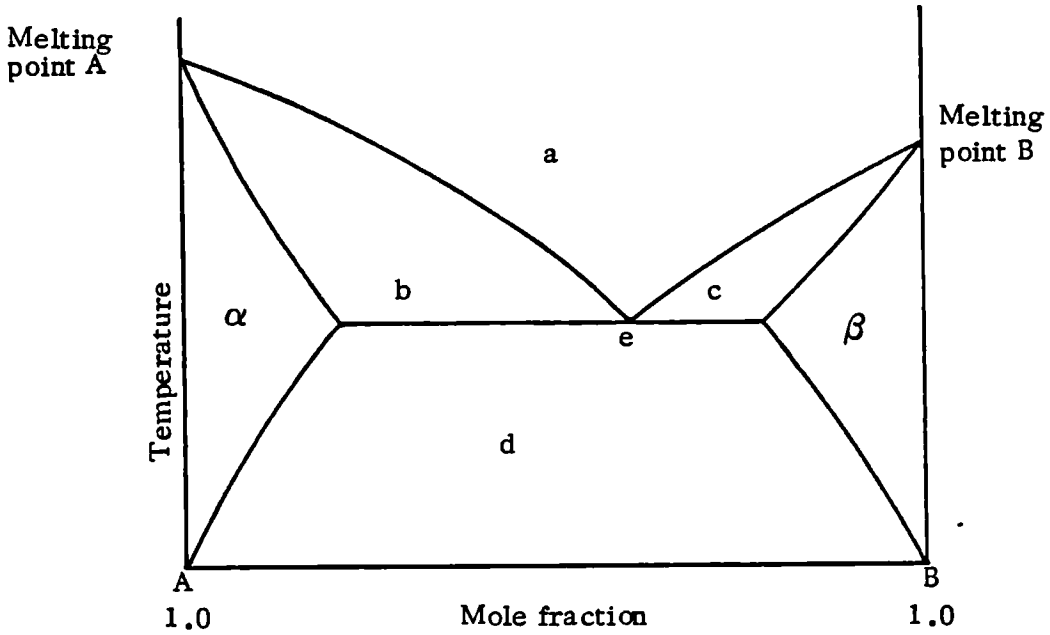

Key:

α, β	unsaturated solid solution
a	liquid
b	saturated solid solution α and liquid
c	saturated solid solution β and liquid
d	two conjugate solid solutions
e	eutectic point

Fig. 1.3. Schematic representation of a substitutional solid solution

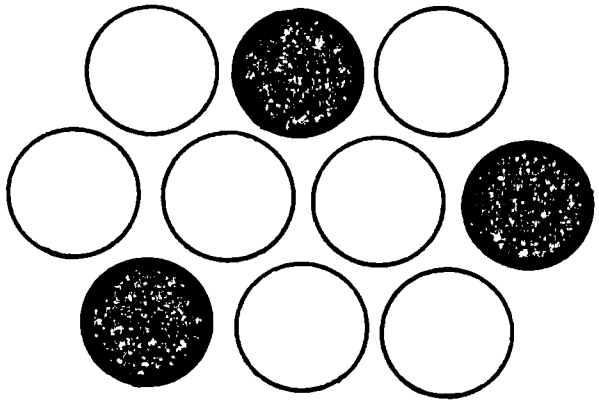

Key Dark circles represent solute atoms/molecules
Open circles represent solvent atoms/molecules

Fig. 1.4. Schematic representation of an interstitial solid solution

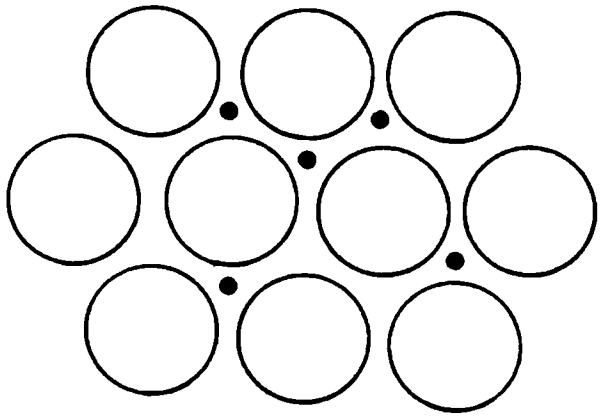

Key As for Fig. 1.3.

solutions to form, the size of the solvent and solute molecules must be as close as possible and the diameter of the solute molecules certainly should not differ by more than 15% from that of the solvent (Reed-Hill, 1964). Another important factor is the degree of lattice distortion produced in the solvent by the solute due to steric factors and chemical interactions. For example, naphthalene forms solid solutions with its α substituted halogen, hydroxyl and amino derivatives but only eutectic mixtures with its β substituted derivatives (Chiou and Riegelman, 1971), indicating the degree of molecular similarity required for substitutional solid solutions to form. These constraints make it highly unlikely that pharmaceutical systems consisting of two diverse chemical entities would form this type of solid solution and indeed no drug-carrier system so far investigated has been shown to have this type of structure.

With interstitial solid solutions, the relative size of the solute molecule is again critical as the interstitial volume of the solvent is limited. For metals, the apparent diameter of the solute molecule should be less than 0.59 of that of the solvent in order to obtain a solid solution (Reed-Hill, 1964). From this, Chiou and Riegelman (1971) calculated that the volume of the solute should be less than 20% of that of the solvent and on this basis suggest that high molecular weight polymers, such as PEGS would be a logical choice as carriers for insoluble drugs. They predict that on solidification, significant amounts of drug will be trapped between the parallel helices of the PEG unit cell.

1.2.3. Glass solutions and suspensions

Chiou and Riegelman (1969) first introduced the concept of glass solutions as a method of enhancing the dissolution rate of drugs. Glass solutions are homogeneous, one phase systems, usually obtained by rapid quenching of the melt to the amorphous form. Glass suspensions consist of precipitated drug particles suspended in a glassy, solid solvent. Examples of carriers which form glasses include citric acid (McGinity et al, 1975), succinic acid (Chiou and Niazi, 1976), and the polymer polyvinyl pyrrolidone (Hoelgaard and Møller, 1975b). Since the amorphous form of any compound possesses the highest free energy, these systems may offer dissolution advantages over even solid solutions. However, many of these systems are metastable and will revert slowly to the more thermodynamically stable but less soluble crystalline form.

1.2.4. Amorphous precipitations in a crystalline carrier

On solidification, the drug may not crystallise but be precipitated as the amorphous form within the crystalline carrier. As mentioned before, the amorphous state possesses the highest surface free energy and should dissolve faster than the crystalline form. For example, the amorphous form of novobiocin has a ten fold higher solubility than the crystalline form (Mullins and Macek, 1960). The properties of the carrier will have an important influence on the final structure of the drug dispersed within it. With PEGS, the viscous nature of the melt may retard crystallisation of the drug due to the difficulty of initiating nucleation and growth of crystals in such a medium. The properties of the drug are also important, Chiou and Riegelman (1971) have postulated that if the drug supercools to any great extent, then this will predispose it to solidify as the amorphous form.

1.2.5. Compound and complex formation

Complexes formed between the drug and carrier may enhance or retard the dissolution of the drug depending on their dissociation constant and intrinsic absorption rate. Chiou and Riegelman (1971) stated that the rate of dissolution and gastro-intestinal absorption may be increased by the formation of a soluble complex with a low association constant. These authors attributed the increased dissolution and absorption of griseofulvin observed in dogs to the formation of such a complex (Chiou and Riegelman, 1970). Conversely, the formation of a complex between PEG 4000 and phenobarbitone was shown to reduce the amount of drug absorbed (Singh et al, 1966). Likewise, decreased absorption of chlorthalidone in PEG 4000 solution compared to a conventional tablet was noted by Williams et al (1982), even though the presence of the polymer increased the solubility of the drug.

1.2.6. Combination systems

The structure of a solid dispersion may not fall entirely into any of the categories described but may be a combination of several systems. Some of the drug may exist in an amorphous form and some as micro-crystalline particles, for example. This complexity may explain why so many solid dispersion systems are difficult to categorise.

1.3. Methods of preparation of solid dispersions

1.3.1. Melting or fusion method

This technique was first utilised by Sekiguchi and Obi (1961) who heated a physical mixture of drug and carrier to just above its melting point in a furnace, before solidifying the material rapidly in an ice bath under vigorous stirring. The final solid mass was then milled and sieved. Subsequent

modifications to this technique have involved mainly changes in the rate of cooling of the solid dispersion. Cooling conditions employed have included pouring the melt onto a glass slab (Hoelgaard and Møller, 1975a) or stainless steel plate cooled by air blown on the opposite side of the plate (Chiou and Niazi, 1976; Chiou and Riegelman, 1971); cooling in a dessicator at 4° C (Kaur et al, 1980a and 1980b) and stirring continuously under ambient conditions until solidification occurred (Daabis and Mortada, 1980: El-Banna and Abdullah, 1980; Said et al, 1974a and 1974b). Faster solidification rates have been obtained by cooling the melt over a dry ice-acetone mixture (McGinity et al, 1984), dry ice (Allen and Kwan, 1969; Brown, 1978) or by immersion in liquid nitrogen (Hargreaves, 1982). In very few instances is the actual melting temperature or time in the molten state recorded and reports exist where no details of the heating and cooling conditions are given. This lack of control of the thermal profile indicates a lack of appreciation of the influence of thermal history on the structure of these systems particularly where polymers such as PEGS are used as the carrier.

1.3.2. Solvent or coprecipitate method

With this method, a physical mixture of the two solid components is dissolved in a common solvent, followed by evaporation of the solvent to leave a co-precipitate of the drug and carrier . It was first proposed by Tachibana and Nakamura (1965) who prepared solid dispersions of β carotene in polyvinylpyrrolidone and subsequently has been used on many occasions to prepare co-precipitates of PEGS with a variety of drugs including griseofulvin and tolbutamide (Kaur et al, 1980a), chloramphenicol (Kassem et al, 1979a) and hydrocortisone (Ho and Hajratwala, 1981). Although this may be a more suitable method of preparation for drugs which undergo thermal decomposition,

problems exist in finding a common, non-toxic solvent for the drug and carrier and in complete removal of the solvent. Furthermore, the relative cost of this method of preparation is high. Careful control of the processing conditions such as the rate of evaporation of the solvent is essential to ensure that the same crystal structure is produced where the drug or carrier can exist in a variety of crystal forms.

1.3.3. Melting/solvent method

An alternative to the melt method which may prove more suitable for some drugs was described by Bajpai and Varma (1981) who dissolved the drug amphotericin B in propylene glycol before mixing with molten PEG 4000 and PEG 6000. However, the usefulness of this technique may be limited by the problem of finding a solvent for the drug which is also miscible and compatible with the carrier and by the fact that only a relatively small percentage of liquid can be incorporated into the carrier without significant loss of its solid property, (Chiou and Smith, 1971).

1.3.4. Molten filling process

In spite of the potential advantages of these systems, as yet no commercial solid dispersion dosage form has been marketed because of the difficulty in manufacturing these materials on a large scale due to their poor processing properties. Chiou and Riegelman (1971) noted that PEG solid dispersions required hardening in a dessicator for at least 24 hours before they could be pulverised. Even so, because of their wax-like nature they are difficult to handle on high speed tabletting and capsule-filling machinery (Wells et al, 1975). Ford and Rubinstein (1980) developed a method of granulating and tabletting indomethacin - PEG 6000 solid dispersions. However, formulations

containing more than 25% $^{w}/w$ drug would not tablet properly because they were tacky and stuck to the upper punch in spite of hardening in a dessicator for 12 hours prior to use. Where the indomethacin concentration was below 20% $^{w}/w$, the size of the tablet required to contain a therapeutic dose was unacceptably large. Thus, for this system, only formulations containing around 20% $^{w}/w$ could be tabletted successfully. Moreover, significant decomposition of indomethacin occurred in the stored tablets, which was later attributed to an interaction with one of the other excipients, magnesium stearate (Ford, 1983). Recently, Walker et al (1980) have developed a process by which liquids, including molten and thixotropic formulations can be filled into hard gelatin capsules on an automatic filling machine. Since this technique is discussed in Chapter 2.2., no further details will be given at this point. However, it does overcome the aforementioned processing difficulties associated with solid dispersions and clearly increases their commercial possibilities.

1.4. Advantages and possible applications of solid dispersions

Although first investigated as a method of improving the dissolution rate profile of poorly soluble drugs, solid dispersion systems, particularly in the form of molten filled hard gelatin capsules, may offer advantages in other respects which can be summarised as follows:

(i) The stability of unstable drugs may be improved by formulating them in a suitable carrier, for example, oxidative degradation would be minimised in a zero porosity matrix.

(ii) Incorporation of liquid or even gaseous compounds into solid dispersion systems is possible. Chiou and Smith (1971) demonstrated that poorly water soluble drugs such as clofibrate and dl-α-tocopheryl acetate could be

successfully formulated in PEG 6000 by the melt method for concentrations of the drugs up to 10% $^{w}/_{w}$.

(iii) Operator handling hazards are decreased and risks of cross-contamination reduced since no dust is generated during the manufacture of molten filled hard gelatin capsules. This is an important consideration when handling toxic drugs such as cytotoxics or allergenic materials such as antibiotics.

(iv) Content uniformity, especially of low dose drugs, can be improved since homogeneity within a melt system is more readily achieved than with conventional powder mixes. Walker et al (1980) reported that molten filled capsules containing a nominal 20 μg of triamterene in PEG 1500 exhibited a lower relative standard deviation in drug content and fill weight variation than conventional powder fill capsules.

(v) Fast release priming doses may be incorporated into sustained release products to provide the initial release of drug. Walker et al (1980) demonstrated that this could be achieved using a matrix of PEG 1500 and polyvinyl alcohol. Rapid initial release of drug was observed due to dissolution of drug dispersed in the water soluble PEG 1500 on the outside of the plug. This was followed by a period of slower release dependent on the rate of diffusion of water through the pores of the polyvinyl alcohol matrix.

(vi) Selection of a carrier with appropriate properties can be used to obtain the release profile desired for the drug. For example, PEGS can be used where a rapid release rate is required as would be desirable with oral hypoglycaemics or analgesics (Geneidi et al, 1981; Froemming et al, 1978). Alternatively, sustained release products may be obtained by using oil/paste formulations as shown by François et al (1982).

1.5. Morphology of PEG 4000

Polymers in the solid state have a complex morphology because of the chain like nature of the constituent molecules which gives rise to crystallisation behaviour and morphologies rarely encountered in small molecule solids, whether organic or inorganic. Knowledge of the morphology of polyethylene glycols is therefore necessary to aid understanding of their behaviour when formulated as solid dispersions, since the structure of the polymer may greatly influence that of the drug and hence the properties of the system.

1.5.1. General formula

The basic monomer unit of polyethylene glycols is the reactive ethylene oxide:

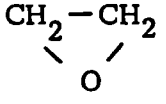

M.Wt = 44

which readily polymerises to form long chain molecules of the general formula HO- $(CH_2CH_2O)nH$, where n is the number of ethylene oxide units or the degree of polymerisation. A wide variety of molecular weights is available ranging from 200 to several million. Lower members of the group, up to molecular weights of approximately 1000 are liquid at room temperature but PEGS of higher molecular weight are hard waxlike solids in appearance (Hoechst, 1977).

1.5.2. Crystallisation

Crystallisation can be defined as the formation of an ordered state from a disordered one which involves nucleation and growth of the new phase within the parent phase. In the molten state the polymer chains are randomly orientated, although some evidence exists for association of the chain ends

(Shimada et al, 1980). As the temperature is lowered, nucleation of crystals can occur by one of two mechanisms.

Homogeneous nucleation involves the random spontaneous aggregation of polymer chains below the melting point. This process is reversible up to the point at which a critical nucleus size is reached, above which subsequent addition of chains is irreversible and growth commences. The closer the crystallisation temperature approaches the melting point, the larger this critical nucleus size is required to be, resulting in the development of only a few nuclei for crystallisation. Conversely, as the temperature is lowered, the critical size of the nucleus required for growth decreases, resulting in the formation of a large number of small nuclei (Meares, 1966). However decreasing the temperature also results in a rapid increase in viscosity which hinders the diffusion of polymer chains through the melt, thereby reducing the rate of nuclei formation. Thus a maximum rate of crystallisation occurs at a temperature where the influence of nucleation and diffusion controlled mechanisms is weakest. If the viscosity of the polymer melt is very high or the temperature is lowered very rapidly, then crystal growth will be inhibited altogether. The polymer will solidify as a glass where the constituent molecules retain the random orientation of the liquid state.

Heterogeneous nucleation arises from nuclei which are already present in the melt and occurs effectively instantaneously, unlike homogeneous nucleation where a finite time is required for the appearance of nuclei. Heterogeneous nuclei may arise from many sources such as extraneous solid impurities, grain boundaries and cavities distributed either randomly throughout the bulk or localised, for example at the surface of the container of the melt (Sharples, 1966). It has also been suggested that thermodynamically

stable minute crystals of polymer with a very high degree of crystalline perfection persist in the melt above the observed bulk melting point (Morgan, 1954). The number, size and stability of such crystal nuclei depend on a number of factors such as time and temperature of melting and previous crystallisation history, which are discussed in section 1.6.

For PEGS, the presence of heterogeneous nucleation sites can be demonstrated. In a thin film of polymer which was crystallised, melted and recrystallised, out of 28 crystallisation sites observed on the first crystallisation, 24 appeared in identical positions on the second crystallisation, (Barnes et al, 1961).

Growth of nuclei is thought to proceed by polymer chains diffusing to the surface of the crystal, where they are pleated into position on the growth face (Hillier, 1966). Crystal growth continues until it is arrested by mutual impingement of growing crystal structures . Many workers have derived equations to describe the overall crystallisation kinetics including Avrami (1939, 1940, 1941) and Hoffman and Lauritzen(1961), but in the case of PEGS, the crystal growth does not follow the predicted kinetics in general (Beech et al, 1972a; Godovsky et al, 1972). The morphological features developed from the melt are now discussed in the following section (1.5.3.).

1.5.3. Morphological features developed from the melt

PEGS are semi crystalline polymers which in the solid state will consist of both crystalline and amorphous regions, in varying proportions according to their previous thermal history. Factors which affect the crystallinity of the polymer are discussed in section 1.6. Total crystallinity is never achieved in any circumstances because of the presence of chain ends, short chain fragments and impurities which cannot pack into crystals and are rejected to

form the amorphous phase.

In the crystalline state, PEG chains exist as a double parallel helix containing seven monomer units (CH_2CH_2O) and two helical turns per fibre identity period of 93 nm. The crystallographic unit cell is monoclinic and contains four molecular chains, (Bailey and Koleske, 1976). The chains have two axes of symmetry, one passing through the oxygen atoms, the other bisecting the carbon-carbon bond. Internal conformations in the solid about the OCH_2, CH_2CH_2 and CH_2O bonds have been assigned as <u>trans</u>, <u>gauche</u> and <u>trans</u> respectively (Koenig and Angood, 1970). The polymer chains form platelike crystals, known as lamellae, with the chain ends rejected onto the surface layer and with the helical chain axis normal to the lamella (Kovacs et al, 1975). In the lamellae, polymer chains are either fully extended or folded a small integer number, n_c, of times (Arlie et al, 1966, 1967) (Fig. 1.5 (a) and (b)). In chain folded crystals, the chain folds are tight with adjacent re-entry. Hydrogen bonding between OH groups of the chain ends on the surface of the lamella contributes to the stability, especially of the extended chain form. It is interesting to note that the melting points of phenoxy or chloro terminated polyethylene oxides are much lower than those of the hydroxy terminated PEGS for this reason (Booth et al, 1972). Extended chain crystals (ecc) are found in PEGS of molecular weights up to about 4000, at which point folded chain crystals (fn_ccc) start to be detected and above PEG 6000, the folded chain morphology predominates. The number of folds per molecule depends to some extent on the molecular weight but is also influenced by crystallisation conditions. For PEG 4000, at least extended and once folded crystals can be formed and for this molecular weight, the latter are metastable with respect to the former. Conversion to the fully

Fig. 1.5. Diagram of cross-section through part of a lamella showing:

(a) Polymer chains in extended chain crystal form

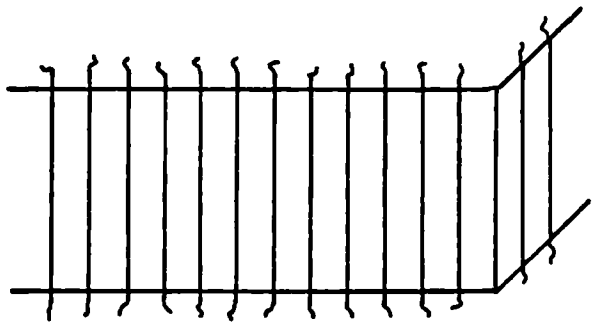

(b) Polymer chains in once-folded chain crystal form

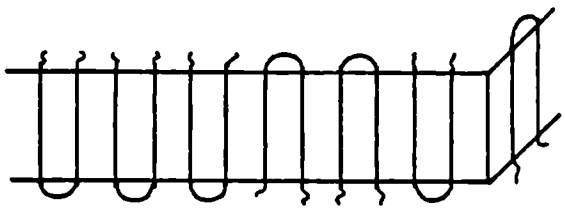

extended form through chain unfolding and lamella thickening will occur under suitable conditions. Evidence for the formation of twice folded crystals of PEG 4000 exists, but they are very unstable so that transformation to the next lowest chain conformation readily occurs (Kovacs et al, 1977). The proportion of f_{1cc} formed will increase as the crystallisation temperature decreases i.e. as the crystallisation rate increases, indicating a preference for this morphology in a rate controlled crystallisation process (Beech et al, 1972a). This can be observed for PEG 4000 on a graph of crystal growth rate as a function of isothermal crystallisation temperature which reveals several discontinuous branches, each of which corresponds to an integral value of n_c(Fig. 1.6.).

The lamellae are in turn organised into spherical structures, usually spherulites, but also hedrites which may range from 4 μm to 1 cm in diameter according to the crystallisation conditions (Bailey and Koleske, 1973). Spherulites are symmetrical birefringent structures with fine radiating branches from a central nucleus. The polymer chains usually lie at right angles to these radial units and hence tangentially with respect to the nucleus. Under crossed polaroids, spherulites composed of lamellae which do not twist as they extend from the apparent nucleus display a dark maltese cross. By comparison, a maltese cross superimposed by concentric extinction bands is observed where lamella twist regularly as they extend outwards (Allen and Mandelkern, 1982). Hedrites have a layered or steplike appearance, apparently grown from a central screw dislocation and appear very similar to spherulites in many respects. However, the maltese cross effect is lost when viewed normal to the basal plane which suggests that one optical axis is perpendicular to this plane (Mikhailov et al, 1978). Under certain

Fig. 1.6. Crystal growth rate as a function of temperature of crystallisation for PEG 3900 (Kovacs & Gonthier, 1972)

Parameter shown is n_c number of folds per molecule

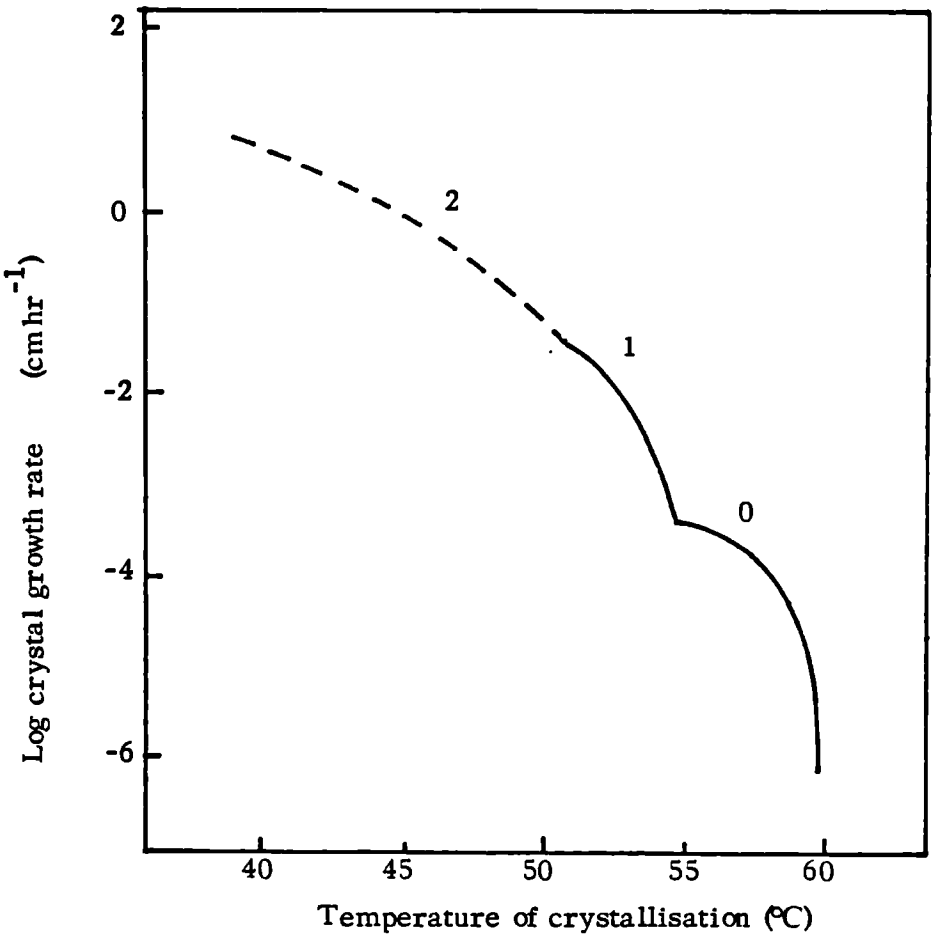

conditions, a morphology which is neither uniquely spherulitic or hedritic in character can be produced.

1.5.4. Melting

Unlike low molecular weight materials, polymers do not show a unique melting point but melt over a range of temperature which may be up to 100°C wide. For PEGS, the melting temperature range increases with molecular weight up to PEG 6000, above which it remains practically the same since for higher molecular weights, the melting point becomes determined by the thickness of the lamella rather than the length of the chains, (Hoechst, 1977). Melting temperature can be considered to be a function of molecular order or crystallinity and will therefore be influenced by such factors as the previous temperature of crystallisation. Samples which have been cooled rapidly from the melt will contain many small crystallites which possess a higher energy per unit volume of crystalline material than would a single large crystal. Furthermore, surfaces between crystallites are regions of poor packing and therefore behave as inherent crystal imperfections, all of this tends to lower the melting point (Meares, 1965). Conversely, samples which have been cooled very slowly will contain larger, more perfect crystals which will possess a higher melting point. Chain ends which are excluded from the crystals also act as imperfections to depress the melting point, an effect which becomes less important as the molecular weight increases since the relative proportion of chain ends decreases (Sharples, 1966). Finally, the crystal type of the polymer can influence the melting temperature. For PEG 4000 which can crystallize as extended chain or once folded chain crystals, the latter are thermodynamically metastable with respect to the former and consequently melt at a lower

temperature (Kovacs et al, 1977).

1.6. Factors affecting the structure of PEG

1.6.1. Time in the molten state and temperature of melting

These factors will influence the degree of chain entanglement and the stability, number and size of surviving nuclei in the melt which in turn govern the subsequent crystallisation rate and size of spherulites developed from the melt. At temperatures not too far in excess of the equilibrium melting point, much of the crystalline conformation of the polymer chain is retained (Matsuura and Miyazawa, 1969), but the persistence of ordered chains in the melt will decrease as the melting temperature or time in the molten state increase. This can be seen from the decreasing number of surviving nuclei observed in samples of polyethylene oxide crystallising at 52.7°C as the temperature at which the polymer had previously been melted increased (Fig. 1.7.). Dependence of crystallisation rate on the melting temperature has been reported for PEG 6000 (Hay et al, 1969). Changing the melting temperature from 80°C to 100°C decreased the rate of crystallisation at 54°C by a factor of thirty, but changing the melting temperature from 100°C to 150°C produced no significant alteration in the crystallisation rate. Although this data implies that above a certain temperature, the history dependence of the sample will disappear, this is not always so. Even if nuclei are destroyed by the high temperature, they can be reformed in cavities or on the surface of foreign particles on cooling to below the melting point (Beech et al, 1972). Furthermore, during the molten filling process, it is desirable that the temperature of the melt is kept as low as possible, certainly below 100°C to minimise thermal decomposition of either the drug or the polymer. This is the region where

Fig. 1.7. Number of heterogeneous nuclei in a sample of polyethylene oxide crystallising at 52.7°C plotted as a function of the previous temperature of melting (Banks & Sharples, 1963)

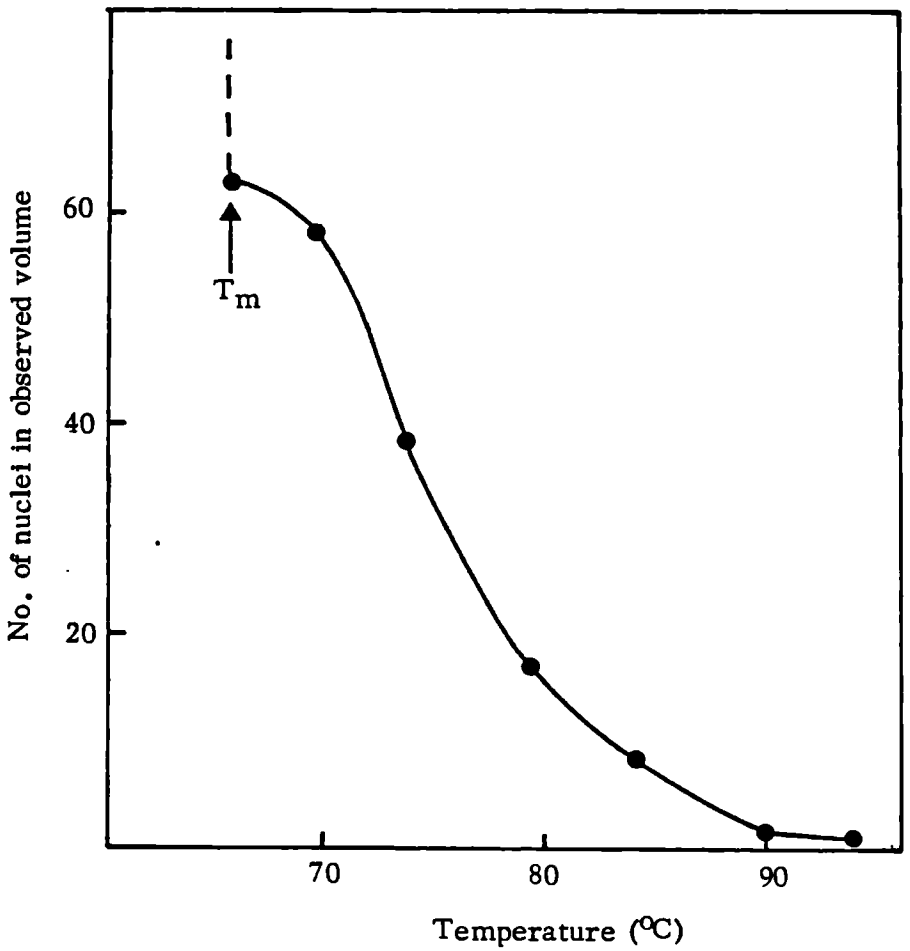

changes in the temperature of melting and time in the molten state would be expected to exert the greatest influence on the subsequent crystallisation process and final structure of the polymer.

1.6.2. Cooling rate

The rate at which a polymer cools from the melt is probably the single most important factor in determining its structure and hence its properties in the solid state. Crystallisation studies have been confined largely to isothermal crystallisation, where the melt is supercooled to a defined temperature and held there, or to rapid quenching of the melt by immersion in liquid nitrogen. However, for most pharmaceutical systems, including the molten filling of solid dispersions into capsules, knowledge of what happens under non-isothermal conditions is necessary to interpret their behaviour, although much information can be inferred from isothermal studies.

Since polymer chains in the melt are randomly orientated, a finite time is required for the nucleation and growth of ordered crystals by chain diffusion through the melt. Thus as the rate of cooling increases, the time for diffusion decreases and becomes hampered by such factors as high viscosity, leading to a decrease in the crystallinity of the polymer. In the extreme case of quenching from the melt, the polymer chains are frozen in their random orientation giving the amorphous form. As this form possesses the highest free energy, it would be expected to have the greatest solubility but also to be the least stable.

For less dramatic rates of cooling, the number of nuclei formed for crystallisation will be dependent on the cooling rate. At relatively slow cooling rates, only a few nuclei will form, resulting in the growth of very large spherulites. Conversely, faster cooling rates will give rise to many

small nuclei and hence a large number of small spherulites will crystallise out. Under isothermal conditions, extended chain crystals preferentially form at high crystallisation temperatures, but with large degrees of supercooling, folded chain crystals become the dominant morphology in PEG 4000 (Kovacs et al, 1975, 1977). An increase in the percentage of amorphous material would be expected at faster cooling rates reflecting the insufficient time for orientation and crystallisation of the polymer chains. Beyene (1981) has demonstrated that even relatively small changes in cooling rate from $7.5^{o}\,CHr^{-1}$ to $3.75^{o}\,CHr^{-1}$ affected significantly the mechanical strength of PEG 6000 due to morphological differences in the structure of the polymer which it is expected would influence other properties as well.

1.6.3. Ageing

Little work has been published on the morphological changes associated with the ageing of polyethylene glycols alone. However, after the completion of the primary crystallisation process, secondary processes are known to occur (Sharples, 1966). These result in a very slow and continual increase in crystallinity often over a period of many months due to perfecting of the existing crystal structure. Crystallisation of the slowly crystallisable components or part of the amorphous region may take place. For PEG 4000, the crystal form may change from the metastable once-folded chain crystal to the completely extended chain crystal by a process of chain unfolding leading to an increase in the thickness of the lamellae (Kambe, 1980). All of these changes will be accelerated by annealing the polymer at a temperature a few degrees below its melting point.

1.6.4. Effect of adding a second component (usually drug)

In addition to forming either a eutectic or solid solution system with the polymer as outlined in section 1.2., the added material may have one of several other actions on the crystallisation of the polymer and thereby influence the final structure of the system. If the added material is present as undissolved or recrystallised particles, it may act as a nucleating agent to increase the number of nuclei present in the polymer melt. This will result in a marked increase in the crystallisation rate of the polymer, as was observed when 2% $^{w}/_{w}$ lead phosphate was added to PEG 6000 (Beech et al, 1972b). Moreover, crystallisation may well take place at a higher temperature which for PEG 4000 might predispose the formation of the more thermodynamically stable extended chain crystals. Rapid crystallisation of the polymer would also hinder any further crystal growth of the other component. Therefore the speed of crystallisation of the PEG may influence the size of the crystals formed by the second component. The nucleating ability of a substance is difficult to predict since the mechanism by which nucleation is induced is not well understood. It is important to note that the mere presence of foreign particles in the melt is not sufficient to initiate nucleation, since for example, addition of mercury droplets to PEG melt resulted in no increase in nucleation (Hay et al, 1969). The surface energy of a substance does not appear to dictate its nucleating ability since both high and low energy surfaces have been shown to be capable of acting as nucleating agents by Chatterjee et al (1975a). However crystallinity of the added material has been identified by these authors as a necessary but not sufficient requirement for nucleating ability.

The added material could also act to inhibit crystallisation of the polymer by hindering chain diffusion and packing resulting a higher percentage of amorphous and imperfectly crystalline material. Studies of the crystallisation of PEGS have shown that low molecular weight fractions and foreign material (which would include the drug) are rejected during the primary crystallisation process, giving a boundary layer of non-crystallisable or slowly crystallisable material and foreign particles at the growth front (Beech et al, 1972b). In the solid state, this wi ll constitute an amorphous region between the crystalline lamellae.

1.7. Methods of studying the structure of solid dispersions

1.7.1. X-Ray Diffraction

Since X-rays are scattered by a crystal according to Bragg's Law, the pattern and intensity of X-ray diffraction from a sample measured as a function of diffraction angle will be characteristic of the material (Vainshtein, 1966). With two component systems, the situation is more complex and a number of possibilities exist. For eutectics, the X-ray diffraction pattern is simply a composite of those of the individual components, whereas with solid solutions the position of the diffraction lines may alter. In the case of substitutional solid solutions, the diffraction lines associated with the solvent crystal may or may not shift according to the size of the solute molecule: while for interstitial solid solutions, the position of diffraction lines associated with the solvent again may or may not change but those of the solute disappear (Chiou and Riegelman, 1971). Complex formation is relatively easy to detect since lattice parameters will always change. Likewise, polymorphic modifications of either the drug or carrier will display different diffraction patterns.

Although X-ray diffraction is a useful technique for investigating the structure of crystalline compounds, it cannot be used to examine amorphous materials, since these scatter X-rays randomly, giving a spectrum consisting of a diffuse 'hump'. This can cause problems also in discriminating between an amorphous precipitation and an interstitial solid solution of drug within a carrier, since in neither case are diffraction peaks of the solute observed. Such difficulties have been experienced in the interpretation of data obtained from systems where low levels of drug were dispersed in PEGS (Chiou and Riegelman, 1971).

1.7.2. Differential scanning calorimetry

Differential scanning calorimetry (DSC) is a technique of non-equilibrium calorimetry where the sample and reference materials, heated at a linear rate, are kept isothermal by changing the current through the heater below the two chambers. By monitoring changes in current, thermal transitions such as melting or polymorphic changes can be measured. The predominant use of DSC in the investigation of pharmaceutical solid dispersions has been the accurate determination of thaw and melting point temperatures over a range of compositions of carrier and drug, (e.g. Hoelgaard and Møller, 1975a and b; Ford and Rubinstein, 1978b; El-Banna and Abdallah, 1980). From this data, a phase diagram of the system can be constructed which should be characteristic of the type of solid dispersion formed. However, information other than simply the melting point of the sample can be obtained from both the shape of the peaks and the area of the transition curve such as the heat of fusion or crystallisation.

1.7.3. Hot stage microscopy

Hot stage microscopy (HSM) is another method which has been used widely in the construction of phase diagrams of pharmaceutical solid dispersion systems (e.g. Ford and Rubinstein, 1978b; Hargreaves, 1982). A thin film of solid dispersion on a microscope slide is heated at a constant rate and observed under crossed polaroids. Crystalline material will appear illuminated against a dark background but on melting, crystallinity is lost and any structures disappear. The melting point data recorded from this technique are obviously subject to operator error and have been reported to be much less reliable than those obtained by DSC (Chiou and Riegelman, 1971 ; Chang et al, 1975). With polymers such as PEGS, the melting points determined by the disappearance of birefringence are 3^{o}- 5^{o} C lower than those determined by thermal analysis methods (Hay et al, 1969). Furthermore, only the thaw and final melting points can be detected by HSM and any intermediate transitions are not observed.

1.7.4. Dissolution rate

Allen and Kwan (1969) proposed a new method for studying what they term the degree of crystallinity in solid-solid equilibria, which they define as the ratio of crystalline drug to that dispersed at a molecular level within a carrier. They compared the dissolution rates of 10% $^{w}/_{w}$ indomethacin in PEG 6000 constant surface area discs prepared by the fusion method with those of a physical mixture and from this data constructed a graph of the degree of crystallinity of indomethacin as a function of dissolution rate. In this method, the authors assume that the indomethacin in the physical mixture was entirely crystalline and in the fusion formulation existed entirely as a molecular dispersion, but no experimental evidence in support of this

was given. Furthermore, the effect on dissolution of the different particle size distributions in the two formulations has not been taken into account. Thus this technique suffers from a number of theoretical and practical limitations.

1.7.5. Other methods

I.R. spectroscopy has been utilised on several occasions to determine whether any complexation existed between PEG and the dispersed drug (Hargreaves, 1982; Kassem et al, 1979b). A number of other methods have been used to examine the polymer alone which have rarely if ever been applied to the study of pharmaceutical solid dispersions. These include nuclear magnetic resonance spectroscopy (Maxfield and Shepherd, 1975; Matsuzaki and Ito, 1974), Raman spectroscopy (Koenig and Angood, 1970), dielectric spectroscopy (Decossas et al, 1982), dilatometry (Ikeda et al, 1975; Price et al, 1975), mechanical relaxation (Hartmann, 1972), electron spin resonance spectroscopy (Törmala et al, 1973; Lang et al, 1977a and b) and scanning electron microscopy (Lovinger et al , 1976). It is possible that a number of these techniques would yield valuable information about the structure of solid dispersions as well.

1.8. Aims of this work

The importance of thermal history in determining the structure and properties of solid dispersions, especially those involving polymers has not been appreciated fully. Therefore, the primary aim of this work is to investigate the structure of PEG 4000 and its solid dispersions with a model drug under various controlled heating and cooling profiles with particular reference to conditions which might be experienced during a molten filling

process. The influence of any changes on the dissolution rate of both the drug and the polymer will be determined. Additionally, structural changes which occur on ageing will be investigated and related to changes in dissolution behaviour.

Difficulties exist in assessing the structure of polymer-drug dispersions in the solid state by conventional techniques which frequently do not provide an unambiguous description of these systems. Thus the second aim of this study is to evaluate a new method of investigating the structure and behaviour of PEG 4000 and its solid dispersions, namely dielectric response. Previous work performed by Shablakh (1982) has already proved the usefulness of this technique in following structural changes on heating and cooling in the cycloalcohols. It is proposed to compare this new technique with established pharmaceutical procedures such as D.S.C. and X-Ray diffraction.

CHAPTER 2

CHAPTER 2 Materials and Process Characterisation and Solid Dispersion Preparation

2.1. Characterisation of materials

2.1.1. Polyethylene glycol 4000

From the wide range of molecular weights available, PEG 4000 was selected as a model because it displays a number of interesting morphological features since both folded chain and extended chain crystals can be formed depending on the crystallisation conditions (see Chapter 1). Secondly, many dissolution studies e.g. Geneidi et al (1980) and Kassem et al (1980) have shown that molecular weights of PEG of this order give the greatest dissolution enhancement of the drug.

The sample of PEG 4000 used in this study was supplied by Hoechst (Batch no. 821336) in the form of hard, white flakes. DSC of the polymer showed that samples melted in the expected range for this molecular weight and details of the technique and results are discussed in Chapter 3, as are the X-ray diffraction studies performed on the material.

One of the most important characteristics of a polymer is its molecular weight distribution and knowledge of this is vital in interpreting physical data. Polymer samples are never monodisperse since during manufacture, the growth and termination procedures which determine the size of individual molecules are often random in nature. This polydispersity will affect properties such as melting point, mechanical strength and crystallinity because on crystallisation, shorter chains in a sample may not pack into crystals as easily as longer chains, leading to fractionation and attenuation of crystal growth (Beech et al, 1972b). Molecular weight analysis was

therefore carried out (at R.A.P.R.A. Technology Ltd., Shawbury) by gel permeation chromatography, a technique which involves non-aqueous fractionation of the different molecular weights by molecular sieve. A 0.1% $^{w}/v$ solution of PEG 4000 in dimethyl formamide at 80°C was passed down a P.L. gel column at 0.5 ml/min. Calibration of the column was carried out using polyethylene oxide standards. From the results, a graph of the molecular weight distribution can be obtained (Fig. 2.1.) and the number average (Mn) and weight average (Mw) molecular weights calculated. The ratio of Mw/Mn gives the polydispersity factor of the material and provides a useful index of the heterogeneity of the molecular weight distribution. In a monodisperse sample, Mw/Mn would be unity, but as the breadth of the distribution increases, so does this ratio. For this sample of PEG 4000, Mn was found to be 4390 and Mw 4960, giving a polydispersity factor of 1.129 which indicates a narrow molecular weight distribution and hence there was no need to fractionate the polymer further.

2.1.2. Trimethoprim

The model drug needed to fulfil certain basic criteria which can be listed as follows:

(a) Chemical stability

(b) Compatibility with PEGS

(c) Easy to assay in aqueous solution

(d) Low solubility in water

(e) Polar nature so that dielectric studies possible

The antibacterial drug trimethoprim complied with all these requirements and, in spite of the fact that it does not suffer from bioavailability problems, was felt to be a suitable model for these studies. Moreover, Meshali et al

Fig. 2.1. Molecular weight distribution of PEG 4000 from gel permeation chromatography studies

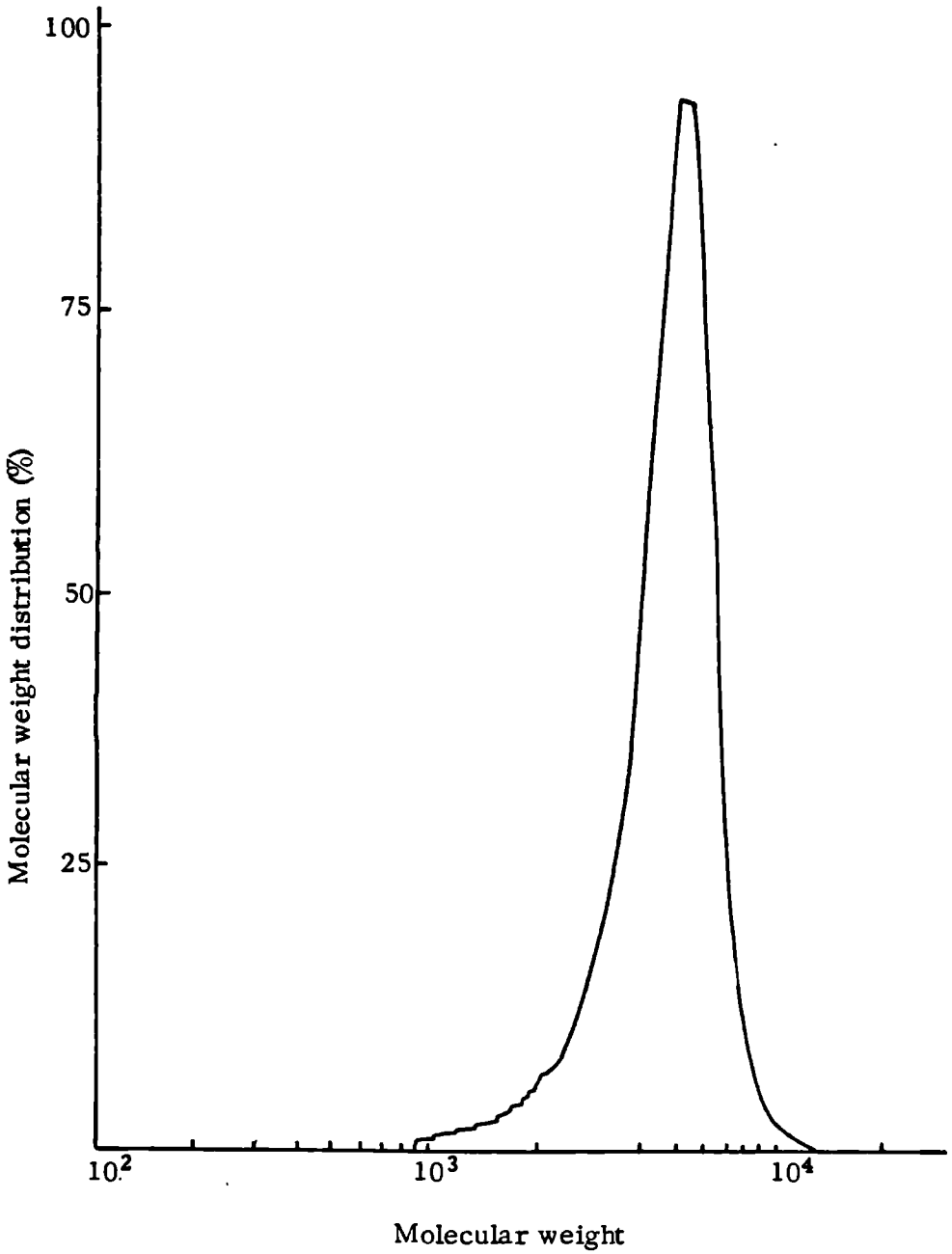

(1983) have demonstrated that an increase in dissolution rate allowing a corresponding dose reduction is possible with sugar glass dispersions of trimethoprim, which might also be expected for PEG dispersions.

Trimethoprim, which has the structure shown in Fig. 2.2. was supplied by Hoechst, batch number L008/OFTTOO, in the form of a fine white powder. The absence of polymorphic forms was confirmed by DSC as only a single exothermic peak at 202°C was observed, which corresponded to Form I of trimethoprim (Bettinetti et al, 1976). X-ray diffraction analysis of the powder produced the expected characteristic spectrum. Details of,and results obtained from,these two techniques will be discussed further in Chapter 3.

Particle size analysis was carried out using a Coulter Counter Model TAII (Coulter Electronics, Harpenden) with a 0.9%^{w}/v aqueous solution of sodium chloride, previously saturated with trimethoprim as electrolyte. The drug was found to have a geometric mean diameter of 10.58 μm (geometric standard deviation 1.46 μm). Scanning electron microscopy (Philips, Model 501B) confirmed the particle size data from the Coulter Counter and also revealed the particles had very broken crystalline surfaces consistent with having undergone micronisation (Plate 2.1.).

2.1.3. Other chemicals used

All other chemicals used in this work e.g. for assay procedures are listed in Table 2.1. together with the supplier, grade and batch number.

Fig. 2.2. Chemical structure of trimethoprim

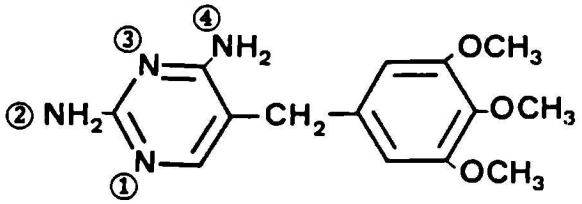

2, 4-diamino-5-[3', 4', 5'-trimethoxybenzyl] pyrimidine

Plate 2.1. Electron micrograph of trimethoprim powder

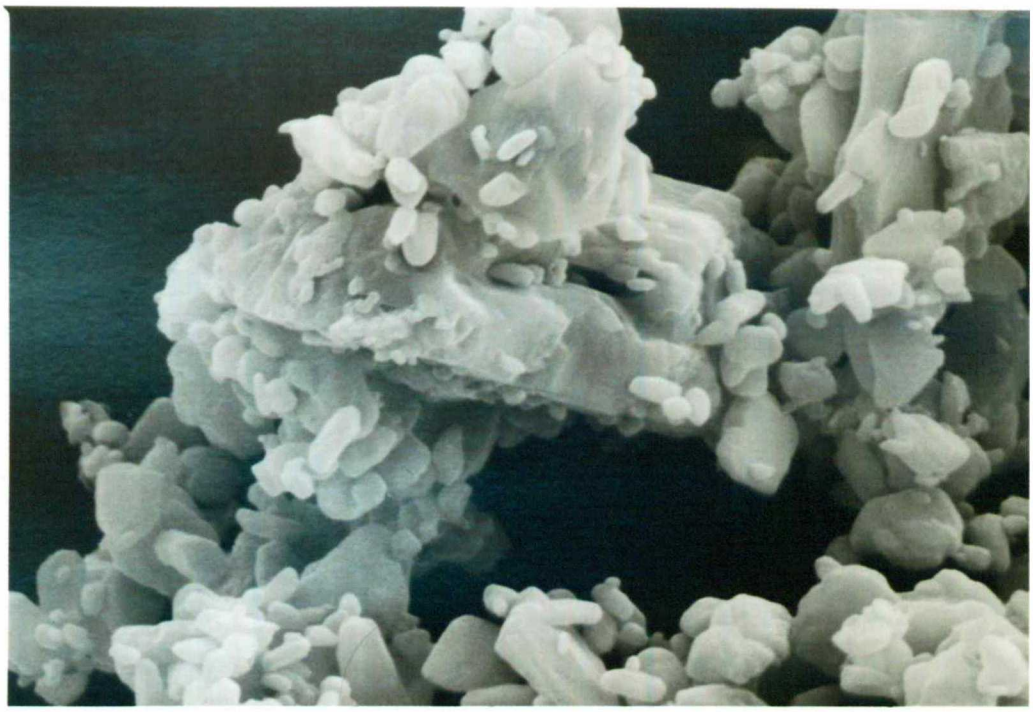

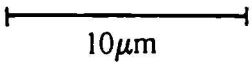

Table 2.1. Details of chemicals used in this work

Chemical	Grade	Supplier	Batch number
Hydrochloric Acid	AR	Fisons, Loughborough	73
Iodine volumetric solution	AR	BDH Chemicals Poole, Dorset	7563990C
Barium chloride	AR	BDH Chemicals Poole, Dorset	9124647H

2.2. Characterisation of the thermal profile of the process for molten filling of hard gelatin capsules

2.2.1. Introduction

Walker et al (1980) have recently described the use of an adapted Zanasi LZ64 automatic capsule filling machine to fill molten formulations, where the dosator tubes and powder hopper have been replaced with a liquid filling

pump and heated reservoir. A schematic diagram of the system is given in Fig. 2.3. Material is pumped from a heated reservoir through a precision pump (Hibar, HBD-1A) and filled into the capsules which are then ejected in the usual manner. A detector system operates to stop the filling cycle if a capsule body is not present and thus prevents soiling of the turntable by the melt. If a capsule body is missing, light from the diode reaches the detector below the turntable and triggers a microswitch which halts filling. As long as a capsule body is present, no light will reach the detector.

During the filling process, material from the same batch will not be subjected to the same heating and cooling conditions. For example, the material will have been in the molten state for a variable length of time, depending on whether it was filled towards the beginning or end of the run. The temperature of the melt in the reservoir may fluctuate during filling. Thirdly, the rate of cooling of the capsules as they are ejected may vary according to their position in the collecting container. As all these factors are known to affect the morphology and hence physical properties of semi-crystalline polymers such as PEGS, it is important to quantify the thermal profile which might be expected and any possible sources of variation which might occur. The effect of different heating and cooling profiles on the structure of the solid dispersion can then be fully investigated and if necessary, temperature controls can be applied at critical stages during processing. Therefore the degree of variation in thermal history during a typical run using the filling system described above was investigated.

Fig. 2.3. Diagram showing molten filling system

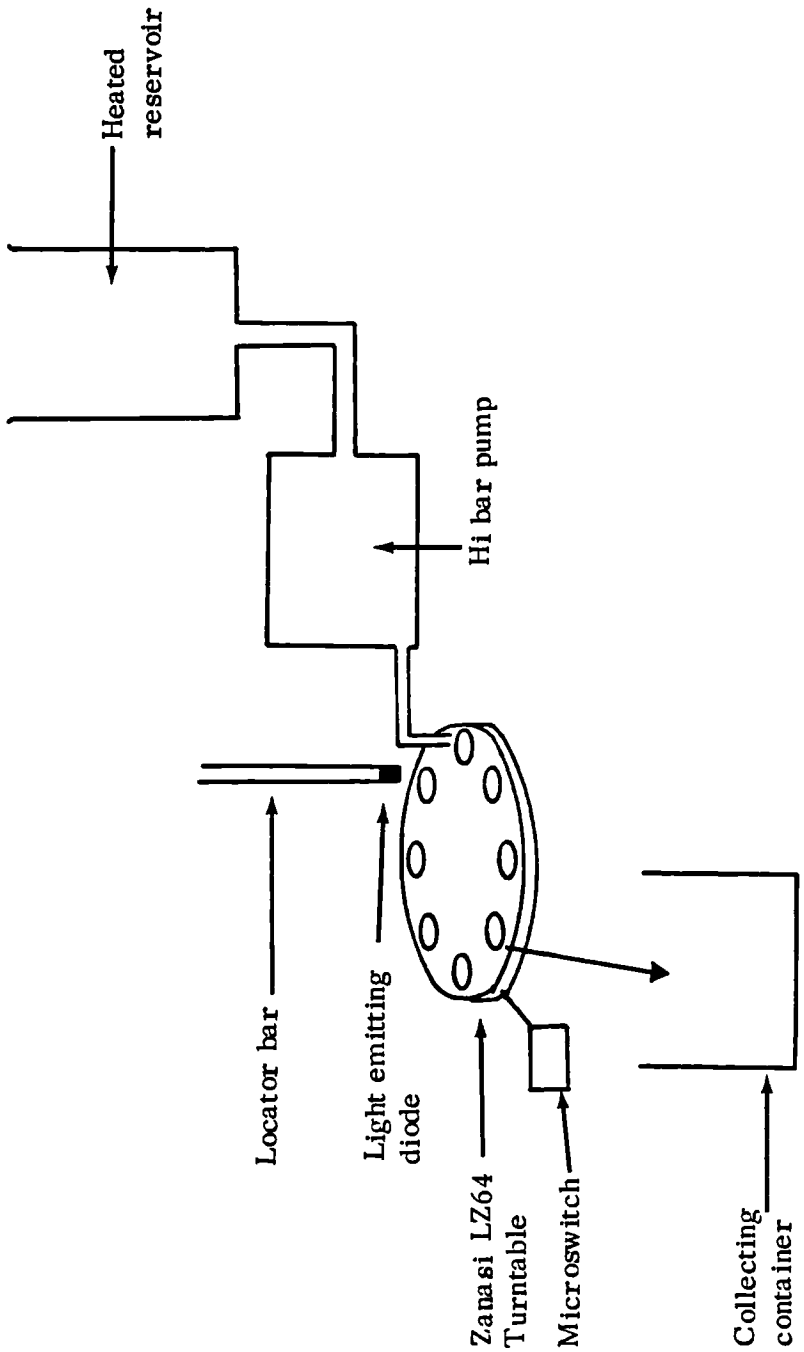

2.2.2. Methods

A batch of approximately 3 kg of PEG was filled into size 3 capsules (fill weight 120 mg) on the adapted Zanasi LZ64 machine. After initially melting the material at 70°C in an oven, it was transferred to the heated reservoir, maintained electrically at 65°C. The temperature at different positions in the reservoir (Fig. 2.4.) was monitored throughout the run using a digitron temperature probe (Model 175, Digitron Instrumentation). The time spent in the molten state was also recorded.

On ejection from the filling machine, capsules were collected into a cylindrical container of diameter 30 cm and height 20 cm. The temperature of the capsules at three different levels in the bulk container was recorded as a function of time using the digitron probe as above. The time taken as zero was when the probe was placed in position as the capsules collected in the container, which took approximately 20 minutes to fill. Cooling profiles were also obtained for the contents of individual, isolated capsules, by inserting the temperature probe directly into the opened capsule after filling.

2.2.3. Results

A graph of the temperature fluctuations with time at various positions in the reservoir is shown in Fig. 2.5. A variation of approximately 8°C in the temperature of the melt at different points in the reservoir was observed, with the coolest material being at the surface in the centre as might be expected. During the run, however, the temperature of the material in the reservoir did not vary by more than 2-3°C, even though the volume of the melt decreased as filling proceeded and no stirring was carried out. The time that the material spent in the molten state ranged from 1 to 7 hours.

Fig. 2.4. Positions in the heated reservoir at which the temperature of the melt was monitored

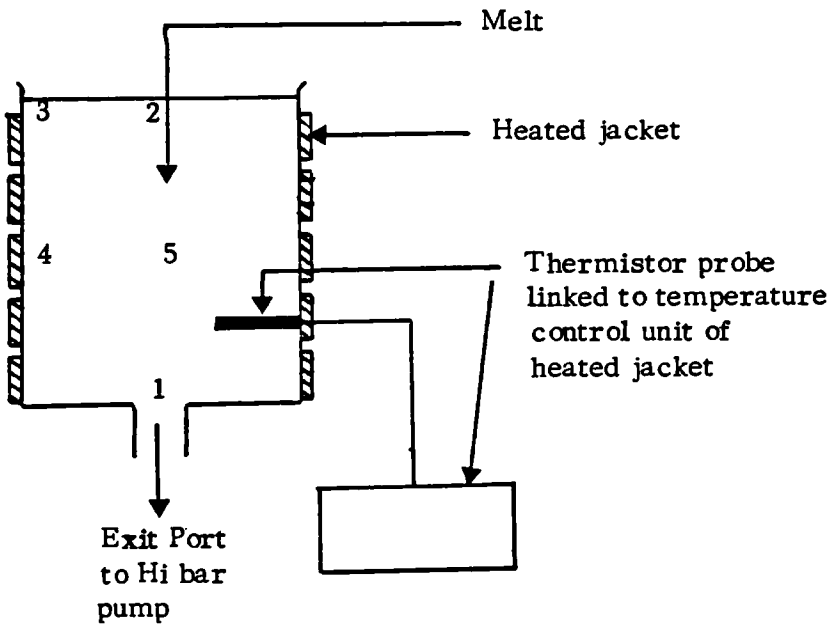

Position 1: Exit port at base

Position 2: Surface of melt, in the centre

Position 3: Surface of melt, at the side

Position 4: Half-way down melt, at the side

Position 5: Centre position in melt

Fig. 2.5. Temperatures at different positions in the heated reservoir as a function of time

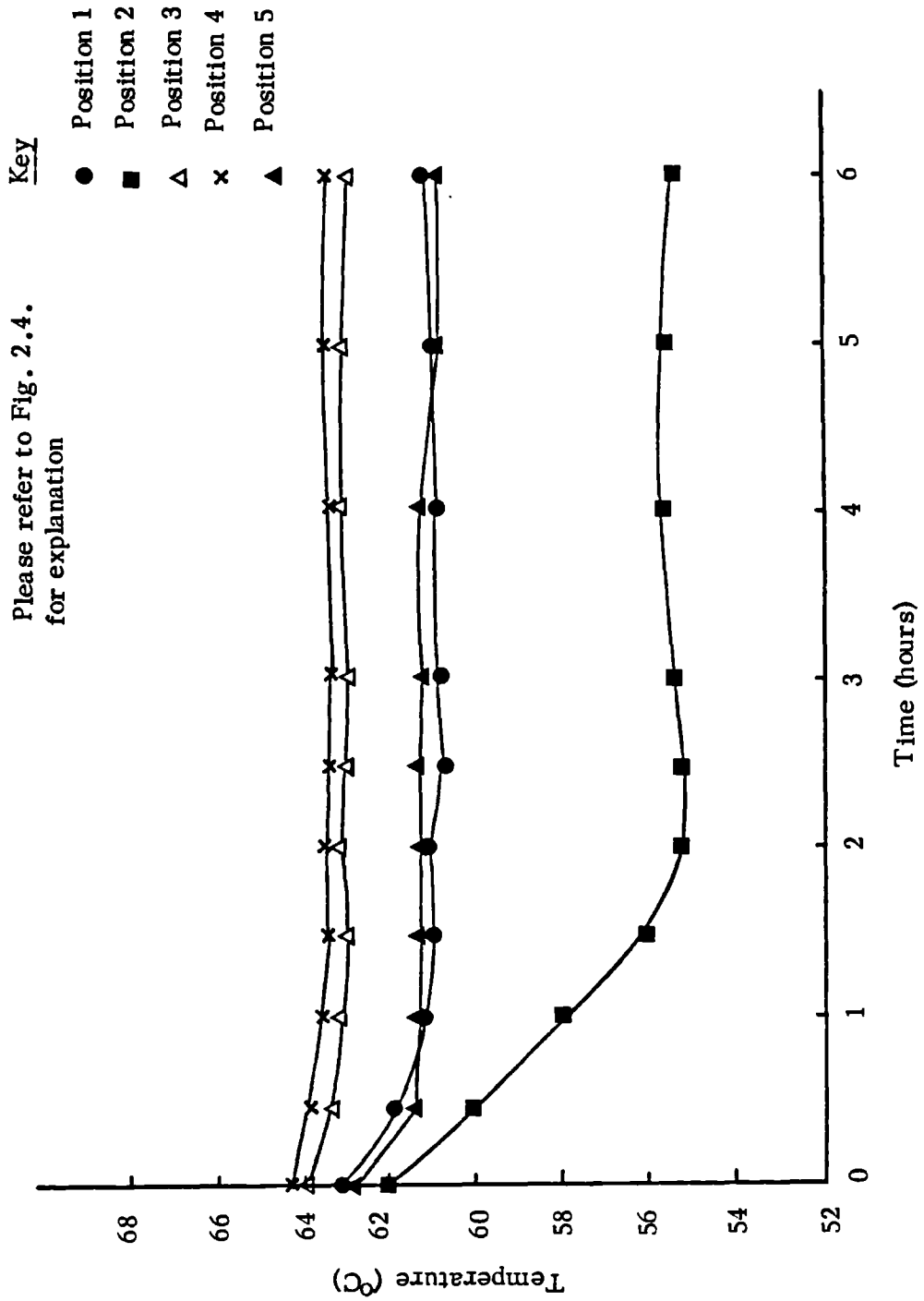

A wide variation was observed in the time that capsules at different levels in the container took to cool to ambient temperatures (Fig. 2.6.) ranging from 1 hr 40 min (capsules on top) to 6 hours (capsules in the middle). Temperature profiles of capsules in the middle and at the bottom of the container showed a rise in temperature of several degrees followed by a plateau region before cooling commenced, which was not observed with capsules on top of the container. Cooling rates (excluding plateau region) were approximately 11, 7 and 6 $^{o}Chr^{-1}$ for the top, bottom and middle positions respectively. The cooling profile for individual capsules followed the behaviour shown in Fig. 2.7. in all samples studied.

2.2.4. Discussion

The range of time that the material spent in the molten state varied between 1 and 7 hours, even for a relatively small batch and might well be expected to increase with larger batch sizes. It is important, therefore, that influence of this factor on the final structure of the polymer is known. Less variation was observed in the temperature of the melt during the run, although again, more variation may be expected with larger batch sizes.

The rise in temperature and subsequent plateau region seen for the cooling profiles of capsules in the bottom and middle of the collecting container is presumably due to the heating effect from warmer capsules on top as they are ejected from the machine. However, some contribution arising from the exothermic heat of crystallisation of the polymer may be involved. Larger collecting vessels might be expected to enhance this temperature gradient, resulting in even greater variations in cooling rates. Individual capsule cooling profiles show a sharp drop in temperature when supercooling of the melt occurs, as is common in polymer systems. The subsequent rise in

Fig. 2.6. Temperature profiles of capsules cooling at different positions in the collecting container

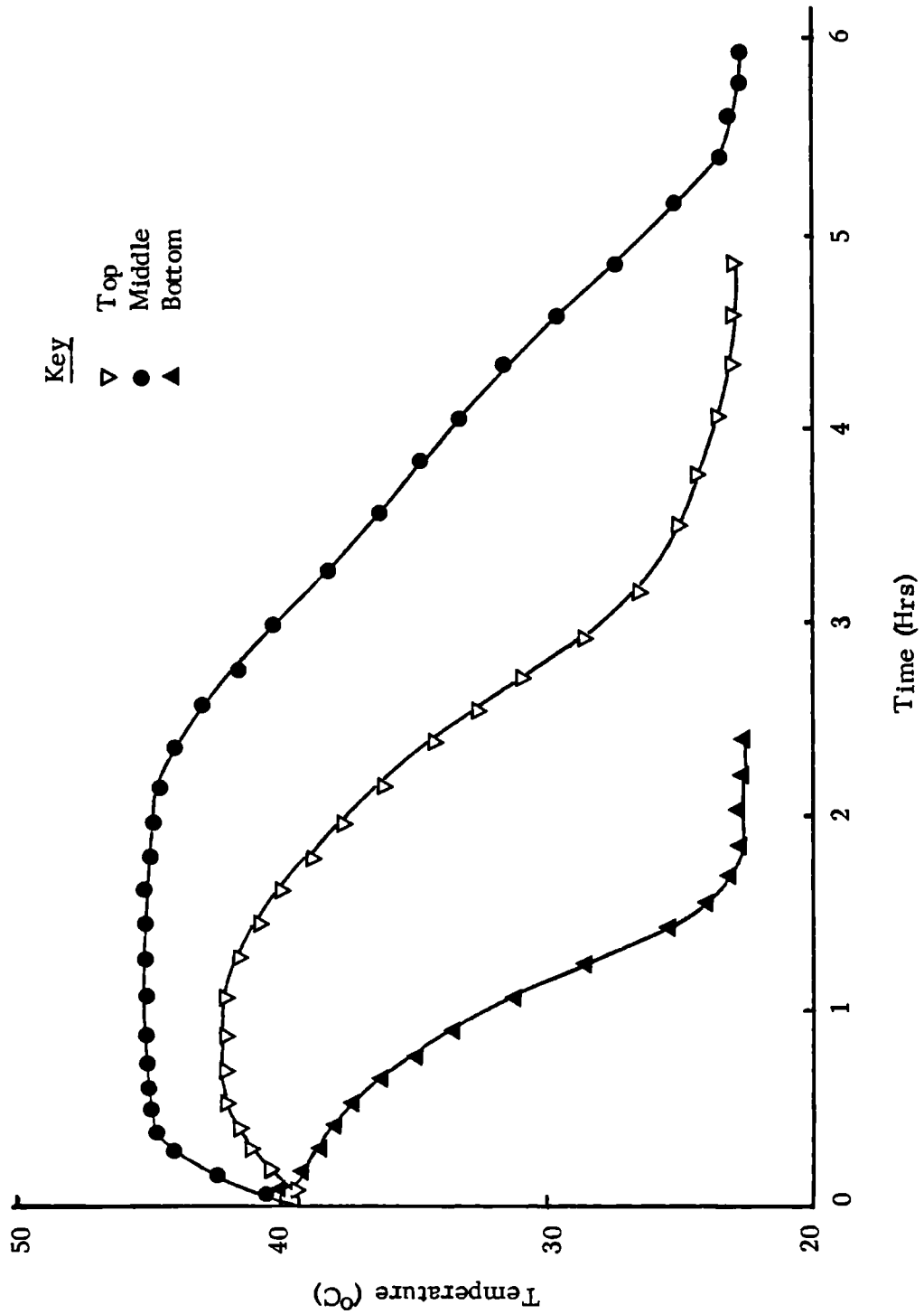

Fig. 2.7. Characteristic cooling profile of an individual capsule

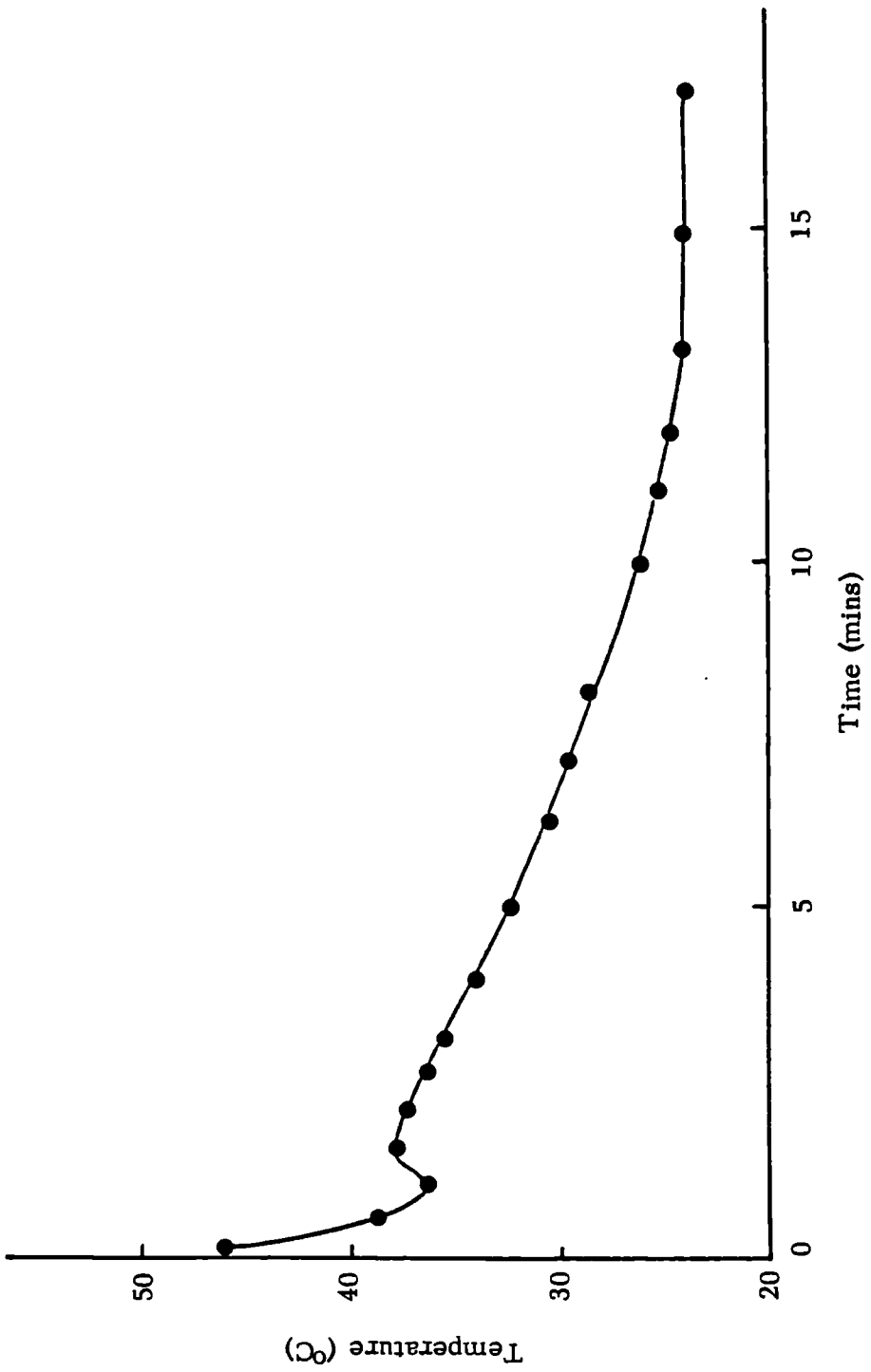

temperature occurs due to the exothermic reaction associated with crystallisation of the polymer. Cooling to room temperature occurs when this transition is complete.

2.2.5. Conclusions

The study carried out above illustrates that capsules from the same batch may have significantly different thermal histories, and the importance of this on the properties of the formulation should be investigated.

2.3. Preparation of solid dispersions

2.3.1. Preparation of samples with different thermal histories

Solid dispersions with different thermal histories were prepared by a fusion method as follows. Quantities of PEG 4000 alone or a physical mixture of polymer and trimethoprim were melted in an oven (LTE Ltd., Oldham, Lancashire) at the required temperature. Subsequently, melts were transferred quickly into either a brass mould with 1.5 cm diameter holes, which produced the discs for dissolution studies or glass slides for examination by X-ray diffraction. The temperature of melting, time in the molten state and rate of cooling of the samples was controlled by means of a clearspan P105T programmer attached to the oven, which also provided a record of the thermal cycle actually undergone. Some of the samples were cooled very rapidly from the melt by immersion in liquid nitrogen. DSC was performed on both discs and slides to ensure that no significant difference in structure resulted from this change in size and shape. Similarly, the thermal equivalence of discs from all positions of the mould was established.

2.3.2. Ageing studies

A range of samples of PEG 4000 and polymer-trimethoprim solid dispersions prepared under different conditions were stored in amber glass bottles protected from light at 25°C, 37°C and 45°C. Changes in dissolution rate and in structure of both polymer and drug as determined by X-ray diffraction and DSC were monitored immediately after preparation and at various intervals up to six months. For every composition, at least duplicate determinations were performed at each time interval. Scanning electron micrographs were obtained for representative samples.

CHAPTER 3

CHAPTER 3 Investigation of structure by DSC, X-ray diffraction and SEM

3.1. Introduction

In this chapter, the application of conventional techniques, namely DSC and X-ray diffraction to the study of PEG 4000 and its solid dispersions is investigated. Since the basis of these techniques has been outlined already in Chapter 1.7., no further introduction to them will be given here.

Although many studies have been performed on the dissolution properties of PEG solid dispersions, relatively few investigations of their physical structure exist. Most workers have characterised these dispersions by constructing phase diagrams, either by DSC or hot stage microscopy (e.g. Ford and Rubinstein, 1978a; Hoelgaard and Møller, 1975b), using X-ray diffraction to substantiate the results obtained from the thermal methods. For most PEG solid dispersion systems investigated, formation of a eutectic at low drug concentrations, typically below 10% $^{w}/_{w}$ drug (e.g. Hoelgaard and Møller, 1975a; Daabis and Mortada, 1980) has been suggested. Other authors have postulated that a degree of solid-solid solubility exists below the eutectic point (e.g. Hargreaves, 1982). However, no unequivocal evidence for the formation of either eutectics or solid solutions has ever been found from X-ray diffraction data. Recently, McGinity et al (1984) suggested that the PEG solid dispersions they studied by X-ray diffraction existed simply as a physical dispersion of drug in the polymer. Thus considerable confusion exists in the literature about the structure of PEG solid dispersions, possibly due to the properties of the polymer itself. Therefore, the first part of the studies described in this chapter concentrate on the behaviour of PEG 4000 alone under different thermal treatments.

3.2. Methods

3.2.1. Differential scanning calorimetry

A differential scanning calorimeter (Model DSC-1, Perkin Elmer Ltd., Beaconsfield) coupled to a galvanometric chart recorder (Model PRR, Texas Instruments, Houston, USA) was calibrated as recommended by the manufacturers using pure materials which melt in the temperature range of interest, namely gallium (mpt = 29.7°C) and indium (mpt = 156.6°C). Samples of between 4 and 5 mg, depending on composition, were weighed to 0.01 mg (Model 1712, Sartorius, Belmont, Surrey) and sealed into aluminium sample pans. Thermograms were obtained at a heating rate of 8°C min^{-1} and a range of 8 mcal sec^{-1} unless otherwise stated, in a nitrogen atmosphere. All determinations were carried out at least in duplicate. Transition temperatures, as determined by the peak maximum method (Wendlandt, 1974) and peak areas were recorded using a graphics tablet connected to a microcomputer (Model II+, Apple).

The heat of fusion or crystallisation was calculated with reference to the indium standard (heat of fusion, ΔH_f = 28.43 kJ kg^{-1}). From these values, the crystallinity of the polymer was estimated by assuming that the heat of fusion of a perfectly crystalline sample of PEG was 196.78 kJ kg^{-1} (Buckley and Kovacs, 1976). Thus:

$$\% \text{ crystallinity of PEG} = \frac{\Delta H_f}{\Delta H_f^*} \times 100 \qquad \ldots 3.1.$$

Where ΔH_f = observed heat of fusion

ΔH_f^* = heat of fusion of perfectly crystalline polymer

3.2.2. X-Ray diffraction

Diffraction patterns were obtained using an X-ray diffractometer (Philips, New Jersey) with CuK_α radiation, wavelength 0.154178 nm, by scanning at 1^o min^{-1} in terms of the 2θ angle over a range from 5^o to 35^o. Duplicate scans were run in all cases. The interplanar d-spacings were calculated according to Bragg's Law:

$$n_x\lambda = 2d \sin\theta \qquad \ldots 3.2.$$

where n_x= order of reflection

λ = wavelength of x-rays

d = distance between planes of atoms

θ = angle of incidence

The intensities of the diffraction peaks were measured and expressed as a percentage of the height of the most intense peak. Degree of crystallinity was estimated by the usual method (Sharples, 1966) based on the relation:

$$\% \text{ crystallinity} = \frac{Oc}{Oc + k_x O_a} \times 100 \qquad \ldots 3.3.$$

where Oc and Oa denote measures of the crystalline and amorphous intensities respectively. The constant, k_x which accounts for the relative scattering intensity of both phases, was taken to be unity as is the convention (Bartel et al, 1979). After a straight background line had been drawn, the diffraction pattern was resolved into its amorphous and crystalline parts as shown in Fig. 3.1. Determination of the areas was performed using a graphics tablet in conjunction with a micro computer (Model II+, Apple).

3.2.3. Scanning electron microscopy

Scanning electron micrographs were obtained (Microscope Model 501B, Philips, Holland) of solid dispersions mounted on stumps with double sided

Fig. 3.1. Resolution of X-ray diffraction pattern into amorphous and crystalline parts

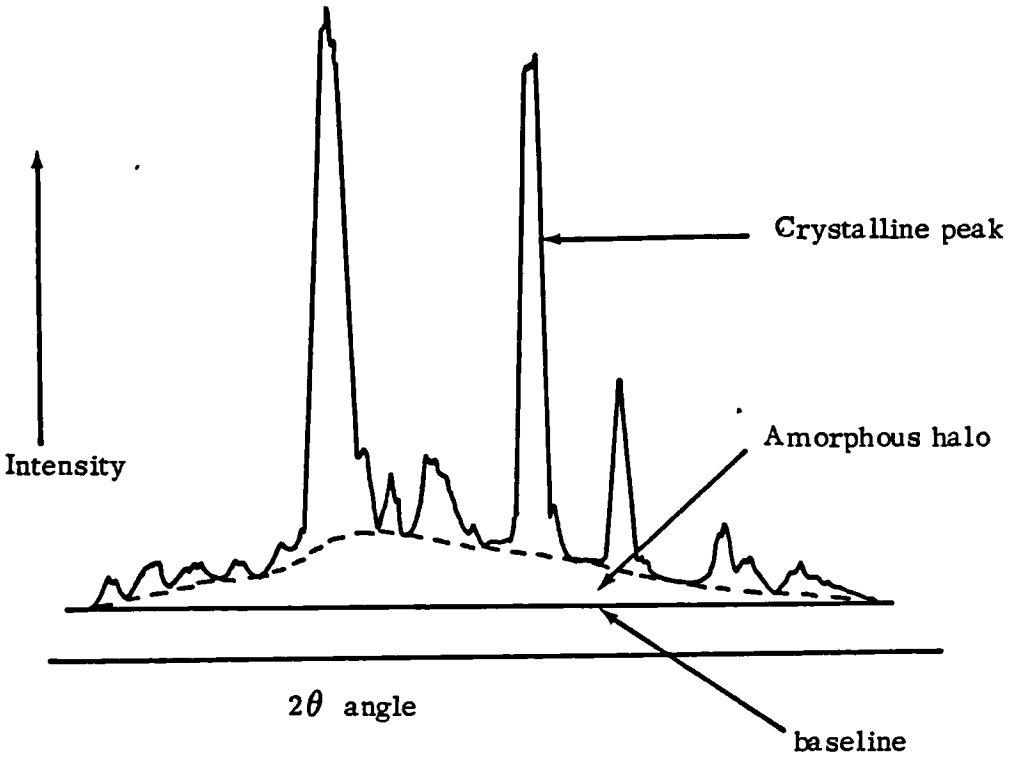

sellotape and sputter coated with gold to a depth of 10-15 nm using an E.M. sputter coating unit (Model E5100, Polaron, Watford).

3.3. Results and discussion

3.3.1. PEG 4000

3.3.1.1. Temperature of melting

Initial investigations of the melting behaviour of PEG 4000 as received by DSC revealed only one melting endotherm with a peak maximum temperature (Tp) of 57.0° C (Table 3.1.) which corresponded to the melting of the extended chain crystal form (Bailey and Koleske, 1976). The average value of the heat of fusion (ΔH_{fl}) was 179.20 $KJKg^{-1}$, equivalent to a crystallinity of 91%, which is in agreement with values from the literature which are quoted as between 167.5 and 193 $KJKg^{-1}$ depending on crystallinity (Hoechst, 1977). After samples had been melted at temperatures of between 60° C and 200°C for 10 minutes they were cooled to room temperature at 8°C min^{-1}. Crystallisation exotherms exhibited only one transition, except for the sample melted at 60°C, where a low temperature shoulder to the peak was observed. Furthermore, the peak crystallisation temperature for this sample of 26.5°C was higher than for any of the other samples which crystallised at ~22°C. The lowest melting temperature of 60°C is only just above the melting point of the polymer and it is expected that relatively large numbers of heterogeneous nuclei will persist in the melt, allowing crystallisation to begin at a higher temperature as the molten PEG 4000 is cooled. Destruction of these nuclei for crystallisation by raising the temperature of melting delays the subsequent recrystallisation as the melt is cooled. Thus samples melted at 80°C or above exhibited a peak crystallisation temperature which was

Table 3.1. Effect of melting temperature on PEG 4000, samples cooled at 8°C min^{-1}

	Temperature of melting (°C)	60	80	100	150	200
Initial melting	ΔH_{f1} ($KJKg^{-1}$)	181.71	177.10	179.61	180.03	177.94
	Peak melting temperature (°C)	57.0	57.0	57.2	57.0	57.1
Crystallisation	ΔH_c ($KJKg^{-1}$)	168.73	169.98	168.31	163.7	164.96
	Peak crystallisation temperature (°C)	26.5	21.8	22.0	22.5	21.0
2nd melting	ΔH_{f2} ($KJKg^{-1}$)	169.57	169.98	172.08	169.57	168.31
	Peak melting temperature (lower) °C	52.0	52.0	52.4	52.5	52.2
	Peak melting temperature (upper) °C	56.7	56.4	57.0	56.8	57.2
	% of lower peak area to total area	60	64	65	71	77
	% of lower peak height	51	52	54	56	59
	% crystallinity	86	86	87	86	86

some 4-5°C lower than samples crystallised from 60°C. Heats of crystallisation ($\Delta H_{c.}$) were always 5-10% less than the respective heats of fusion due to an increase in the amorphous fraction, which arises from the material which is rejected during this primary crystallisation process and crystallises only very slowly or not at all.

Subsequent remelting of the polymer invariably produced a melting endotherm with two distinct transitions, with peak melting temperatures of ~52°C and 57°C which can be assigned to the melting of once folded and extended chain crystals respectively (Buckley and Kovacs, 1976). Representative melting, crystallisation and remelting thermograms are shown in Fig. 3.2. The effect of cooling PEG 4000 at a slower rate was also investigated by preparing samples in the oven at a cooling rate of 0.33°C min^{-1} (20°C hr^{-1}). Subsequent examination of these samples by DSC revealed similar melting behaviour to that at a cooling rate of 8°C min^{-1} (Table 3.2.). Under both cooling conditions, the percentage of folded chain crystals formed, as measured by the ratio of the lower melting peak area to the total area, increased as the previous temperature of melting was raised (Figs. 3.3. and 3.4.). This increase was reflected also in the relative increase in the peak heights of the lower temperature transitions, which are shown on the same diagrams. However, a higher proportion of extended chain crystals was formed under all melting conditions with samples cooled at the slower rate of 20°C hr^{-1}. No significant difference in the position of the two melting peaks nor in the total heat of fusion on remelting was observed. It is known that the crystallisation temperature has a marked effect on the relative proportion of the two crystal types (Beech et al, 1972a). An increase in the crystallisation temperature will be paralleled by a rise

Fig. 3.2. Typical DSC thermograms for PEG 4000

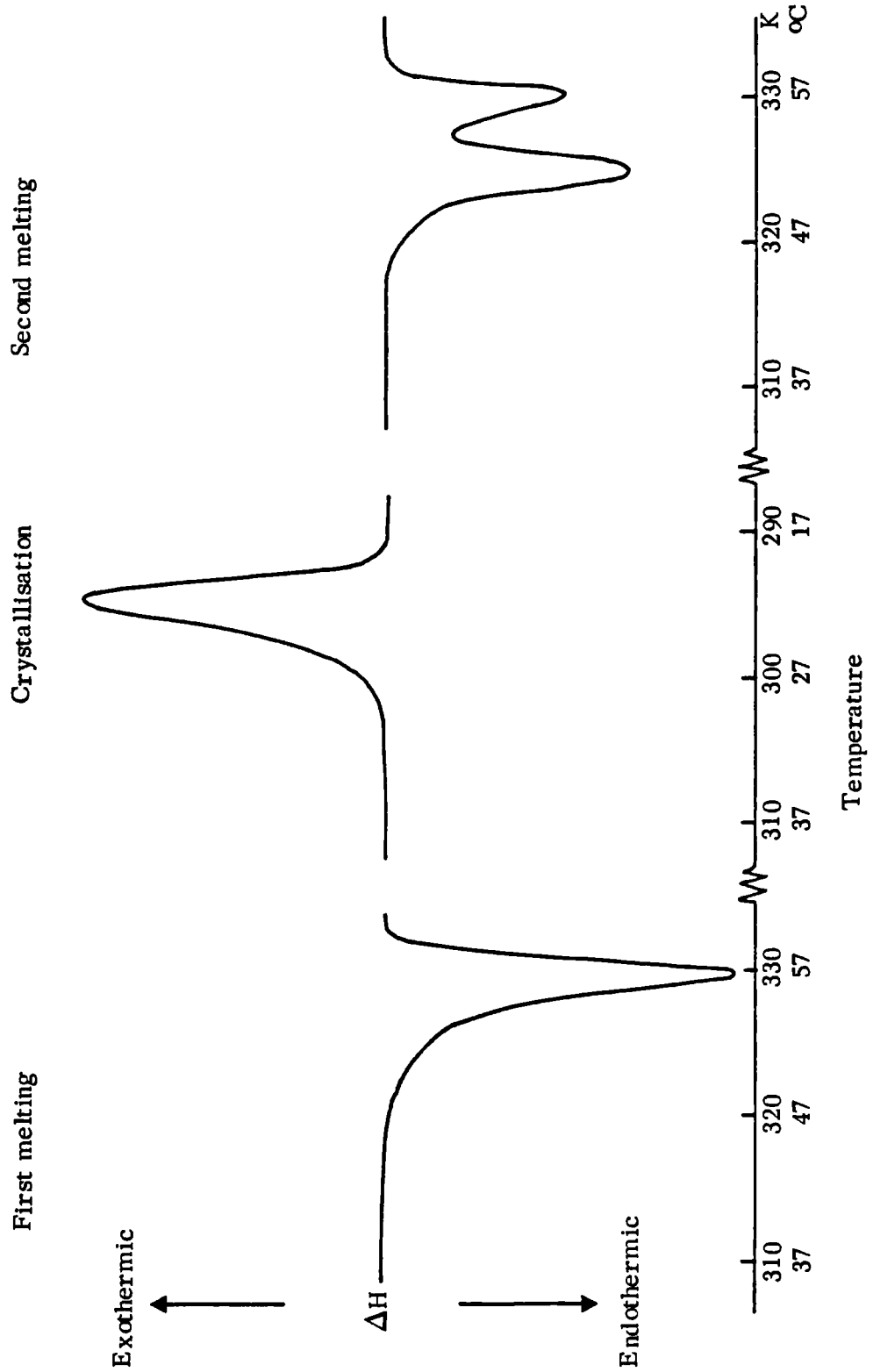

Table 3.2. Effect of melting temperature on PEG 4000, samples cooled at $20^{\circ}C\ hr^{-1}$

Temperature of melting ($^{\circ}C$)	60	80	100	150	200
ΔH_{f2} ($KJKg^{-1}$)	172.5	175.8	173.8	170.8	171.2
Peak melting temperature (lower) ($^{\circ}C$)	52.0	52.8	52.2	52.2	53.0
Peak melting temperature (upper) ($^{\circ}C$)	56.5	57.0	56.8	56.8	57.4
% of lower peak area to total area	35	39	39	43	45
% of lower peak height	26	27	28	29	31
% crystallinity	88	89	88	87	87

Fig. 3.3. Relative proportion of folded chain crystals formed as a function of the previous temperature of melting (samples cooled at 8°C min^{-1})

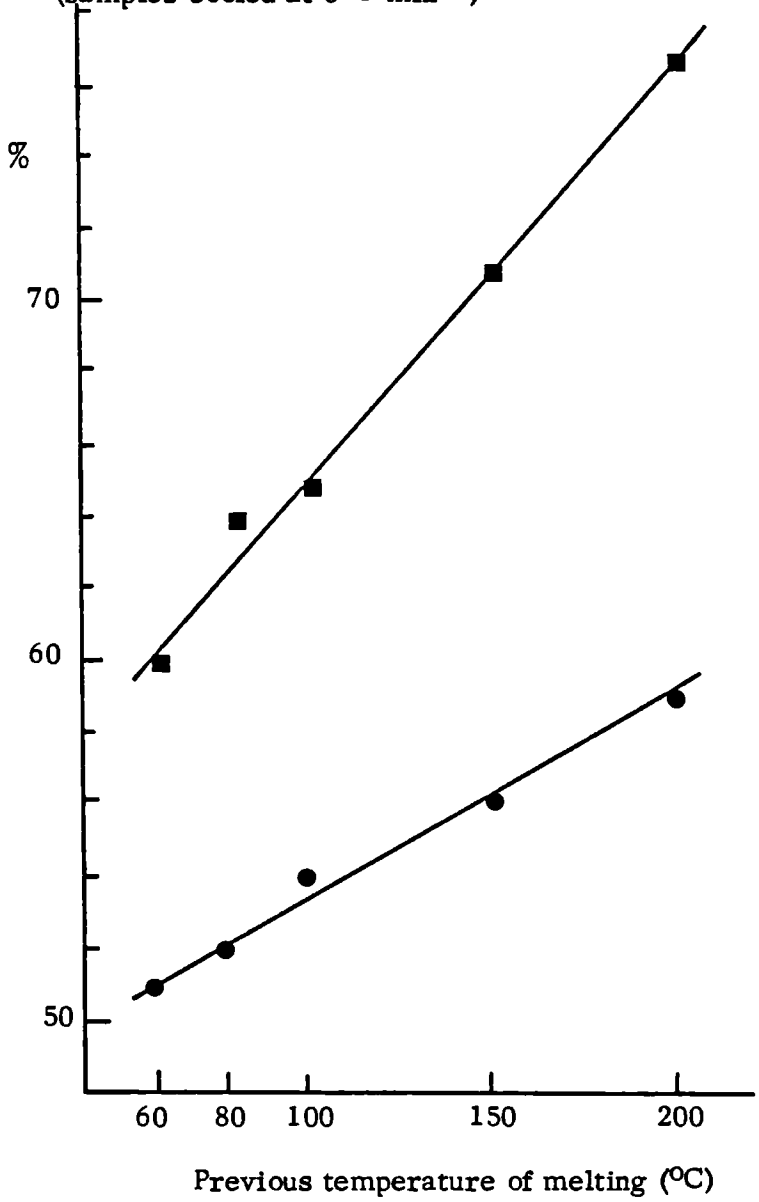

Key

● Peak heights
■ Peak areas

Fig. 3.4. Relative proportion of folded chain crystals formed as a function of previous temperature of melting (samples cooled at 20°C hr^{-1})

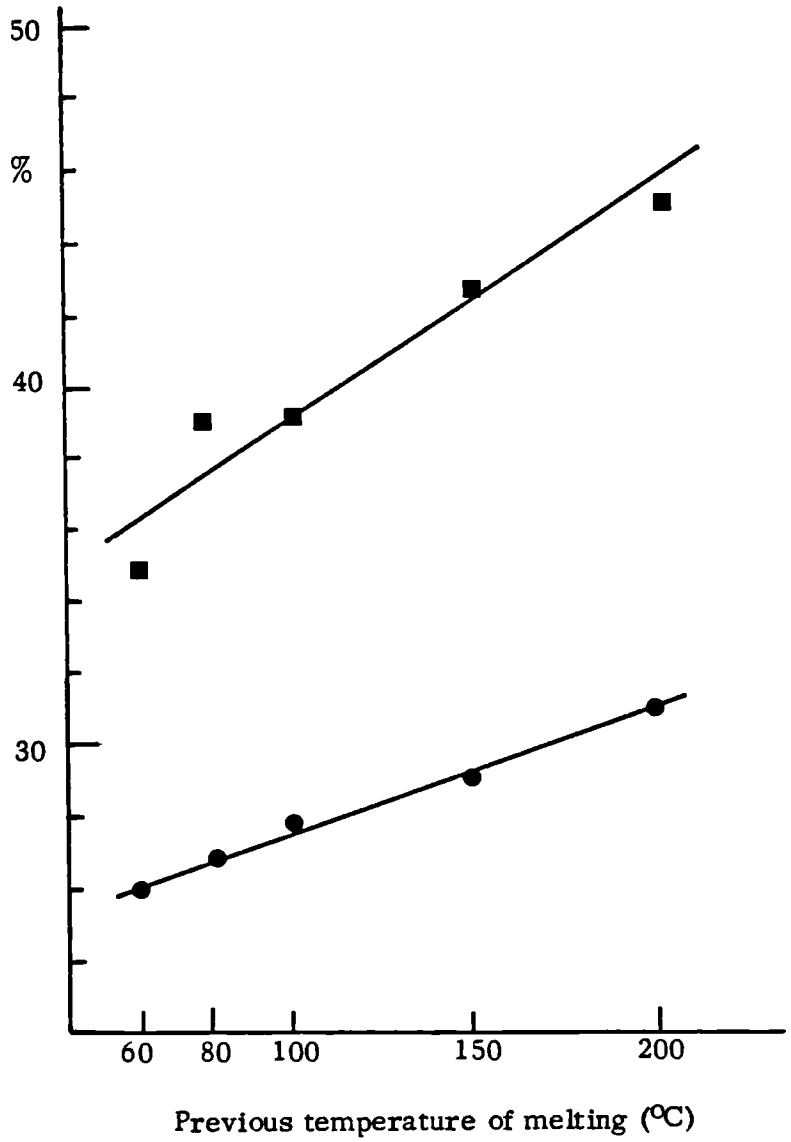

Key

● Peak heights

■ Peak areas

in the proportion of the higher melting point extended chain crystals and vice versa. Thus, as previously mentioned, increasing the melting temperature will destroy surviving nuclei in the melt, tending to decrease the temperature at which crystallisation commences predisposing the formation of folded chain crystals.

A typical X-ray diffraction spectrum of PEG 4000 as received together with the d-spacings and relative peak intensities are presented in Fig. 3.5. and Table 3.3. respectively. The degree of crystallinity was determined to be 94% which is in good agreement with that calculated from the calorimetric measurements. Variations in the melting temperature, under either cooling condition., did not alter the diffraction spectrum from that of the original material, although a small decrease in crystallinity to 90% occurred in both cases as was observed also from the DSC data.

3.3.1.2. Time in the molten state

Samples of PEG 4000, melted at temperatures from just above the melting point of the polymer up to 200°C, were maintained in the molten state for periods of time ranging from 10 minutes to 10 hours before being cooled at 20°C hr^{-1} to room temperature and subjected to DSC and X-ray diffraction studies.

The melting endotherms of some samples did not show two distinct peaks, but rather a low temperature shoulder to the main higher temperature melting peak, or in the case of samples kept at 200°C for 10 hours, two very broad overlapping peaks. The proportion of folded chain to extended chain crystals could not be calculated where this occurred (Table 3.4.).

At 60°C, the time in the molten state does not seem to influence particularly the subsequent structure of the polymer. Neither the degree of crystallinity

Fig. 3.5. X-ray diffraction spectrum of PEG 4000

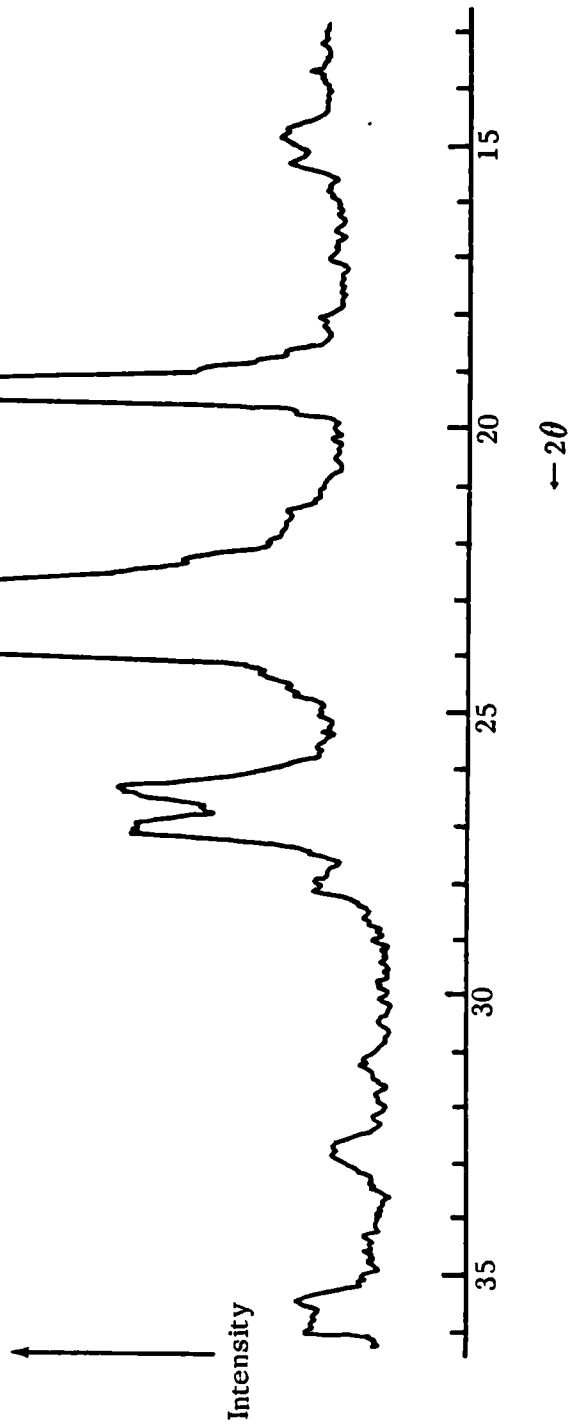

Table 3.3. d-spacings and relative intensities of X-ray diffraction peaks for PEG 4000

2θ	d-spacing (nm)	Relative intensity (I/I_0)
13.61	0.6505	2
14.65	0.6047	4
15.10	0.5867	4
19.2	0.4630	75
21.57	0.4121	7
22.10	0.4022	11
23.30	0.3818	100
26.20	0.3401	16
26.92	0.3314	16
27.90	0.3199	4
31.00	0.2885	2
32.93	0.2720	4
35.42	0.2534	6
36.30	0.2475	5

nor the peak melting temperatures (Table 3.4.(a)) changed significantly, indicating that no degradation of polymer chains had occurred. Furthermore, the proportion of folded chain to extended chain crystals obtained on crystallisation from the melt remained virtually unchanged even after 10 hours, with a predominance of the extended chain type.

Although little difference was seen at 100°C for samples melted for up to 1 hour, there was a slight decrease in the heat of fusion for samples of PEG 4000 maintained at this temperature for 10 hours (Table 3.4.(b)). A more marked decrease in the heat of fusion from 171.2 to 153.7 $KJKg^{-1}$ resulted after melting the polymer for 10 hours at 200°C (Table 3.4.(c) and Fig. 3.6.), with a consequent decrease of approximately 3°C in the peak melting temperatures. Furthermore, the melting endotherms obtained for these samples were very broad and commenced some 5°C lower than those for other samples. After 10 hours at either 100°C or 200°C, polymer melts turned yellow, as is often observed when PEGS are kept at high temperatures for long periods (Hoechst, 1977). An increase in the amorphous halo of the X-ray diffraction spectrum was apparent after melting at 200°C for 10 hours, but no other changes were observed. This instability of PEG 4000 to prolonged heating results from the break up of the polymer chains into lower molecular weight fragments. These cannot pack effectively into the crystals and tend to be rejected during the crystallisation process, resulting in a larger fraction of amorphous material, which is reflected in the decreased heats of fusion measured. However, long melting periods at high temperatures seem to be required before appreciable break up occurs and below 100°C, degradation of polymer chains is minimal.

Table 3.4. Effect of time in molten state on PEG 4000

(a) Temperature of melting = 60°C

	Time in molten state		
	10 mins	1 hour	10 hours
ΔH_{f2} ($KJKg^{-1}$)	172.5	171.2	171.7
Peak melting temperature (lower) °C	52.0	53.0	52.9
Peak melting temperature (upper) °C	56.5	57.0	58.0
% lower peak area to total area	35	-	-
% lower peak height	20	26	24
% crystallinity	88	87	87

(b) Temperature of melting = 100°C

	Time in molten state		
	10 mins	1 hour	10 hours
ΔH_{f2} ($KJKg^{-1}$)	173.8	168.3	163.3
Peak melting temperature (lower) °C	52.2	52.4	53.0
Peak melting temperature (upper) °C	56.8	57.2	57.5
% lower peak area to total area	39	-	-
% lower peak height	28	26	18
% crystallinity	88	86	83

Table 3.4. cont.

(c) Temperature of melting = 200°C

	Time in molten state		
	10 mins	1 hour	10 hours
ΔH_{f2} ($KJKg^{-1}$)	171.2	167.5	153.7
Peak melting temperature (lower) °C	53.0	52.0	50.0
Peak melting temperature (upper) °C	57.4	56.0	54.0
% lower peak area to total area	45	-	-
% lower peak height	35	40	38
% crystallinity	87	85	78

Fig. 3.6. Effect of time in the molten state on the enthalpy of fusion of PEG 4000

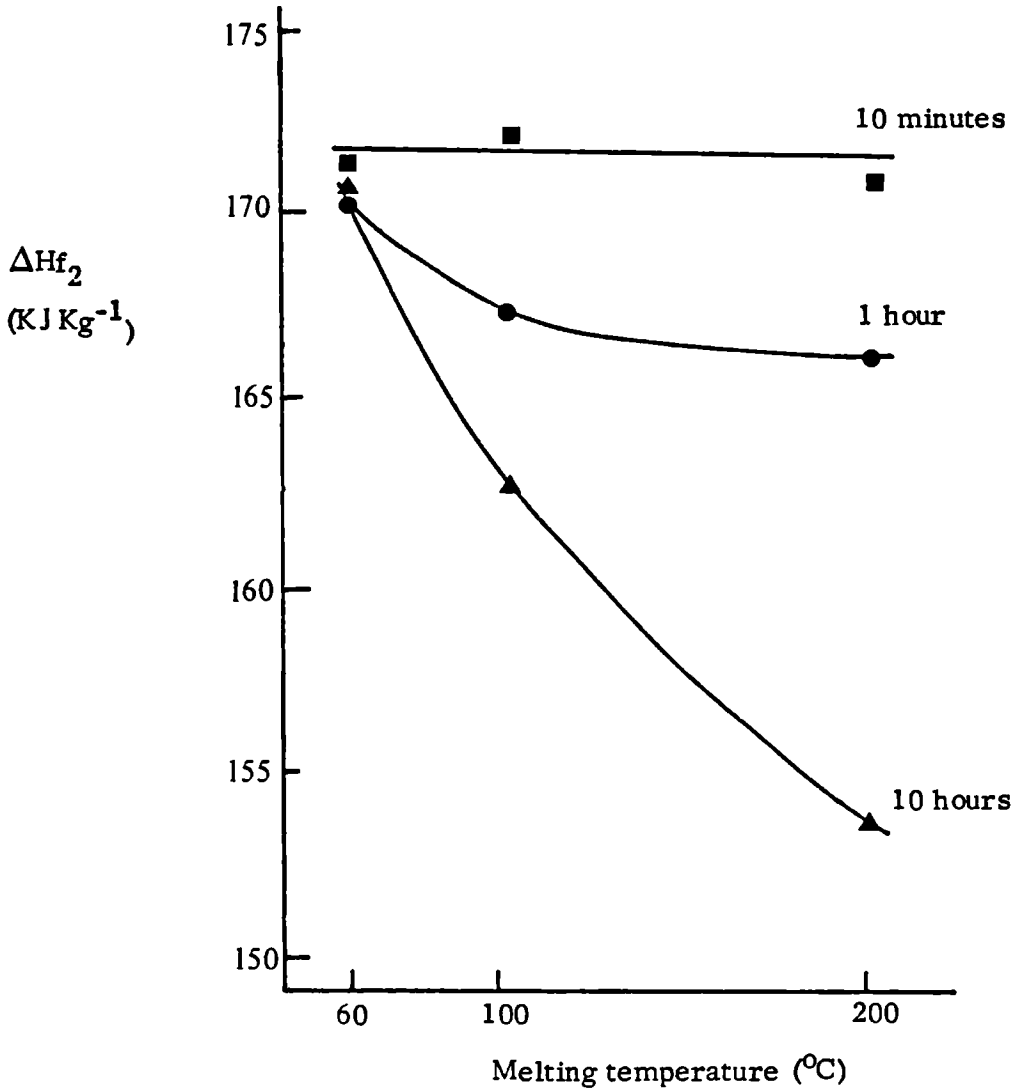

3.3.1.3. Cooling rate

Following melting at 100°C, samples of PEG 4000 were cooled at rates ranging from rapid quenching in liquid nitrogen to cooling at 5°C hr^{-1}. After cooling at the slowest rate, 5°C hr^{-1}, PEG 4000 displayed only one endothermic transition at 57°C arising from the melting of extended chain crystals and a relatively high degree of crystallinity~91%, when investigated by DSC (Table 3.5.). This high degree of crystallinity was confirmed by the X-ray diffraction pattern, which was unchanged from that of the original polymer. Presumably the slow cooling rate favours the formation of extended chain crystals, since crystallisation at higher temperatures may take place, although isothermal crystallisation studies suggest that the limiting temperature above which only this type of crystal is formed is around 55°C (Beech et al, 1972a). Alternatively, annealing of folded chain crystals which may be formed initially could occur during the slow cooling process, resulting in chain extension.

DSC thermograms of polymer samples cooled at faster rates of between 0.33°C min^{-1} and 32°C min^{-1} revealed that two melting peaks reappeared indicating the presence of both folded and extended chain crystals. A gradual increase was noted in the proportion of folded chain crystals formed up to ~72% at a cooling rate of 32°C min^{-1}, indicating a preference for this crystal type in a rate-controlled process as reported by Beech et al (1972a). From their isothermal studies, the proportion of folded chain crystals was found to increase as the crystallisation temperature was lowered with a consequent increase in the crystallisation rate. No changes in the melting temperatures of either folded or extended chain crystals were observed. The slight decrease in the heat of fusion for these samples, especially those cooled at 32°C min^{-1},

Table 3.5. Effect of cooling rate on PEG 4000

Cooling rate °C/min	ΔH_{f2} (KJKg^{-1})	% Crystallinity	Lower peak Melting temp. °C	Upper peak Melting temp. °C	% lower peak to total peak area	% lower peak height
0.083 (5°Chr^{-1})	180.0	91	-	57.0	-	-
0.33 (20°Chr^{-1})	173.8	88	52.2	56.8	39	28
0.5	173.3	88	52.0	56.7	49	38
1.0	172.5	88	52.0	56.3	54	44
2.0	171.7	87	52.3	56.8	58	49
4.0	172.1	87	52.0	56.2	60	51
8.0	172.1	87	52.4	57.0	65	54
32.0	167.9	85	52.8	56.5	72	59
Quenched in cardice	156.2	79	-	55.1	-	-
Quenched in liquid nitrogen	89.6	46	-	54.8	-	-

in comparison to PEG 4000 cooled at the slowest rate of $5^{o}C\ hr^{-1}$ reflected both the higher proportion of folded chain crystals and a decrease in their crystalline perfection.

PEG 4000 was found to be extremely difficult to quench and a completely amorphous form could not be produced by immersing samples in either cardice or liquid nitrogen. Quenching in cardice or liquid nitrogen did nevertheless reduce the crystallinity to 79% and 46% respectively. DSC thermograms of these samples showed somewhat surprisingly that the lower melting peak disappeared rather than the higher temperature transition, indicating that crystallisation which occurred took place in the extended chain form. Similar findings were reported by Guven and Sengar (1978) from their investigations of the melting behaviour of irradiated and quenched PEG 4000. However, the peak transition temperatures of these samples were some $2^{o}C$ lower than those recorded for the melting of extended chain crystals produced from more slowly cooled material, suggesting that the crystals formed were extremely small and contained many defects. Visual examination tended to confirm this since no spherulites were seen and much of the material was glassy and transparent in appearance. X-ray diffraction spectra of PEG 4000 quenched in liquid nitrogen (Fig. 3.7.) showed that peak heights were markedly reduced with a corresponding increase in the amorphous halo.

3.3.1.4. Effect of ageing

The effect of ageing on PEG 4000 was investigated by following changes in the structure of samples cooled at different rates after storage at 25, 37 or $45^{o}C$ for periods of up to six months. Under all storage conditions studied, irrespective of their previous thermal history, an increase in the heat of fusion of the samples was observed (Fig. 3.8.). This was noticeable after

Fig. 3.7. Effect of quenching on X-ray diffraction spectrum of PEG 4000

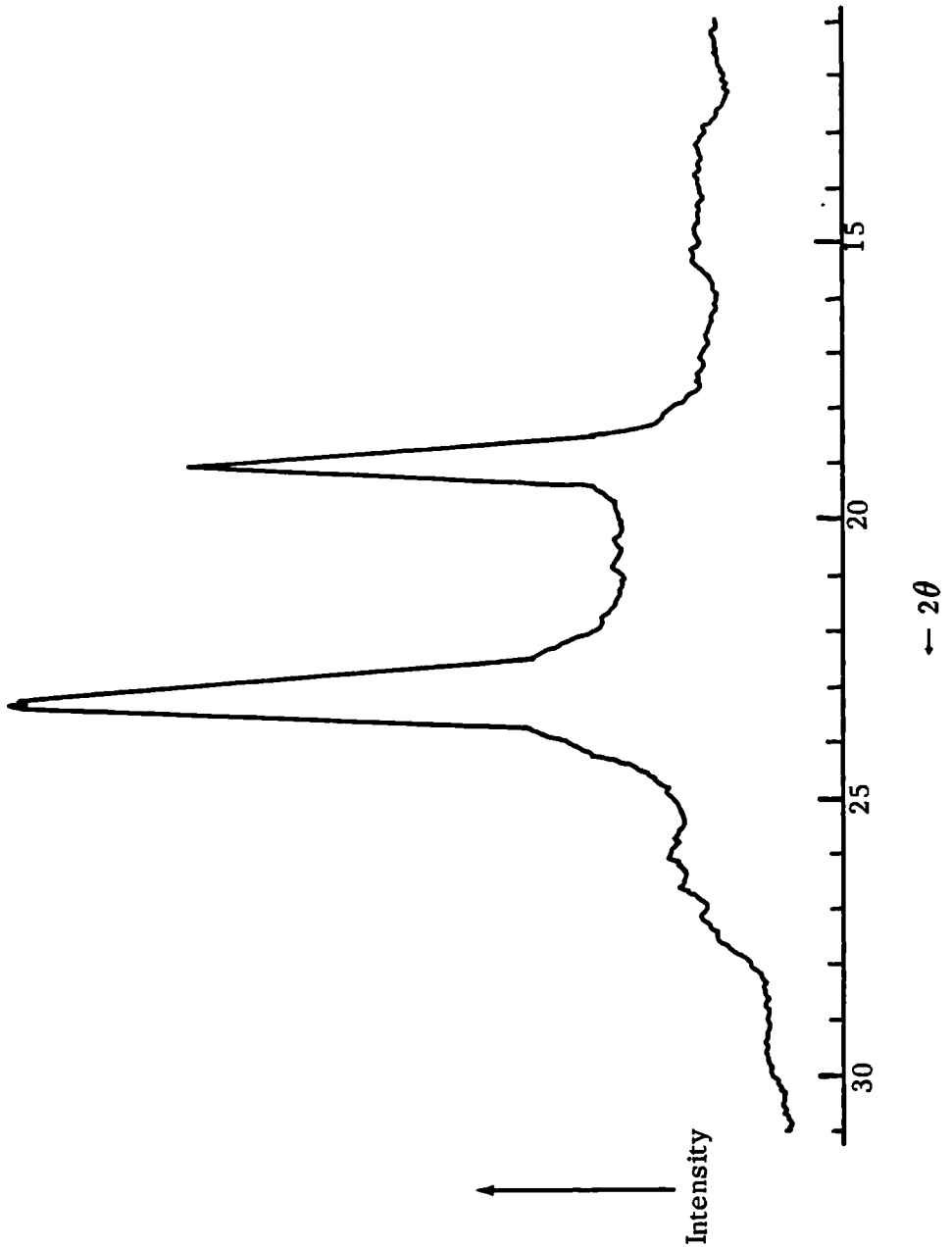

Fig. 3.8. Effect of ageing on various samples of PEG 4000

(a) Stored at 25°C

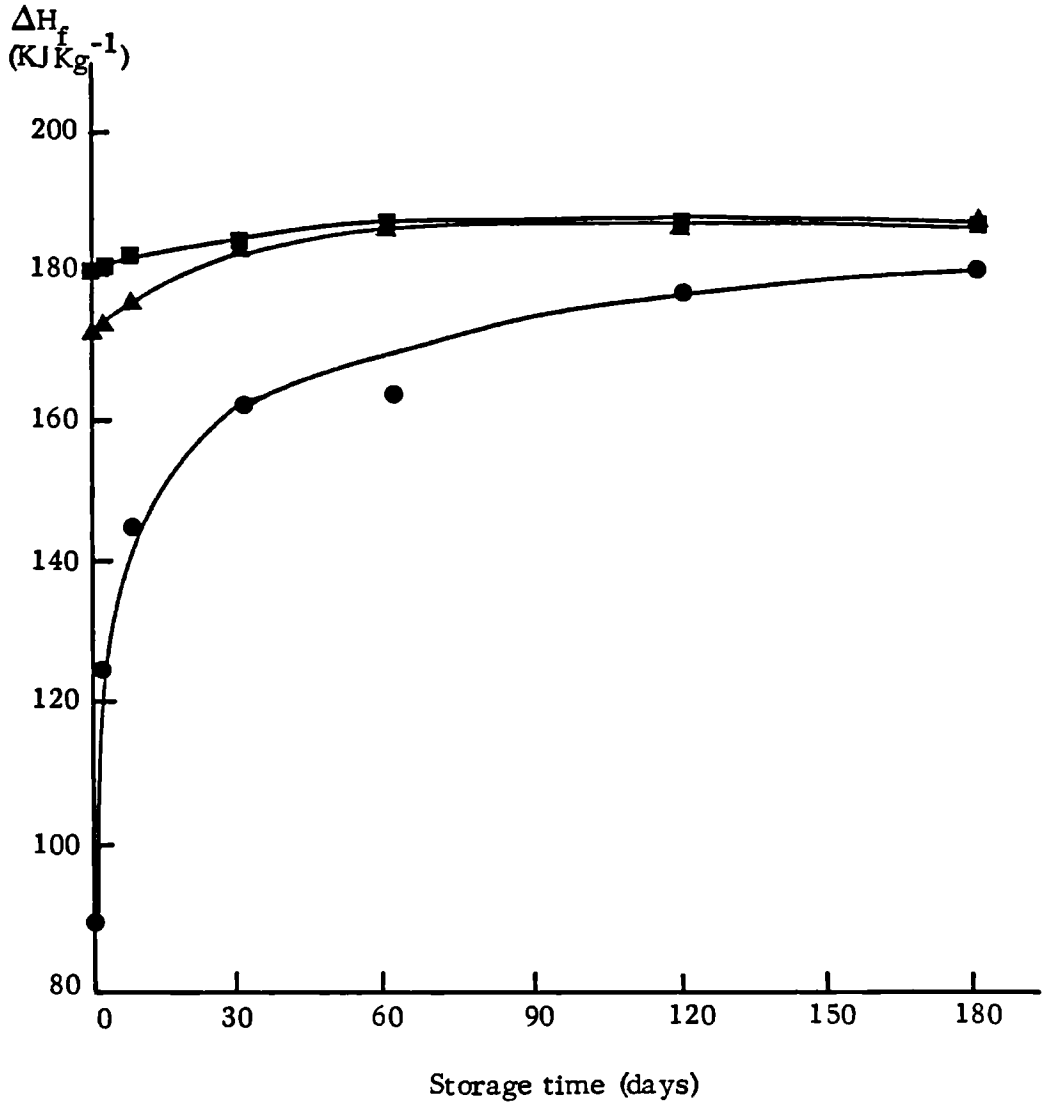

Fig. 3.8. (b) Stored at 37°C

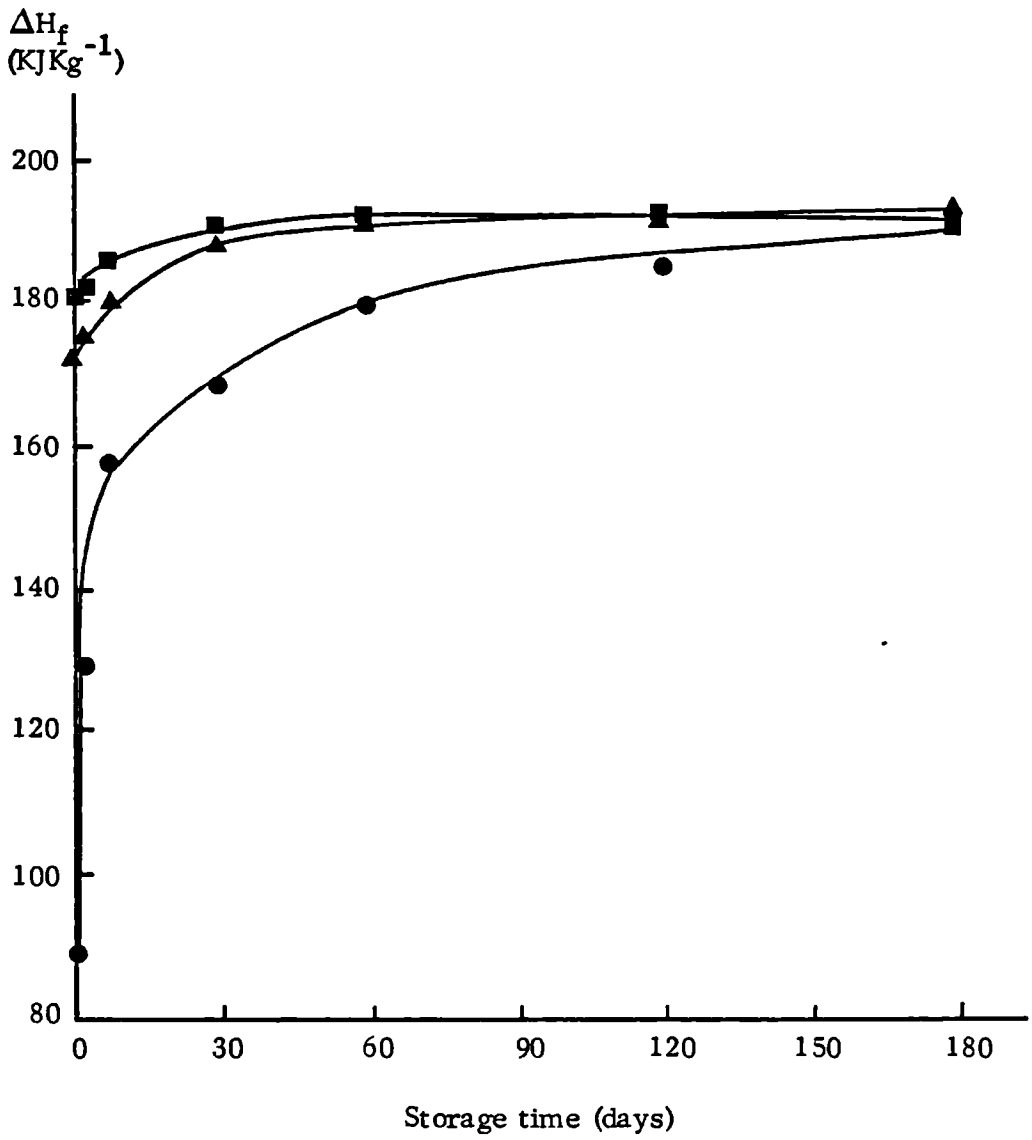

Fig. 3.8. (c) Stored at 45°C

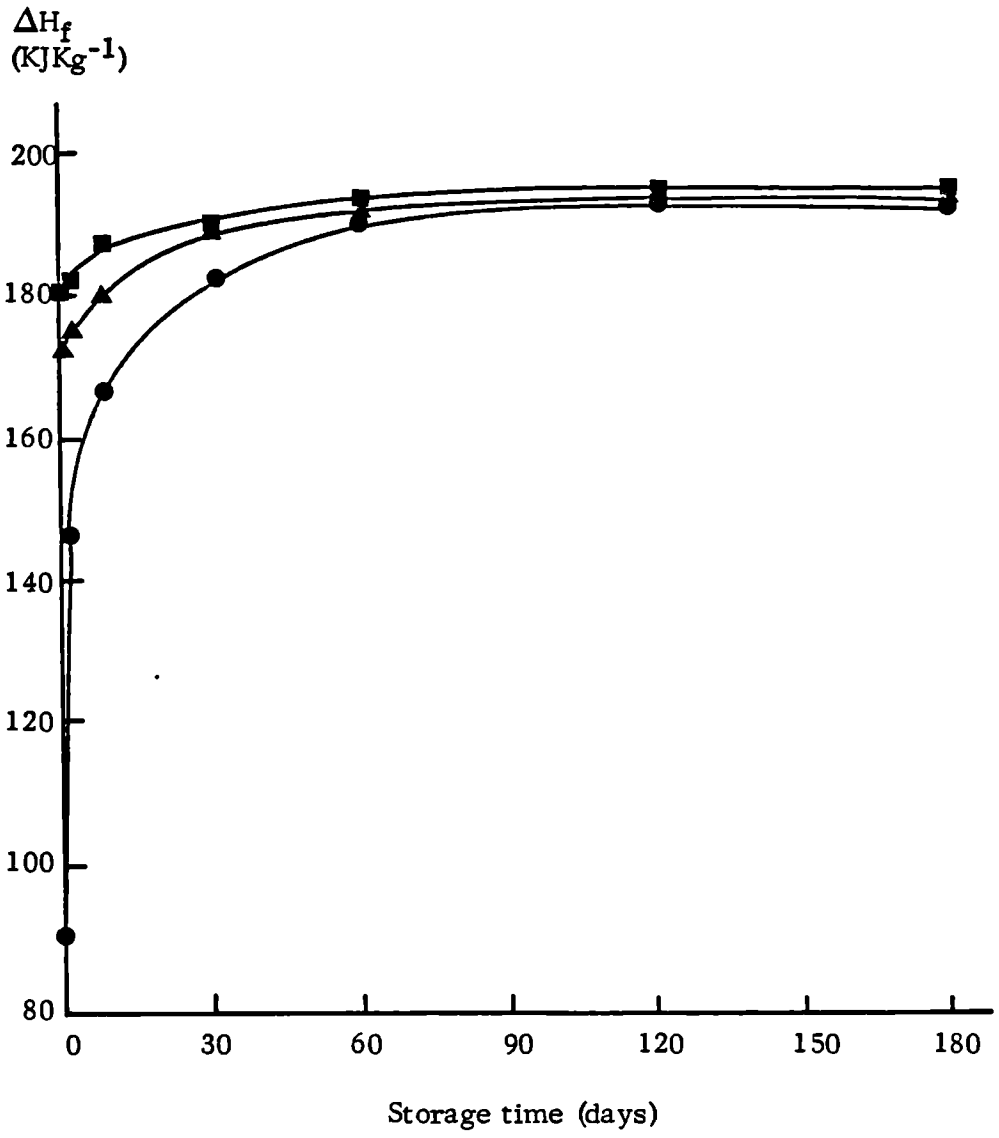

Key

● samples quenched in liquid nitrogen

▲ samples cooled at 20°C hr^{-1}

■ samples cooled at 5°C hr^{-1}

only 24 hours especially where the polymer had been quenched in liquid nitrogen previously. The increase in crystallinity was most rapid for polymer stored at the highest temperature of 45°C, but even at 25°C, changes in structure occurred relatively quickly. Most of the observed increase in the heat of fusion took place in the first two months of storage at all temperatures. After six months, all samples exhibited approximately similar heats of fusion indicating an equivalent degree of crystallinity. X-ray diffraction data substantiated these results and confirmed the degree of crystallinity present. No new diffraction peaks appeared and although some minor changes in the relative intensities of the peaks occurred, these were simply due to changes in the preferred orientation in particular samples.

The DSC thermograms of PEG 4000 cooled at 20°C hr^{-1} showed that a gradual conversion from folded to extended chain crystals occurred, resulting in the disappearance of the lower temperature melting peak (Fig. 3.9.). This conversion was most rapid at a storage temperature of 45°C, since chain unfolding can take place more easily as the melting point of the polymer is approached. The polymer samples cooled at 5°C hr^{-1} contained the largest initial percentage of stable extended chain crystals and the highest degree of crystallinity. Thus the changes observed on ageing at any of the storage temperatures were small in comparison to the other two batches, since only a limited amount of annealing could take place in these samples. Nevertheless, the small fraction of folded chain crystals present were converted to the extended chain form and the degree of crystallinity did increase slightly.

The most dramatic increase in crystallinity on ageing was observed in PEG 4000 which had been quenched to a semi-amorphous state. Possibly,

Fig. 3.9. DSC thermograms of PEG 4000 after ageing for different periods of time at 25°C (sample previously cooled at 20°C hr^{-1})

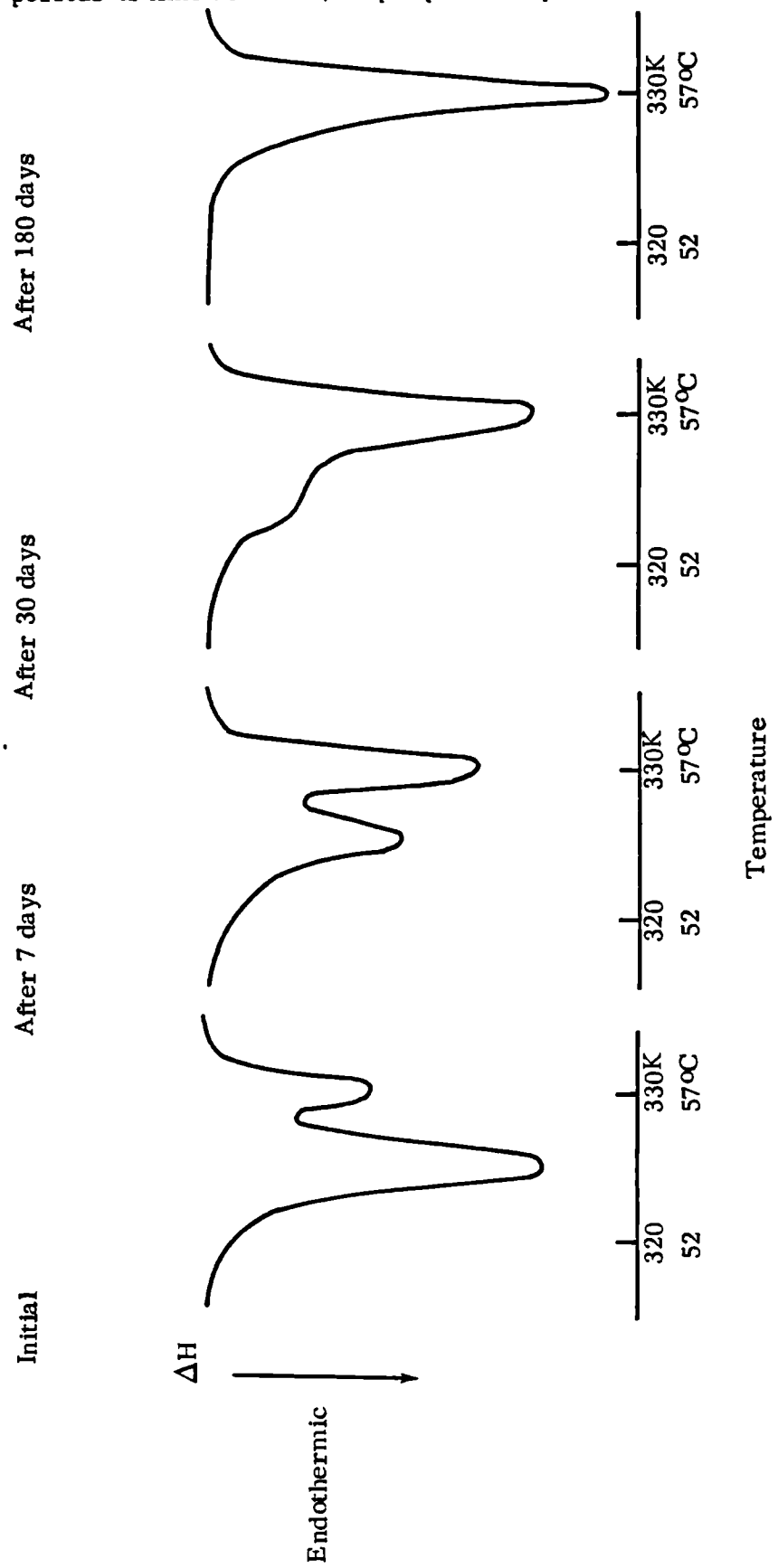

the residual crystalline regions present acted as nuclei for recrystallisation of the amorphous fraction. The melting point of the initial samples before ageing was approximately 55°C and corresponded to the melting of extended chain crystals. As already stated, this was some 2°C lower than that measured for this crystal form in other samples of PEG 4000 but was probably due to the small size of crystals which were formed and their high degree of imperfection. During ageing, the rise in the degree of crystallinity was mirrored by a concurrent increase in the melting point of the crystals to the expected value for extended chain crystals of 57°C. However, the melting points measured for this crystal type of PEG 4000 cooled at either 20°C hr^{-1} or 5°C hr^{-1} initially did not change by more than 0.5°C during the period of storage. This would be expected, since the melting point is influenced by the thickness of the lamella, which cannot increase once the extended chain form is present.

These ageing studies seem to indicate that reversion to the most stable crystal form of the polymer - extended chain crystals for this molecular weight - will eventually occur regardless of the initial structure or the temperature of storage, providing sufficient time is allowed. Even slowly cooled samples of PEG 4000 do not exist in a totally stable state and will change slowly with time. The changes in structure which occur are accelerated by higher storage temperatures, since lamella thickening and recrystallisation will be facilitated, but the final level of crystallinity is almost equivalent at all storage temperatures after 6 months.

3.3.2. PEG 4000 and trimethoprim

3.3.2.1. Phase diagrams

Phase diagrams have been used successfully on numerous occasions to elucidate the structure of binary systems. However, problems in interpretation can exist where one of the components is a polymer, in that the co-ordinates of the apparent eutectic point may vary according to the thermal conditions of the experiment. Gryte et al (1979) reported that, for the polyethylene oxide - glutaric acid system changing the crystallisation temperature from 24°C to 50°C altered the position of the eutectic point from a polyethylene oxide mole fraction of 0.85 and temperature of 45.5°C to a mole fraction of 0.82 at 52°C. These authors concluded that the eutectic point, and hence the shape of the phase diagram, will depend on the nature of the polymer crystal species involved. Furthermore, a thermodynamically stable situation is not realisable where folded chain crystals of PEG are present, as exists with all molecular weights over ~4000. Thus care must be exercised in interpreting such phase diagrams and in the conclusions drawn from them.

In spite of these reservations, phase diagrams were constructed for solid dispersions of PEG 4000 and trimethoprim from the peak melting point data obtained by DSC as described by Hager and Macrury (1980). Dispersions were prepared under a variety of heating and cooling profiles to allow a wide range of morphologies to develop.

With dispersions maintained at 100°C for 10 mins prior to cooling at $20^{\circ}C\,hr^{-1}$, dissolution of the drug in the polymer melt was incomplete at concentrations greater than 1%w/w trimethoprim. Electron micrographs of the cooled dispersions revealed that the drug particles appeared to be

homogeneously dispersed in the PEG matrix, with no large agglomerates or aggregates visible. The morphology of the polymer in the presence of the drug was found to be similar to that of the polymer alone. Spherulites were visible, both to the naked eye and under the electron microscope (Plate 3.1.). The step-like structure of the lamellae could be seen very clearly in fractured surfaces (Plate 3.2.). In many cases, the distorted and twisting appearance of the lamellae suggested that the polymer had crystallised around the drug particles (Plates 3.3. and 3.4.).

Subsequent DSC thermograms of these samples showed that for concentrations of up to 10%w/w trimethoprim, two transitions were observed. These were a low temperature shoulder at ~52°C and a main peak at ~57°C which can be attributed as before (Chapter 3.3.1.1.) to the melting of folded and extended chain crystals of PEG 4000 respectively. Above this concentration, a third, rather broad endothermic transition appeared which corresponded to the melting of trimethoprim. The pure drug displayed a sharp melting endotherm at 202°C.

The partial phase diagram for this system (Fig. 3.10.) resembles that of a monotectic, i.e. a eutectic where one 'arm' of the diagram is missing and the lower melting component, PEG 4000, replaces the eutectic composition. The upper rising curve corresponds to the solubility curve of the drug in the molten excipient. This type of system for PEG dispersions has been reported previously by only two authors. Firstly, Kaur et al (1980a), who found this response for griseofulvin and tolbutamide solid dispersions with PEG 2000 irrespective of their method of preparation, whether solvent, fusion or simply a physical dispersion. Hargreaves (1982) also reported a monotectic system for physical mixtures of betamethasone

VOLUME CONTAINS CLEAR OVERLAYS

OVERLAYS SCANNED SEPERATELY AND OVER THE RELEVANT PAGE.

Plate 3.1. Electron micrograph of PEG 4000 spherulites 5%^{w}/w trimethoprim dispersion

Plate 3.2. Electron micrograph showing lamellar structure of PEG 4000 in 7%^{w}/w trimethoprim dispersion

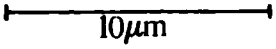

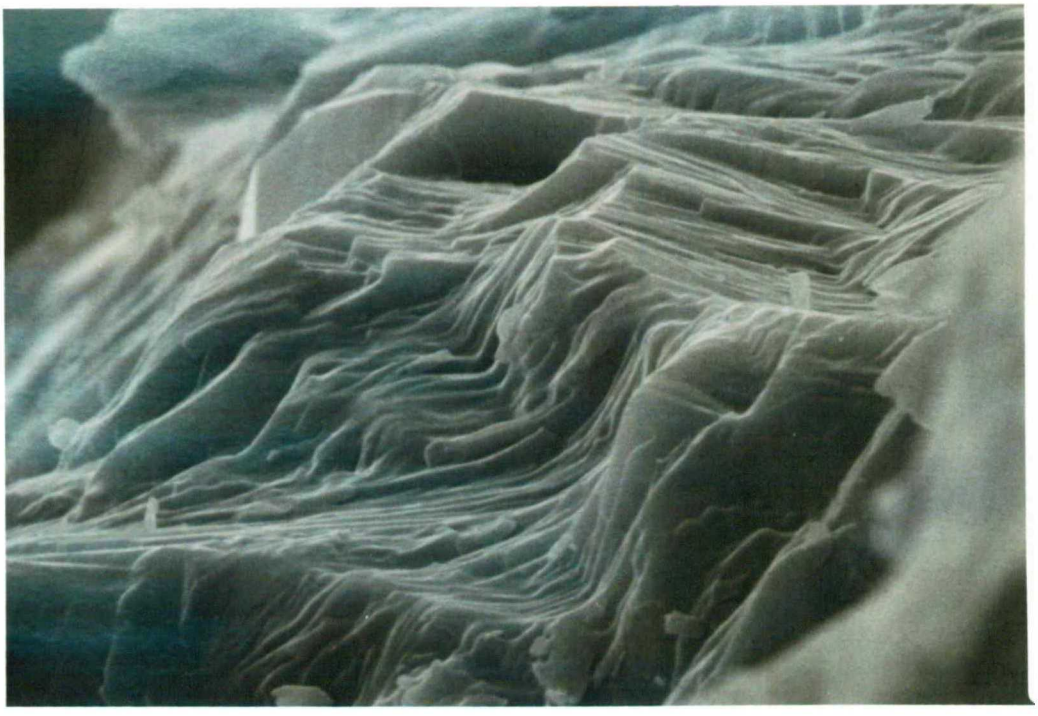

Plate 3.1. Electron micrograph of PEG 4000 spherulites 5%^{w}/w trimethoprim dispersion

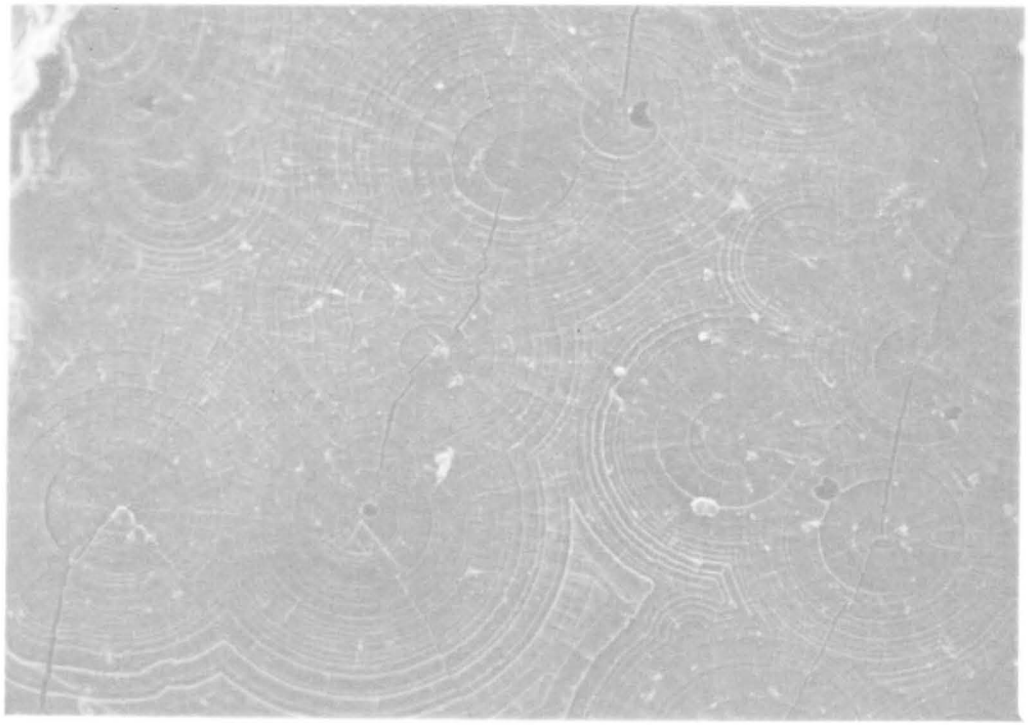

100μm

Plate 3.2. Electron micrograph showing lamellar structure of PEG 4000 in 7%^{w}/w trimethoprim dispersion

10μm

Plate 3.3. Electron micrograph of 10%^{w}/w trimethoprim-PEG 4000 dispersion

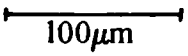

Plate 3.4. Electron micrograph of 20%^{w}/w trimethoprim-PEG 4000 dispersion

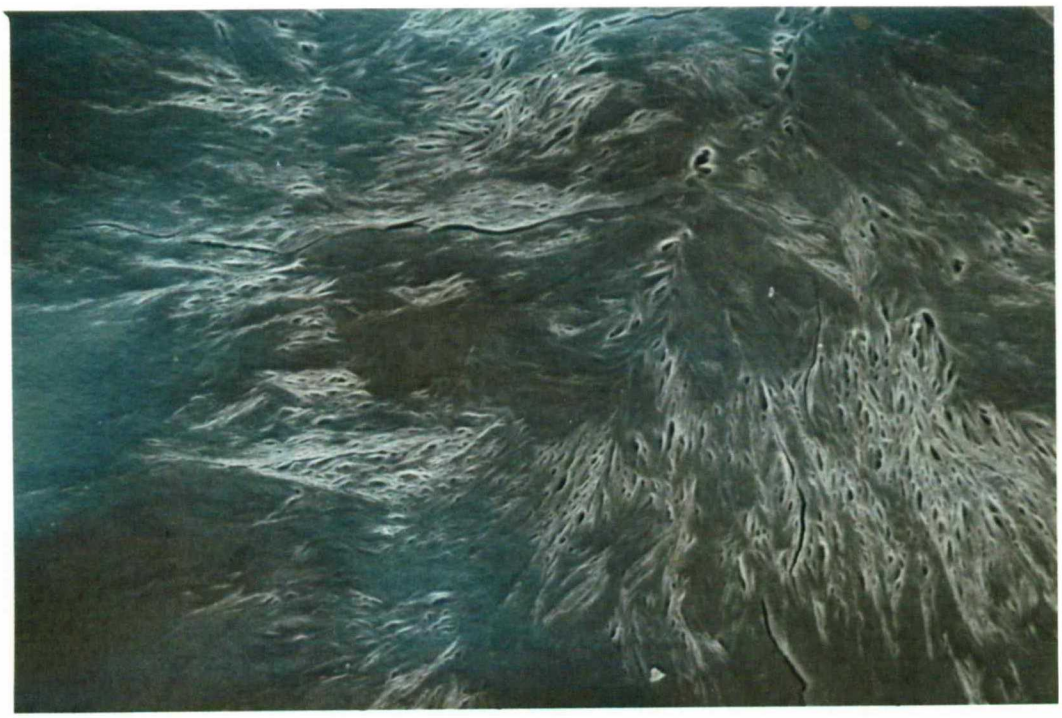

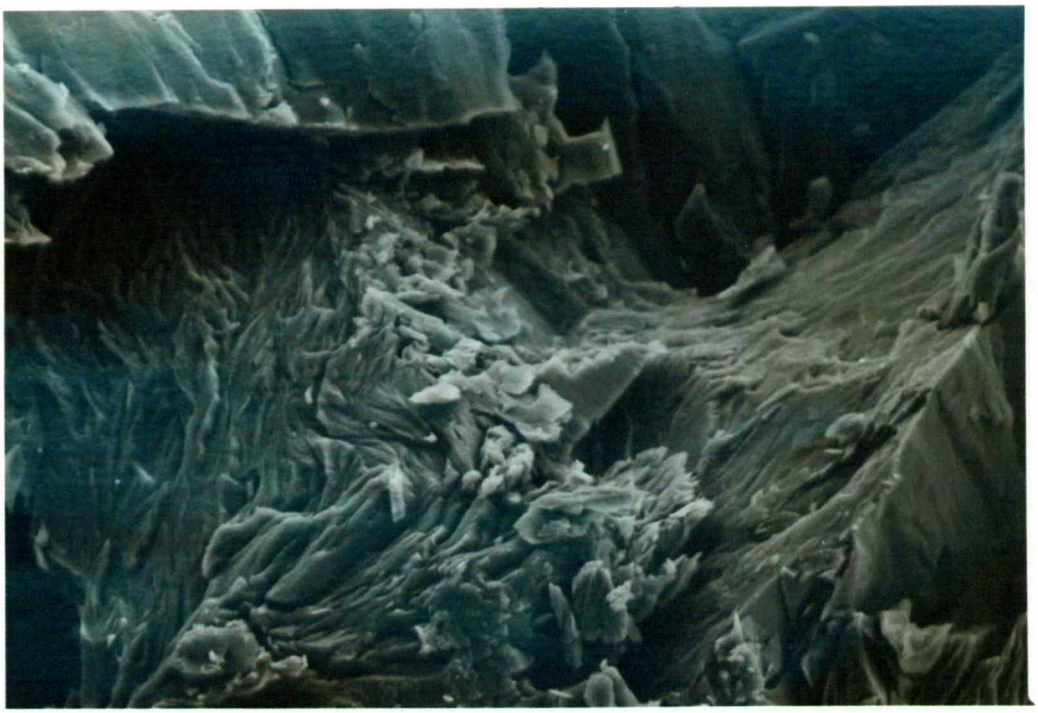

Plate 3.3. Electron micrograph of 10%^{w}/w trimethoprim-PEG 4000 dispersion

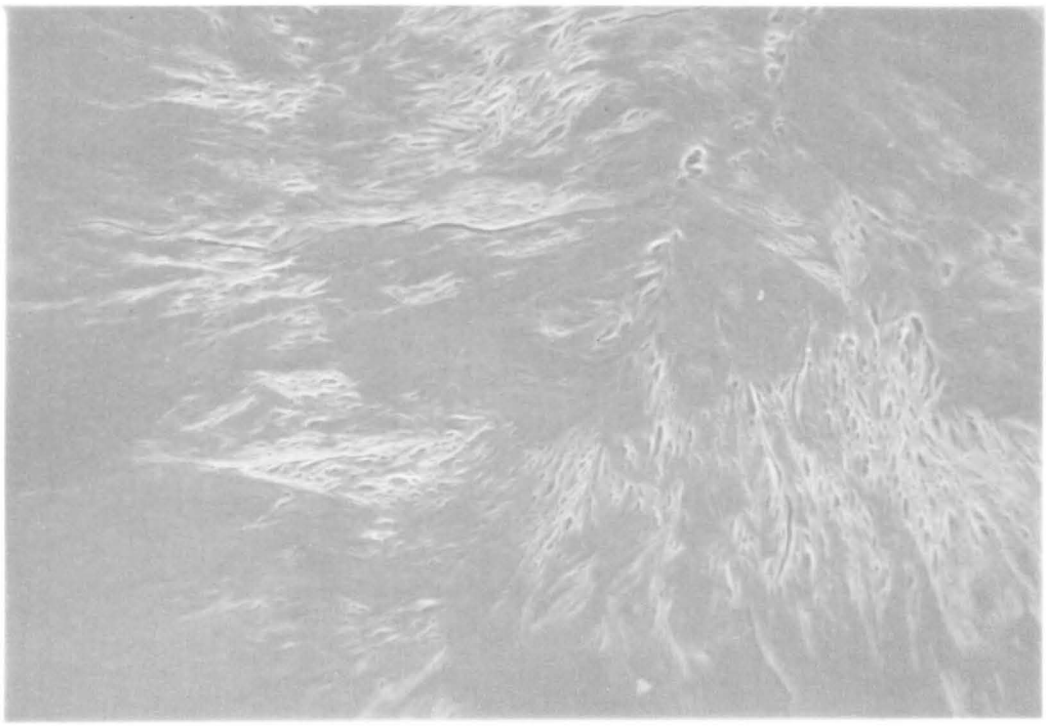

100μm

Plate 3.4. Electron micrograph of 20%^{w}/w trimethoprim-PEG 4000 dispersion

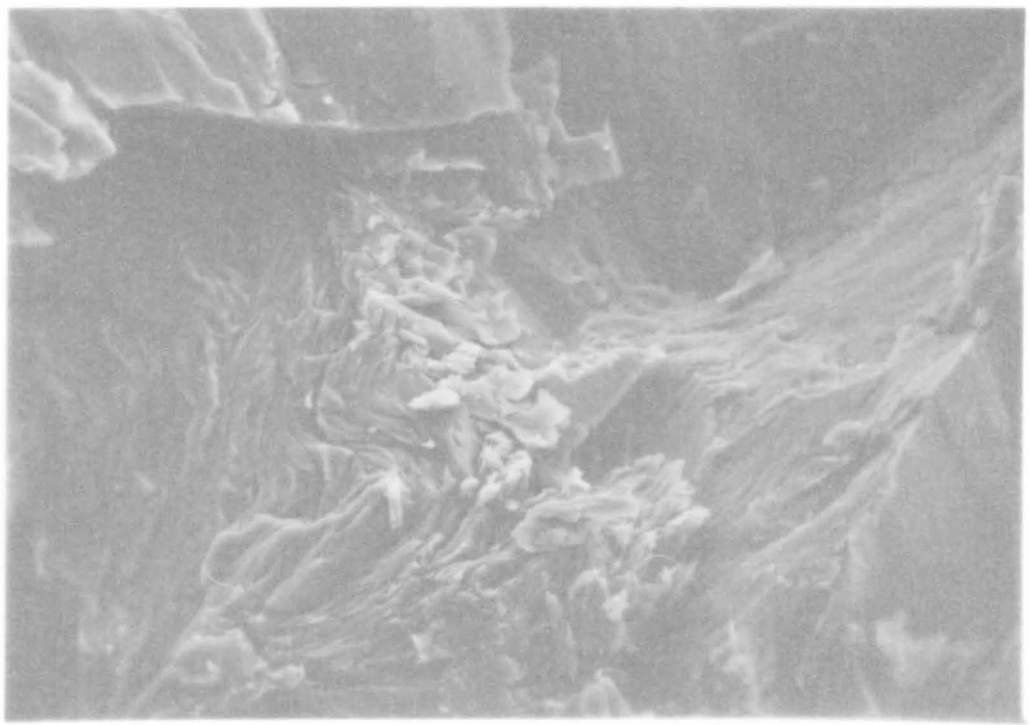

10μm

Fig. 3.10. Partial phase diagram for PEG 4000 -trimethoprim system, previously melted at 100°C for 10 mins and cooled at 20°C hr^{-1}, constructed from DSC melting transition data

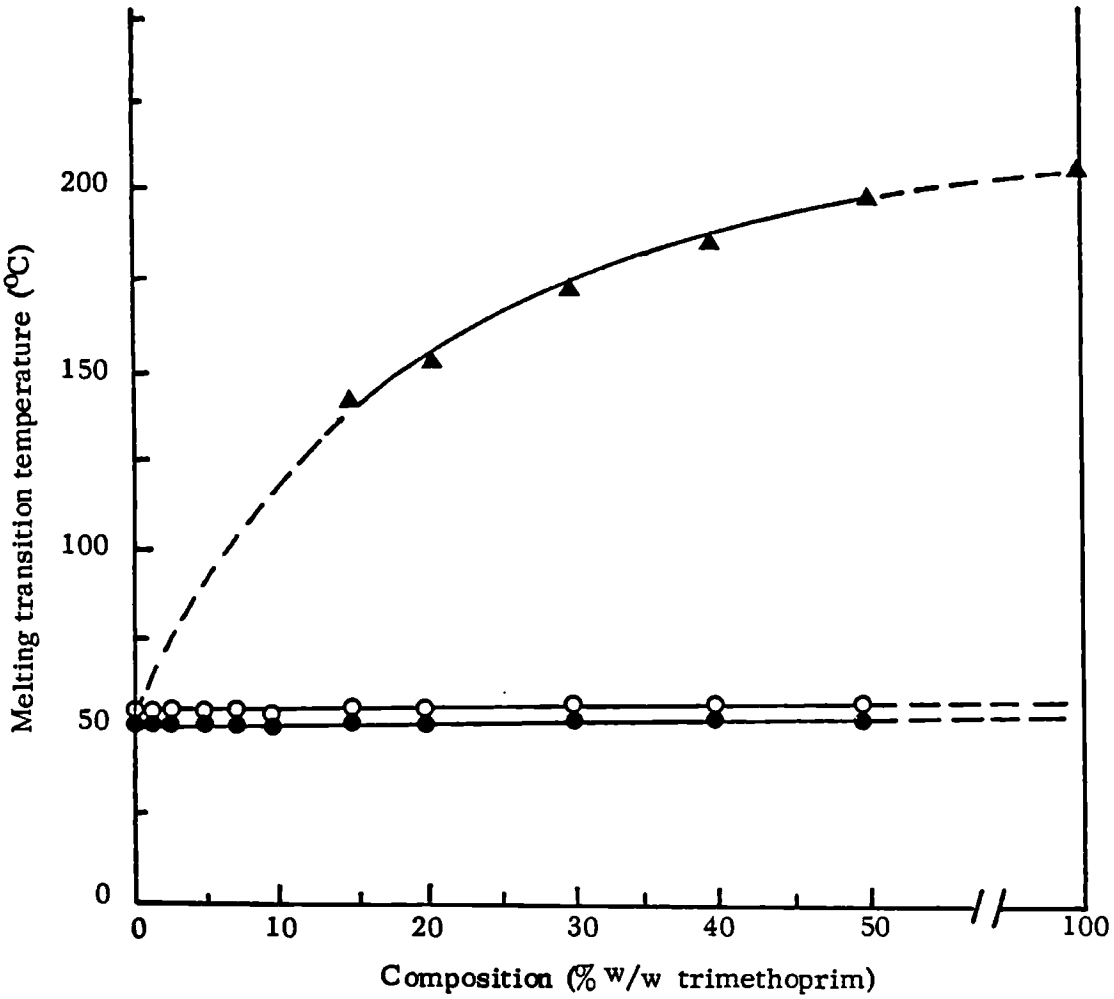

Phase transitions:

▲ **Trimethoprim**

o PEG 4000 - extended chain crystals

● PEG 4000 - once-folded chain crystals

alcohol and PEG 6000, which had not been melted together previously. In this latter case, as here, no melting transitions were observed by DSC for the drug at concentrations of 10%w/w or less. It appears that at low concentrations, very gradual dissolution and melting of the drug occurs which cannot be detected by DSC. Depression of the melting point of trimethoprim, due to the presence of the polymer diminished as the drug concentration rose. No melting point depression of the polymer by the drug was apparent, except for 50%w/w dispersions where a small decrease of 2°C was observed. This is again similar to the results reported by Hargreaves (1982) on heating physical mixtures of betamethasone alcohol and PEG 6000, where the melting point of the polymer was depressed by up to 6.5°C, apparently by the physical presence of the drug. It is interesting to note that Harrison and Runt (1980) reported that single crystals of polyethylene embedded in totally incompatible matrices of other polymers, with which no chemical reaction was possible, showed a melting point depression of up to 5°C. The effect was most marked where the matrix was crystalline rather than amorphous. This degree of depression would be a significant part of that reported for compatible systems.

Although the phase diagram suggested that no eutectic or solid solution was present, there is some degree of uncertainty as to the behaviour at low concentrations of trimethoprim since no melting transition for the drug could be detected in this region. However, additional information about the structure can be obtained if the enthalpies of fusion for the polymer and drug are plotted as a function of the percentage weight of the polymer. A typical diagram where a eutectic is formed, for the PEG 4000-water system (Hager and Macrury, 1980), is illustrated in Fig. 3.11. If a eutectic point

Fig. 3.11. Enthalpy of melting obtained by DSC as a function of % weight of polymer (Hager and Macrury, 1980)

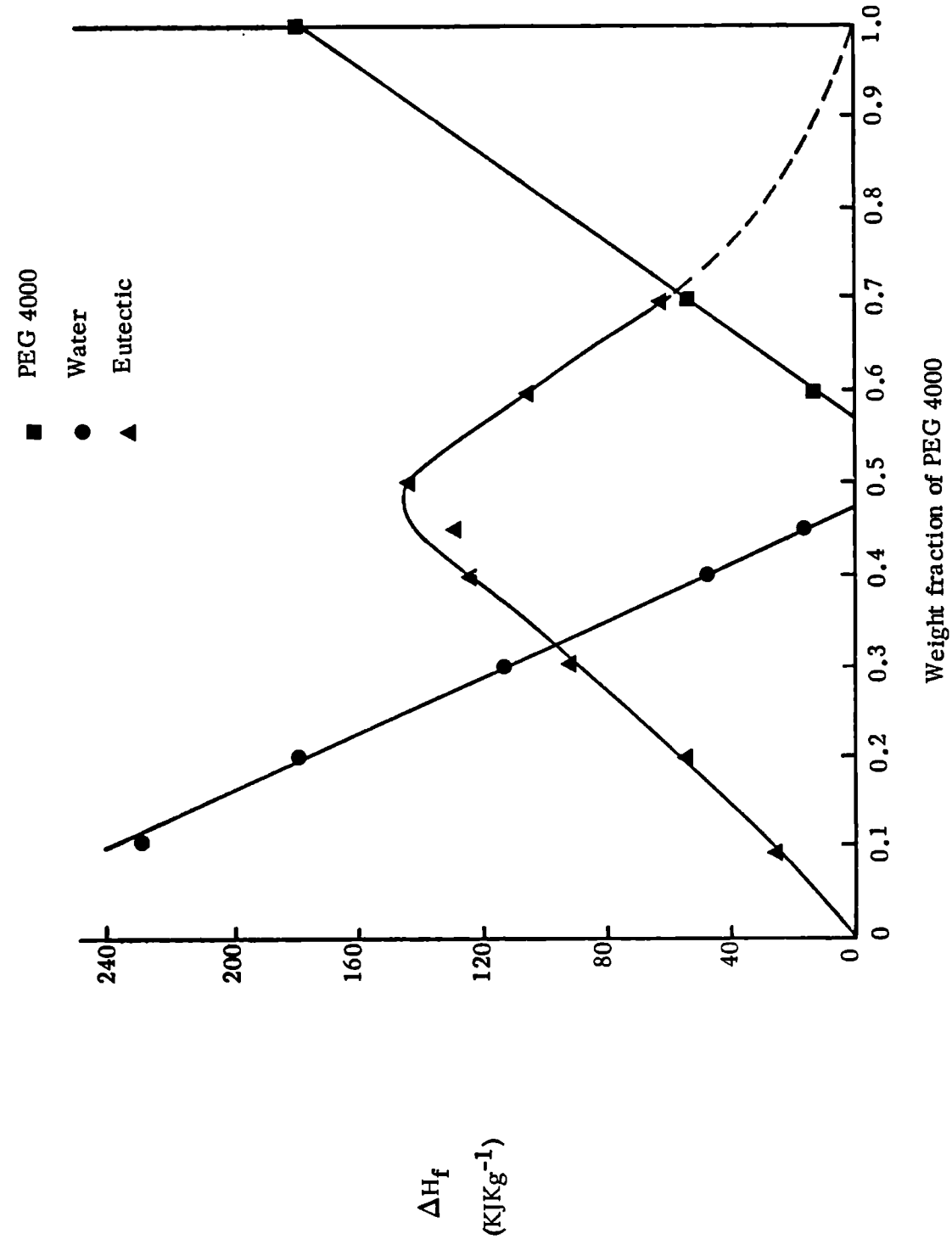

exists, then the enthalpy of fusion of the non-polymeric component per gram of sample should decrease as the concentration of the polymer increased, eventually to zero at the eutectic point. The enthalpy of fusion of the eutectic should increase as more eutectic forms, reaching a maximum at the eutectic composition and then decreasing as excess polymer is added. This decrease is paralleled by a rise in the enthalpy of fusion of the crystalline PEG 4000.

A similar diagram constructed for this system (Fig. 3.12.) revealed that although there was a decrease in the enthalpy of melting of trimethoprim at high concentrations of PEG 4000, it did not fall to zero, as might have been expected for a eutectic system. Furthermore, there was no appreciable increase in the enthalpy of fusion of PEG 4000 as has been reported by Prud'homme (1982) for the solid solution formed between PEG 4000 and PEG 1000. There, the presence of the small percentage of PEG 1000 molecules trapped inside the PEG 4000 crystals resulted in an apparent increase in the heat of fusion of the latter. The only change in the enthalpy of melting of PEG 4000 here however, was a small decrease at high concentrations of trimethoprim. This probably arises from the high concentration of drug particles hindering the orientation and diffusion of polymer chains in the melt, resulting in a lesser degree of crystalline order and hence lower heat of fusion. The observed decrease in the heat of fusion of trimethoprim as its concentration decreased, may reflect the fact that gradual dissolution of the drug in the polymer melt is also occurring.

X-ray diffraction patterns of these samples were found to be composites of those of the two individual components, except below 2%^{w}/w trimethoprim, where no diffraction lines characteristic of the drug could be detected. Typical X-ray diffraction spectra of trimethoprim powder as received and

Fig. 3.12. Enthalpy of melting obtained by DSC as a function of % weight of PEG 4000, for trimethoprim solid dispersions previously melted at 100°C for 10 mins before cooling at 20°C hr^{-1}

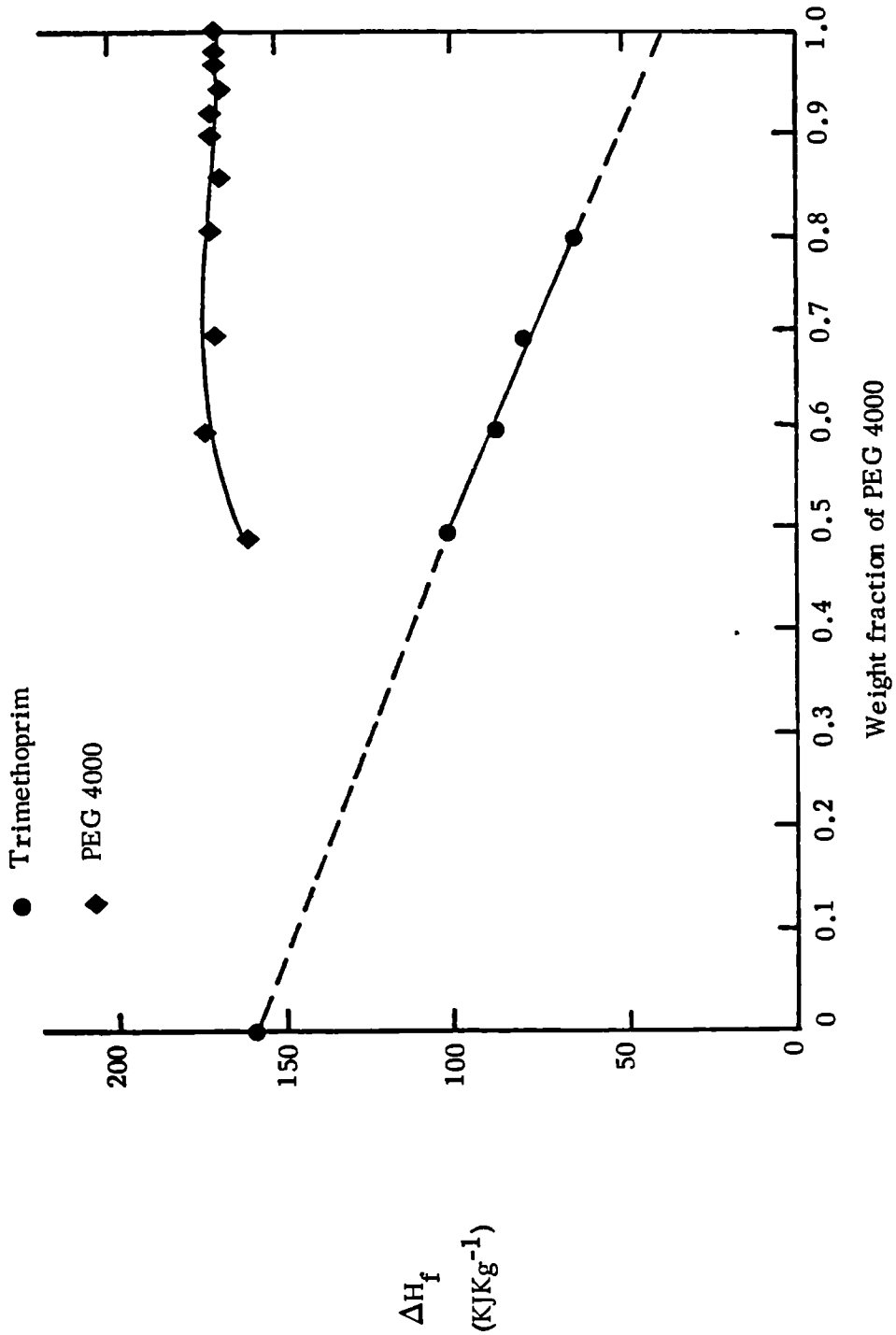

a number of solid dispersions are presented in Fig. 3.13. and the d-spacings for polymorphic form I of trimethoprim in Table 3.6. Although a second polymorphic form of trimethoprim is known to exist (Bettinetti et al, 1976), it did not appear to be present to any detectable extent in the original powder or the solid dispersions.

As expected where the drug did not dissolve completely in the polymer melt, the subsequent dispersions existed as a physical dispersion of drug particles in the polymer matrix. A different structure might be expected and in fact has been reported (e.g. Hargreaves, 1982), where the two components have previously been fused together. However, a similar phase diagram i.e. monotectic, was obtained with solid dispersions which had been prepared by totally melting the polymer and drug at 200°C, prior to cooling at $60^{\circ}C\,hr^{-1}$. A faster rate of cooling than from 100°C was chosen to minimise thermal degradation (Fig. 3.14.). Moreover, a similar relationship existed between the enthalpy of melting and percentage composition (Fig. 3.15.). The melting points of both PEG 4000 and trimethoprim were not significantly changed from those measured for the physical dispersions. X-ray diffraction spectra were again composites of the two components but diffraction peaks of trimethoprim were absent at concentrations below $5\%^{w}/w$. No polymorphic forms of trimethoprim were detected, in either the dispersions or in samples of drug which had been fused and cooled, nor was there any significant decrease in the intensity of the diffraction peaks.

An alternative to using DSC melting data to construct a phase diagram is to use the crystallisation data (Smith and Pennings, 1977). Additionally, this should provide information as to whether PEGS inhibit the crystallisation

Fig. 3.13. Typical X-ray diffraction spectra for trimethoprim and its and its solid dispersions with PEG 4000 previously heated at 100°C for 10 minutes and cooled at 20°C hr^{-1}

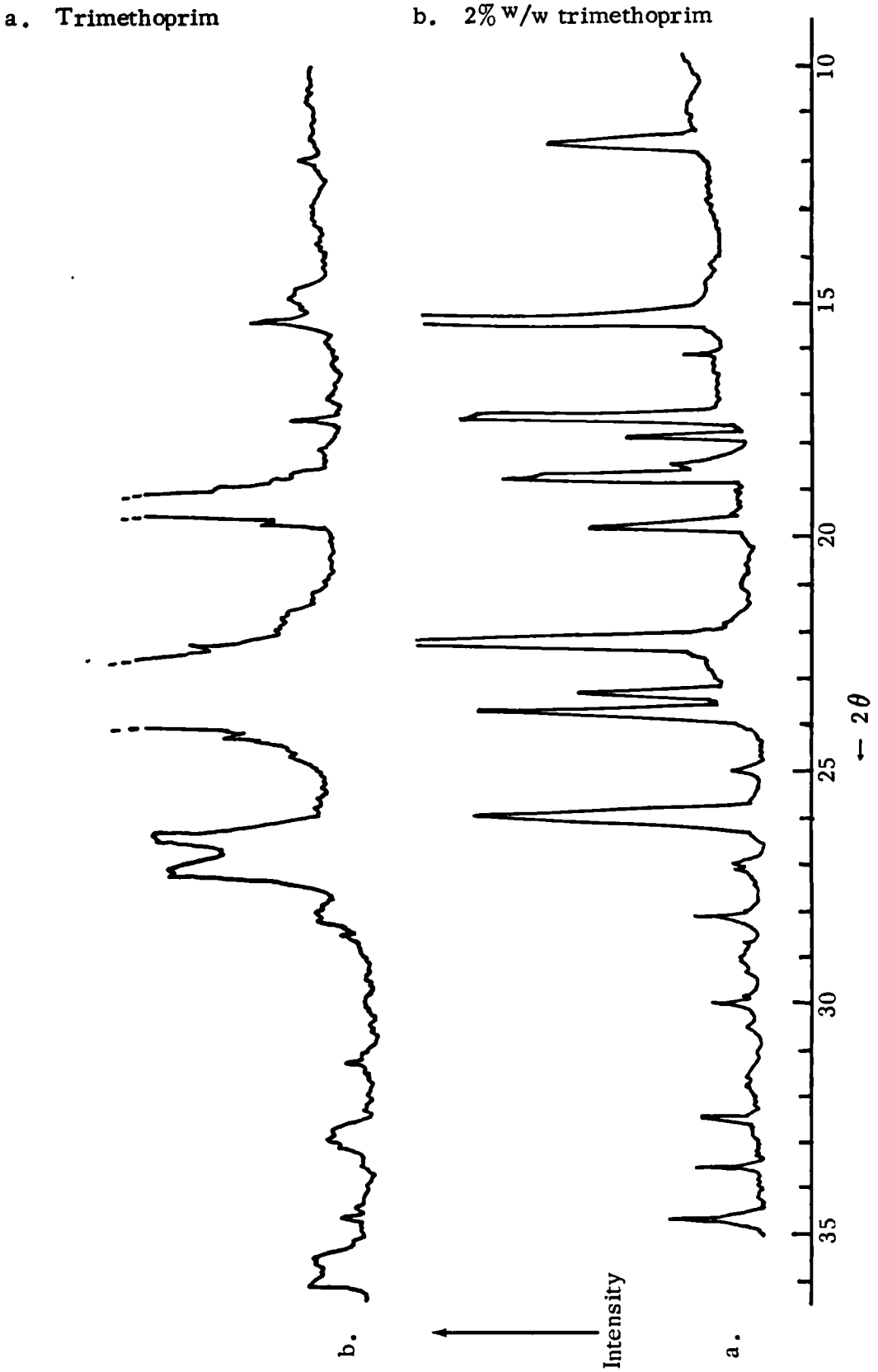

Fig. 3.13. c. 10% w/w trimethoprim d. 50% w/w trimethoprim

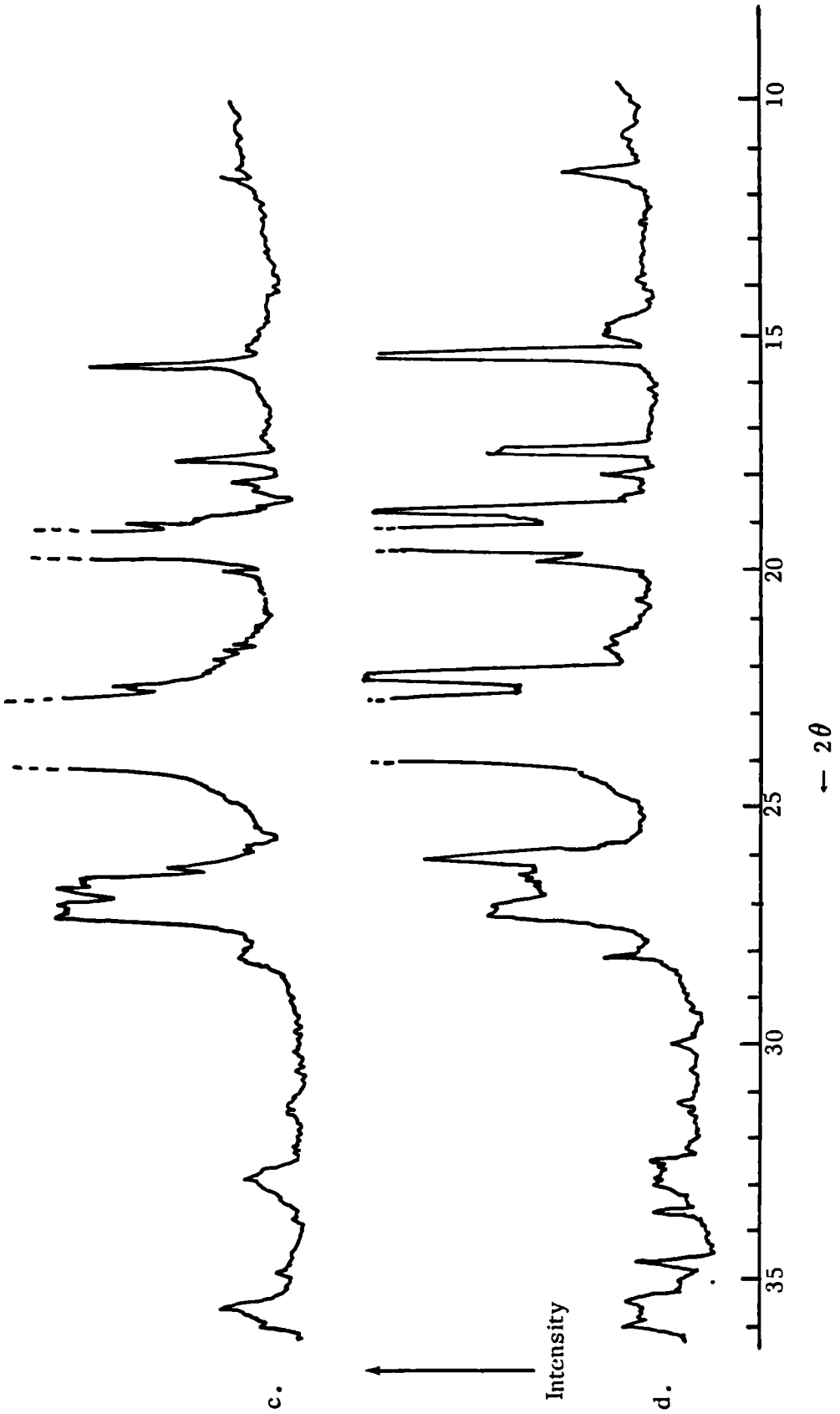

Table 3.6. d-spacings and relative intensities of X-ray diffraction peaks for trimethoprim (Form I)

2θ	d-spacing	Relative intensity I/I_o
7.46	11.88	43
5.8	15.30	100
5.5	16.14	17
5.07	17.52	60
4.94	17.96	26
4.82	18.44	14
4.75	18.71	55
4.46	19.91	34
4.03	22.09	2
3.97	22.39	93
3.85	23.10	36
3.73	23.85	62
3.53	25.23	18
3.43	25.98	62
3.29	27.15	7
3.17	28.20	17
3.11	28.70	4
2.97	30.14	8
2.89	30.94	17
2.83	31.67	2
2.74	32.68	12
2.66	33.69	17
2.58	34.77	26

Fig. 3.14. Partial phase diagram for PEG 4000 - trimethoprim system, previously melted at 200°C for 10 mins and cooled at 60°C hr^{-1}, constructed from DSC melting data

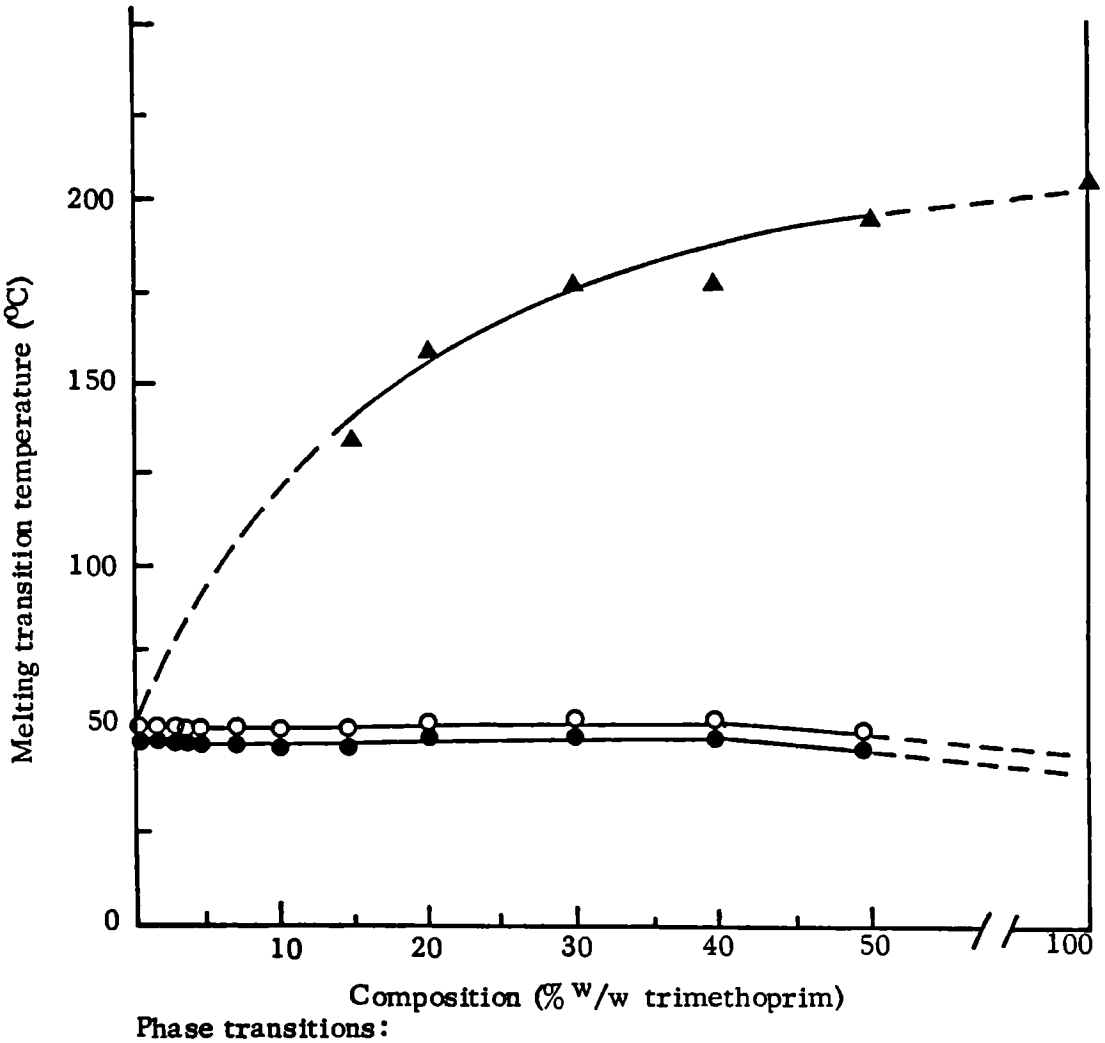

Phase transitions:

▲ Trimethoprim

o PEG 4000 extended chain crystals

● PEG 4000 once-folded chain crystals

Fig. 3.15. Enthalpy of melting obtained by DSC as a function of % weight of PEG 4000, for trimethoprim solid dispersions previously melted at 200°C for 10 mins before cooling at 60°C hr^{-1}

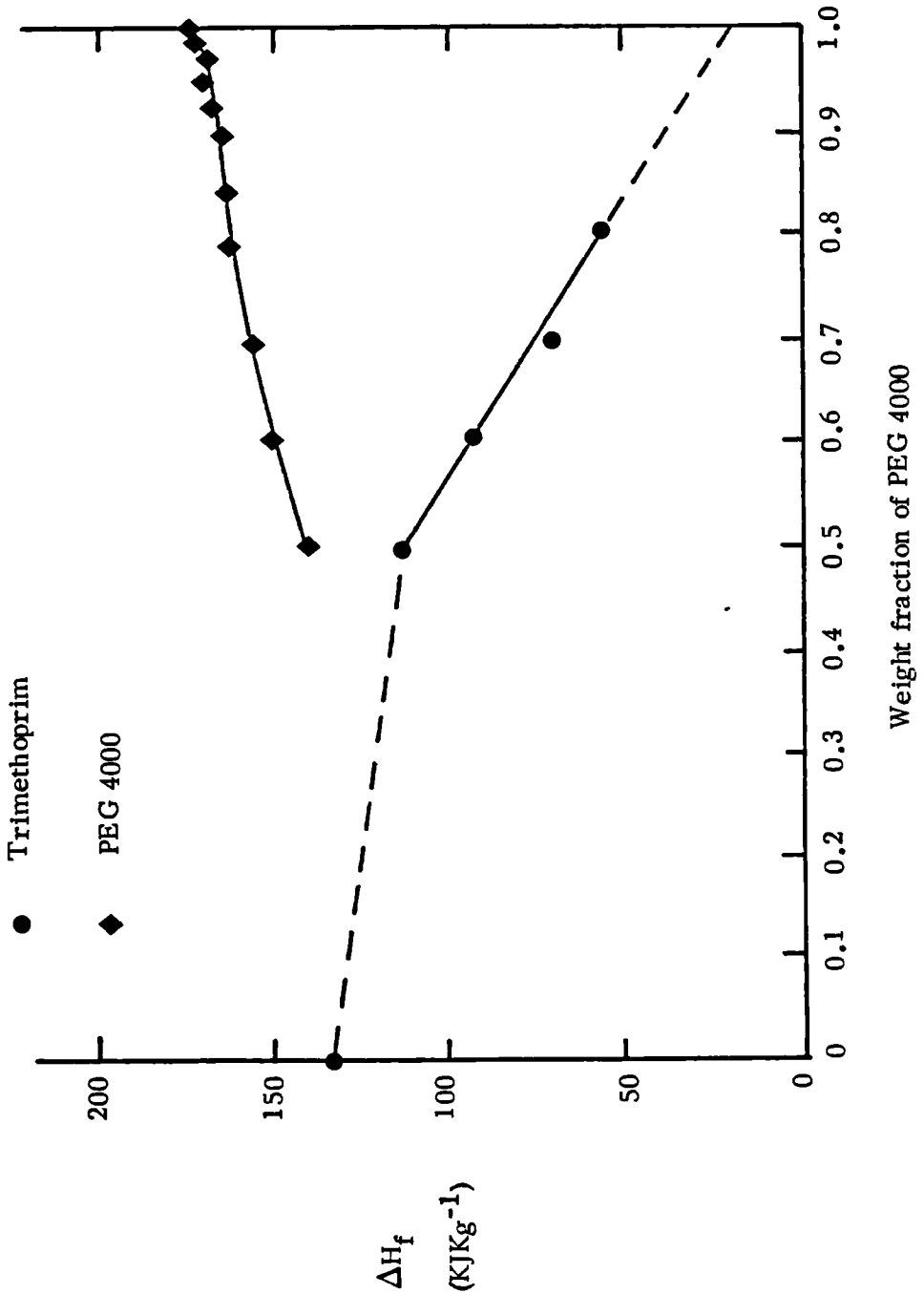

of drugs dissolved in them, as has often been suggested (El-Banna and Abdallah, 1980; Salib et al, 1976) but never conclusively demonstrated. DSC thermograms of the crystallisation exotherms of solid dispersions of PEG 4000 and trimethoprim melted at 200°C for 10 mins and cooled at 8°C min^{-1} were obtained. The relatively rapid cooling rate was chosen because faster cooling is known to facilitate the formation of eutectics and solid solutions, due to the lack of time for complete fractionation of the two components (Prud'homme, 1982).

On cooling the pure drug, which melted at 202°C, a significant degree of supercooling occurred before recrystallisation at 149°C. Obviously though, the amount of supercooling will be dependent on the cooling rate used. Only one exothermic peak was observed, thus it is likely that only one polymorphic form of trimethoprim recrystallised. This was confirmed on remelting, since these samples displayed only one endothermic peak as before. If the other known polymorphic form of trimethoprim had also been present, then a second transition at ~170°C would have been observed, corresponding to the conversion of the metastable Form II to Form I (Bettinetti et al, 1976). Crystallisation transitions for trimethoprim could only be detected for concentrations between 20%^{w}/w and 50%^{w}/w. Below this, only one exothermic peak arising from the crystallisation of PEG 4000 was observed. The phase diagram and enthalpy of crystallisation as a function of polymer composition data (Fig. 3.16. and 3.17. respectively) are again of the pattern obtained earlier.

Below 20%^{w}/w trimethoprim, where no recrystallisation peak for the drug is observed, a number of explanations for this behaviour can be postulated. Firstly, the formation of a eutectic or solid solution would be

Fig. 3.16. Partial phase diagram for PEG 4000 - trimethoprim system constructed from DSC crystallisation data, fused at 200°C for 10 mins and cooled at 8°C min^{-1}

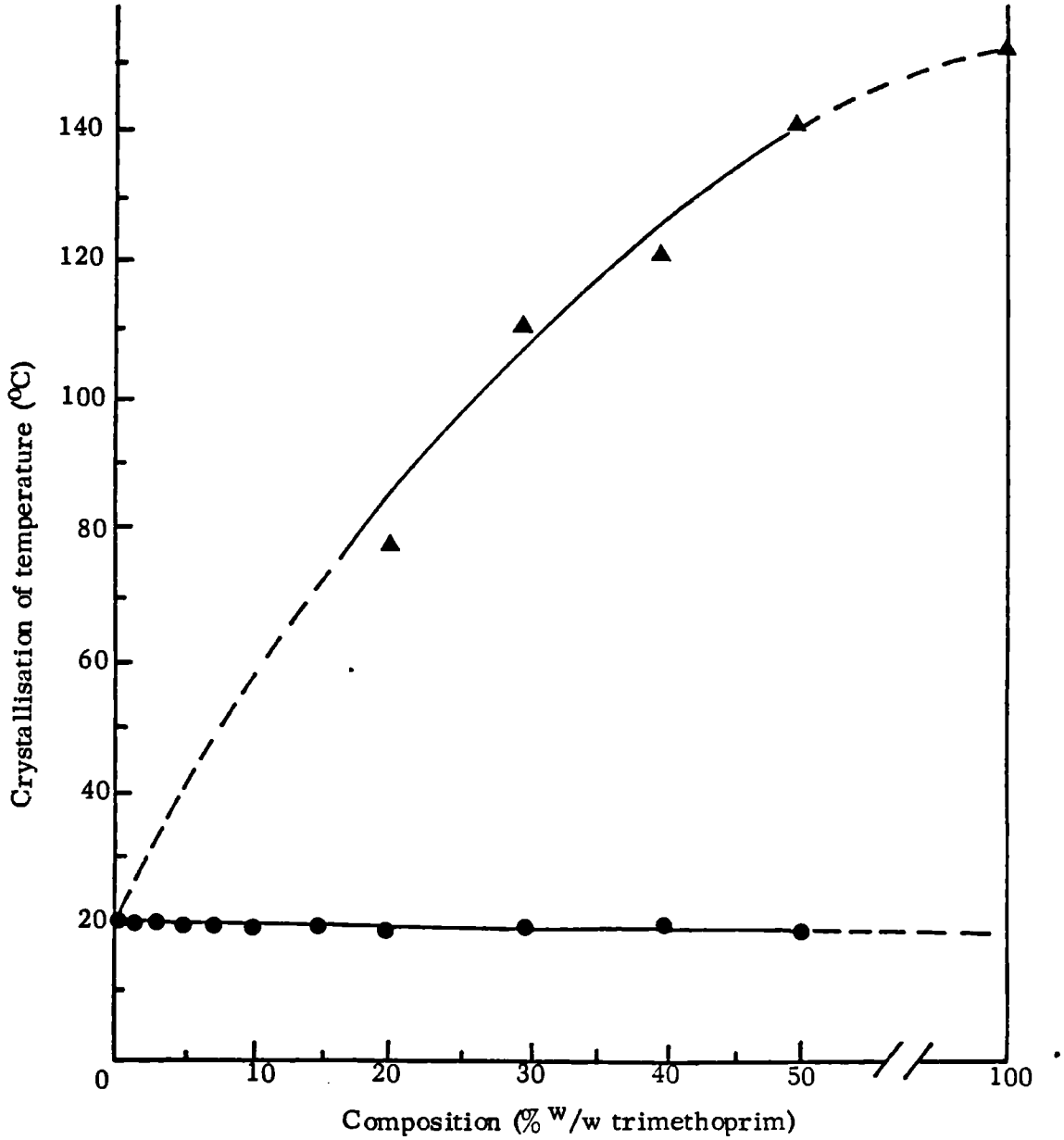

Phase transitions:

● PEG 4000

▲ Trimethoprim

Fig. 3.17. Enthalpy of crystallisation obtained by DSC as a function of % weight of PEG 4000, for trimethoprim solid dispersions fused at 200°C for 10 mins and cooled at 8°C min^{-1}

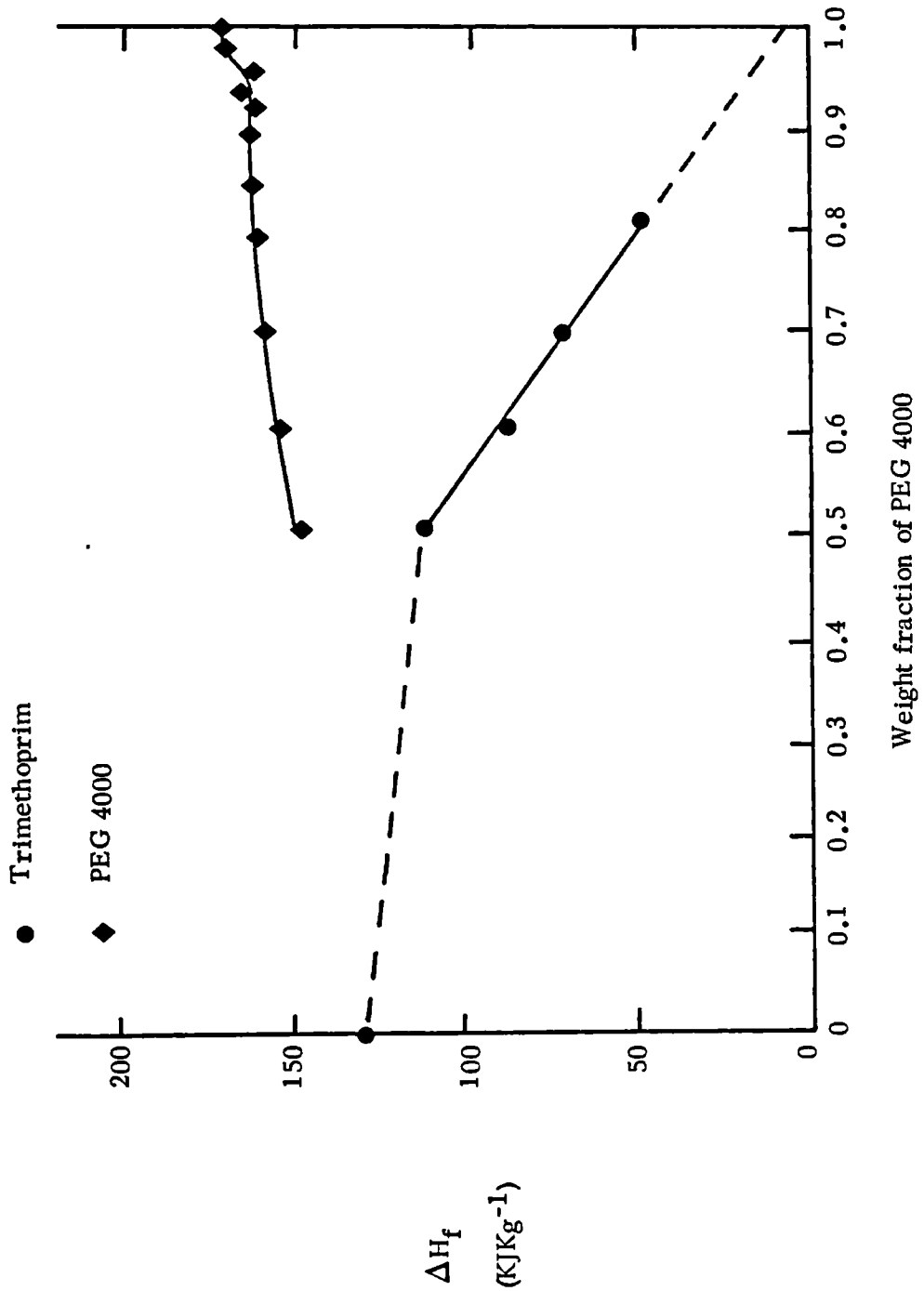

a possible reason. However, no corresponding increase is observed in the enthalpy of crystallisation of the transition attributed to PEG 4000, nor does the extrapolated curve for the enthalpy of crystallisation of trimethoprim fall to zero. Alternatively, the technique of DSC may be too insensitive to detect the heat of crystallisation of small amounts of drug in the molten polymer. However, the most likely explanation would be that the crystallisation of the drug is inhibited to a certain extent in the polymer melt due to its high viscosity. Thus on cooling, some of the drug molecules fail to recrystallise and are rejected by the growing polymer crystals as foreign impurities. Thus, they are forced into the amorphous regions which exist between the crystal branches of spherulites and in between lamellae. This suggestion is consistent with the X-ray diffraction data observed for dispersions which previously had been fused totally, where the absence of diffraction peaks for trimethoprim below 5%w/w drug could be due to the presence of the drug in an amorphous form. It is difficult to envisage the formation of a solid solution of drug inside the polymer lamellae, since foreign particles and even low molecular weight chains are rejected by the growing crystals. Furthermore, considerations of the size of the interstitial space available within the PEG helix suggest that trapping of drug molecules between the parallel helices of PEG chains, as has been postulated by Chiou and Riegelman (1971) is not feasible. The cross-sectional diameter of the PEG helix is of the order of 0.5 nm (Takahashi and Tadokoro, 1973) which would be insufficient to accommodate trimethoprim molecules and still allow crystallisation of the polymer.

Thus from theoretical considerations of PEG morphology, crystallisation and from the data presented in this section, it appears that negligible solid

solution or eutectic formation occurs between PEG 4000 and trimethoprim. Nevertheless, the structure of both components may be influenced by the other and by their thermal history, further studies of which are presented in the following sections.

3.3.2.2. Temperature of melting

As the morphology of PEG 4000 was found to be dependent on its previous thermal history (Chapter 3.3.1.), the addition of a second component was of interest in terms of the effect on both the drug and the polymer. A representative range of concentrations of trimethoprim, 2%^{w}/w, 10%^{w}/w and 50%^{w}/w, were chosen for study. After melting at temperatures of between 60°C and 200°C for 10 minutes, samples were cooled at 8°C min^{-1} to room temperature. Dissolution of the trimethoprim particles in the polymer melt as assessed visually was incomplete for 2%^{w}/w dispersions below 100°C, for 10%^{w}/w dispersions below 150°C and at all melting temperatures except 200°C for 50%^{w}/w dispersions.

DSC melting endotherms for all samples showed two lower temperature transitions corresponding to the melting of once folded and extended chain crystals of PEG 4000 as before (Buckley and Kovacs, 1976). In addition, the 50%^{w}/w solid dispersions displayed a third endothermic peak which resulted from the melting of the drug. The observed melting temperatures and enthalpies of fusion for PEG 4000 in the 2%^{w}/w dispersions were not significantly different to those for the polymer in the absence of the drug. At a trimethoprim concentration of 10%^{w}/w, a slight decrease in the enthalpy of fusion of ~5% compared to the polymer alone was observed, whereas the melting temperatures were unchanged, for samples previously

melted at 150°C or 200°C. However, for 50%^{w}/w dispersions, a decrease in both the melting temperature, of ~2°C and the enthalpy of fusion, of ~10% in relation to the pure polymer was apparent where the previous melting temperature exceeded 100°C. The percentage of once folded chain crystals increased with the previous temperature of melting (Fig. 3.18.), as was observed for PEG 4000 alone. Differences between dispersions containing various concentrations of trimethoprim were not very marked, and the proportion of each crystal type formed was of the same order as PEG 4000 in the absence of any drug. Nevertheless, there appeared to be slightly more folded chain crystals in samples containing 50%^{w}/w trimethoprim at all melting temperatures studied.

X-ray diffraction studies did not reveal any new diffraction lines for any of the dispersions, indicating that no polymorphic forms of trimethoprim had appeared. The characteristic peaks for trimethoprim were absent in 2%^{w}/w dispersions melted at 100°C or above, but present in the diffraction patterns for all other samples, which were composites of the two components. Apart from a slight increase in the amorphous halo for 50%^{w}/w dispersions melted at 150°C or 200°C, there were no detectable changes in crystallinity.

Overall, these results suggest that at low concentrations of drug, around 2%^{w}/w, the presence of the drug does not interfere significantly with the crystallisation of the polymer. This appears to be true for both the crystalline drug, as was present in the dispersions melted below 100°C, and for the amorphous form , as was probably present in dispersions previously melted at or above 100°C. At this low concentration, trimethoprim which dissolves or melts in PEG 4000 does not seem to recrystallise on cooling, due to the inhibitory effect of the high melt viscosity. Thus,

Fig. 3.18. Relative proportion of folded chain crystals formed as a function of previous temperature of melting for various concentrations of trimethoprim in PEG 4000 dispersions

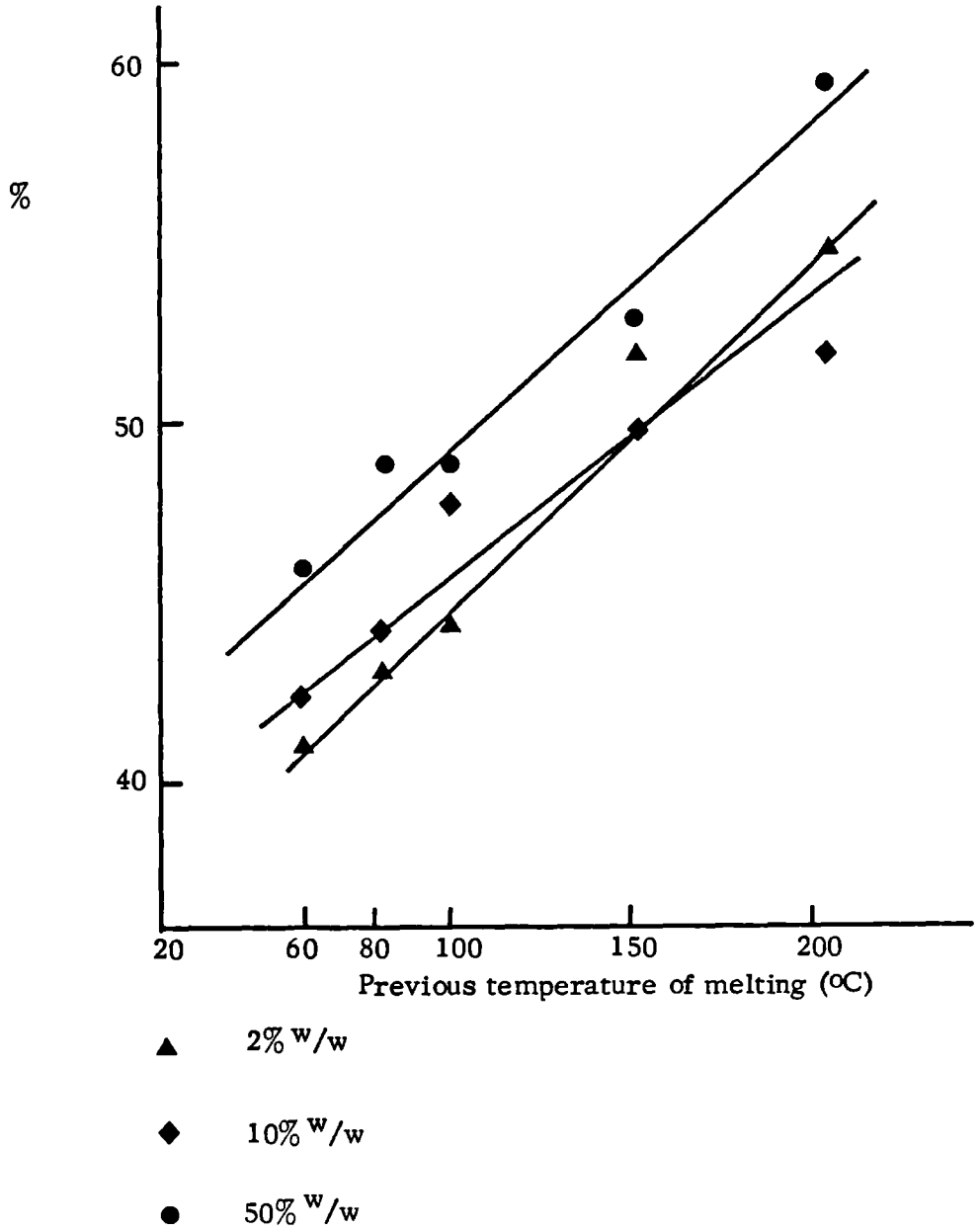

as the temperature is lowered, and crystallisation of the polymer commences, drug molecules will be rejected as impurities by the growth front of the crystal and form part of the amorphous region (Beech et al, 1972b). At this concentration, no effect on crystallinity is detectable. Trimethoprim which is present as particles does not appear to nucleate crystallisation of the polymer to any significant extent.

At a concentration of 10%^{w}/w trimethoprim, there is no evidence to suggest that the drug present in particulate form behaves as a nucleating agent. As for 2%^{w}/w dispersions, some of the drug in dispersions previously melted at high temperatues does not recrystallise on cooling and exists in the amorphous state. Some disruption of the crystallisation process of the polymer is apparent from its reduced enthalpy of fusion and hence crystallinity with samples melted at 150^{o}C or 200^{o}C.

For low melting temperatures below 100^{o}C, the presence of 50%^{w}/w trimethoprim on the morphology of PEG 4000 was not marked. The decrease in the melting temperatures and enthalpies of fusion for dispersion previously melted at or above 100^{o}C indicates that a higher proportion of amorphous material is formed. This, together with the higher percentage of metastable folded chain crystals formed suggests that the crystallisation of the polymer is hindered. Reasons for this may include the higher viscosity of polymer melts containing 50%^{w}/w trimethoprim which will decrease the mobility and rate of diffusion of the polymer chains. A decrease in the temperature at which crystallisation took place would favour the formation of a higher percentage of folded chain crystals. Also, crystallisation of the polymer in the presence of a high concentration of drug particles would be hindered simply because the growth of the crystals would have to take place around

the drug particles, resulting in a less perfect crystalline structure.

3.3.2.3. Time in the molten state

The effect of the time in the molten state on solid dispersions of trimethoprim and PEG 4000 was studied, with respect to its influence on the subsequent morphology produced, rather than the kinetics of degradation of the drug at elevated temperatures. Investigations were performed as for PEG 4000 (Chapter 3.3.1.2.) except that only times of 10 minutes and 10 hours were studied.

The behaviour of dispersions containing 2%^{w}/w trimethoprim was very similar to that of PEG 4000 alone with an equivalent degree of reduction in the enthalpy of fusion and melting temperatures under all conditions studied. For dispersions of 10%^{w}/w or 50%^{w}/w trimethoprim maintained in the molten state for 10 minutes, a slight reduction in the enthalpy of fusion and melting temperatures was observed by DSC and X-ray diffraction studies, especially at high melting temperatures. These results have been discussed in the preceding section. After 10 hours at 200^{o}C, 10%^{w}/w dispersions were very yellow and displayed a very broad melting endotherm with a markedly reduced heat of fusion. 50%^{w}/w dispersions maintained at 100^{o}C or 200^{o}C for 10 hours failed to recrystallise on cooling to room temperature, and were dark yellow-brown in colour, indicating that significant decomposition of the polymer and probably the drug also had occurred. However, at the lowest melting temperature studied, 60^{o}C, the dispersions remained relatively stable, even after 10 hours, as was observed for PEG 4000. The effect of time in the molten state at different temperatures enthalpy of fusion of the various dispersions is illustrated in Fig. 3.19. As would be expected, melts maintained at the lowest temperatures are the most stable

Fig. 3.19. Effect of time in the molten state on the enthalpy of fusion of various solid dispersions of PEG 4000 and trimethoprim

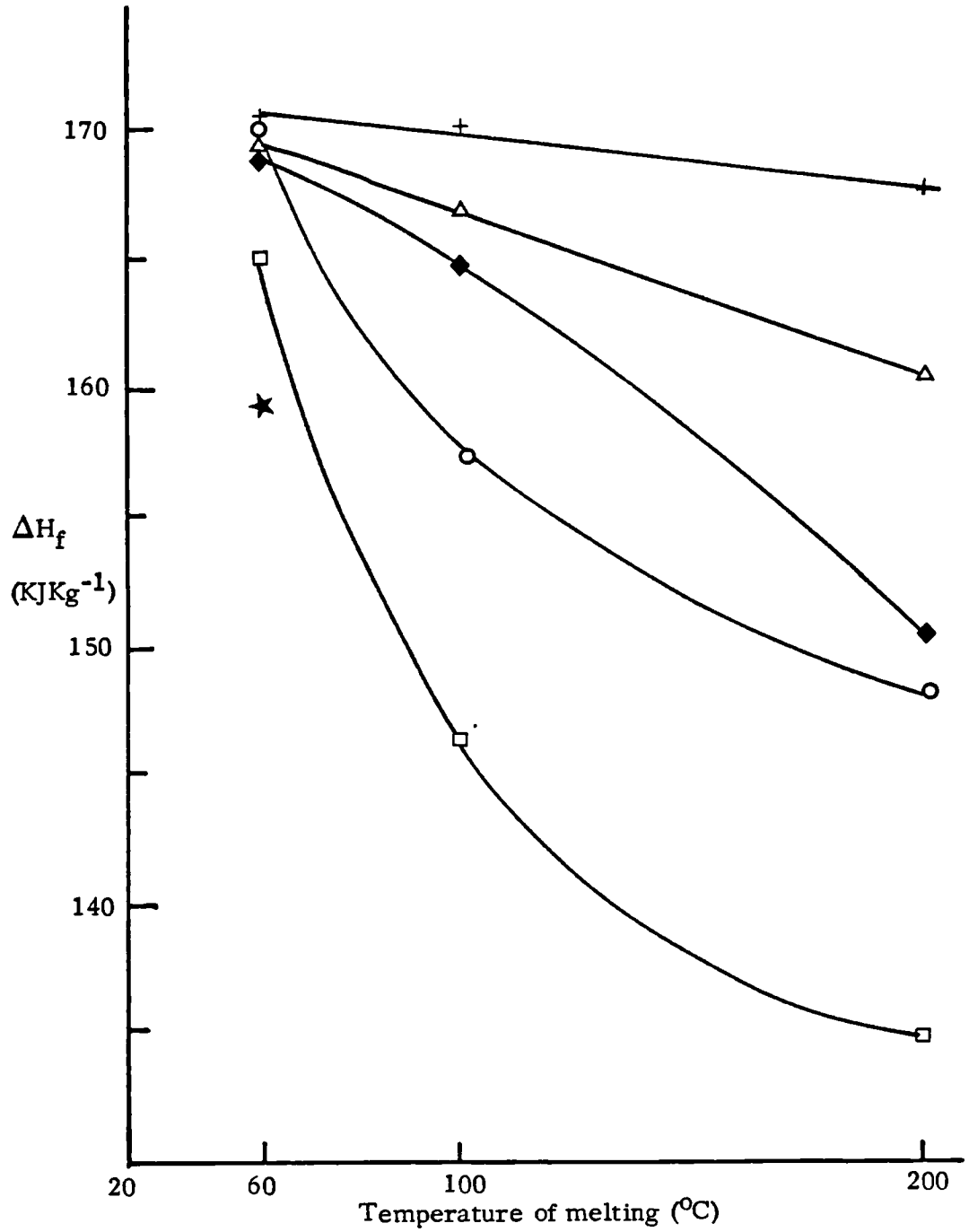

to thermal degradation and chain scission of the polymer. The rate of degradation of the melt appears to accelerate considerably above ~100°C.

3.3.2.4. Cooling rate

As the rate of cooling from the melt was shown to exert a strong effect on the subsequent morphology of PEG 4000, the influence of this variable on the morphology of its solid dispersions is of particular interest.

Quenching in liquid nitrogen of solid dispersions previously fused at 200°C markedly reduced the crystallinity of both components, as would be expected. For 2%^{w}/w and 10%^{w}/w trimethoprim dispersions, no X-ray diffraction peaks which could be attributed to the drug could be discerned, suggesting that both the rapid cooling rate and the high viscosity of the polymer melt had inhibited the drug's crystallisation, giving an amorphous form. By contrast, diffraction peaks corresponding to Form I of trimethoprim were apparent for 50%^{w}/w dispersions, albeit of a very weak intensity. At all concentrations studied, the characteristic X-ray diffraction peaks for PEG 4000 were present, but of reduced intensity, reflecting the decrease in crystallinity of the polymer. DSC thermograms failed to reveal any melting endotherm for trimethoprim, even at 50%^{w}/w, which tends to confirm the lack of crystallinity of the drug observed by X-ray diffraction data. The melting point of PEG 4000 was depressed by ~2°C for 2%^{w}/w and 10%^{w}/w quenched dispersions and to a slightly greater degree, ~3°C, for 50%^{w}/w dispersions, similar to the behaviour observed for PEG 4000 alone. Again, the crystal form present is extended chain rather than folded chain lamellae. Reduction of the crystallinity of the polymer to ~44% was observed for both 2%^{w}/w and 10%^{w}/w dispersions, which again is of the same magnitude as

for PEG 4000 in the absence of trimethoprim. At the highest concentration of drug, the slightly greater reduction in the crystallinity of PEG 4000 to ~40% probably reflects the increased difficulty of nucleation and orientation of polymer chains in the presence of large amounts of drug.

The effect of cooling at 8°C min^{-1} (480°C hr^{-1}), 60°C hr^{-1} and 20°C hr^{-1} after melting at 200°C for 10 minutes on the morphology of these solid dispersions has already been discussed in detail in the preceding sections. Cooling rates slower than ~20°C hr^{-1} led to an unacceptably high degree of thermal degradation of the dispersions.

3.3.2.5. Ageing

The effect of ageing on 2, 10 and 50%^{w}/w dispersions prepared under a variety of conditions was investigated as for PEG 4000. Although the effect of ageing at different temperatures on the dissolution performance of solid dispersions has been studied by several workers (e.g. Ford and Rubinstein, 1979, 1980; Hargreaves, 1982; Khalil and Mortada, 1978), very few investigations of the corresponding changes in their physical structure exist. Generally, however, a deterioration in the dissolution rate is observed, which is usually attributed to crystal growth and coarsening of the eutectic particles of drug with age (Chiou and Riegelman, 1971).

Dispersions containing 2%^{w}/w and 10%^{w}/w trimethoprim, which had been melted at 100°C for 10 mins and cooled at 20°C hr^{-1}, showed a similar increase in the heat of fusion and crystallinity of the polymer with time to that of PEG 4000 alone (Section 3.3.1.4.). Conversion of the polymer folded chain crystals to the extended chain form did not appear to be hindered by the presence of the drug as it occurred over a similar time-scale to that of PEG 4000. No DSC transitions appeared which could be

attributed to the melting of the trimethoprim, although X-ray diffraction spectra showed the drug to be present in the crystalline form. There appeared to be a slight increase in the crystallinity of these dispersions from X-ray diffraction data, but there is no means of quantifying this increase in terms of one or other of the two components. Scanning electron micrographs did not show any gross changes in structure on ageing. For 50%^{w}/w dispersions, the increase in crystallinity of the polymer was slower at all storage temperatures studied than for dispersions containing 2%^{w}/w or 10%^{w}/w drug, and was paralleled by a correspondingly slower conversion of folded chain lamellae to the extended chain form. A slight increase to ~56^{o}C was observed for the melting temperature of the extended chain crystal type, but this is still less than the value for PEG 4000 alone. Since no increase in the heat of fusion of the drug occurred (Fig. 3.20a.), most of the trimethoprim probably initially existed in a stable crystalline state. As for the 2%^{w}/w and 10%^{w}/w dispersions, a slight decrease in the amorphous halo of the X-ray diffraction patterns was discernible, but scanning electron micrographs failed to reveal any significant changes in structure. These results are in good agreement with those reported by Hajratwala and Ho (1984) for their X-ray diffraction and SEM studies on the ageing of 40%^{w}/w hydrocortisone-PEG 4000 dispersions.

Very similar behaviour to that described above was observed for dispersions which had previously been melted at 200^{o}C for 10 minutes and cooled at 60^{o}C hr^{-1}, except for a few minor points. No X-ray diffraction peaks which could be attributed to trimethoprim were apparent in the spectra of 2%^{w}/w dispersions, even after 6 months. Thus, at low concentrations, the recrystallisation of the drug seems to be inhibited by the polymer, even

Fig. 3.20. Effect of ageing at different temperatures on 50% w/w trimethoprim - PEG 4000 dispersions, prepared by:

a. Melting at 100°C for 10 mins and cooling at 20°C hr^{-1}

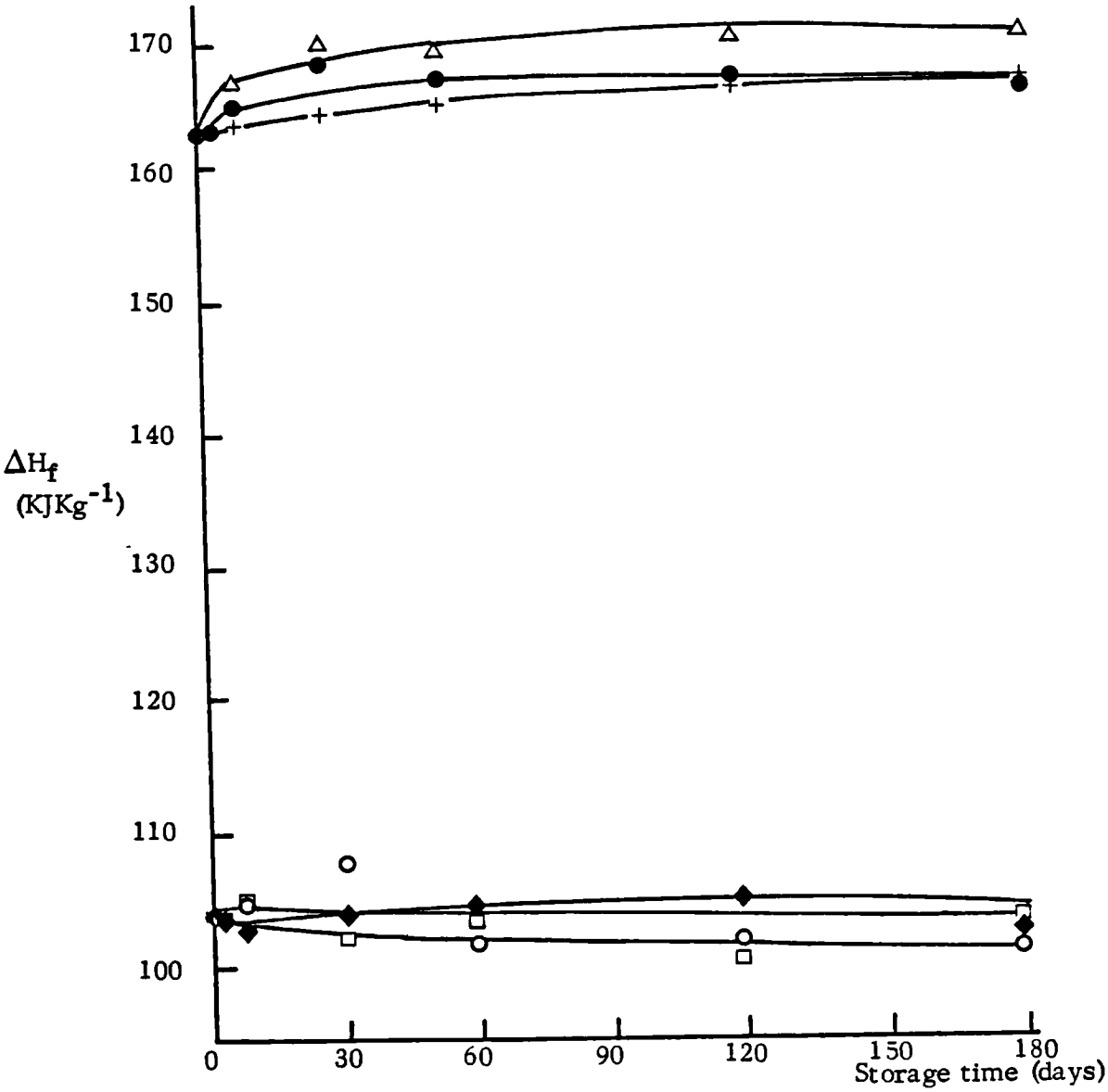

Storage temperatures:

Trimethoprim		PEG 4000	
◆	25°C	+	25°C
□	37°C	●	37°C
○	45°C	△	45°C

Fig. 3.20. b. Melting at 200°C for 10 mins and cooling at 60°C hr^{-1}

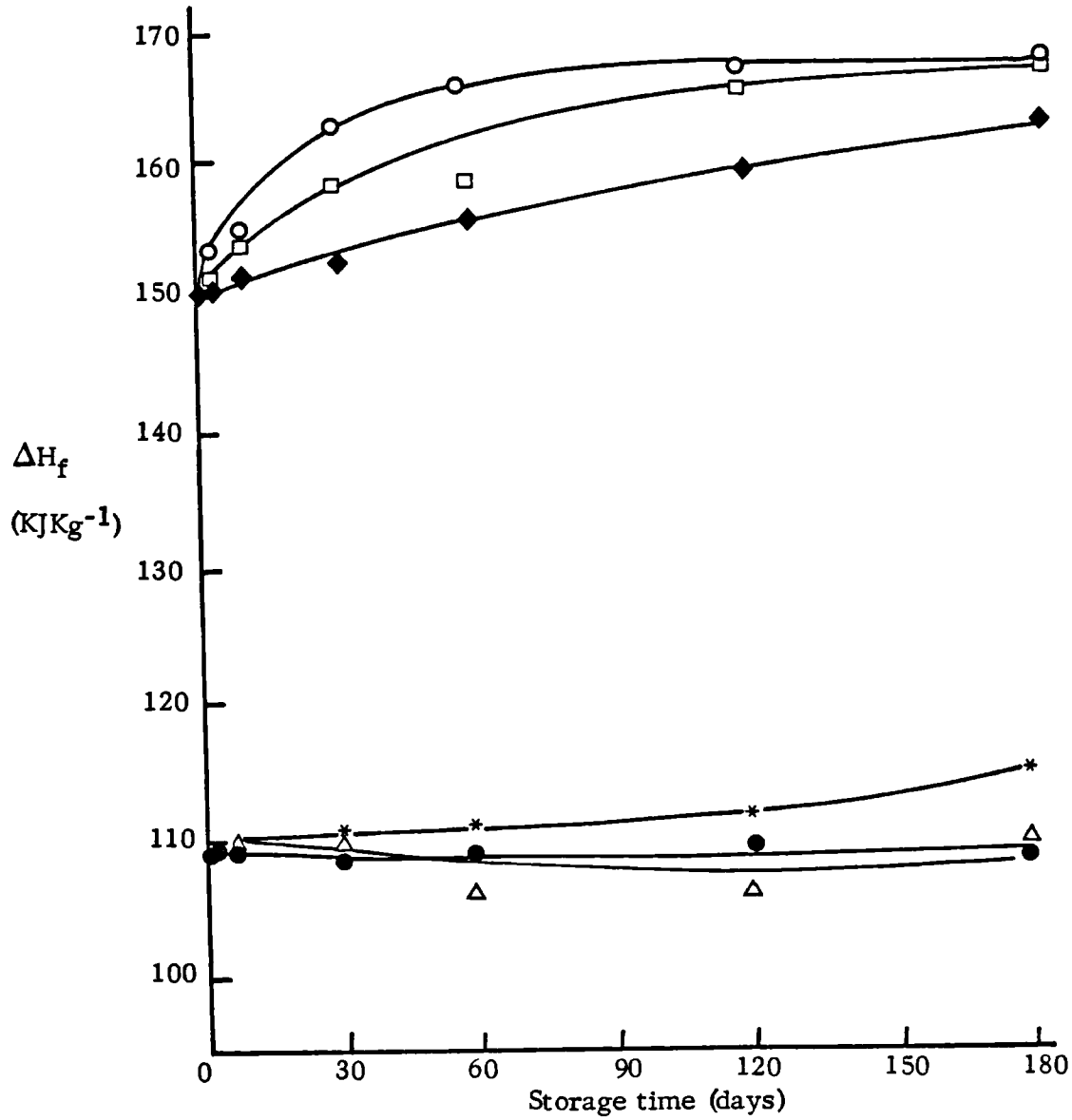

Storage temperatures:

● 25°C	◆ 25°C
△ 37°C	□ 37°C
* 45°C	o 45°C
Trimethoprim	PEG 4000

Fig. 3.20. c. Melting at 200°C for 10 mins and quenching in liquid nitrogen

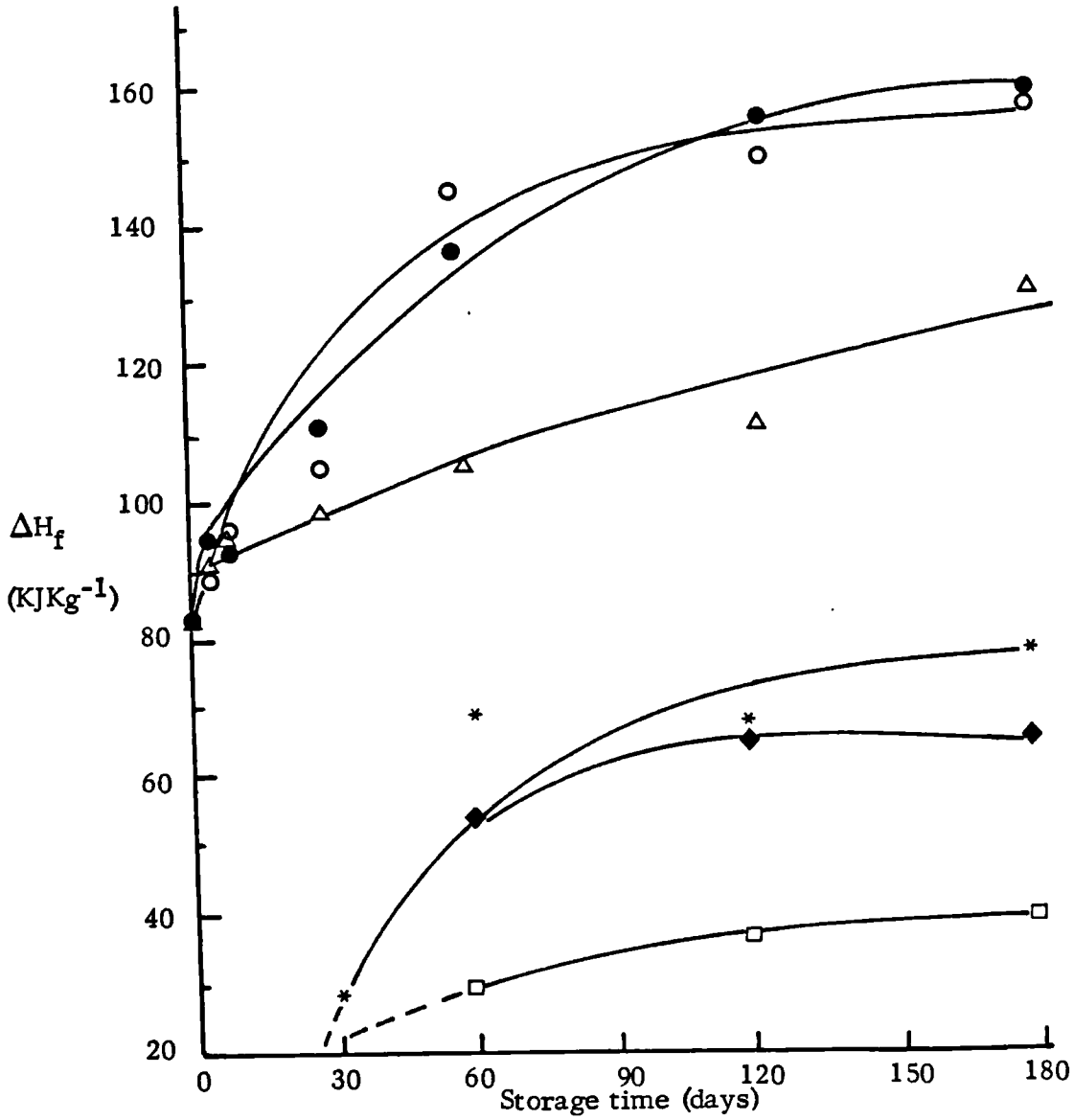

Storage temperatures:

□	25°C	△	25°C
◆	37°C	○	37°C
*	45°C	●	45°C
Trimethoprim		PEG 4000	

though chain unfolding and lamella thickening of the PEG 4000 apparently takes place unhindered. Dispersions containing 50%^{w}/w trimethoprim showed a slight increase in the heat of fusion of the drug after 6 months at 45^{o}C (Fig. 3.20b.) which may be indicative of some recrystallisation of the drug. Merely increasing the size of the drug crystals in the polymer matrix would not necessarily result in an increased enthalpy of fusion.

As for the polymer in the absence of trimethoprim, the largest changes on ageing occurred in samples which had been quenched in liquid nitrogen after fusing at 200^{o}C for 10 mins. The increase in the crystallinity of PEG 4000 in 2%^{w}/w and 10%^{w}/w trimethoprim dispersions was as for the polymer alone. No characteristic diffraction peaks for the drug could be detected on X-ray spectra for 2%^{w}/w dispersions at any storage temperature investigated, even after 6 months. Weak trimethoprim diffraction lines appeared on X-ray spectra for 10%^{w}/w dispersions but only after 6 months at either 37^{o}C or 45^{o}C. The melting point of the extended chain crystals of PEG 4000 present rose from 55^{o}C to 57^{o}C as their crystalline order increased, as has been observed previously (Section 3.3.1.4.). Again, it seems that the polymer is able to recrystallise more readily than the drug, which may be due in part to the nearness of the storage temperatures to the melting point of the former, presumably facilitating molecular flexibility and movement. X-ray diffraction peaks corresponding to the recrystallisation of trimethoprim from quenched 50%^{w}/w dispersions appeared sooner than with 10%^{w}/w dispersions, and were paralleled by the appearance of a DSC melting transition. A greater degree of recrystallisation of both drug and polymer occurred at the two highest storage temperatures, 37^{o}C and 45^{o}C, as determined by measurements of the enthalpy of melting (Fig. 3.20c.).

However, compared to the polymer alone, recrystallisation of PEG 4000 was slower in these dispersions.

Overall, it appears that the secondary crystallisation and lamella thickening processes, which occur in PEG 4000 on ageing are not affected by the presence of low concentrations of trimethoprim, and only inhibited to a relatively minor extent even at 50%^{w}/w trimethoprim. Conversely the recrystallisation of small amounts of amorphous drug is hindered within the polymer matrix, even at the higher storage temperatures. Recrystallisation of trimethoprim from dispersions containing high concentrations of drug occurs to a much greater extent and appears to be facilitated as the temperature of storage increases.

CHAPTER 4

CHAPTER 4 Investigation of Structure by Dielectric Spectroscopy

4.1. Introduction

4.1.1. General introduction

The technique of dielectric spectroscopy has been applied successfully to the study of the structure and properties of a wide variety of materials, including polymers. Furthermore, it has been demonstrated that alterations in structure arising from changes in the thermal history can be detected from studies of dielectric behaviour for polymers such as polyoxymethylene (McCrum et al, 1967), which is structurally related to PEG. It was hoped therefore, that the application of this technique to the study of PEG 4000 and its solid dispersions would yield additional information about their structure to that obtained from DSC and X-ray diffraction. Since dielectric measurements can be performed over a range of temperature in both the liquid and solid states, potential advantages exist over either of these methods. The following sections of this introduction outline the theories of dielectric behaviour and the measurement of dielectric response.

4.1.2. Polarisation and polarisation mechanisms

If an external electric field (E) is applied to a dielectric, then dipoles within the sample will attempt to align themselves in the direction of the field, thus giving rise to a net charge on the surface of the material. This effect, known as polarisation (P), can be defined in terms of the charge per unit area of the surface. Hence the response of a dielectric material to an electric field can be expressed as the difference in polarisation produced on the plates of a capacitor in a vacuum and in the presence of the dielectric.

Polarisation will be time dependent since dipole reorientation occurs at different times and is not instantaneous. The general response for any function which varies arbitrarily with time and which is assumed to be linear in the field is therefore given by the time superposition principle (McCrum et al (1967) as:

$$P(t) = \int_{-\infty}^{t} \Phi(t-t_0)\, E(t')\, dt' \qquad \ldots 4.1.$$

where $\Phi(t-t_0) = \Phi(t')$ is the response function which is defined according to the type of electric field applied. When the field takes the form of a delta function (Fig. 4.1.a.)

$$E(t') = E_o\, \delta(t) \qquad \ldots 4.2.$$

where E_o is the amplitude of the field, then $P(t) \equiv 0$ at $t<0$ (no response before application of field) and $P(t) \equiv 0$ at $t \to \infty$ (no permanent polarisation at infinite time after removal of field) and it is found that:

$$\Phi(t) = P(t) \qquad \ldots 4.3.$$

In other words, the response function can be expressed as the time dependency of polarisation following the application of a delta function field.

In the case where the field takes the form of a step function (Fig. 4.1.b.), defined as:

$$E(t') = E_o \text{ at } t>0 \qquad \ldots 4.4.a.$$

$$E(t') = 0 \text{ at } t<0 \qquad \ldots 4.4.b.$$

Then it can be shown that:

$$P(t) = \int_{o}^{t} \Phi(t')\, E_o\, dt' \qquad \ldots 4.5.$$

Thus $\Phi(t) = \frac{dP(t)}{dt} = J(t)$ defines the response function in terms of the current flow, $J(t)$, in the system. This forms the basis of time domain measurements for the determination of dielectric response.

Fig. 4.1. Types of Electric field and response to them

Type of field applied	Response defined in terms of:
Fig. 4.1a. Delta Function	
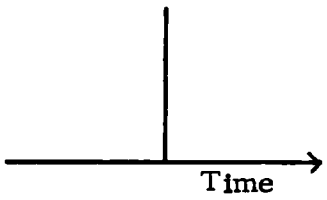	POLARISATION P(t)
Fig. 4.1b. Step Function	
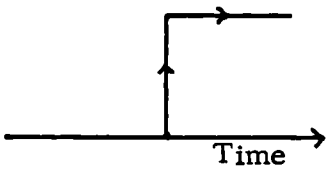	CURRENT J(t)
Fig. 4.1c. Oscillating	
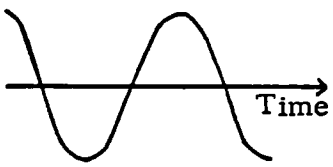	SUSCEPTIBILITY $\chi(t)$

Thirdly, when the applied field takes an oscillating form (Fig. 4.1.c.):

$$E(t') = E_0 \exp(i\omega t') \qquad \ldots 4.6.$$

ω = angular frequency

where $\exp(i\omega t) = \cos(\omega t) - i\sin(\omega t)$ ... 4.7.

Then equation 4.1. becomes:

$$P(t) = \int_{-\infty}^{t} \Phi(t-t_0)\, E_0 \exp(i\omega t')\, dt' \qquad \ldots 4.8.$$

which by Fourier transform, from time to frequency domain, yields:

$$P(\omega) = E_0 \exp(i\omega t)\ \chi(\omega) \qquad \ldots 4.9.$$

where $\chi(\omega) = \int_0^{\infty} \Phi(t') \exp(-i\omega t)\, dt$ ... 4.10

$\chi(\omega)$ is a complex function of frequency known as the dielectric susceptibility, which can be written in terms of its real and imaginary components as:

$$\chi(\omega) = \chi'(\omega) - i\chi''(\omega) \qquad \ldots 4.11.$$

When measurements are performed in the frequency domain, results are usually expressed in terms of capacitance (C) and loss (G/ω). These will be proportional to the real and imaginary parts of the susceptibility since the capacitance, as a function of frequency $C(\omega)$ can be related to $\chi'(\omega)$ by

$$C(\omega) = \frac{\epsilon_0 A}{d'} \left\{\chi'(\omega) + \epsilon(\infty)\right\} \qquad \ldots 4.12.$$

Similarly, the loss as a function of frequency $G(\omega)/\omega$ is linked to $\chi''(\omega)$ by the relationship:

$$G(\omega)/\omega = \frac{\epsilon_0 A}{d'}\ \chi''(\omega) \qquad \ldots 4.13.$$

$\epsilon(\infty)$ is the baseline response of the material and arises from polarisable elements within the material which respond instantaneously at the audio and lower frequencies used for measurement here. A is the area of the electrodes

on the sample and d'is the distance between them, therefore $\frac{\epsilon_0 A}{d'}$ is a constant for a particular experimental cell.

Molecular polarisation in a dielectric can arise from three different components which will respond at different frequencies. These are as follows:

(a) Electronic polarisation - where the application of an external electric field causes a small displacement of the electrons with respect to the nucleus. Only a small shift is seen because the applied field is relatively weak in comparison to the atomic field due to the nucleus. This type of polarisation occurs at optical frequencies and is responsible for such effects as the refraction of light.

(b) Atomic polarisation, here the application of an electric field can distort the arrangement of atomic nuclei within the molecule or lattice. As nuclei respond more slowly than electrons, this type of polarisation is not seen above infra-red frequencies.

(c) Orientational polarisation, if molecules possess permanent dipole moments, that is where the centres of gravity of the positive and negative charges do not coincide, then there is tendency for these to align within an applied electric field to give a net polarisation in that direction. For molecules with no permanent dipole moment, an induced net moment will be seen as the result of separation of centres of gravity of positive and negative charges. Orientational polarisation is seen at frequencies below those of the infra-red band.

A plot of molar polarisation as a function of frequency (Fig. 4.2.) will show that as frequency increases, there is a characteristic stepwise fall in polarisation as successive components become unable to relax quickly enough

Fig. 4.2. Dispersion of molar polarisation in a dielectric
From Blythe (1979)

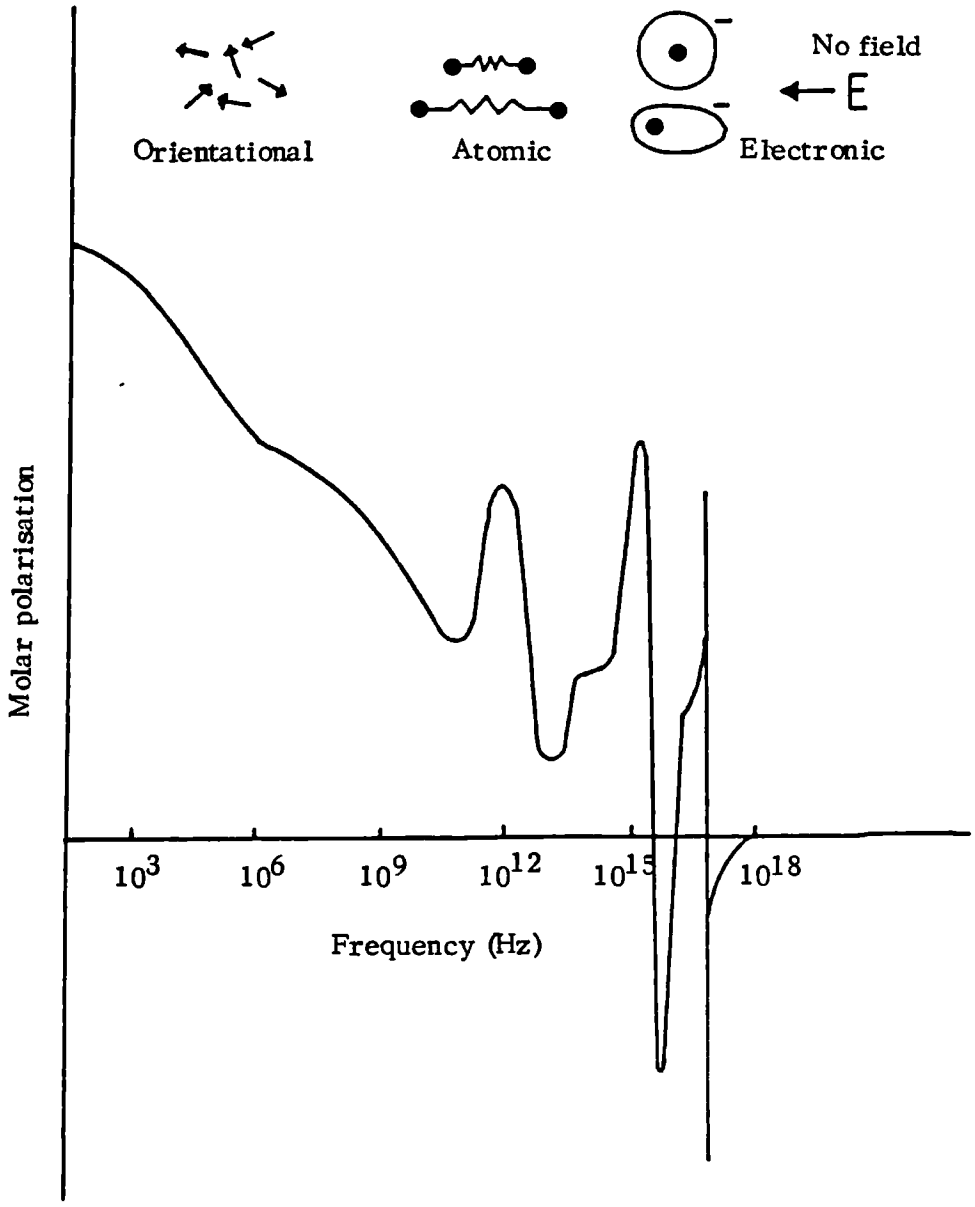

to contribute to the response. Elements which give rise to the electronic and atomic polarisation will respond instantaneously at the audio and lower frequencies used for measurements here and hence will only be observed as the baseline response, $\epsilon(\infty)$.

4.1.3. Debye Theory of Relaxation

Debye (1912, 1945) examined the dynamics of the response of a charged dipole embedded in a viscous medium and proposed a general model for all types of relaxation behaviour, whether it be acoustic, magnetic, dielectric or mechanical. His model is based on a physical approach which assumes dipole elements to be non-interacting, thus Boltzmann's superposition principle will apply. This states that the total magnitude of the susceptibility will be given by the sum of the responses and each exhibits an identical relaxation time. Approach to equilibrium will be exponential, therefore the decay of polarisation after excitation can be expressed as:

$$\frac{dP(t)}{dt} = -\frac{P(t)}{\tau} \qquad \ldots 4.14$$

τ is the characteristic Debye relaxation time for the polarisation process and is related to the viscosity of the medium. It is often an activated function of temperature.

$$\tau(T) = \tau_{\infty} \exp(\Delta/kT) \qquad \ldots 4.15.$$

Equation 4.14. has as its solution the decay function:

$$P(t) = P_0 \exp(-t/\tau) \qquad \ldots 4.16.$$

$$\text{or } P(t) = \chi(o)E \exp(-t/\tau) \qquad \ldots 4.17.$$

Where $\chi(o)$ is the magnitude of the real part of the susceptibility at zero frequency.

Equation 4.15. gives the response function $\Phi(t)$ as:

$$\Phi(t) = \chi(o)\ \tau^{-1} \exp(-t/\tau) \qquad \ldots 4.18.$$

Thus the corresponding frequency domain susceptibility function is:

$$\chi(\omega) = \chi(o)\ \tau^{-1} \int_0^{\infty} \exp(-i\omega t)\exp(-t/\tau)\, dt \qquad \ldots 4.19.$$

Which is equivalent to

$$= \chi(o)\ \left\{ \frac{1}{1+\omega^2\tau^2} - i\,\frac{\omega\tau}{1+\omega^2\tau^2} \right\} \qquad \ldots 4.20.$$

If $\chi(\omega)$ is written in terms of its real and imaginary components $\chi'(\omega)$ and $\chi''(\omega)$ as in equation 4.11., then:

$$\chi'(\omega) = \frac{\chi(o)}{1+\omega^2\tau^2} \qquad \ldots 4.21.$$

and

$$\chi''(\omega) = \frac{\chi(o)\,\omega\tau}{1+\omega^2\tau^2} \qquad \ldots 4.22.$$

The complex nature of the susceptibility function $\chi(\omega)$ reflects the delay of the response of the exponential time decay seen in Equation 4.16. Thus the Debye response can be characterised by two parameters, namely, the magnitude of the susceptibility, $\chi(o)$ and the relaxation time, τ .

If $\chi'(\omega)$ and $\chi''(\omega)$ are plotted as a function of frequency on a log-log scale, then the characteristic Debye dispersion curves in Fig. 4.3. are obtained. On this presentation, the dielectric loss curve $\chi''(\omega)$ is symmetrical about ωp, with a slope of +1 or -1 on both sides and a half height width of 1.144 decades. The maximum loss value occurs when $\omega\tau = 1$ and corresponds to a loss peak frequency of $\omega p = 1/\tau$. At frequencies lower than ωp, $\chi'(\omega)$ becomes constant with a limiting value of $\chi(o)$, while at frequencies higher than ωp, it decreases rapidly with a gradient of -2.

Fig. 4.3. Debye Dielectric dispersion curves

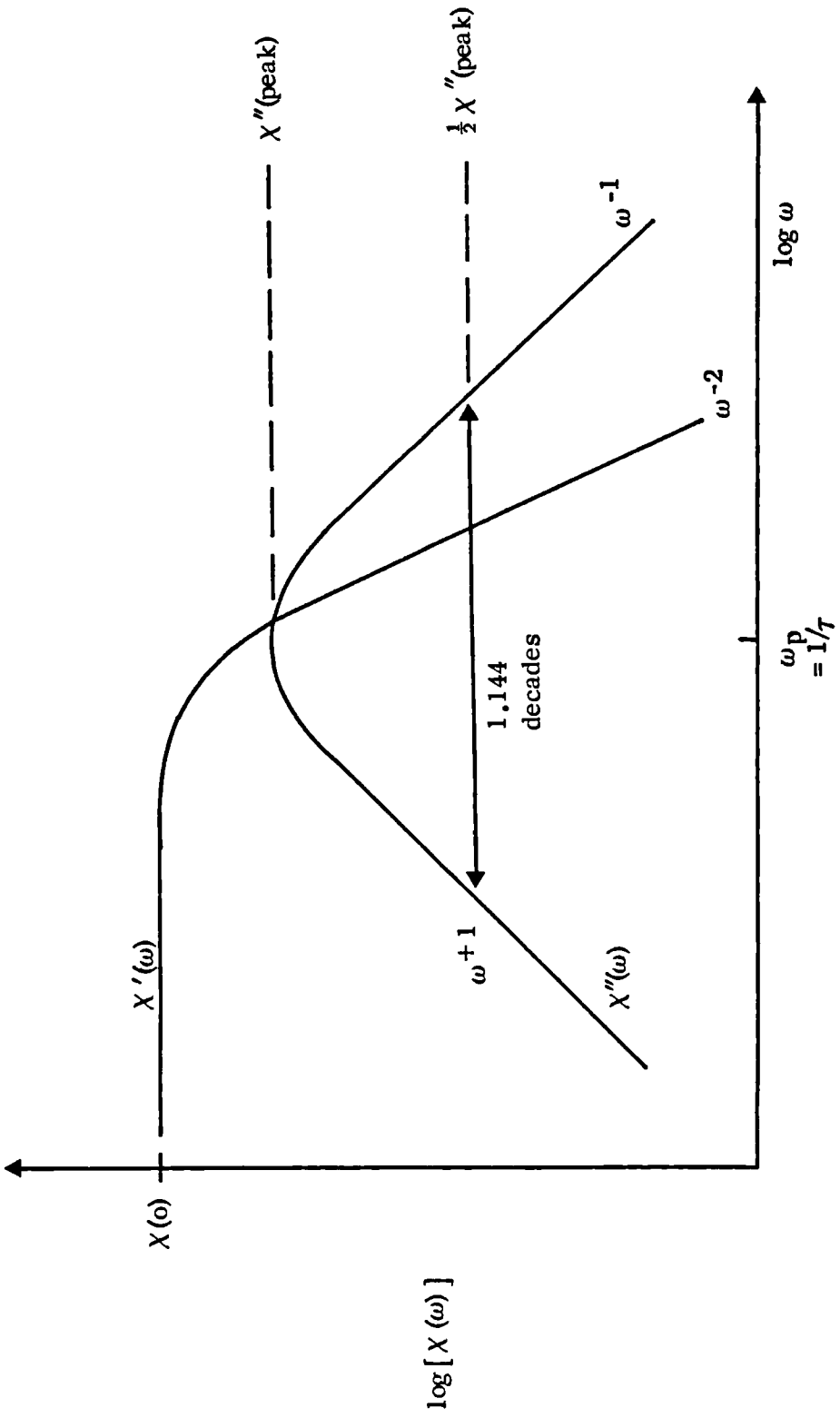

4.1.4. Other susceptibility presentations

Experimentally, Debye's model is found to apply only to systems such as weak concentrations of gases, where the conditions assumed by this theory, i.e. independently relaxing dipoles, hold true. Liquids and solids will always show deviations from the Debye response, since the particle-particle interactions present play an important role in relaxation. In real systems, the dielectric loss peak broadens to give a half height width much greater than the 1.144 decades seen in the Debye response. Furthermore, the loss peak maxima are lower than predicted and the loss curve may be asymmetrical.

This led Cole and Cole (1941) to propose a semi-empirical model to describe the observed behaviour, where they presented the data as a plot of $\chi''(\omega)$ as a function of $\chi'(\omega)$. For Debye's theory, this presentation gives a semi-circle passing from the origin in the complex susceptibility plane, diameter $\chi(o)$, and with its centre lying on the real axis of susceptibility (Fig. 4.4.).

The empirical relationship proposed by Cole and Cole to explain dielectric relaxation in polymers was of the form:

$$\chi(\omega) = \chi(0) \frac{1}{\{1 + (i\omega/\omega p)^{1-\alpha'}\}} \qquad \ldots 4.23.$$

α' was limited to values between 0 and 1 and was an experimental constant for the material under investigation. It was suggested that there was a range of relaxation times with a symmetrical distribution about τ. The empirical shape parameter, α', was introduced because it was realised that the two parameters of the Debye model were too restrictive to describe the experimental situation. When $\alpha' = 0$, the Debye response is recovered, but as $\alpha' \rightarrow 1$, the arc of the Cole-Cole plot becomes increasingly truncated

Fig. 4.4. Cole-Cole presentation of Debye response

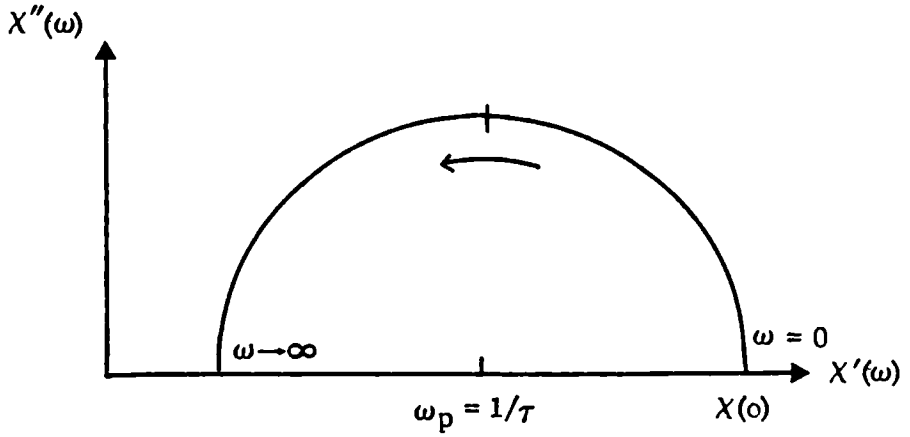

Fig. 4.5. Cole-Cole presentation when $\alpha' > 0$

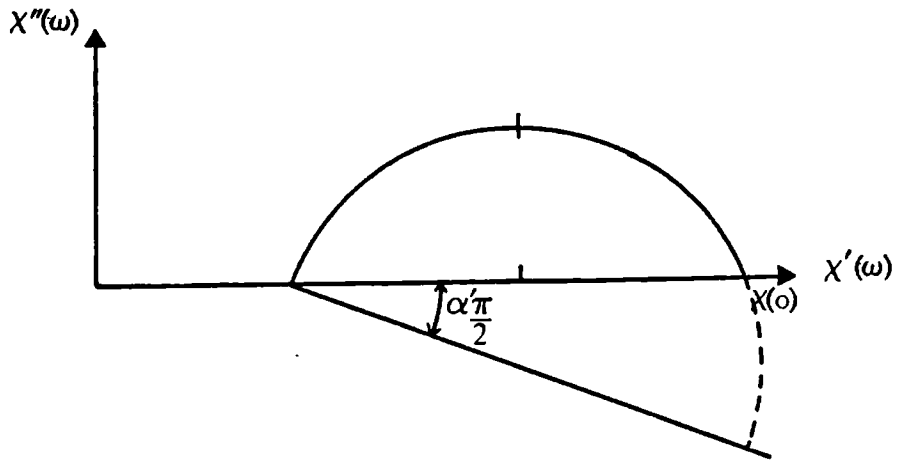

Fig. 4.6. Davidson-Cole response when $\beta' < 1$

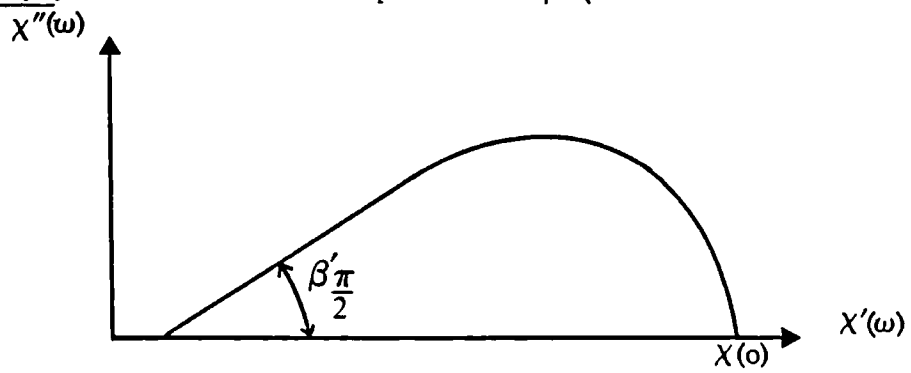

(Fig. 4.5.). This corresponds to the half width of the loss peak broadening and the loss peak maximum decreasing on the Debye dispersion curves. However, the power law behaviour, as seen in Equations 4.21. and 4.22., is still retained at the high and low frequency limits with respect to ωp. This proposed spread of relaxation times was seen as a likely explanation of the broadness of the relaxation in systems which consisted of long chain, tangled molecules, where a wide range of forces inhibiting the independent reorientation of dipole elements could be expected.

Davidson and Cole (1951) proposed a slightly different relationship, (Fig. 4.6.), where the distribution of relaxation times about τ is assumed to be skewed.

$$\chi(\omega) = \chi(0) \frac{1}{(1 + i\omega/\omega p)^{-\beta'}} \qquad \ldots 4.24.$$

Again, β' is a parameter between 0 and 1 and is constant for the material under investigation, the Debye response being obtained when $\beta' = 1$. Although no physical explanation of this relationship was proposed, it does provide a good fit to some sets of experimental data.

More recently, Cook, Watt and Williams (1970) suggested that the approach to equilibrium may not in fact be exponential as assumed by Debye, and that this could lead to the observed breadth of dispersion in polymers. A decay function was proposed as follows:

$$\Psi(t) = \exp(-t/\tau)^{\gamma'} \qquad \ldots 4.25.$$

Where γ' is a parameter between 0 and 1. This again shows good agreement with some sets of experimental data, but no physical explanation has yet been established.

However, some experimental results were found not to fit any of the single parameter empirical models proposed above. This led Havriliak and

Negami (1966) to propose the first bi-parametric susceptibility function, in order to fit data which tails off at the high and low frequency limits on a Cole-Cole plot (Fig. 4.7.).

$$\chi(\omega) = \chi(0) \frac{1}{[1 + (i\omega\tau)^{1-\alpha'}]^{\beta'}} \qquad \ldots 4.26.$$

Where $0 < \alpha' < 1$

$$\beta' < (1 - \alpha')^{-1}$$

Recently, Jonscher (1977) observed power law behaviour in a large number of materials in both the real and imaginary parts of the susceptibility function at frequencies higher than ωp, which are interrelated by the expression:

$$\chi'(\omega) = \chi''(\omega) \tan(n\pi/2) \propto \omega^{n-1} \qquad \ldots 4.27.$$

Where $0 < n \leq 1$

This relationship, known as the universal law of dielectric response, states that the ratio of energy lost per cycle to that stored per cycle is constant. Thus on a Cole-Cole presentation, this corresponds to a straight line on the high frequency side (Fig. 4.8.). The universal law can be derived from current many body theory, as will be shown later.

Hill (1978) proposed a more general empirical susceptibility formula which will give power law behaviour at frequencies below as well as above the loss peak frequency.

$$\chi(\omega) \propto \frac{\omega^m}{(\omega_p^{2s} + \omega^{2s})^{\frac{m+1-n}{2s}}} \qquad \ldots 4.28.$$

Where $1 < n, m, s < 0$

The constant, s, is only significant where $\omega \approx \omega p$.

It is important to remember that all the presentations described above, except Debye's, are empirical mathematical formulae which have no physical basis. They do not explain the causes of deviation from Debye's model.

Fig. 4.7. Cole-Cole plot showing tailing behaviour at high and low frequency limits

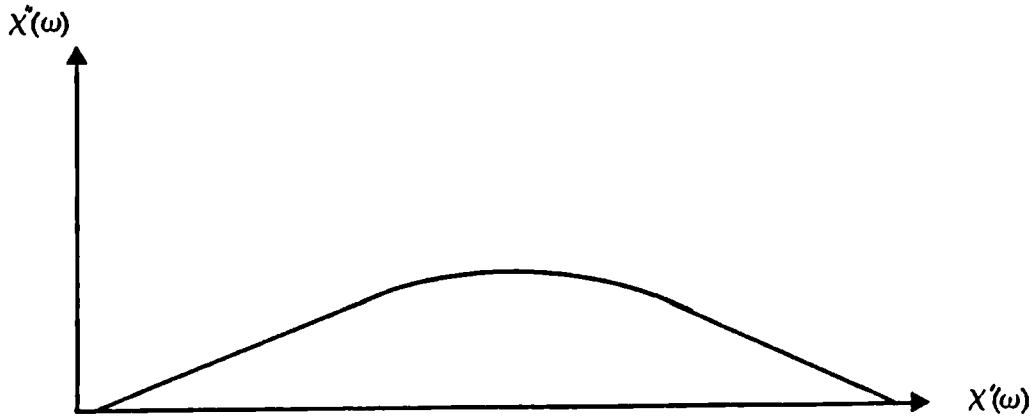

Fig. 4.8. Cole-Cole presentation of Jonscher's universal law of dielectric response

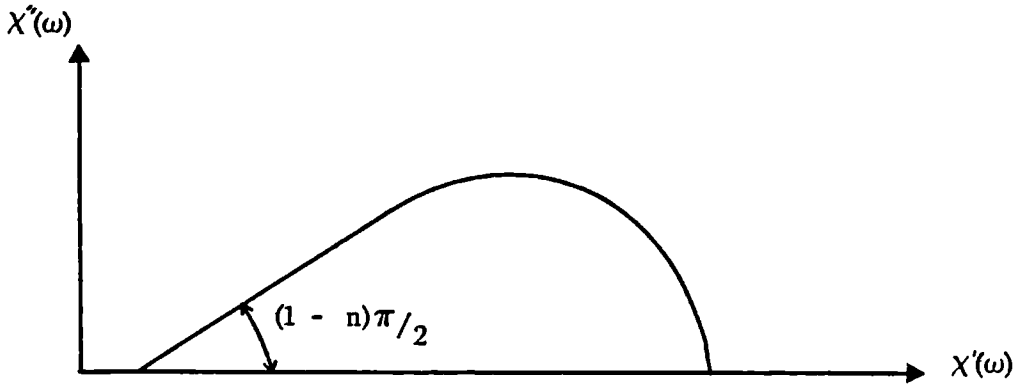

4.1.5. Dissado-Hill theory of dielectric response

This theory, based on the concept of a many body co-operative model is capable of giving a complete description of dielectric susceptibility. Furthermore, both Hill's empirical relationship and Jonscher's universal law of dielectric response can be derived mathematically from it.

Since particle-particle interactions are always present in solids and liquids, Dissado and Hill (1979) consider a system which consists of coupled particle displacement motions. As a consequence of this, relaxation of any particle must necessarily modify a group of others and thus its environment. This is in contrast to the Debye model which postulates independently relaxing dipoles. Moreover, it is assumed that the system has locally correlated motion up to some finite extent. The spatial extent of these local vibrational modes can be defined as a cluster. Not all clusters are identical, giving rise to a dynamic distribution of cluster types. Hence, over a period of time, each cluster will adopt all the possibilities allowed within the cluster system. This is not equivalent to the distribution of relaxation times proposed by Cole and Cole (1941) as an explanation for non-Debye behaviour. These authors stated that although the environments of the particles were different, they were not modified during relaxation, i.e. there was a static distribution of environments.

Dissado and Hill (1979) noted that correlated motions in clustering systems, such as ferromagnetics, are known theoretically to give t^{-n} behaviour for the relaxation of dipole displacements. Secondly, they noted that the origin of the fractional power law behaviour lay in the time development of the probability of finding the particles of the cluster at their original displacements. These concepts have been developed by Dissado and Hill to form the basis of

their general model for relaxation. It should be remembered that this theory does not only apply to dielectric phenomena, but can also be used to explain other types of relaxation behaviour, e.g. mechanical.

The formal relaxation function of the cluster is proposed to be (Dissado and Hill, 1979, 1983):

$$\langle \Phi(t) \rangle \propto \omega_p \exp(-\omega_p t) t^{-n} \; {}_1F_1 \; (1 - m; 2 - n; \omega_p t) \quad \ldots 4.29.$$

with ${}_1F_1$ (; ;) the confluent hypergeometric function (Slater, 1960). This gives the susceptibility as:

$$\chi(\omega) \propto \left\{ \frac{\omega_p}{\omega_p + i\omega} \right\}^{1-n} \; {}_2F_1 \left(1 - n, 1 - m; 2 - n; \frac{\omega_p}{\omega_p + i\omega}\right) \quad \ldots 4.30.$$

with ${}_2F_1$ (, ; ;) the Gaussian hypergeometric function (Slater, 1966).

Equation 4.28. shows that at frequencies higher than ω_p, both the real and imaginary parts of the susceptibility are proportional to ω^{n-1}, which is identical to the relationship proposed by Jonscher (1977) and Hill (1978). At frequencies lower than ω_p, the imaginary part of the susceptibility function is proportional to ω^m and the real part to $\chi'(0) - A' \chi''(\omega)$, where A' is a constant. This again is in agreement with Hill's (1978) empirical relationship.

Jonscher (1978) has also identified a new type of response found in dipolar systems formed from charge carriers, which may move from their original clusters or sites. The polarisation response, due to charge separation over substantial distances, seen in these systems has been termed low frequency dispersion (L.F.D.) and its susceptibility function can be defined as (Dissado and Hill, 1984a):

$$\chi_{LFD}(\omega) = N_S \left(\frac{\delta e a}{kT}\right)^2 \frac{\Gamma(1 - p - n)}{\Gamma(1 - n)\Gamma(1 - p)} \; F(\omega/\omega_c) \quad \ldots 4.31.$$

Where N_S is the number density of occupied sites and $F(\omega/\omega_c)$ is the dielectric shape function equivalent to:

$$\left\{ \frac{\omega_c}{\omega_c + i\omega} \right\}^{1-n} {}_2F_1 \left(1 - n, 1 + p; 2 - n; \frac{\omega_c}{\omega_c + i\omega}\right) \quad \ldots 4.32.$$

The Dissado-Hill theory can be outlined as follows:

(1) Materials that exhibit dielectric relaxation will contain structural imperfections and thus, on a localised scale, the existence of groups of dipoles (clusters) can be expected.

(2) The motion of any particular cluster can be organised into a hierarchy of sub-units which are arranged according to the number of irreducible dipole elements they contain. Also, the motion of each of the sub-units takes place in the rigid environment of all other elements of the cluster. Each dipole element is involved in a fraction of all possible sub-unit motions. These range from the element behaving as an independent dipole, up to the whole cluster as a rigid body. From these considerations, Dissado and Hill (1979) have calculated that the probability of finding a dipole element in its original displacement is t^{-n}, where the parameter n lies between 0 and 1 and indexes the extent to which dipole displacements are correlated. Alternatively, it is possible to define n in terms of the degree to which the structural organisation of a sub-unit is reproduced by increasing its size to a sub-unit of larger number, i.e. a scaling index. In practice, n will always be less than unity because the dipole elements constituting the cluster do not have full translational symmetry.

Recently, Dissado (1984) has related the process giving rise to the t^{-n} behaviour to the change in configurational entropy of the cluster as a specified configuration relaxes. This provides a link between the Dissado-Hill theory and the thermodynamics of relaxation, thus emphasizing the

relationship of the result to environmental changes during relaxation.

(3) Cluster fragmentation and coalescence is allowed by Dissado-Hill theory as follows. Correlation of sub-unit motions with those of other clusters in the cluster array can take place, usually in a different co-ordinate to that of the local cluster. This produces a description of the cluster ensemble in terms of a dynamically fluctuating system, with an instantaneous distribution of cluster types. The long time decay, $t^{-(1+m)}$ is due to the influence of these fluctuations on the random thermal contributions to the cluster relaxation. The index m ($\equiv$ p) is a measure of the degree to which clusters interact, i.e. a measure of the extent and correlation of transfer processes between clusters. This index defines the shape of the distribution, (Fig. 4.9.).

It can be seen that the case of $m = 0$ refers to the case where all clusters are identical and that the distribution changes continuously from this delta function to the case of $m = 1$, which is exponential over the range $0 < y < \infty$. These distributions describe the fluctuations that arise from inter-cluster transfers.

Dissado and Hill (1984b) have recently shown that the recovery of the dynamic steady state distribution during relaxation can be described by the evolution of an array configurational entropy, at the expense of individual cluster configurational entropies during the relaxation phase in which excess energy is returned to the heat bath. In this way, the thermodynamic causes of relaxation can be seen to determine the experimentally observed relaxation behaviour.

Thus the Dissado-Hill theory as outlined above offers a new and fundamental approach to the understanding of dielectric relaxation. This model will

Fig. 4.9. Distribution of fluctuations for the parameter m(≡p) (Hill et al, 1981)

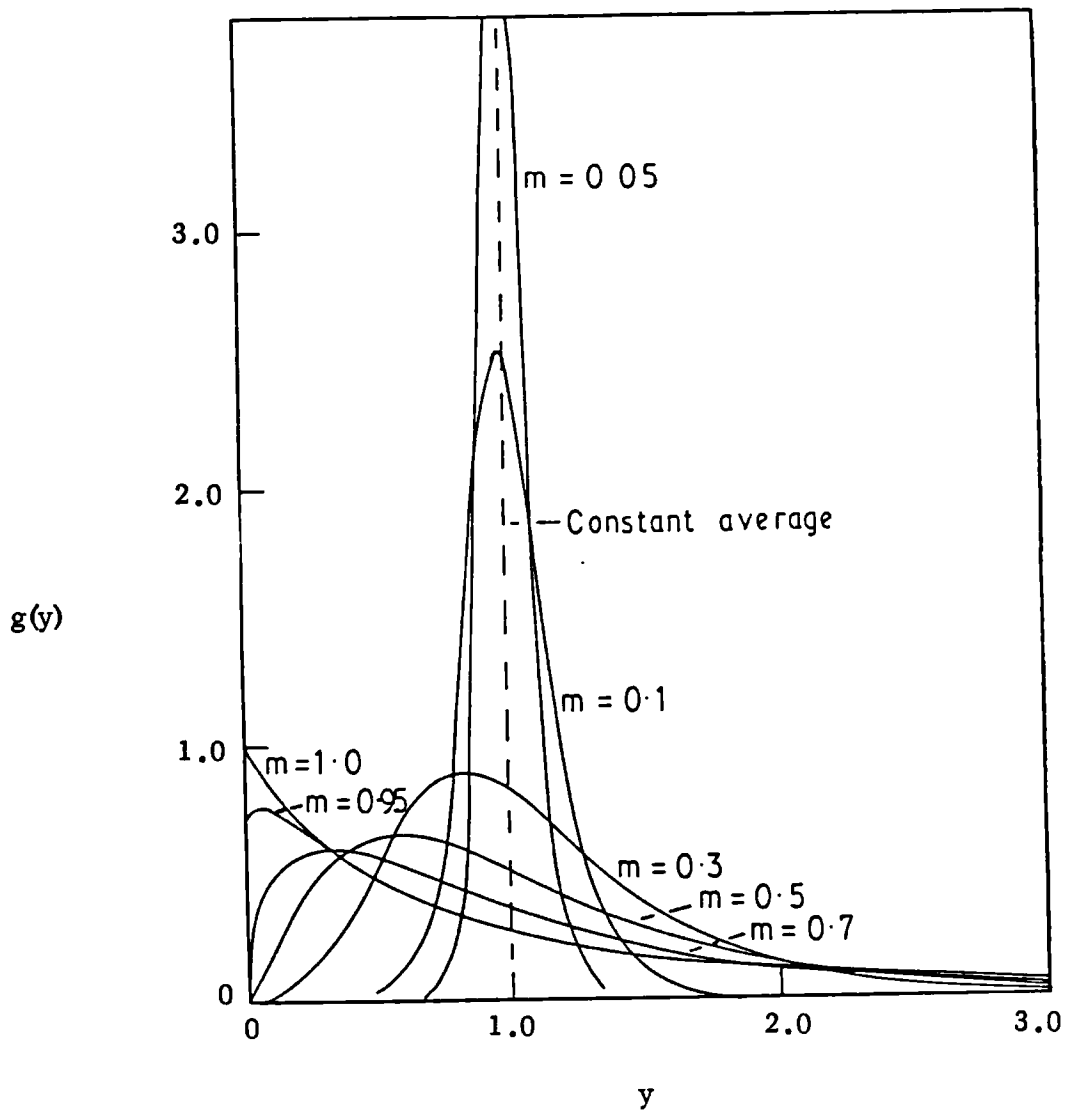

therefore be used to interpret the experimental data obtained from the work on PEG 4000 and its solid dispersions with Trimethoprim.

4.1.6. Dielectric relaxation in polymers

Several discrete relaxation processes, which arise from the different types of molecular motion, can often be distinguished in polymers in the solid state. A scan of dielectric loss at constant frequency with increasing temperature often reveals several loss processes. These are associated with the different molecular mobilities becoming energetically favourable, hence enabling dipole elements to reorientate and contribute to the dielectric response. By convention, dielectric relaxation processes are arbitrarily labelled as α, β, γ, etc., starting from the high temperature end (Fig. 4.10.). On a frequency scan, this is equivalent to starting at the low frequency limit and working upwards in frequency.

Different relaxation processes will be associated with the amorphous and crystalline regions of the polymer and either one or both types may be present. The symbols α, β, γ are used to describe processes in both regions, but it should be remembered that this does not imply that the same molecular mechanisms are responsible in each case. The same relaxation processes are generally thought to be occurring in both the dielectric and mechanical dispersions observed in polymers, but the relative magnitudes of the response may be different. Thus, in a semi-crystalline polymer such as PEG 4000, the relaxation spectrum may be complex. In order to aid identification of the phase from which any relaxation process arises, the physical structure of the polymer can be altered by, for example, varying the rate of cooling from the melt. If polytetrafluoroethylene (PTFE) is taken as an example, the unheat-treated material shows a strong α crystalline

Fig. 4.10. Schematic dielectric loss curve at constant frequency (Blythe 1977)

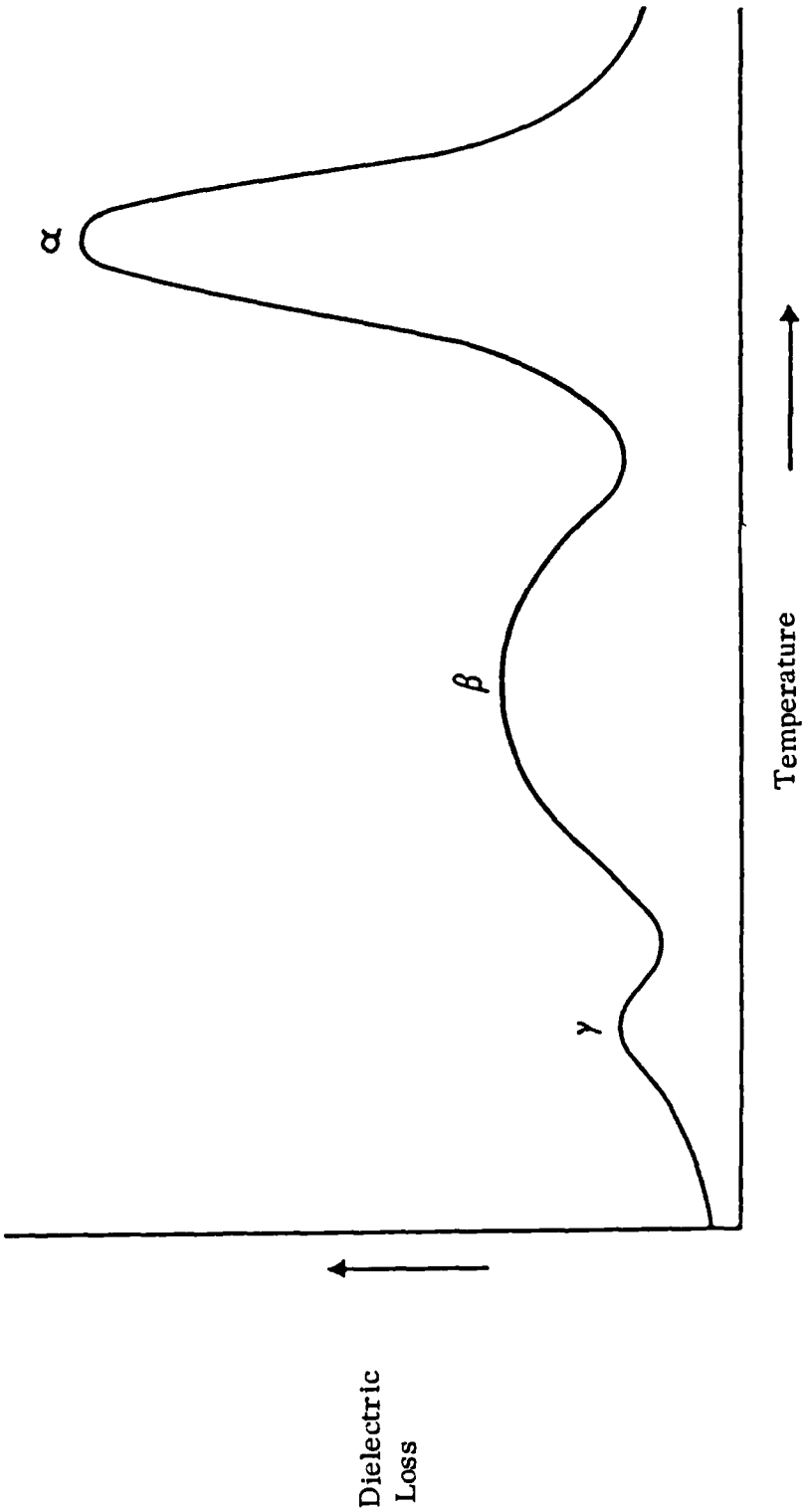

relaxation (Fig. 4.11.). The magnitude of this process is enhanced by annealing as the degree of crystallinity increases, whereas quenching the material to the amorphous form will decrease the magnitude of the response. Conversely, for relaxation processes arising from molecular motions within the amorphous phase, annealing the material would have decreased and quenching increased the observed response.

In the liquid state, the polymer will exist as randomly orientated, tangled chains with a high degree of molecular mobility. However, there will be little coordinated molecular motion.

4.1.7. Dielectric relaxation in a solid dispersion

The effect of adding a second component, such as a drug, to the polymer is difficult to predict and is complicated by the fact that the drug may exhibit a separate dielectric response. Thus three possibilities exist - the relaxation processes associated with either material may be enhanced, inhibited or unaffected by the presence of the other component. This would depend largely on the configuration and orientation adopted by the two components relative to each other as well as on their chemical structure. It is envisaged that the degree to which the response is affected could well be dependent on the concentration of drug to polymer.

Fig. 4.11. Temperature dependence of dielectric loss tangent at 10^3 Hz in the α_c relaxation region for three samples of polytetrafluoroethylene(PTFE) (Krum and Müller, 1959)

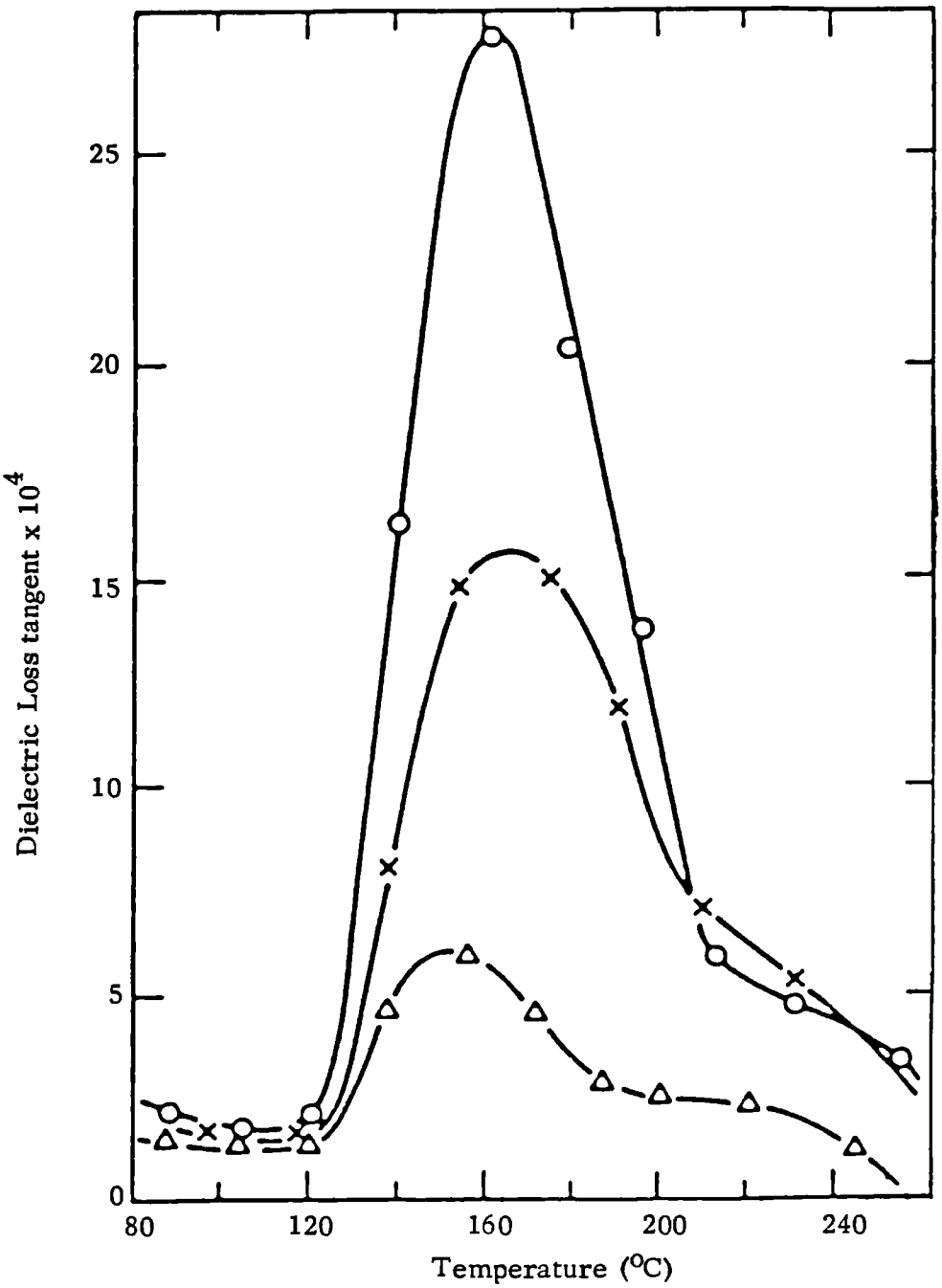

Key

× Unheat-treated sample
△ Quenched sample - most amorphous
○ Annealed sample - most crystalline

4.2. Methods

4.2.1. Dielectric Measuring System

4.2.1.1. Dielectric cell and temperature control

The work here was performed using a dielectric cell consisting of two nominally plane and parallel stainless steel electrodes mounted in a copper jacket, (Fig. 4.12.), which is a design that previous studies (Shablakh, 1982) have shown to be optimal for this type of system. This cell was positioned on a copper heating block from which it was electrically insulated by a thin mica sheet. The temperature was controlled by a platinum resistor temperature sensor mounted in the heating block and a Eurotherm controller connected to a specially designed Servo power supply; a method which has been shown to be accurate to better than + or -0.5°C, (Shablakh et al, 1982). The dielectric cell, heater and leads were placed inside an Edwards high vacuum system and evacuated to 10^{-1} Torr. This degree of vacuum was found to be adequate to avoid water vapour condensing on the leads at low temperatures. The sample, however, remained at atmospheric pressure within the cell.

4.2.1.2. Frequency Domain Measurements

A computer controlled frequency response analyser (F.R.A.) was used which measures the voltage across and current flowing through a dielectric sample in response to an applied a.c. field, over a frequency range from 10^{4} to 10^{-4} Hz. Loss angle ($\tan \delta$) resolution is better than 10^{-3} for most practical applications (Morse, 1974). A schematic diagram of the system and peripheral instruments is given in Fig. 4.13. A variety of software was available and the programmes used will be discussed later. The results

Fig. 4.12. Dielectric Cell

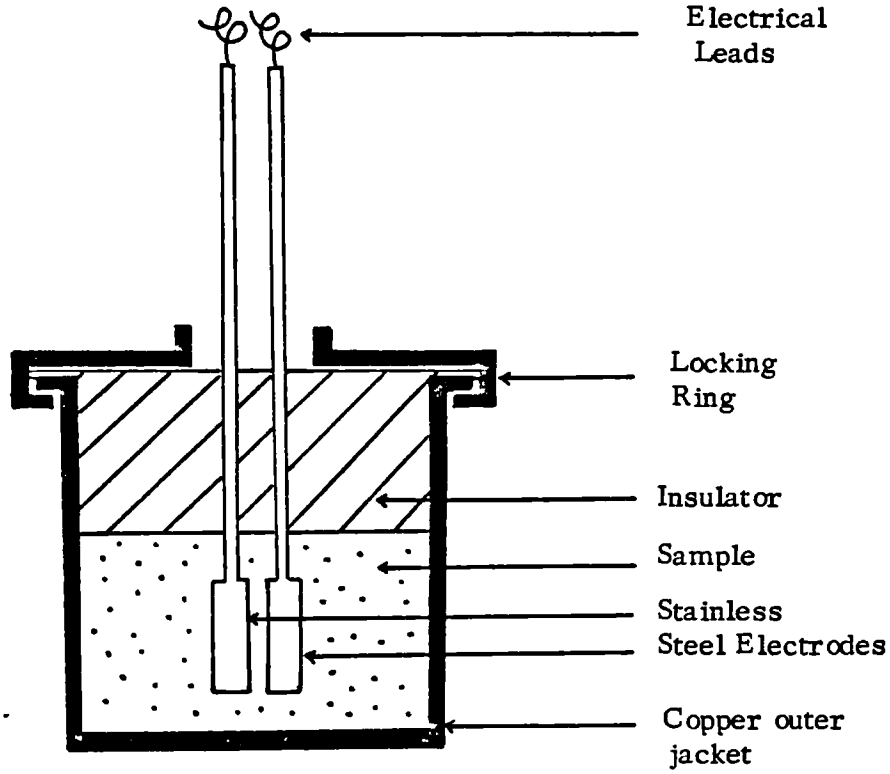

Fig. 4.13. Diagram of computer controlled frequency response analyser and peripheral instruments

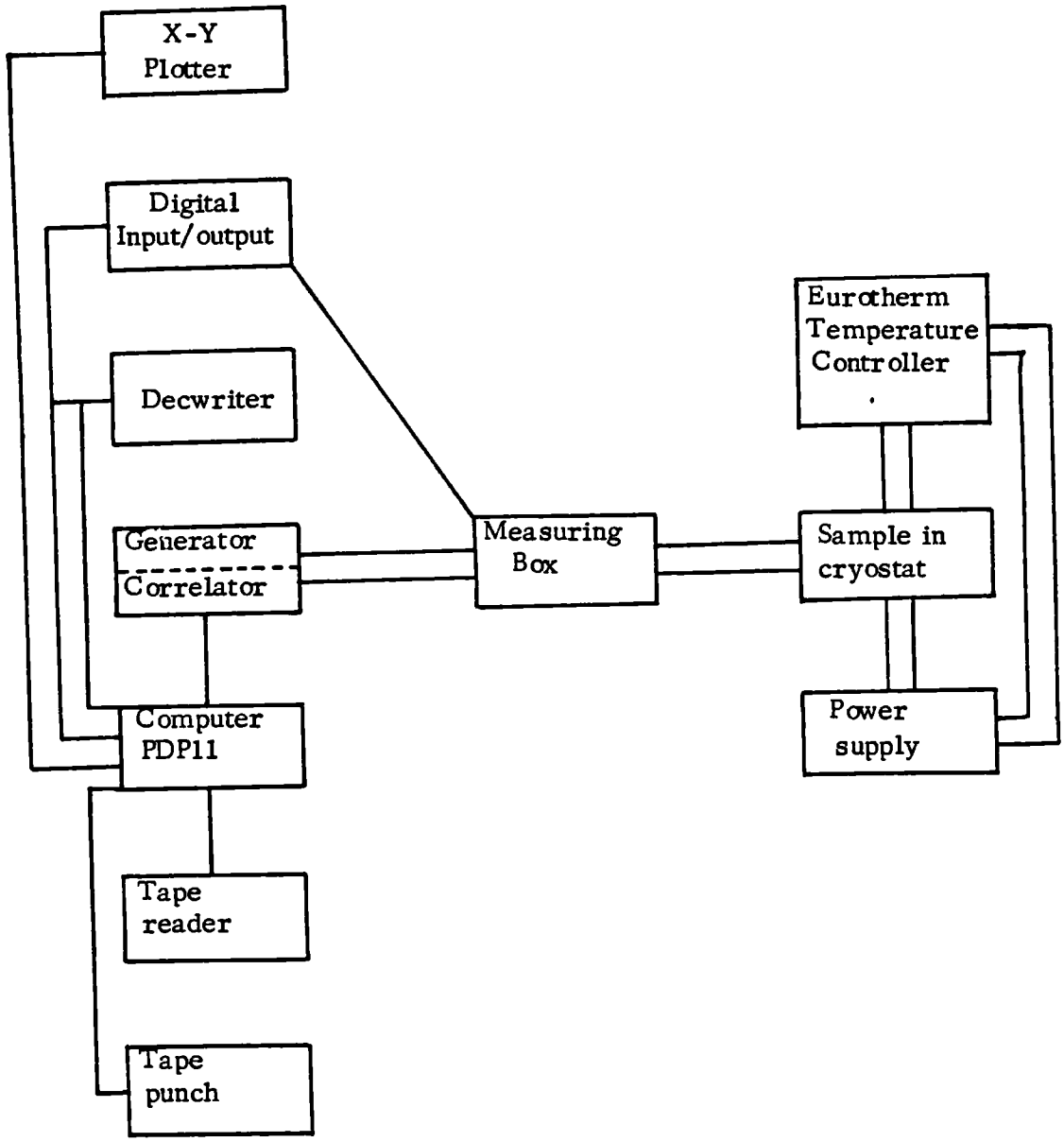

obtained were recorded on tape, as a print-out and plotted on an X-Y recorder.

4.2.1.3. Principle of Operation of the F.R.A.

The F.R.A. consists of two main parts - a generator and a correlator. Sine waves of a previously programmed amplitude are produced by the generator using one of two methods according to the region of frequency in which it is operating. Above 150 Hz, smooth sine waves are produced by conventional techniques. Below this frequency, waveforms are synthesized digitally, giving a sine wave signal consisting of 2000 staircase steps per cycle. Smoothing of step edges, which would otherwise degrade the signal, is effected by means of a low pass filter, positioned at a suitable point in the measuring circuit. The signal is then applied across the dielectric sample, in series with a suitable resistor/capacitor combination, which is selected automatically by the measuring box as that which gives the most effective standard impedance for that sample and frequency. The correlator then determines the in phase and quadrature components of the input signal with respect to a reference signal produced by the generator. Following this, the results are processed by the computer and recorded as required.

4.2.2. Types of experiments

The following methods were used to study the dielectric response of PEG 4000, trimethoprim and systems containing various proportions of both.

(i) Frequency scans - Capacitance and loss were measured over a range of frequency at intervals in temperature of 10K from 363K to 223K for both heating and cooling cycles. All samples containing PEG 4000, both with and without the drug were heated at 363K for 1 hour prior to

measurement to ensure complete randomisation of polymer chains and thus remove any possible influence of thermal history.

(ii) Capacitance as a function of time - At a previously selected frequency and temperature, changes in capacitance were recorded against time. This type of scan was used to study the time dependence of the phase changes, either melting or crystallisation, of PEG 4000 on its own and in the presence of the various concentrations of trimethoprim.

4.2.3. Circuit analysis of the response

The data obtained can be presented as a dielectric circuit response for each temperature. A dielectrically active circuit can be described in terms of a dispersive process, a parallel "infinite frequency" capacitance and a parallel resistance or conductance, (Fig. 4.14.). The dispersive element can be characterised by four parameters:

(i) The characteristic frequency, ω_p, which is the relaxation rate for the process being observed.

(ii) The zero frequency susceptibility magnitude, $C_{(0)}$, which is a measure of the strength or number of responding elements.

(iii) Two Dissado-Hill spectral shape parameters, n and m, where n indexes the degree of local structural order and m the efficiency of the intercluster exchange process.

A computer curve fit procedure is used to obtain the magnitude of each of the individual elements.

Since the measurement of dielectric response requires electrodes to be positioned on the sample, in this instance on opposite faces, then it is necessary to consider two such elements in series with each other. This allows for the effect of the contacts on the sample, e.g. there may not be

Fig. 4.14. Typical dielectric circuit

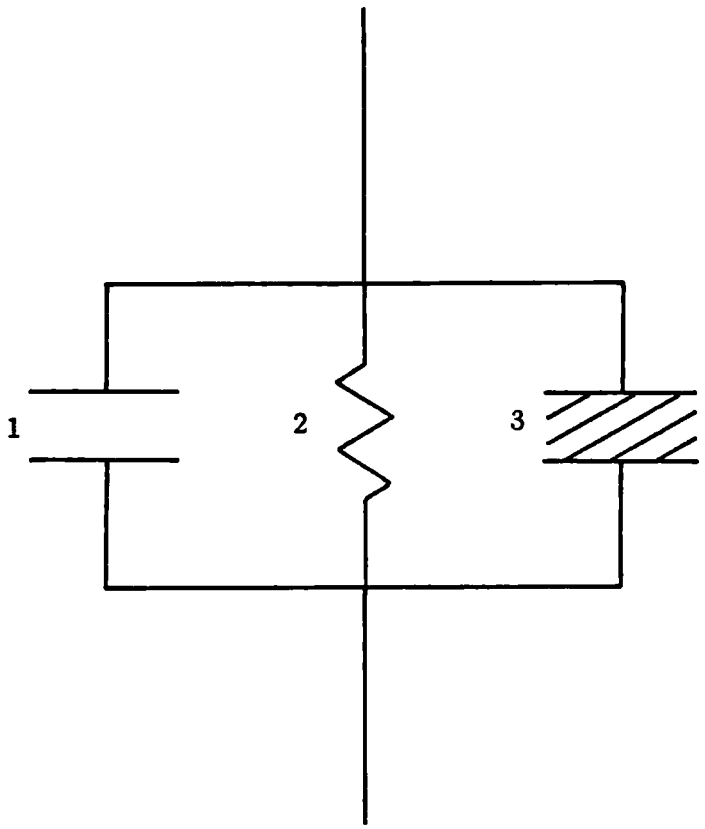

1 Frequency dependent or dispersive capacitance

2 Frequency independent or infinite frequency capacitance

3 Resistance ($\equiv$ 1/conductance)

a perfect exchange of charge between the electrodes and the material. The sample is assumed to have a bulk response, associated with the bulk of the material, and a surface response associated with the two regions in the proximity of the electrodes. The response of each of the surface elements is assumed to be equivalent in the presence of an a.c. field.

Dielectric circuit analysis allows complete characterisation of the response in terms of the parameters discussed above, which can then be interpreted in terms of their physical basis to give useful information on the structure of the material under investigation.

4.3. Results and discussion

4.3.1. PEG 4000

4.3.1.1. PEG 4000 liquid

Since the dimensions of the experimental cell cannot be measured as accurately as the dielectric response, the results are presented in terms of capacitance (C) and loss (G/ω) which, apart from geometric scaling factors, are identical to the real and imaginary parts of the susceptibility function $\chi(\omega)$. Where possible, the dielectric measurements are subjected to a normalisation technique (Ferry, 1970; Hill, 1978) in which the sets of results obtained from the frequency scans at different temperatures are rescaled in frequency and amplitude to produce a master response curve. Normalisation of the results is only possible where the different components which give rise to the overall response exhibit the same temperature dependence with respect to each other. If a datum point is recorded from the frequency scan at each temperature, then the relative shift of the response with each temperature can be observed and used to determine the temperature

dependence of the characteristic frequency and amplitude.

Frequency scans of PEG 4000 equilibrated at 363K gave a response which characterised the liquid state. Values of capacitance and loss both rise with decreasing frequency and the behaviour of the liquid appears to be dominated by a R-C circuit combination at low frequencies, while towards the high frequency end, the capacitance tails off to a limiting value. This behaviour persisted down to temperatures of 323K, as can be seen from the composite graph in Fig. 4.15. Normalisation of the data from the liquid phase proved difficult as the components of the frequency response showed different shifts relative to each other as the temperature changed.

From dielectric circuit analysis, it was found that the data could be modelled in terms of the circuit diagram given (Fig. 4.15.) that is by:

(i) A frequency dependent barrier of surface capacitance (C_s) in series with

(ii) A frequency independent capacitance (C_∞) and

(iii) A conductance (G_b) which arises from a d.c. charge transport process. Both (ii) and (iii) were associated with the bulk response.

The values of the individual characteristic parameters at different temperatures are given in Table 4.1. and were obtained by the curve fitting procedure outlined in Chapter 4.2.3.

From the circuit analysis it can be seen that there are two components to the dielectric response - one associated with the bulk and one associated with the region adjoining the electrodes. The bulk response is dominated by a high conductance arising from a d.c. charge transport process which is unusual in saturated organic polymers of this type, being approximately nine orders higher than that of its closest homologue, polymethylene oxide

Fig. 4.15. Composite graph of frequency response molten PEG 4000, scaled at 323K

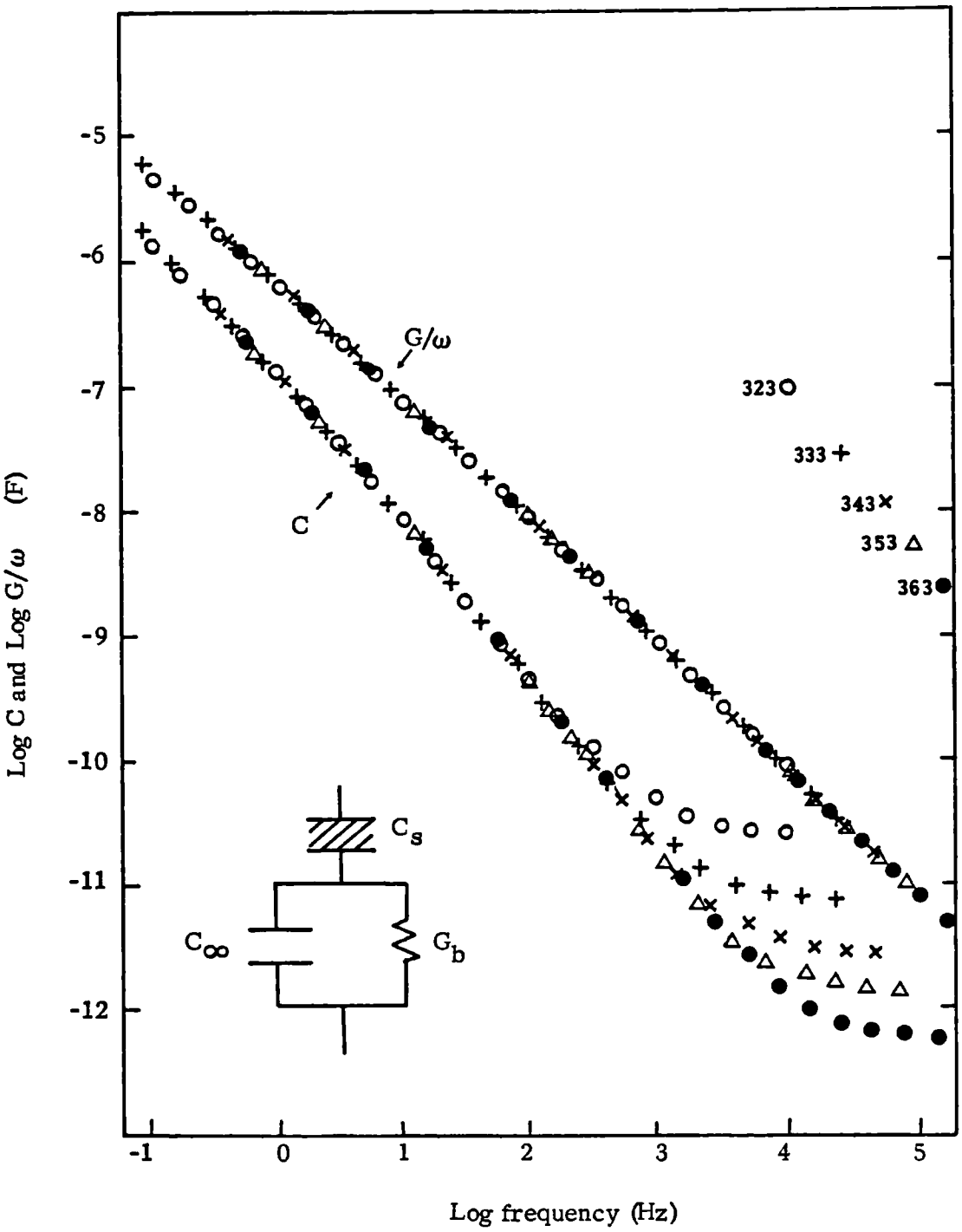

Table 4.1. Characteristic dielectric circuit parameters of molten PEG 4000 at different temperatures

Temperature (K)	Parameters associated with barrier capacitance				Bulk response	
	Dissado-Hill parameters		ω_p (Hz) x 10^5	C(0) (F) x 10^4	C_∞ (F) x 10^{11}	G(Ω^{-1}) x 10^6
	m	n				
323	-	0.3	25	7.5	3	5.9
333	-	0.3	10	30	2.5	9.4
343	-	0.3	5	70	2.6	11
353	-	0.3	2.6	150	2.5	11.5
363	-	0.3	1.4	300	2.5	13

(Binks and Sharples, 1968). Conductances of this magnitude are usually only observed in more complex polymeric structures such as those which contain double bonds, where electronic conduction processes can occur through overlapping π orbitals. It has, however, been established (Binks and Sharples, 1968) that this high conductance is not due to the presence of sorbed water or any ionogenic impurities which might be left from the polymerisation process and is thus an inherent property of the material.

The temperature dependence of the bulk conductance was determined by constructing an Arrhenius plot from the data at different temperatures (Fig. 4.16), excluding that obtained at 323K, since the graph becomes non-linear as the crystallisation temperature is approached. From this, the activation energy of the process was calculated to be 0.106 eV. In the molten state, the polymer chains possess considerable flexibility and mobility and have no preferred direction of orientation (Maxfield and Shepherd, 1975). The decrease in the conductance with decreasing temperature indicates that the d.c. charge transport process from which it arises becomes more difficult as the temperature is lowered. This is consistent with the polymer chains becoming less mobile as the crystallisation temperature is approached. The activation energy of 0.106 eV corresponds to a wavelength of approximately 851 ν cm^{-1}. No absorption at this wavelength is seen for polyethylene glycol in the molten state when investigated by Raman spectroscopy (Koenig and Angood, 1970). However, I.R. spectroscopy reveals a band at 855 ν cm^{-1}, which corresponds to a CH_2 rocking movement and a C-O bond stretch (Matsuura and Miyazawa, 1969). Molecular motion observed at this frequency thus involves a change in dipole moment and is therefore likely to be involved in the charge transport process.

Fig. 4.16. Arrhenius plot for d.c. charge transport process in molten PEG 4000

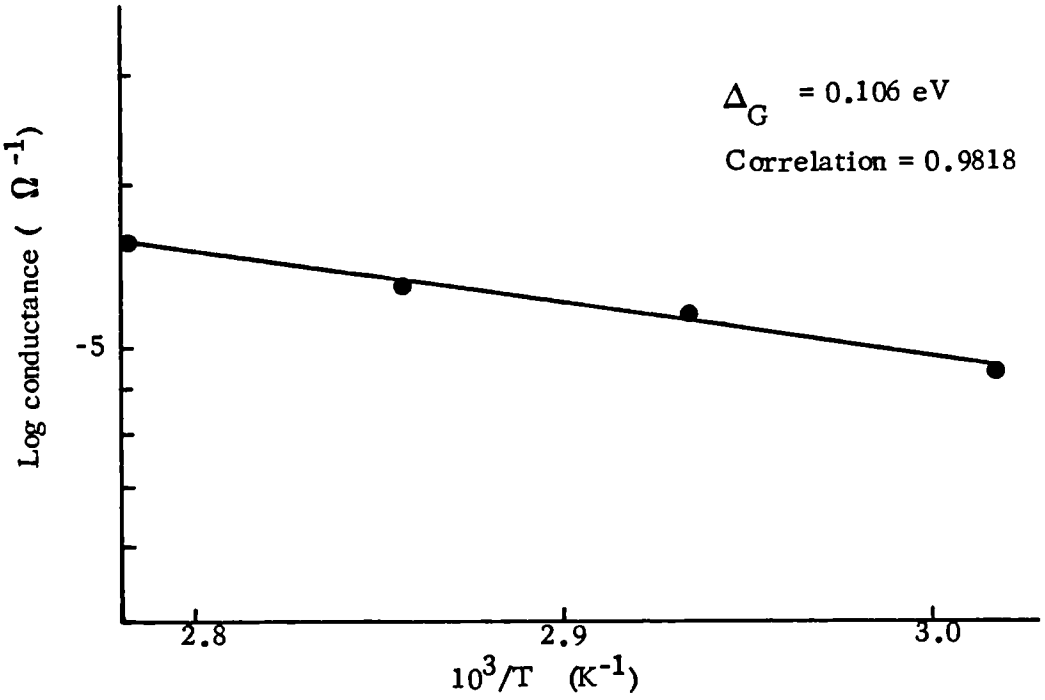

It has been suggested that the conductance may occur through one of two possible mechanisms. NMR spectroscopy has revealed that one relaxation route occurs via the flip-flop process in Fig. 4.17. (Kimmich and Schmauder, 1977) requiring an activation energy of 0.113 eV, similar to that calculated here. This movement would allow transport of charge through the system by the interaction of oxygen atoms along the polymer chain and correlates well with the suggested involvement of the molecular motion observed by I.R. spectroscopy. Alternatively, charge may pass through the system by the mechanism of inherent proton generation proposed by Binks and Sharples (1968). They suggested that protons are removed from the polymer chains and transported via the ether oxygen atoms through local segmental motions such as molecular rotations. Again, it is very likely that this mechanism would involve the CH_2 rocking and C-O stretching movements implicated by I.R. data. The proposed transport mechanism for protons is illustrated in Fig. 4.18a. and that for the negative charge in Fig. 4.18b.

The behaviour of the polymer in the region adjoining the electrodes differs from that observed for the bulk material, in that it is a non-conducting layer which only allows a slow dielectric relaxation. Arrhenius plots constructed for the loss peak frequency (Fig. 4.19.) and loss peak magnitude (Fig. 4.20.) of the barrier response gave activation energies of -0.683 and 0.800 eV respectively. The temperature dependence of the loss peak frequency is unusual in that the relaxation rate appears to increase as the temperature decreases. The apparent activation energy of the loss peak frequency ($\Delta\omega_p$) of the barrier relaxation can be related to the activation energies of the bulk conductance (Δ_G) and barrier loss peak magnitude (Δ_C) since:

Fig. 4.17. Relaxation route from which the charge transport process in molten PEG 4000 could arise (Kimmich and Schmauder, 1977)

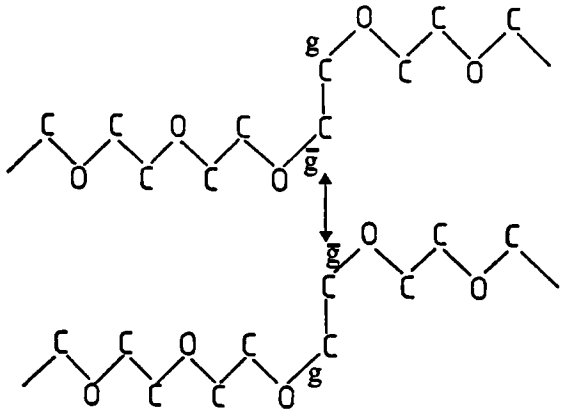

g, $\bar{g}$ are positive and negative gauche conformations

Fig. 4.18a. Ionic proton transport mechanism from which charge transport in molten PEG 4000 could arise (Binks and Sharples, 1968)

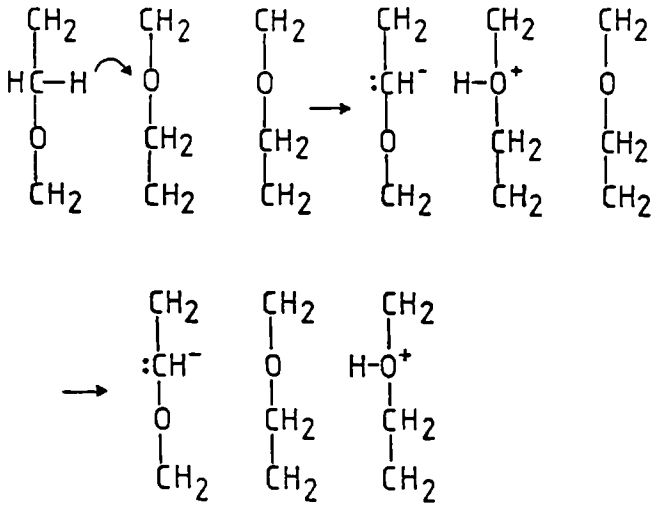

Fig. 4.18b. Mechanism for the transport of negative charge in molten PEG 4000

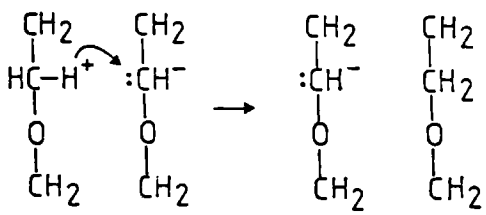

Fig. 4.19. Arrhenius plot of the barrier loss peak frequency in molten PEG 4000

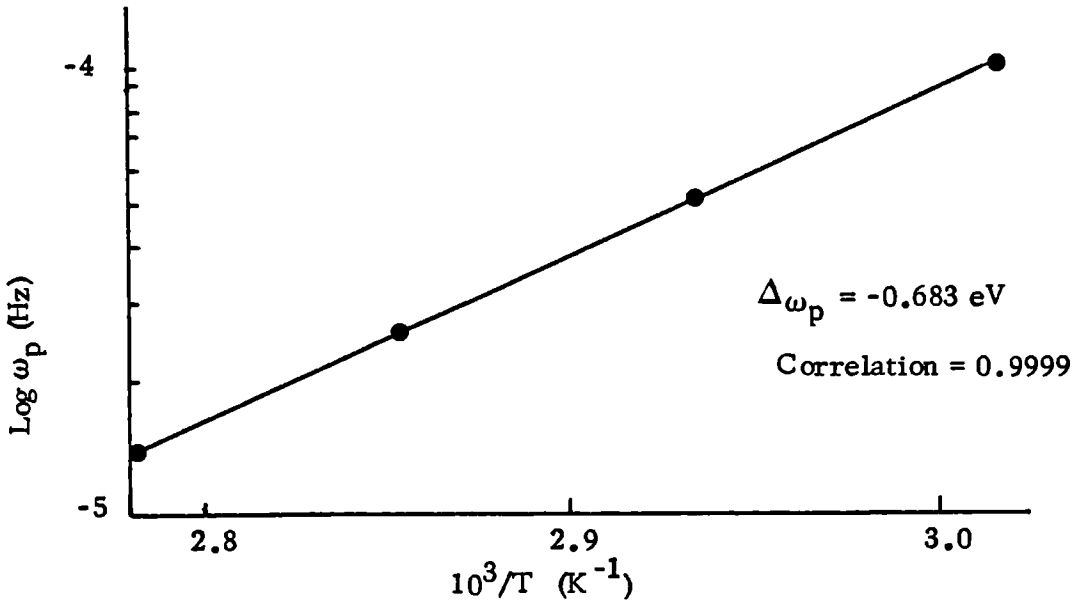

Fig. 4.20. Arrhenius plot of the barrier loss peak magnitude in molten PEG 4000

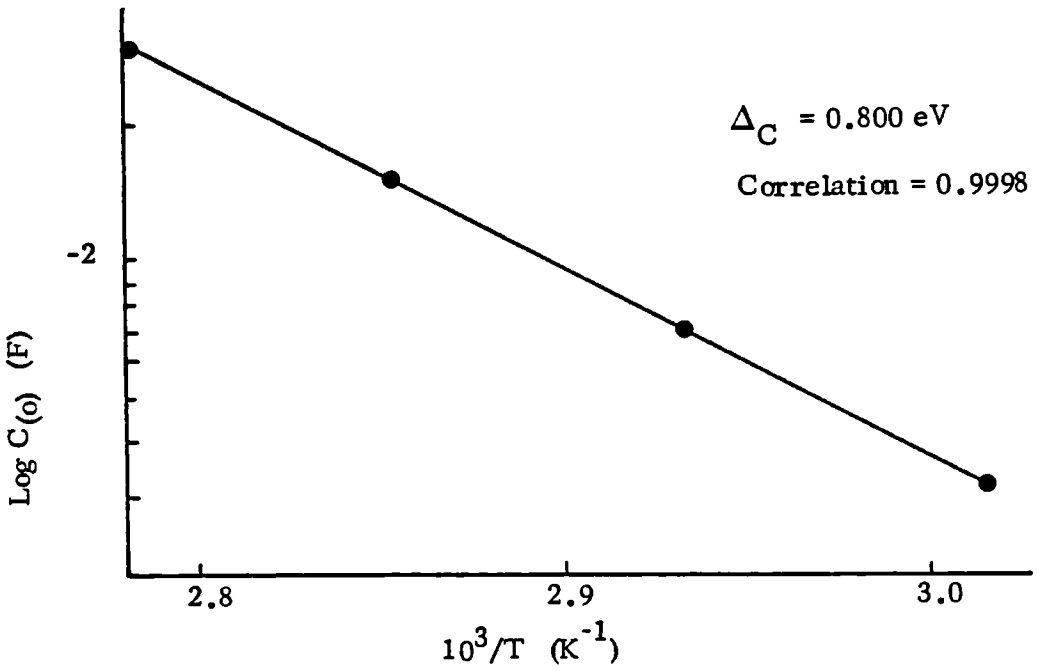

$$\Delta\omega_p = \Delta_G - \Delta_C \qquad \ldots 4.33.$$

$$= 0.106 - 0.800$$

$$= -0.693 \text{ eV}$$

which is very close to the value of -0.683 eV observed for $\Delta\omega_p$. This interrelationship between the magnitude and relaxation rate of barrier shows that the process attributed to the barrier is not that of a reorientating dipole, but rather a region of charge diffusion. This is in spite of the fact that its frequency dependence ($\omega^{-0.7}$) is not that expected classically ($\omega^{-0.5}$) (de Gennes, 1982). However, it has been noted that segmental diffusion in polymer melts gives this form of behaviour (Klymko and Kopelman, 1983). Charge transport through a partially disordered matrix also gives the same frequency dependence (Shapiro and Abrahams, 1981).

Thus it appears that the behaviour of the polymer at the barrier is consistent with a restricted movement of charged segments or kinks of the polymer chain which are adsorbed onto the electrode. In the bulk of the liquid, conduction can occur through the d.c. transport process observed because of the freedom of movement of the polymer chains, allowing the possibility of molecular transport of the charge. However, in the barrier, molecular motion is restricted because parts of the molecule are presumably "tied" to the surface of the electrode. Charge transfer is therefore forced to occur via transfer of the chain distortion through the chain itself. This motion is obviously more difficult since the activation energies associated with the barrier response are higher than that calculated for the bulk conductance.

The barrier layer can therefore be visualised as a single layer of PEG 4000 molecules adsorbed onto the surface of the electrode via the

Fig. 4.21. Possible structure of barrier layer in molten PEG 4000

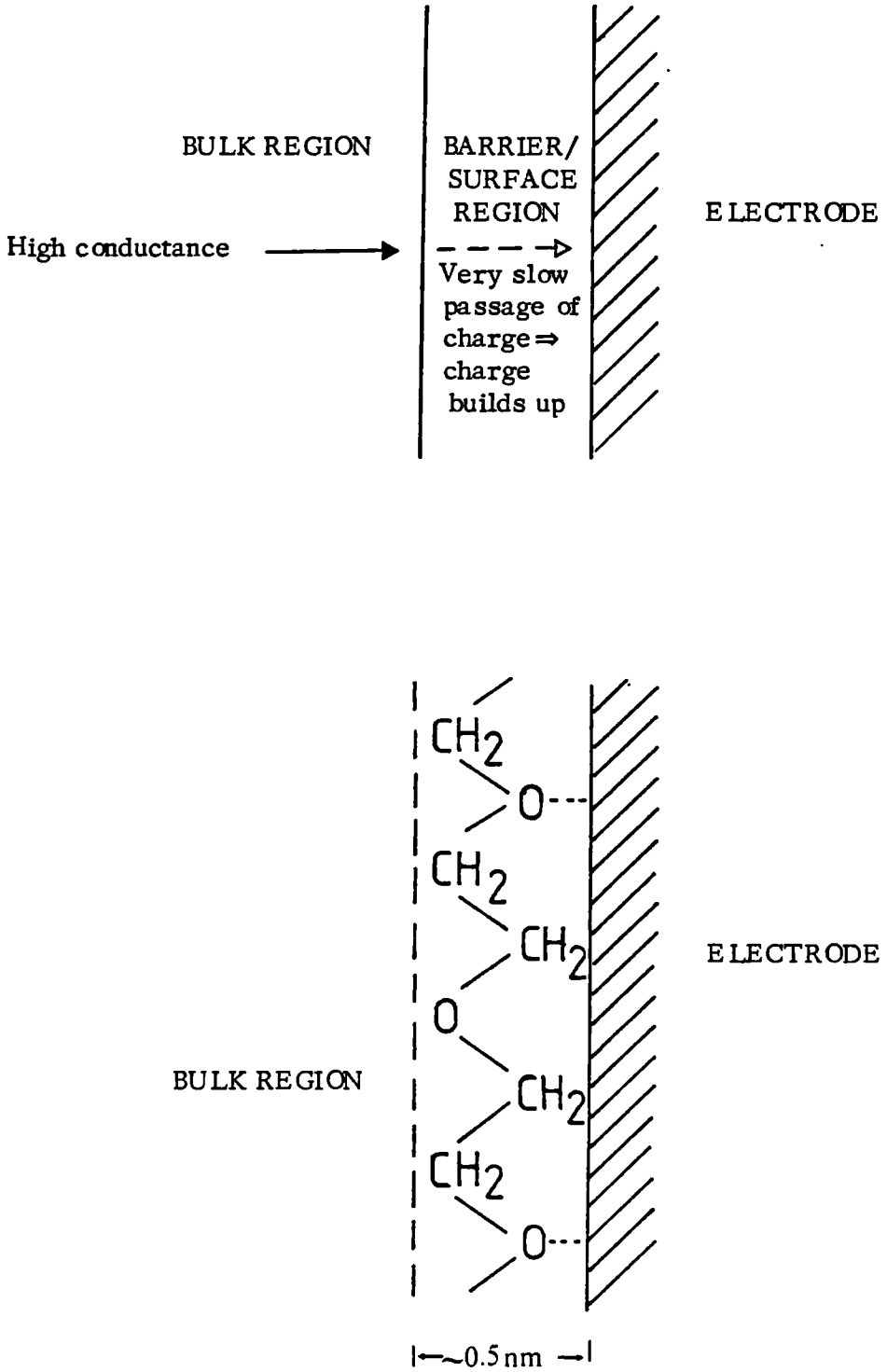

ether oxygens of the polymer chain (Fig. 4.21.). The magnitude of the barrier capacitance supports this contention since a rough estimate of the barrier thickness is of the order of 0.5 nm, approximately equivalent to the cross-sectional diameter of one polymer molecule.

4.3.1.2. PEG 4000 solid state

Samples equilibrated below the melting point of the material showed responses typical of the solid, which could be normalised over the temperature range investigated. It is important to note that the solid and liquid dielectric responses are very different and do not normalise together. Results obtained during the cooling and heating cycles (Fig. 4.22a. and b. respectively) were essentially similar apart from some hysteresis, seen as a shift to lower frequencies on the heating curve. On cooling, a maximum was observed in the loss at around 10^3 Hz at 313K which was absent during the heating cycle.

Circuit analysis (Fig. 4.22.) revealed that the barrier layer present in the liquid was retained intact on solidification with minimum modification to its structure, although presumably molecular exchange with the bulk was now prevented. Estimates of the thickness of this layer at about 0.5 nm on each electrode corresponded to those obtained in the liquid are therefore consistent with the structure proposed in 4.3.1.1. The similarity of the Dissado-Hill parameter, n for the barrier in the solid and liquid provided further evidence for this view.

A new element is introduced into the bulk response as a result of crystallisation, seen as a frequency dependent capacitance. In addition, a conductance arising from a d.c. charge transport process was present, as in the liquid. The other frequency dependent capacitance is common to both bulk and barrier responses and thus behaves as a parallel circuit element.

Fig. 4.22. Normalised curve of frequency response of PEG 4000 solid
a. On cooling cycle

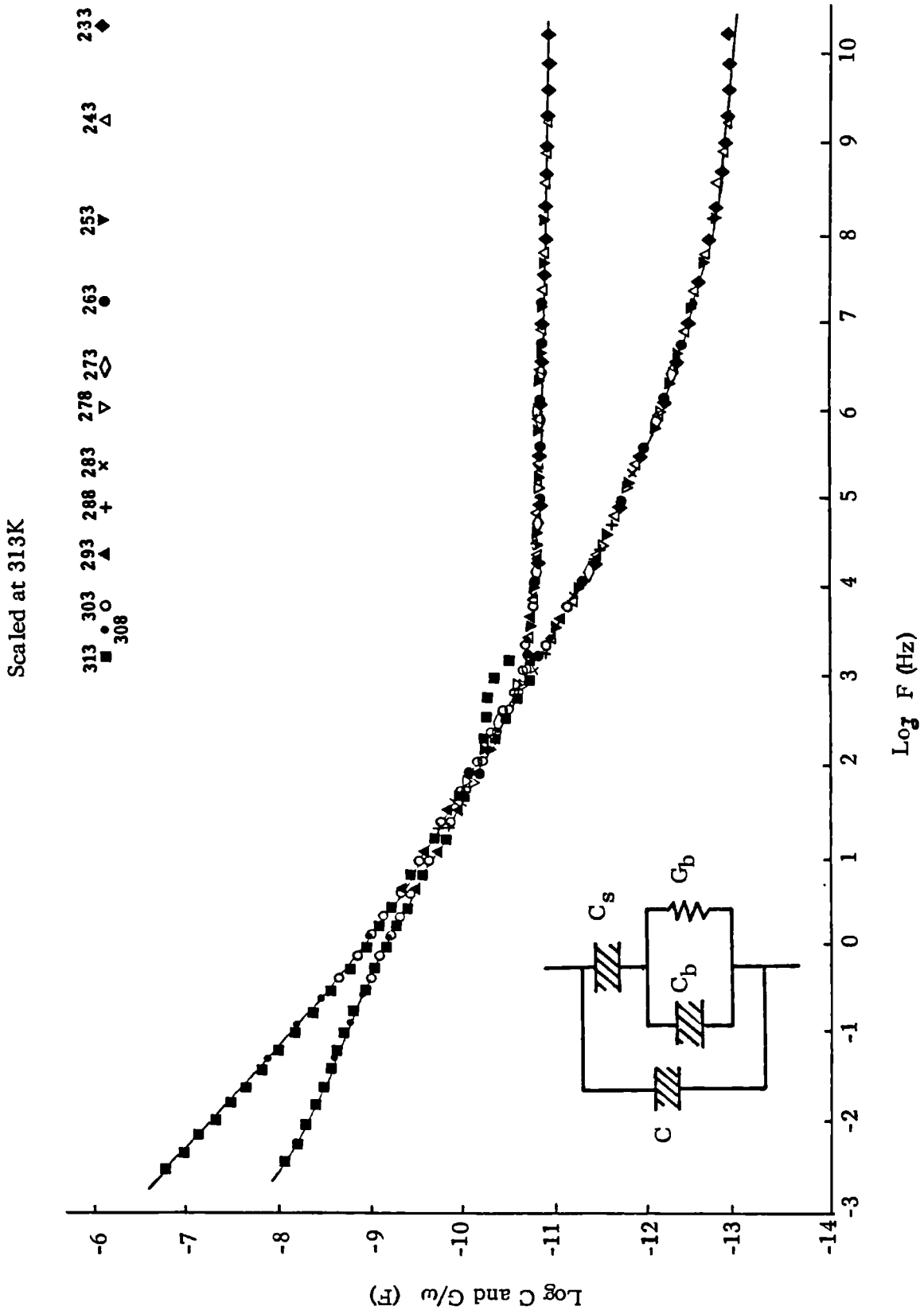

Fig. 4.22b. On heating cycle

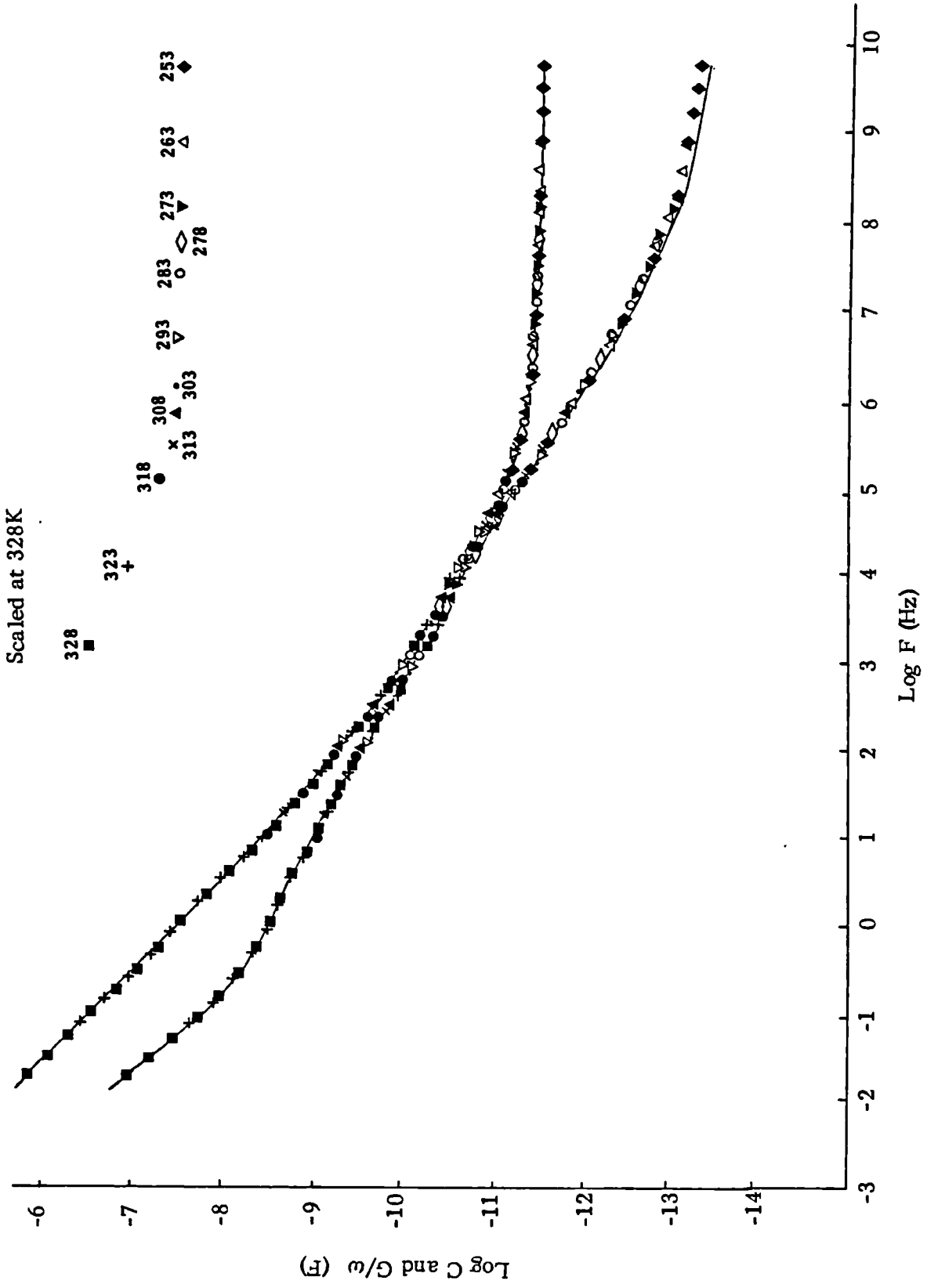

Scaling of the magnitude of the individual components at different temperatures was carried out by the usual curve fitting procedure and the results are given in Tables 4.2. and 4.3. for cooling and heating cycles respectively.

The Dissado-Hill shape parameters remained constant throughout the heating and cooling cycles for both bulk and barrier responses. From the values of $m = 0.4$ and $n = 0.45$ for the dispersion in the bulk, it can be concluded that the system contains a fairly wide range of constructions but there is some degree of local correlated motion.

On the cooling cycle, no temperature dependence was observed in the amplitudes of the loss processes ($C_{(0)1}$ and $C_{(0)2}$), which is in contrast to the behaviour on heating where these values remain constant only up to 318K and then become temperature dependent. Arrhenius plots of the loss peak frequencies, ω_{p1} and ω_{p2} and the conductance arising from the d.c. transport process, G_{02}, were constructed for both heating and cooling data (Fig. 4.23. and 4.24. respectively). Very similar activation energies of around 1.1 eV were determined for these parameters. In all cases, data obtained above 318K on the heating curve did not lie on the straight line formed by the lower temperature data and hence were not used to calculate activation energies.

Since the loss peak frequency in both bulk and barrier responses and the conductance during heating (up to 318K) and cooling cycles all show the same temperature dependence, it can be assumed that the same molecular relaxation route governs all these elements. Furthermore, this relaxation must be associated with the crystalline lamella of the polymer because the Arrhenius plots obtained are linear and thus do not show the characteristic behaviour of a relaxation arising from the amorphous region where an increase in

Table 4.2. Characteristic dielectric circuit parameters of PEG 4000 in the solid state at different temperatures on cooling cycle

Temperature (K)	Dissado-Hill parameters				Barrier ω_{p1} (Hz) x 10^{10}	Bulk ω_{p2} (Hz) x 10^{4}	Barrier $C_{(0)1}$ (F) x 10^{3}	Bulk $C_{(0)2}$ (F) x 10^{9}	Bulk G_{02} (Ω^{-1}) x 10^{12}	C_{∞} TOTAL (F) x 10^{11}
	Barrier		Bulk							
	m	n	m	n						
313	-	0.2	0.4	0.45	18,000	18,000	4	4	40,000	1
308	-	0.2	0.4	0.45	14,000	14,000	4	4	28,000	1
303	-	0.2	0.4	0.45	7,000	7,000	4	4	12,000	1
293	-	0.2	0.4	0.45	1,600	1,600	4	4	2,800	1
288	-	0.2	0.4	0.45	630	630	4	4	1,100	1
283	-	0.2	0.4	0.45	250	250	4	4	440	1
278	-	0.2	0.4	0.45	140	140	4	4	210	1
273	-	0.2	0.4	0.45	32	32	4	4	48	1
263	-	0.2	0.4	0.45	7.8	7.8	4	4	12	1
253	-	0.2	0.4	0.45	1	1	4	4	1.5	1

Table 4.3. Characteristic dielectric circuit parameters of PEG 4000 in the solid state at different temperatures on heating cycle

Temperature (K)	Dissado-Hill parameters				Barrier ω_{p1} (Hz) x 10^{11}	Bulk ω_{p2} (Hz) x 10^{5}	Barrier $C_{(0)1}$ (F) x 10^{4}	Bulk $C_{(0)2}$ (F) x 10^{10}	Bulk G_{02} (Ω^{-1}) x 10^{13}	C_{∞}TOTAL (F) x 10^{12}
	Barrier		Bulk							
	m	n	m	n						
328	-	0.2	0.4	0.45	1 x 10^{7}	1 x 10^{7}	6.7	6.7	4.2 x 10^{6}	1.7
323	-	0.2	0.4	0.45	5.3 x 10^{6}	5.3 x 10^{6}	10	10	3.3 x 10^{6}	2.5
318	-	0.2	0.4	0.45	130,000	130,000	40	40	370,000	10
313	-	0.2	0.4	0.45	85,000	85,000	40	40	210,000	10
308	-	0.2	0.4	0.45	45,000	45,000	40	40	100,000	10
303	-	0.2	0.4	0.45	23,000	23,000	40	40	46,000	10
293	-	0.2	0.4	0.45	6,300	6,300	40	40	11,000	10
283	-	0.2	0.4	0.45	1,300	1,300	40	40	2,300	10
278	-	0.2	0.4	0.45	530	530	40	40	930	10
273	-	0.2	0.4	0.45	170	170	40	40	300	10
263	-	0.2	0.4	0.45	40	40	40	40	70	10
253	-	0.2	0.4	0.45	6.5	6.5	40	40	9.8	10

Fig. 4.23. Arrhenius plots for bulk and barrier loss peak frequencies on heating and cooling cycles for PEG 4000 solid

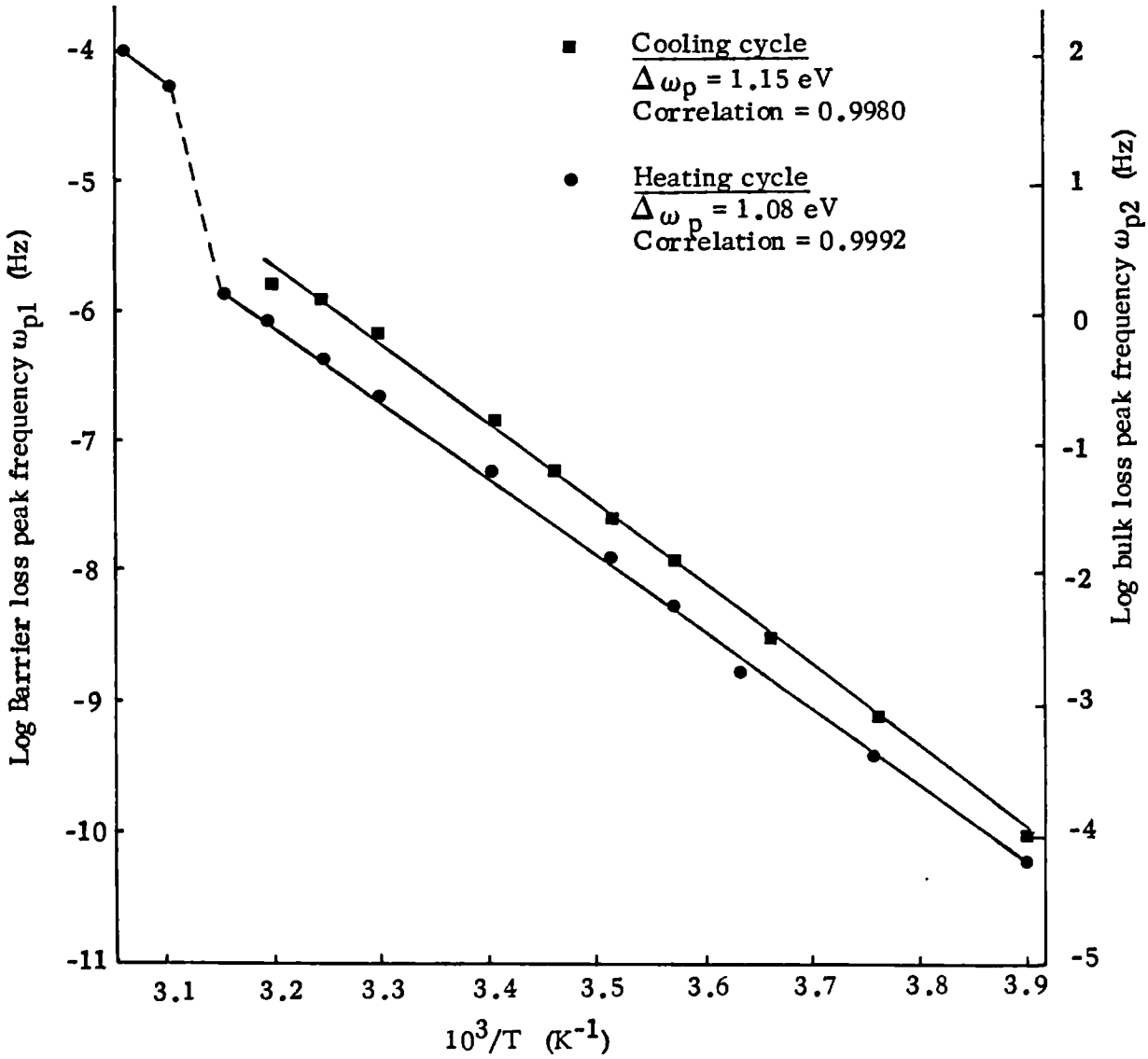

Fig. 4.24. Arrhenius plots for bulk conductance on heating and cooling cycles for PEG 4000 solid

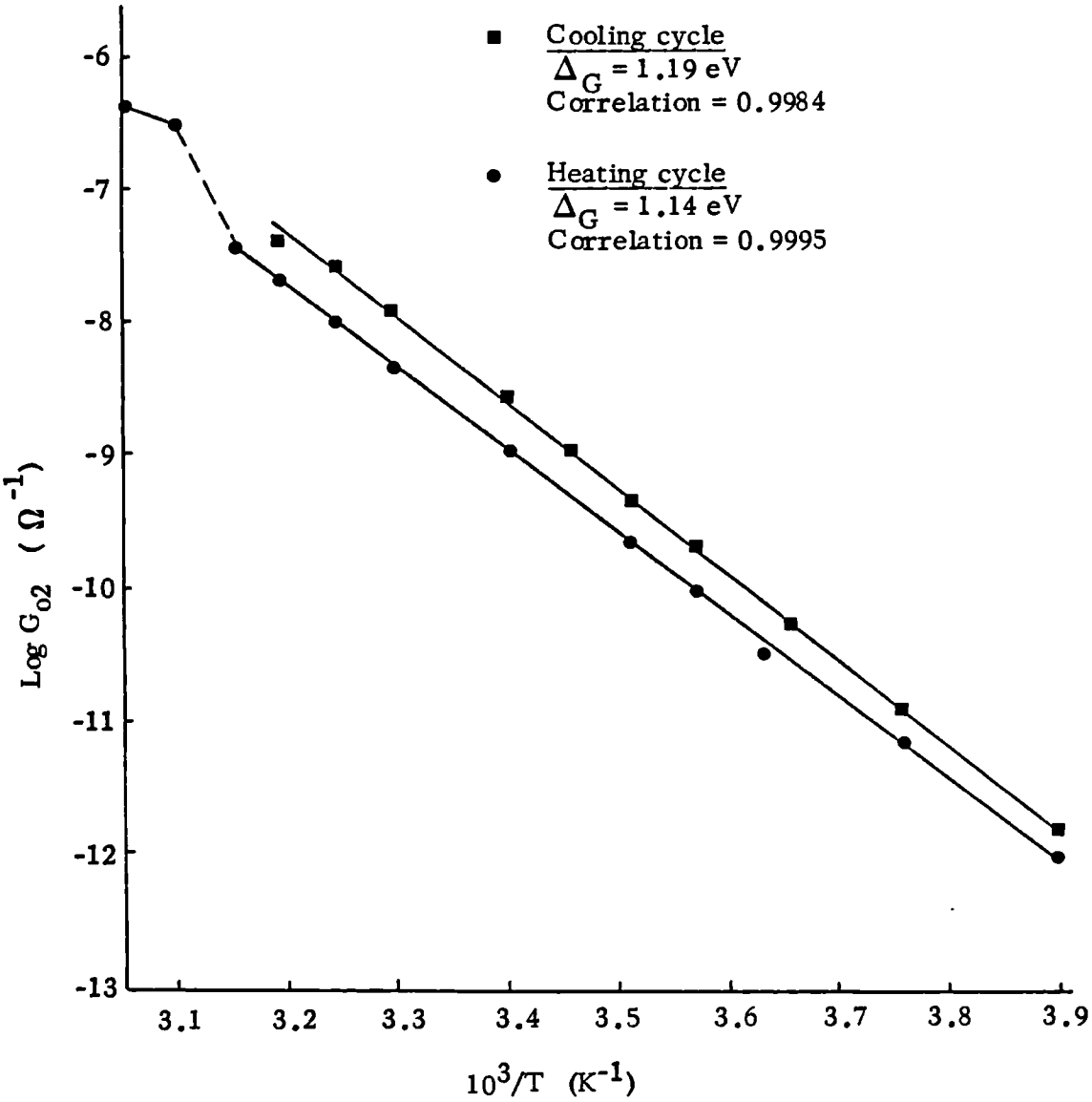

gradient would be expected as the temperature is lowered, giving a curve (Blythe, 1979). Decossas et al (1982), who carried out dielectric measurements from 77-400 K at various frequencies between 500 and 10^6 Hz, report evidence for a high temperature αc relaxation associated with the crystalline region. They found that this process, observed as a shoulder on the loss curve as here, was difficult to investigate fully because of the strong conductivity also associated with the response at high temperatures, thus preventing any calculations of the activation energy involved. In this work however, circuit analysis of the dielectric response has allowed full characterisation of the individual components. Investigation by DSC and ESR (Lang et al, 1977a, 1977b) again reveals the presence of a high temperature αc relaxation region below the melting point. From the ESR data, the activation energy was estimated as approximately 2.19 eV (equivalent to 50 Kcal $mole^{-1}$) although the authors suggest that their sample began to melt in this region. NMR spectroscopy (Hikichi and Furuichi, 1965) of a sample of PEG 4000 shows that rapid narrowing of the broad component occurred between 270K and the melting point, which was assigned as arising from an αc crystal disordering mechanism. From these results and from measurements of dielectric response performed over a very limited range of frequency, the authors concluded that molecules in the crystalline regions must move without destruction of their helical structure, involving rotational or oscillatory movements around the helical axis. However, this assumption is based on the fact that they observe no dispersion in the dielectric response over the temperature range in which the NMR line width narrows, indicating that dipole reorientation was not involved in the molecular motion seen. Closer examination of their dielectric data, however, reveals that a small dispersion

is in fact present and hence dipole motion is involved in the relaxation, as is found in this present work and that of Decossas et al (1982). Hikichi and Furuichi (1965) give a rough estimate of the activation energy of the process as 1.73 eV (40Kcal $mole^{-1}$), which is of the same order as that calculated here.

The αc relaxation probably occurs mainly on the surface of the lamella, involving both the chain ends of the molecules which are excluded from the crystal and the chain folds. Some whole chain motion may be present, leading to distortion of the lamella itself. This is in agreement with the NMR data of Hikichi and Furuichi (1965) which shows that the temperature at which the broad component narrows is not dependent on molecular weight in the range they studied (PEG 1000-PEG 4000) suggesting that only a small proportion of the molecule is involved. The d.c. charge transport process giving rise to the conductance could also arise from this mechanism.

From 318-328 K in the heating cycle, there is a discontinuous increase in the conductance and capacitance values obtained from circuit analysis such that they do not fit with the rest of the results. However, this is not due to the material melting since frequency scans of the response still normalise with lower temperatures and correspond to that of the solid phase.

The sample of PEG 4000 investigated here had been crystallised under non-isothermal conditions before being heated, which will give rise to both extended and folded chain crystal forms, (Kovacs et al, 1977). Frequency scans were then performed at discrete temperature intervals in the heating cycle, this stepwise increase in temperature is equivalent to successive heat treatments (Lang et al, 1977b). Therefore, the thermodynamically less stable material (i.e. that which previously crystallised as once folded chain

crystals) will begin to melt as the temperature is raised and will subsequently recrystallise as the more thermodynamically stable extended chain crystal form with a higher melting point (Point and Kovacs, 1980). DSC results and direct microscopic observation suggest that this chain unfolding does not involve large scale melting followed by recrystallisation, but rather that the two processes occur simultaneously (Buckley and Kovacs, 1976).

It is expected that the same relaxation route via the chain ends located on the surface of the lamella would be possible whether extended or folded chain crystals or a mixture of the two species were present. This is borne out by the fact that frequency scans performed at 323K and 328K normalise with those obtained at lower temperatures. However Decossas et al (1982) noted that chain folding will reduce the number of chain ends which are found on the surface of the lamella in any given area, thus the extended chain form will possess the highest density of chain ends on the surface. There is also good evidence that hydrogen bonding occurs where the concentration of hydroxyl groups on the surface of the lamella is sufficiently high (Buckley and Kovacs, 1976). Both of these suggest that the extended chain crystal form supports faster relaxation and charge transport rates than the folded chain crystal lamellae, which is consistent with the sharp increase in frequency factors seen above 318K on the Arrhenius plots in Figs. 4.23. and 4.24.

As previously mentioned, the heating and cooling curves exhibit hysteresis with respect to each other which can be shown more clearly if a graph of capacitance as a function of temperature at fixed frequency is constructed (Fig. 4.25.). Temperature lag effects were eliminated as an explanation of this phenomenon, since examination of the response at two different cooling rates, namely $1^{o}C\ min^{-1}$ and $10^{o}C\ hr^{-1}$ produced similar results.

Fig. 4.25. Capacitance as a function of temperature cycling at fixed frequency (10 Hz) of PEG 4000

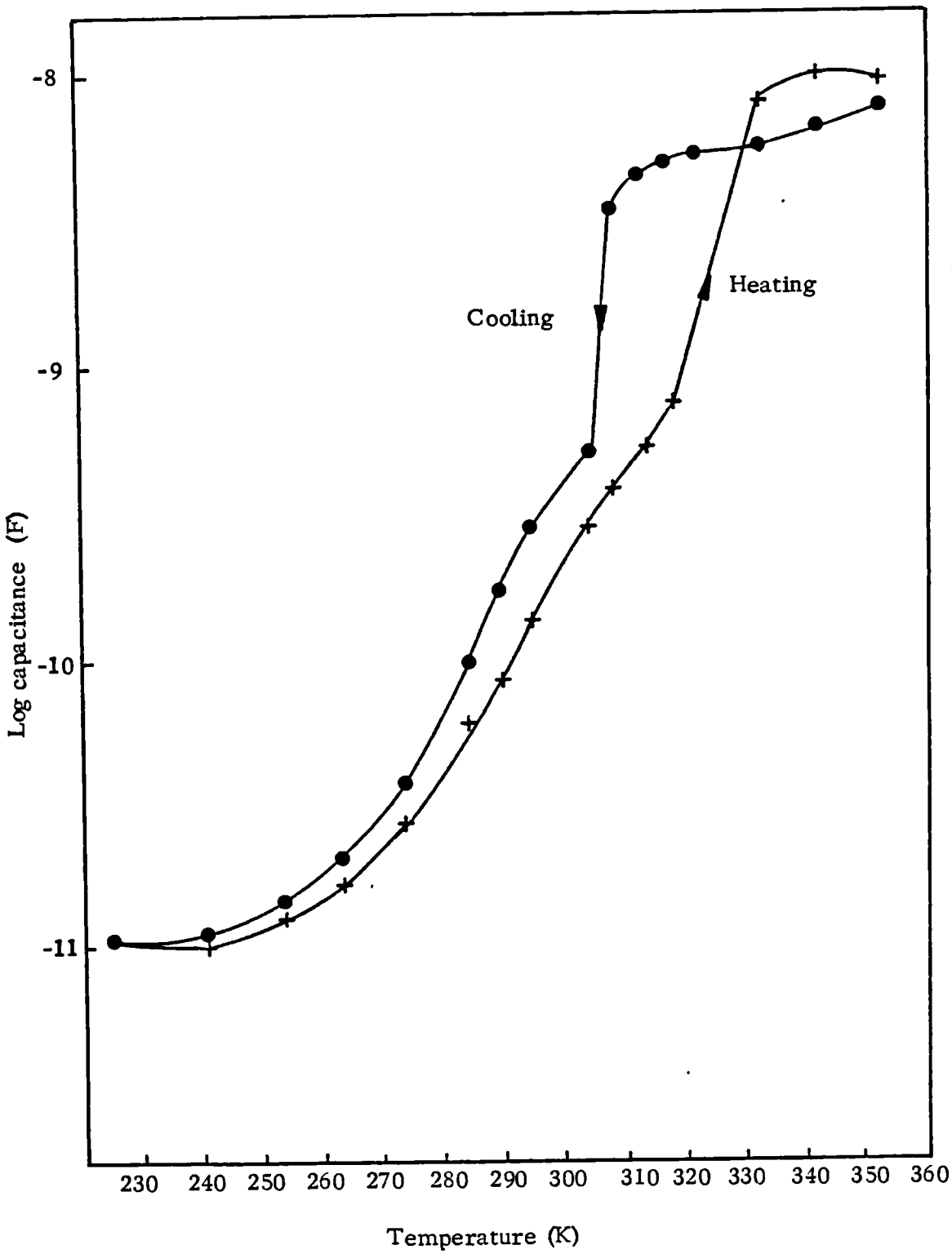

On cooling, the phase transition from liquid to solid, seen as a sharp drop in capacitance at 10Hz, occurred between 318 and 313K. This was followed by a steady decrease in the capacitance which tailed off towards a limiting value at low temperatures. The heating curve ran almost parallel to but did not coincide with the cooling curve and the rise in capacitance associated with the return to the liquid state occurred between 328 and 333K. This is consistent with the data obtained by DSC (Chapter 3.3.1.) where the melting point of extended chain crystals of PEG 4000 was found to be 330K. Therefore a significant degree of supercooling of the liquid below the melting point occurred, even at relatively slow cooling rates. This is a common feature of polymer melts (Sharples, 1966) and reflects the finite time required for the nucleation and growth of crystals. The polymer exhibited an increased capacitance on first forming the liquid state and to clarify this behaviour, a further investigation of the melting and crystallisation transitions of PEG 4000 was carried out as detailed in the following two sections, (Chapter 4.3.1.3. and 4.3.1.4.).

The effect of different thermal treatments on the dielectric response of PEG 4000 in the solid state was also investigated. Quenching of the material by solidification in liquid nitrogen was carried out to produce a more amorphous form of the polymer. Previous experiments (Chapter 3.3.1.) however, had shown that it was extremely difficult to remove all crystallinity and produce a totally amorphous material. A frequency scan at 293K showed that this treatment enhanced the magnitude of the low temperature dispersive process and reduced the αc response compared with material which had been cooled at the normal slower rate (Fig. 4.26.). Since the low temperature process arises from a β_a relaxation which is associated with local segmental motions

Fig. 4.26. Effect of quenching on frequency response of PEG 4000 at 293K

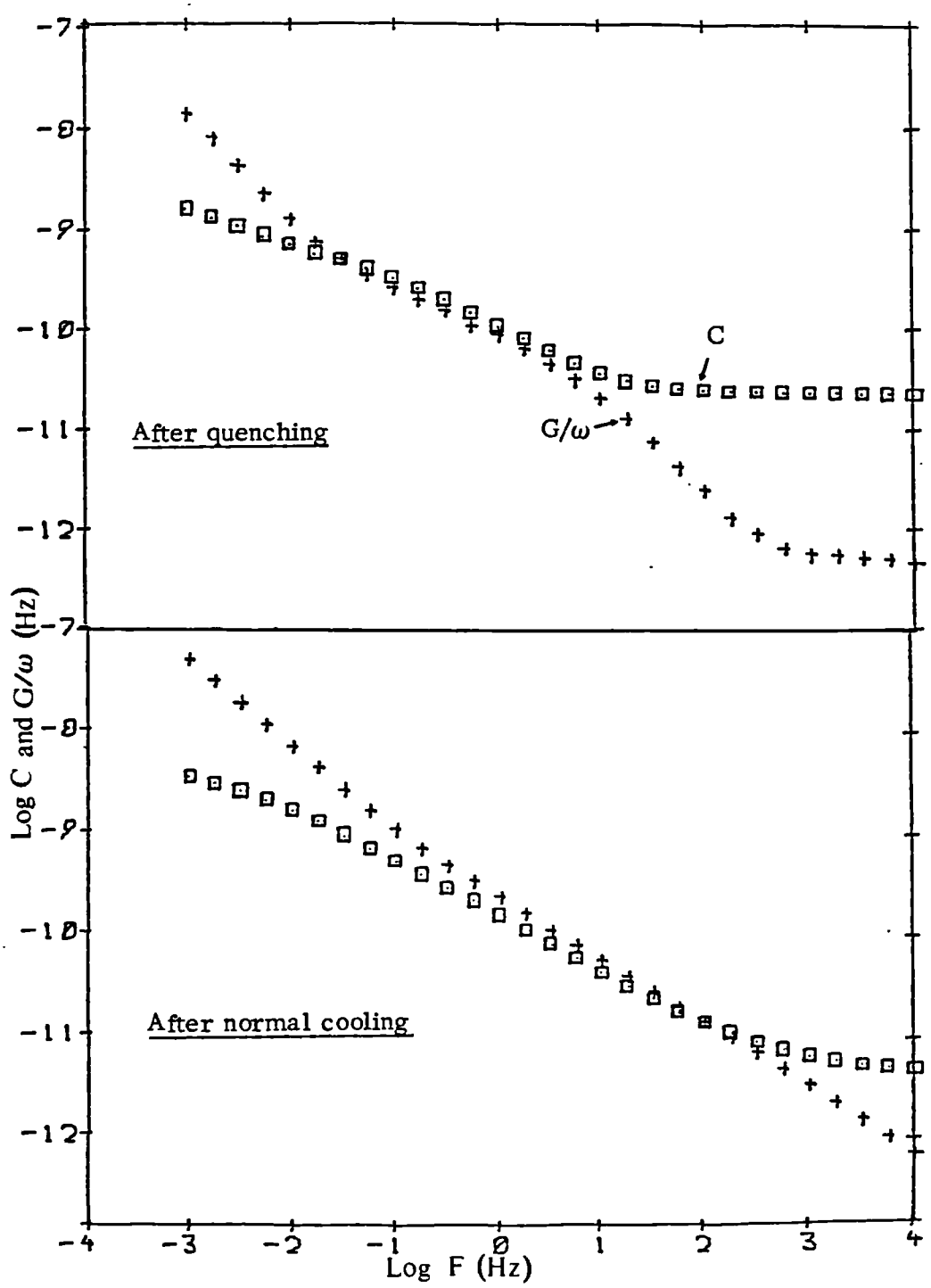

of the main chains in the amorphous region (Connor et al, 1964), these results demonstrate a decrease in the crystallinity. Annealing of PEG 4000 was achieved by cycling the sample between 333K, just above its melting point and the solid at 293K. A frequency scan of the polymer at 293K after the first cooling and heating cycle showed the response typical of that normally observed at this temperature. However, after the third temperature cycle, the dielectric behaviour of the sample (at 293K) was similar to that which would be expected at higher temperatures such as 323K (Fig. 4.27.), indicating that a shift in the frequency response to higher frequencies had occurred. As a consequence of the rapid heating and cooling cycles, only partial melting can take place before the subsequent recrystallisation process, which favours the more thermodynamically stable material, in this case the extended chain crystal form of the polymer. This means that as the temperature is raised, the metastable folded chain crystals melt first but the extended chain crystals tend to persist, since insufficient time for complete fusion is allowed. On cooling, recrystallisation as the extended chain form on the extended chain crystals already present will occur. As Figs. 4.23. and 4.24. show, extended chain structures lead to an increase in the frequency factors for the different dielectric processes, which causes the observed shift to higher frequencies following annealing.

It can be concluded therefore, that changes in the structure of PEG 4000 which result from alterations in its thermal history can be detected from measurements of dielectric response.

Fig. 4.27. Effect of temperature cycling on frequency response of PEG 4000

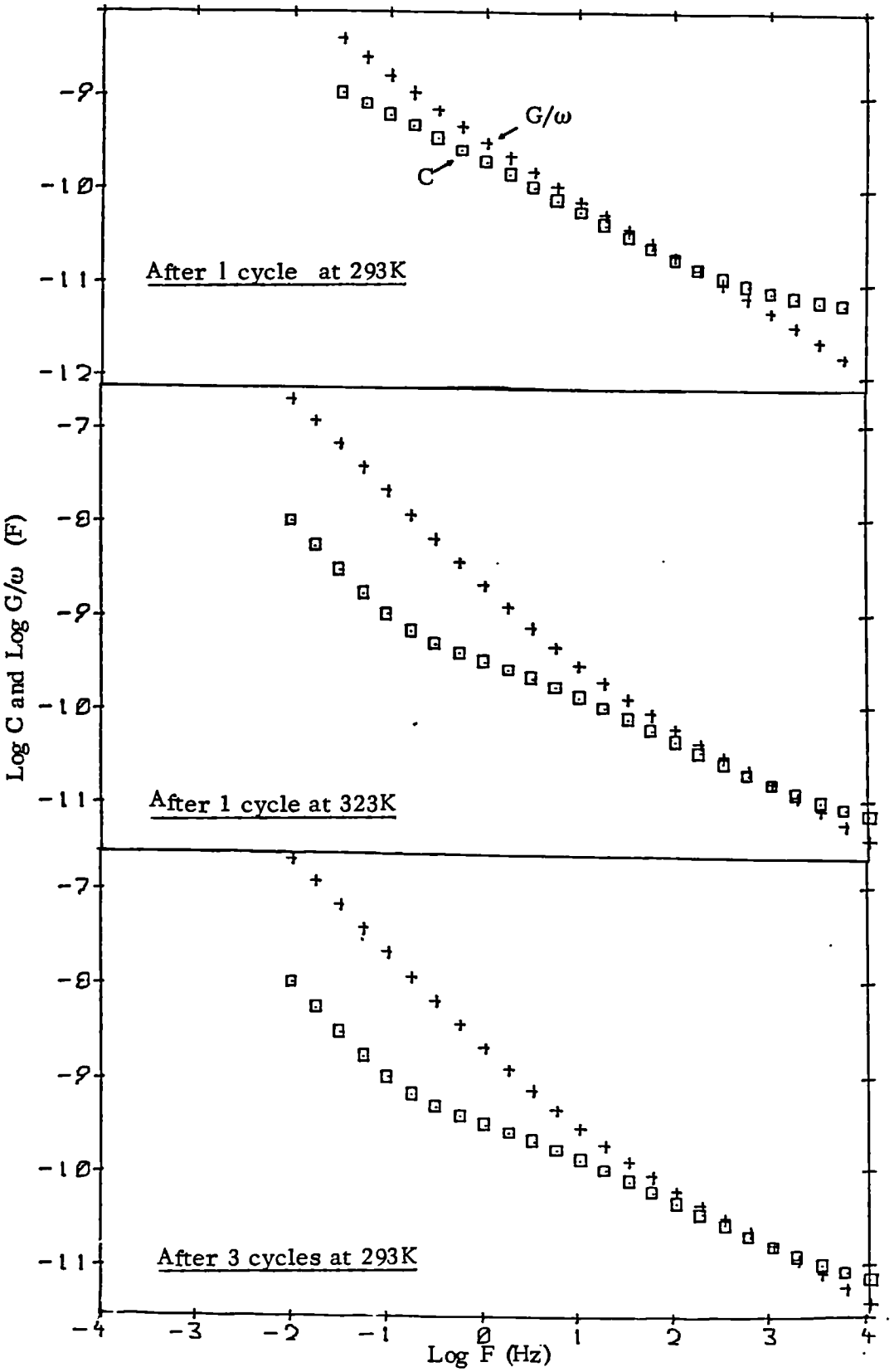

4.3.1.3. Crystallisation behaviour

The temperature and time dependence of the crystallisation of PEG 4000 was investigated between 318 and 308K by measuring changes in capacitance with time at a fixed frequency of 1778 Hz. Subsequently, frequency scans were performed to check that the dielectric response associated with the solid was present. Sigmoidal shaped graphs of capacitance as a function of time were obtained for polymer crystallised at 318 and 313K, as would be expected (Fig. 4.28). This is in contrast to the behaviour observed at the lowest crystallisation temperature, 308K, where a peak was present (Fig. 4.29.), suggesting that some differences occur in the crystallisation process at this temperature. However, frequency scans performed after crystallisation were identical at all temperatures to those obtained from earlier measurements of the solid.

It is therefore possible that the time dependencies of the components which influence the measured capacitance were different. For example, the decrease in the bulk conductance on solidification could occur more slowly than the change in bulk capacitance. A graph of capacitance as a function of time, would show an apparent increase in the capacitance initially, followed by a fall as the conductance starts to drop, giving the peak observed at 308K. Alternatively, the influence of the conductance and capacitance components on the observed capacitance may vary according to the temperature of crystallisation.

It is expected that the crystallisation of PEG 4000 would follow Avrami growth kinetics (Avrami, 1939, 1940, 1941), where the equation for the nucleation and growth of a new phase within another can be expressed as:

Fig. 4.28. Capacitance at 1778 Hz as a function of time for crystallisation of PEG 4000 at 313K

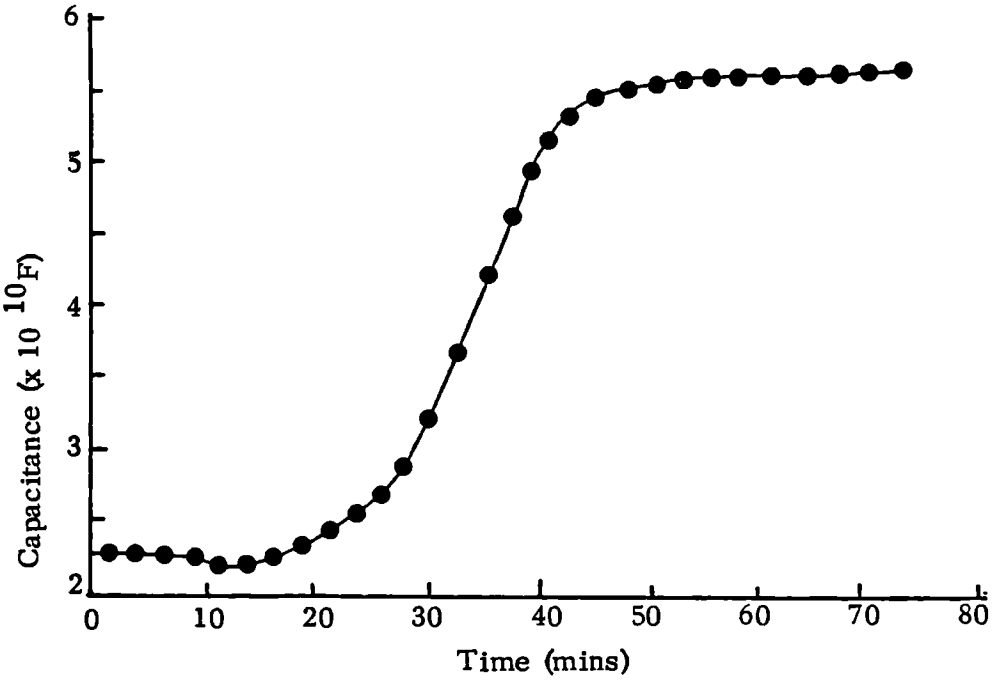

Fig. 4.29. Capacitance at 1778 Hz as a function of time for crystallisation of PEG 4000 at 308K

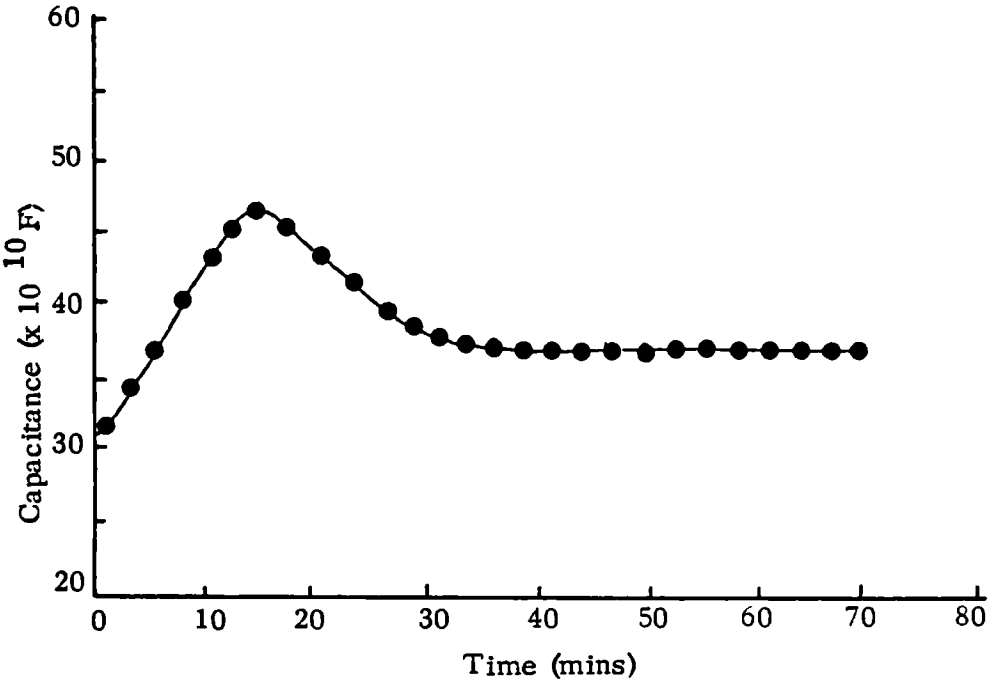

$$\ln \left| \frac{C_{\infty}' - C_t}{C_{\infty}' - C_o} \right| = -k_r t^{n_a} \qquad \ldots 4.34.$$

where C_{∞}' = capacitance at infinite time after start

C_t = capacitance at time t after start

C_o = capacitance at t = 0

$-k_r$ = rate constant

n_a = Avrami exponent which has a value between 1 and 4 characterising the dimensionality time dependence of growth

For example, if $n_a = 4$, nucleation must be homogeneous (i.e. time dependent) and growth must be three dimensional. However, for $n_a = 3$, two interpretations are possible: either nucleation is heterogeneous (i.e. effectively instantaneous) and growth is three dimensional or nucleation is homogeneous and growth is two dimensional. The exponent is not necessarily an integer since values of $n_a = 1.5$, 2.5 or 3.5 are obtained where diffusion controlled transport to the growth boundary occurs.

The value of the Avrami exponent is obtained through constructing co-logarithmic plots of $\ln \left| \frac{C_{\infty}' - C_t}{C_{\infty}' - C_o} \right|$ as a function of time, the gradient of which will correspond to n_a. A typical Avrami plot for crystallisation at 313K is presented in Fig. 4.30. It was not possible to interpret the results at 308K in this way due to the peak in capacitance/time curve. If this, for example, arose as a result of two competing processes, then the maximum value of the capacitance would not correspond to the true value of C_{∞}' which would affect the calculated Avrami exponent.

Fig. 4.30. Avrami plot for PEG 4000 crystallising at 313K

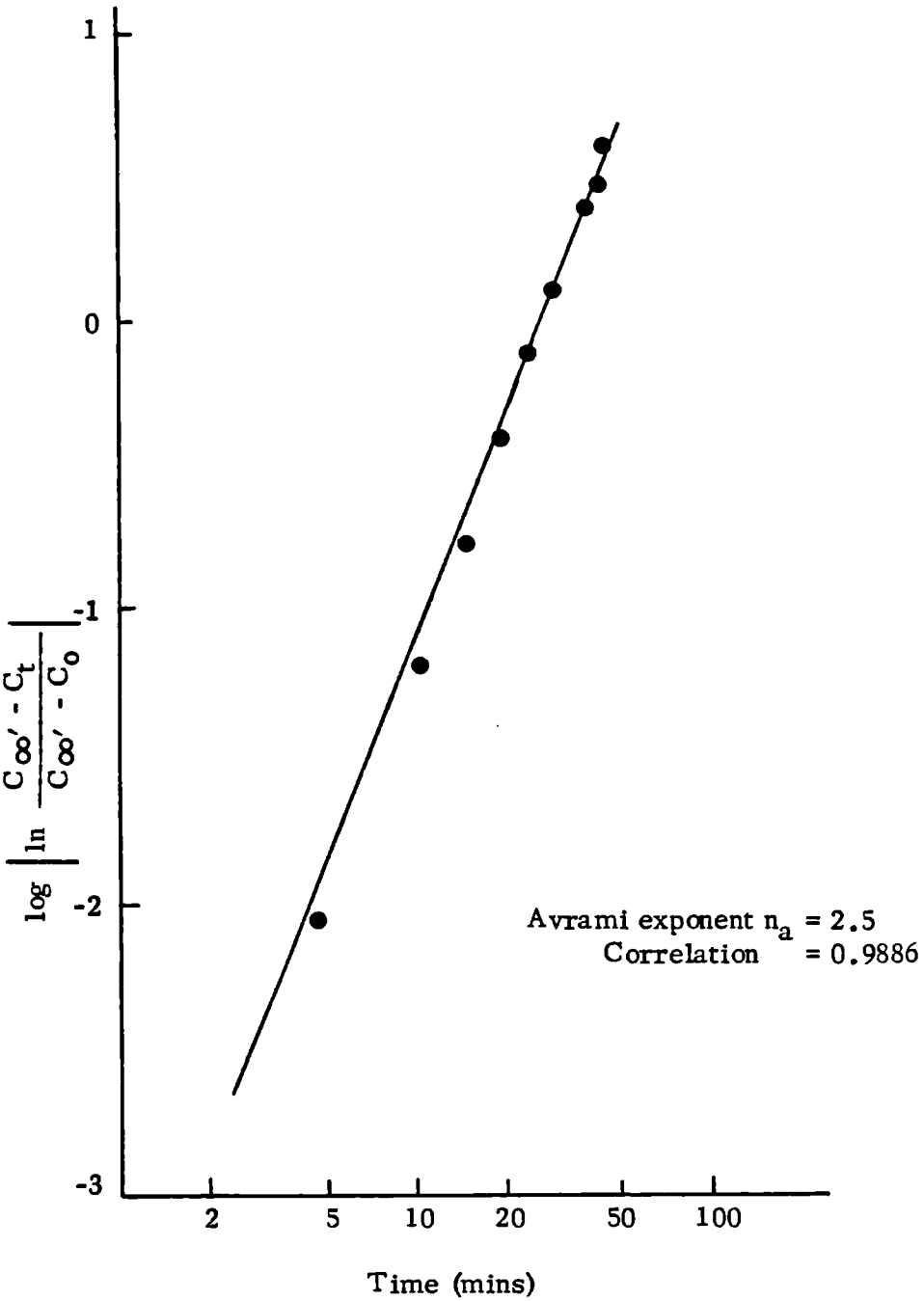

The values obtained here for n_a (Table 4.4.) are less than the expected value of 3 or 4 which is predicted where the growth of three-dimensional spherulites is seen. However, PEG crystallisation cannot be fitted to a single Avrami equation in general and a wide range of values for n_a has been observed with the different methods used to study the crystallisation kinetics. For example, n_a was found to vary from 2.2. to 3.2. when determined by dilatometry, but from 1.4. to 1.8. when determined by calorimetry (Godovsky et al, 1972). Many causes of the deviation from Avrami growth kinetics have been postulated. Results obtained by DSC (Hay et al, 1969) showed the Avrami exponent to be dependent on preheating time and temperature. However, removal of any thermal history such as was carried out here by maintaining samples in the molten state at 363K for 1 hour prior to crystallisation should eliminate any differences between samples. Beech et al (1972b) suggested that deviations from the expected value of n_a arose as a result of secondary crystallisation processes. Fractionation by molecular weight could occur, leading to attenuation of the crystallisation rate as the crystallisation proceeded. Alternatively, the growing fronts of the spherulites could impinge on each other, which means that crystallites formed initially as spheres would become constrained to form discs (Hay et al, 1969). This would correlate with experimental data where the value of n_a is determined to be approximately 2, such as is observed here. Godovsky et al (1972) have also suggested that the deviation occurs because the Avrami equation applies only to primary crystallisation processes i.e. those involving crystallites. They argued that spherulites are just secondary aggregates which do not contribute essentially to the energy parameters for either crystallisation or fusion, since the heat of fusion for samples consisting of

Table 4.4. Crystallisation half times and Avrami exponents for PEG 4000

Crystallisation Temperature (K)	Crystallisation half time $t_{c\frac{1}{2}}$ (mins)	Avrami exponent n_a
318	38	1.9
313	22	2.5
308	16	-

either a large number of small spherulites or a few large spherulites is equal provided the degree of crystallinity is the same in both cases.

The calculated half times to crystallisation ($t_{c\frac{1}{2}}$) decrease as the temperature of crystallisation is lowered (Table 4.4.) indicating that the rate of crystallisation increases with the degree of supercooling as would be expected. From calorimetric and dilatometric studies, Godovsky et al (1972) estimated the $t_{c\frac{1}{2}}$ of PEG 4000 at 319.9K as 17.4 mins which is shorter than the value of 38 mins at 318K determined here. However, since even small differences in experimental conditions and choice of the beginning and end point of crystallisation will affect significantly the results obtained, the values of $t_{c\frac{1}{2}}$ can be considered to be in reasonable agreement.

4.3.1.4. Melting behaviour

The time and temperature dependence of melting of PEG 4000 was investigated between 328 and 343K, above which temperature the transition occurred too quickly to follow accurately. No melting transition was observed in samples equilibrated at 328K although a rise in capacitance occurred corresponding to the conversion to the extended chain form, as was confirmed by a subsequent frequency scan which revealed that the dielectric response of the solid was still present.

For temperatures from 333 to 343K, capacitance as a function of time was measured at frequencies of 1778 and 10 Hz. Graphs of data at the former frequency exhibited peaks, whereas at the latter frequency, sigmoidal shaped graphs were obtained. Typical examples for the melting transition at each frequency at 333K are given in Fig. 4.31. and 4.32. respectively. Melting half times ($t_{m\frac{1}{2}}$) at the two frequencies show good agreement and increase as the temperature is lowered (Table 4.5.). The effect of different thermal

Fig. 4.31. Capacitance at 1778 Hz as a function of time for melting transition of PEG 4000 at 333K

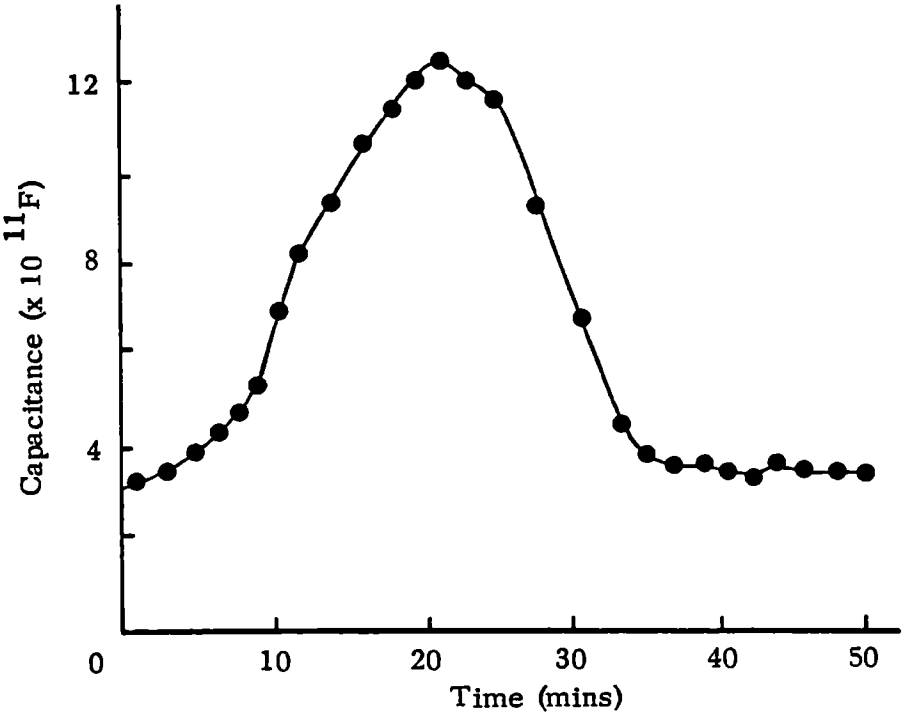

Fig. 4.32. Capacitance at 10 Hz as a function of time for melting transition of PEG 4000 at 333K

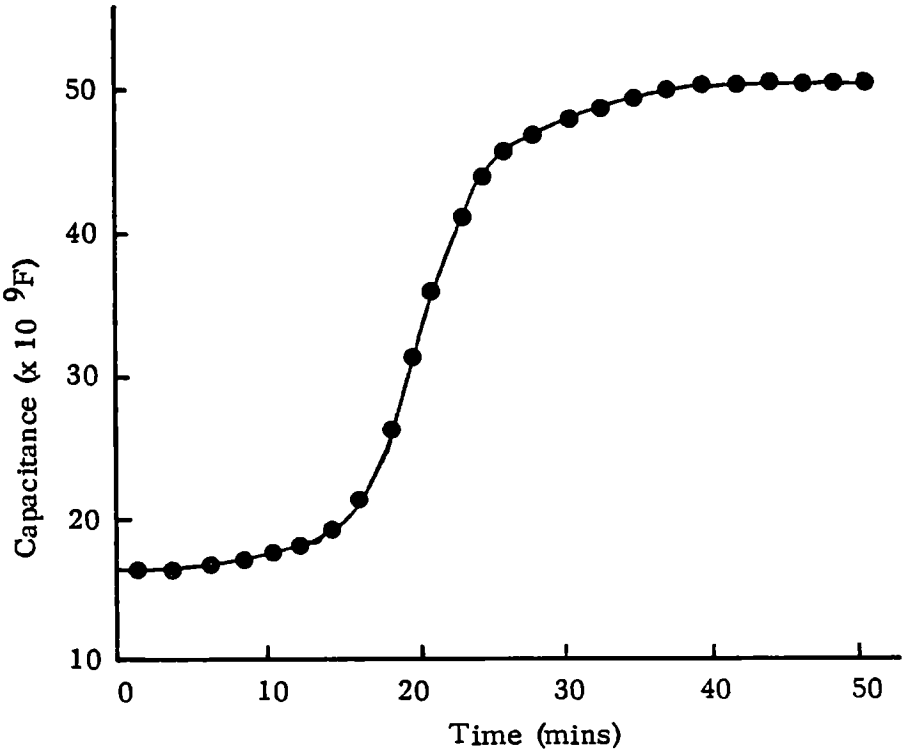

Table 4.5. Melting transition half times ($t_{m\frac{1}{2}}$) for PEG 4000

Temperature of melting (K)	Melting half time ($t_{m\frac{1}{2}}$) mins	
	10 Hz	1778 Hz
343	5.0	4.5
338	6.5	7.0
333	21.0	18.0
333 Annealed sample	45.0	-
333 Quenched material	16.0	-

Table 4.6. Values of Avrami exponent for melting obtained from data at 10 Hz for PEG 4000

Temperature of melting (K)	Avrami exponent, n_a
343	0.4
338	1.9
333	2.4
333 Annealed sample	2.5
333 Quenched material	2.7

treatments on the time dependent behaviour of melting was also investigated. PEG 4000 which had been annealed, by cycling three times between the solid and liquid states showed a two-fold increase in the melting half time. This reflects the increase in the crystallinity and the higher proportion of extended chain crystals present in this material, giving it a greater thermal stability and hence increasing the time required for melting compared to unannealed polymer. However, PEG 4000 which had been solidified by quenching in liquid nitrogen showed at most a small decrease in the melting half time.

Since melting can be regarded as a process which involves nucleation and growth of a new phase within another, it can be treated as a simple reverse of crystallisation and thus Avrami growth kinetics may be expected to apply. The values of the Avrami exponents calculated from the data at 10Hz for the different melting temperatures are presented in Table 4.6. and range from 0.4 to 2.7. It has been postulated that nucleation occurs at corners or lattice defects in the crystals since direct observation of PEG single crystals embedded in liquid shows melting occurs by progressive lateral shrinkage, often starting at the corners (Buckley and Kovacs, 1976). These authors concluded that for the melting of extended chain crystals, a model which involves closely packed crystalline lamella without an intervening layer of molecules in the liquid state is appropriate, as has been suggested for melting in other polymers. It is expected that the Avrami parameter for this mechanism would be 3 or 4. However, melting is a complex transition and may be influenced by many factors. Thus it is not surprising that the Avrami parameters calculated from the results here showed a wide range of values and that no trends could be established.

4.3.2. Trimethoprim

The dielectric response of trimethoprim in the solid was investigated over a temperature range from 363 to 293K, below which temperature the dielectric loss became too low to measure accurately.

The results could be normalised over the temperature range studied and a normalisation curve is presented in Fig. 4.33. Circuit analysis of the response showed that the system could be represented by:

(i) A frequency dependent capacitance in parallel with

(ii) A frequency independent capacitance

These two elements which characterised the barrier response were in series with:

(iii) A frequency independent capacitance

(iv) A frequency dependent capacitance

(v) A conductance

All of these three elements were associated with the bulk response. The characteristic parameters at the different temperatures are given in Table 4.7. Temperature independent behaviour over the temperature range studied was displayed by the Dissado-Hill shape parameters, the frequency independent capacitances $C_{\infty 1}$ and $C_{\infty 2}$ and the amplitude of the loss processes, $C_{(0)1}$ and $C_{(0)2}$ for both barrier and bulk responses. However, Arrhenius plots of the loss peak frequencies ωp_1 and ωp_2 as well as the bulk conductance, Go_2 revealed two different regions of temperature dependent behaviour which were similar for all three parameters. Between 363K and 333K, the observed process exhibited only weak temperature dependence with a calculated activation energy of ~ 0.2 eV in all cases. Below 333K, a sharp increase in the gradient of the Arrhenius plots was observed, with the calculated activation energies

Fig. 4.33. Normalised curve of frequency response for trimethoprim

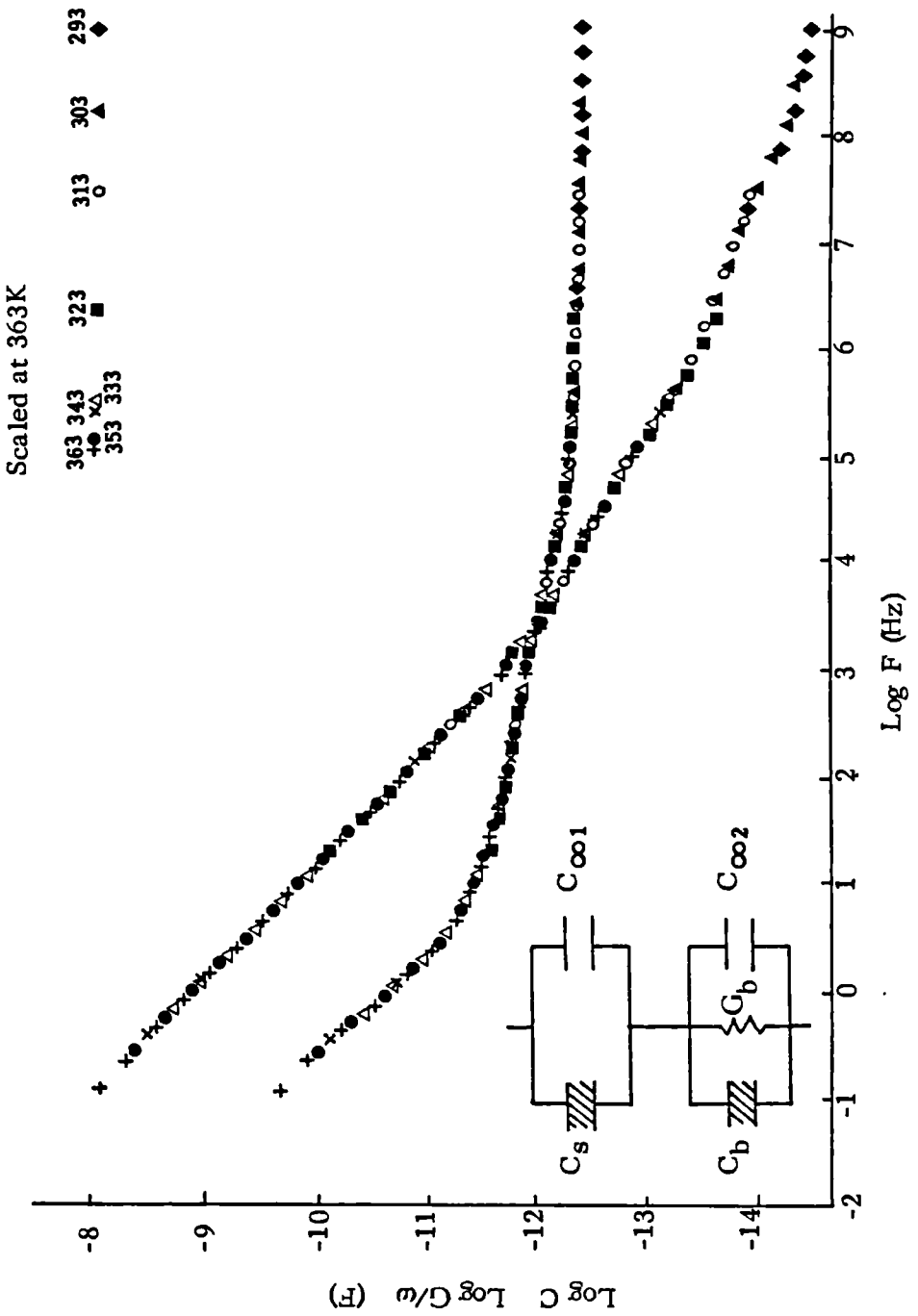

Table 4.7. Characteristic dielectric circuit parameters of trimethoprim

Temperature (K)	Dissado-Hill parameters				Barrier $C_{\infty 1}$ (F) x 10^{11}	Bulk $C_{\infty 2}$ (F) x 10^{12}	Barrier ω_{p1} (Hz) x 10^{10}	Bulk ω_{p2} (Hz) x 10^{3}	Barrier $C_{(0)1}$ (F) x 10^{4}	Bulk $C_{(0)2}$ (Hz) x 10^{11}	Bulk G_{02} (Ω^{-1}) x 10^{13}
	Barrier		Bulk								
	m	n	m	n							
363	-	0.15	0.5	0.7	1.7	4.7	280,000	85,000	2.4	1.7	84,000
353	-	0.15	0.5	0.7	1.7	4.7	220,000	67,000	2.4	1.7	67,000
343	-	0.15	0.5	0.7	1.7	4.7	180,000	53,000	2.4	1.7	53,000
333	-	0.15	0.5	0.7	1.7	4.7	160,000	47,000	2.4	1.7	47,000
323	-	0.15	0.5	0.7	1.7	4.7	14,000	4,200	2.4	1.7	4,200
313	-	0.15	0.5	0.7	1.7	4.7	1,500	450	2.4	1.7	450
303	-	0.15	0.5	0.7	1.7	4.7	120	33	2.4	1.7	33
293	-	0.15	0.5	0.7	1.7	4.7	8.9	2.7	2.4	1.7	2.7

Fig. 4.34. Arrhenius plot for bulk loss peak frequency for trimethoprim

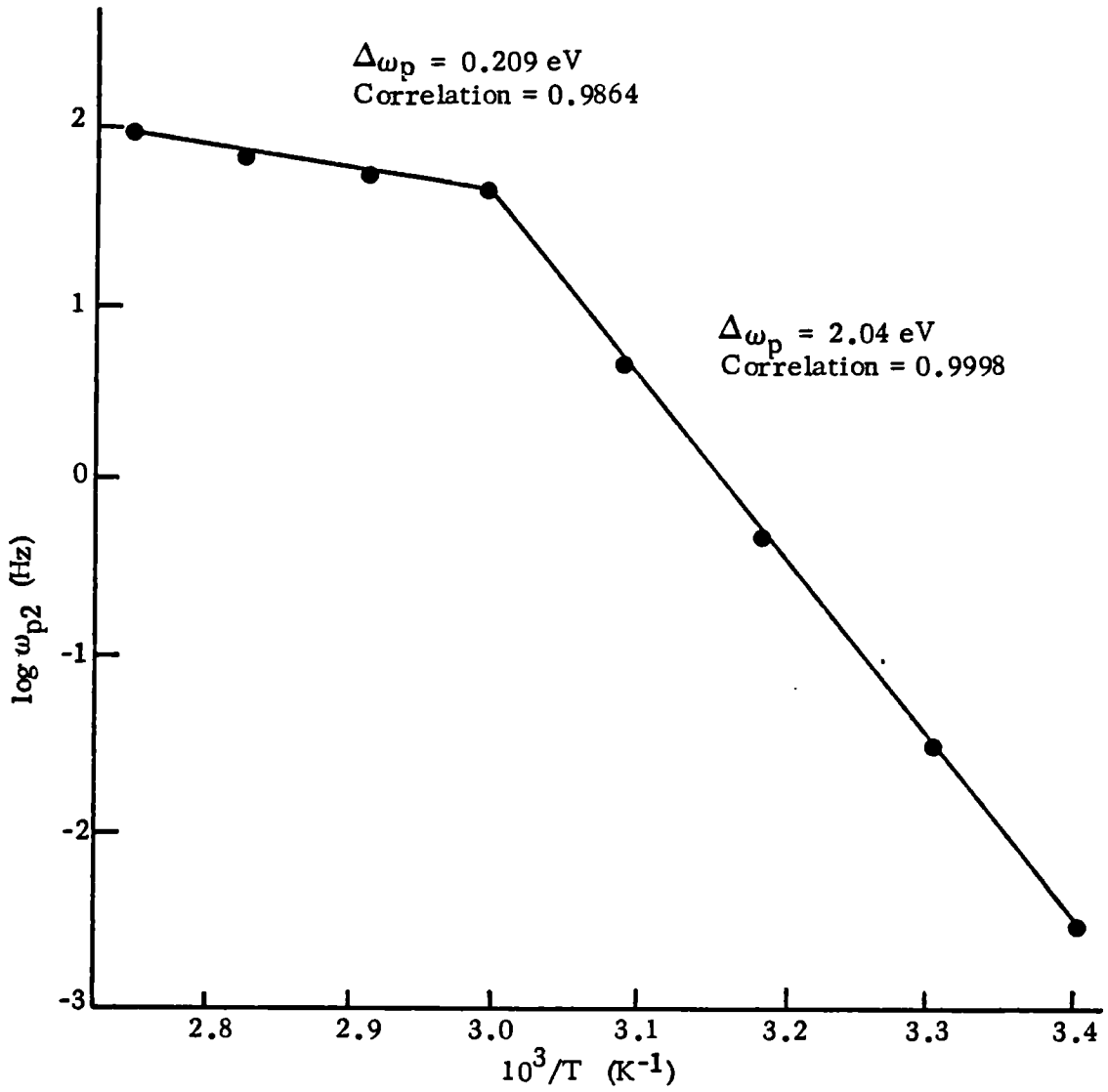

Table 4.8. Activation energies of characteristic parameters of trimethoprim determined from circuit analysis

Parameter	High temp. process (363—333K) Δ (eV)	Correlation	Low temp. (333—293K) Δ(eV)	Correlation
ω_{p1}	0.195	0.9851	2.05	0.9997
ω_{p2}	0.209	0.9864	2.04	0.9998
G_{o2}	0.209	0.9864	2.04	0.9998

rising to ~2.05 eV. A typical Arrhenius plot of the barrier loss peak frequency (ωp_1) is presented in Fig. 4.34., and the values of the activation energies for all three parameters in Table 4.8.

Since all the temperature dependent processes exhibit the same activation energy, it appears that the conduction and dipole relaxation, which must occur in a crystalline environment, arise through hydrogen bond transfer, coupled to $-OCH_3$ side group rotations and twisting about the $-CH_2$ bond. Neutron diffraction studies (Koetzle and Williams, 1976) indicate that extensive hydrogen bonding can occur to give a ribbon like network, with N(1) and N(2) of the pyrimidine ring acting as receptor and donor respectively across one centre of symmetry, and N(3) and N(4) acting similarly across another. At high temperatures, the activation energy for the process of ~0.2 eV corresponds to ~1650 $\nu\,cm^{-1}$. I.R. studies (Bettinetti et al, 1976) show a strong absorption band at this wavelength.

At low temperatures, the high activation energy of ~2.0 eV is consistent with transport of charge by hydrogen bond 'hopping', which occurs together with dipole reorientation, and is likely to involve twisting of the CH_2 bridge.

4.3.3. Solid dispersions of PEG 4000 and Trimethoprim

4.3.3.1. Liquid state

Dispersions containing 2%, 10% and 50% $^{w}/_{w}$ of trimethoprim in PEG 4000 were fused completely at 473K for 10 minutes prior to pouring into the dielectric cell at 363K, which was the highest temperature that could be achieved with this experimental system. Frequency scans of the solid dispersions were performed as for PEG 4000 and composite curves of the response at different temperatures for each concentration are given in Fig. 4.35a., b. and c.

Fig. 4.35. Composite graph of frequency response for molten PEG 4000 and various concentrations of trimethoprim

a. 2%^{w}/w trimethoprim

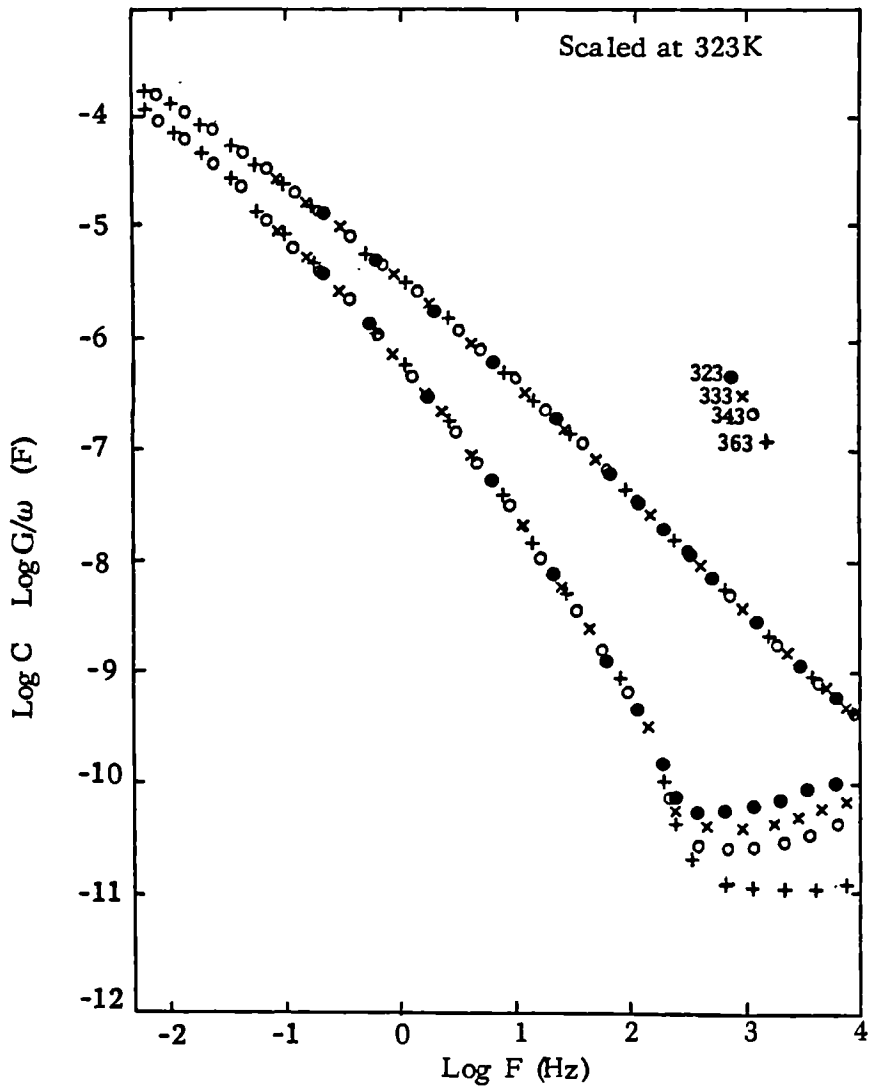

Fig. 4.35. b. 10%^{w}/w trimethoprim

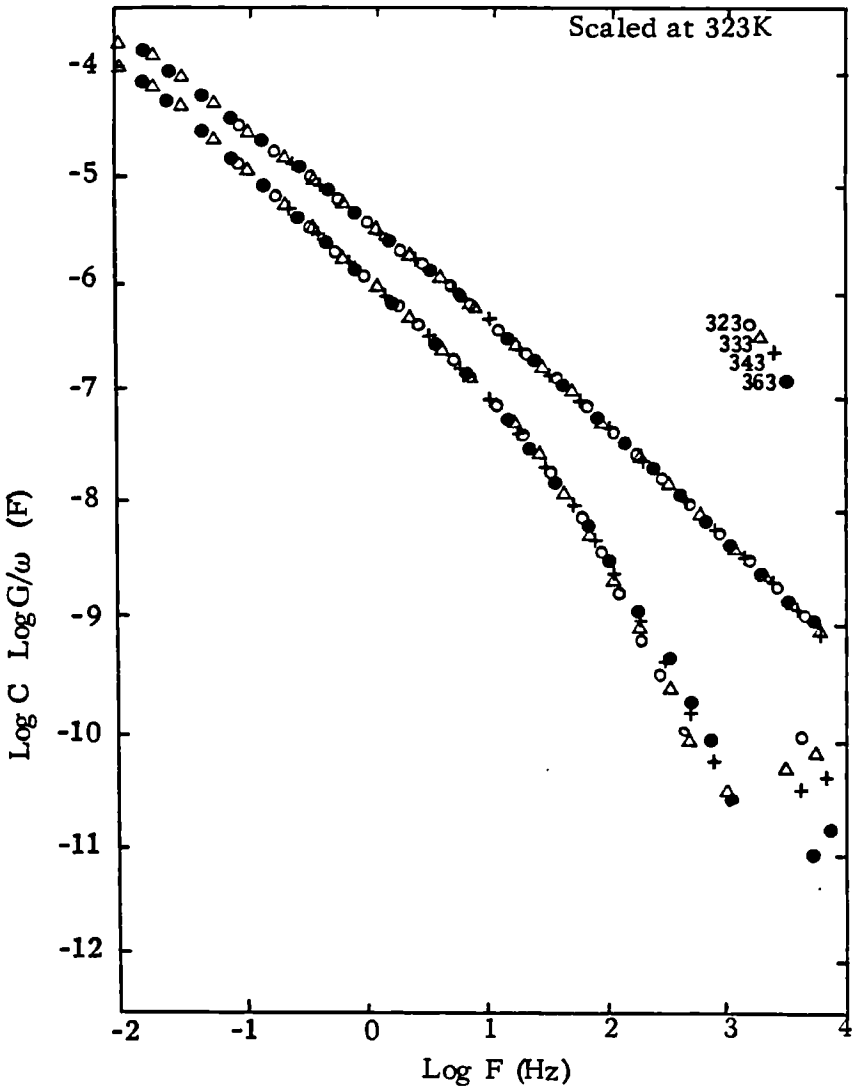

Fig. 4.35. c. 50%^{w}/w trimethoprim

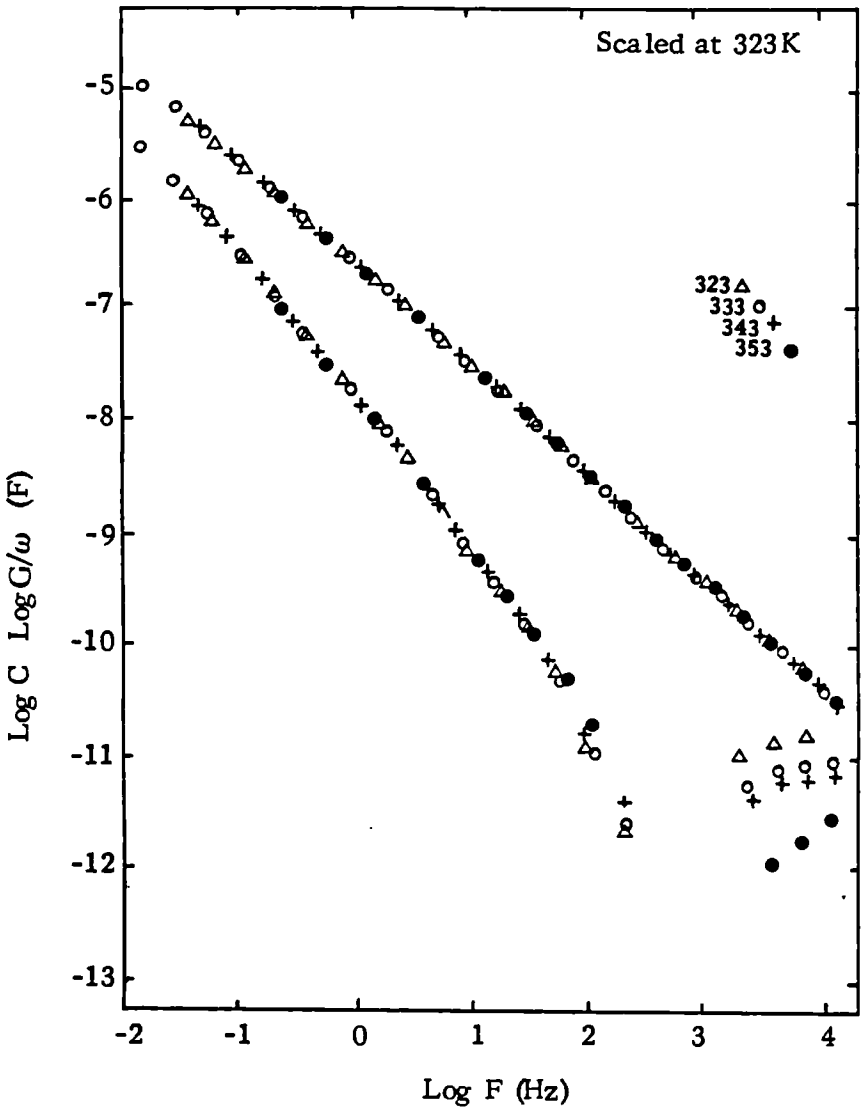

Normalisation of the data could not be carried out since the components of the response displayed different temperature dependent behaviour relative to each other. As can be observed from the composite graphs of the dielectric response, there is an anomalous decrease in the capacitance at frequencies of approximately 10^3Hz for all concentrations of trimethoprim, which often became more pronounced as the temperature was lowered. This type of behaviour is usually observed where resonance effects are present. Since this behaviour was never observed for PEG 4000 alone, electrode bending or resonating effects can be eliminated as the cause, which tends to suggest that the resonance effect arises from the presence of the drug. The oscillation is probably due to the effect of polarisation induced by the field on the particles of drug since it is enhanced as the drug content increases (Armstrong and Edmondson, 1973). At high frequencies, the induced charges are not able to respond to the field, except within the particle itself, thus the capacitance is positive. At lower frequencies, the positive ions drawn to the drug particles overcompensate for the induced negative charges on the drug particles (and vice versa) and the capacitance becomes negative. For very low frequencies, the conductance in series with the barrier contributes to give a positive capacitance.

Unfortunately, circuit analysis of the responses could not be carried out because of the high frequency behaviour of the capacitance, which led to an unacceptably high degree of uncertainty in the curve fitting procedure. However, estimates of the conductivity can be obtained from the loss curve for each concentration of trimethoprim. There is an increase in the conductivity at all concentrations of drug, relative to that of the polymer melt alone, suggesting that some of the trimethoprim has dissolved and is acting

as a charge donor. The conductivity of the 10% ^{w}/w and 50% ^{w}/w dispersions is reduced compared to that of the 2% ^{w}/w dispersions, as would be expected, since the volume fraction of the polymer has decreased.

4.3.3.2. PEG 4000 and Trimethoprim solid dispersions - solid state

The frequency responses of PEG 4000 and trimethoprim solid dispersions investigated in the solid state as for the polymer alone could be normalised for all concentrations of drug. Normalised curves of the data are presented in Fig. 4.36. to Fig. 4.38. As with PEG 4000, the results obtained in the liquid and solid states cannot be fitted together. Moreover, hysteresis between the cooling and heating cycles is again observed.

The dielectric response of the solid dispersions could be interpreted at all the concentrations of drug studied in terms of the circuit diagram given for PEG 4000. Even at the highest concentration of 50% ^{w}/w trimethoprim, no separate dielectric response attributable to the drug was observed and that of the polymer predominated. The Dissado-Hill shape parameter $n = 0.2$ associated with the barrier response remained unchanged in the presence of the drug, suggesting that the behaviour and structure of the barrier is similar to that postulated for PEG 4000. It is possible that the polymer is preferentially 'adsorbed' onto the electrode surface rather than the drug, or that the amount of drug molecules present in the barrier layer is insufficient to influence its behaviour.

Scaling of the magnitudes of the individual parameters was achieved by the usual computer curve fitting procedure and the results are given in Tables 4.9. to 4.14. for cooling and heating cycles of 2%, 10% and 50% ^{w}/w trimethoprim solid dispersions. The Dissado-Hill shape parameters at all concentrations are similar to those obtained for PEG 4000, indicating a fairly wide range of

Fig. 4.36. Normalised curve of frequency response for PEG 4000 and 2%w/w trimethoprim solid dispersion

a. On cooling cycle

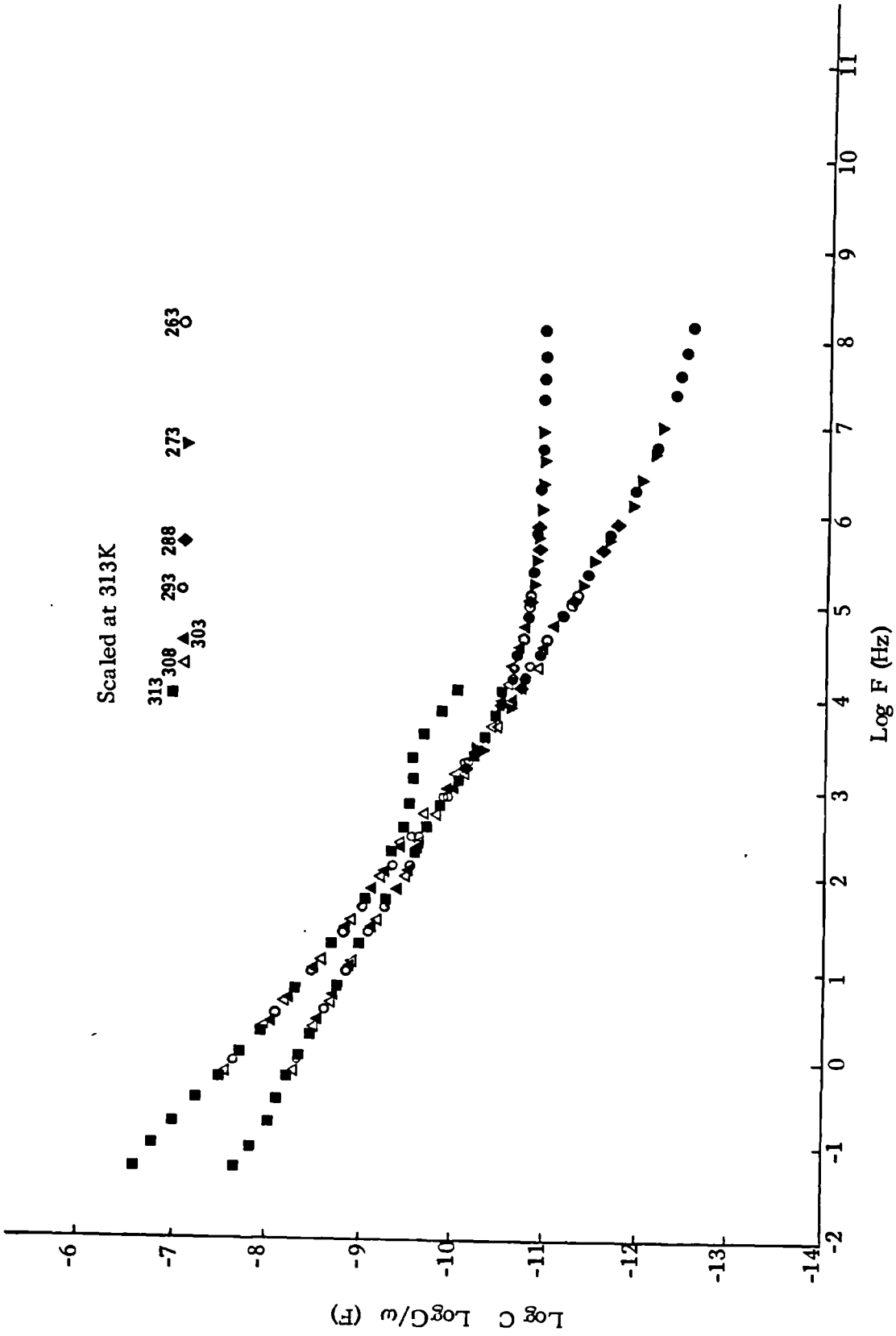

Fig. 4.36. b. On heating cycle

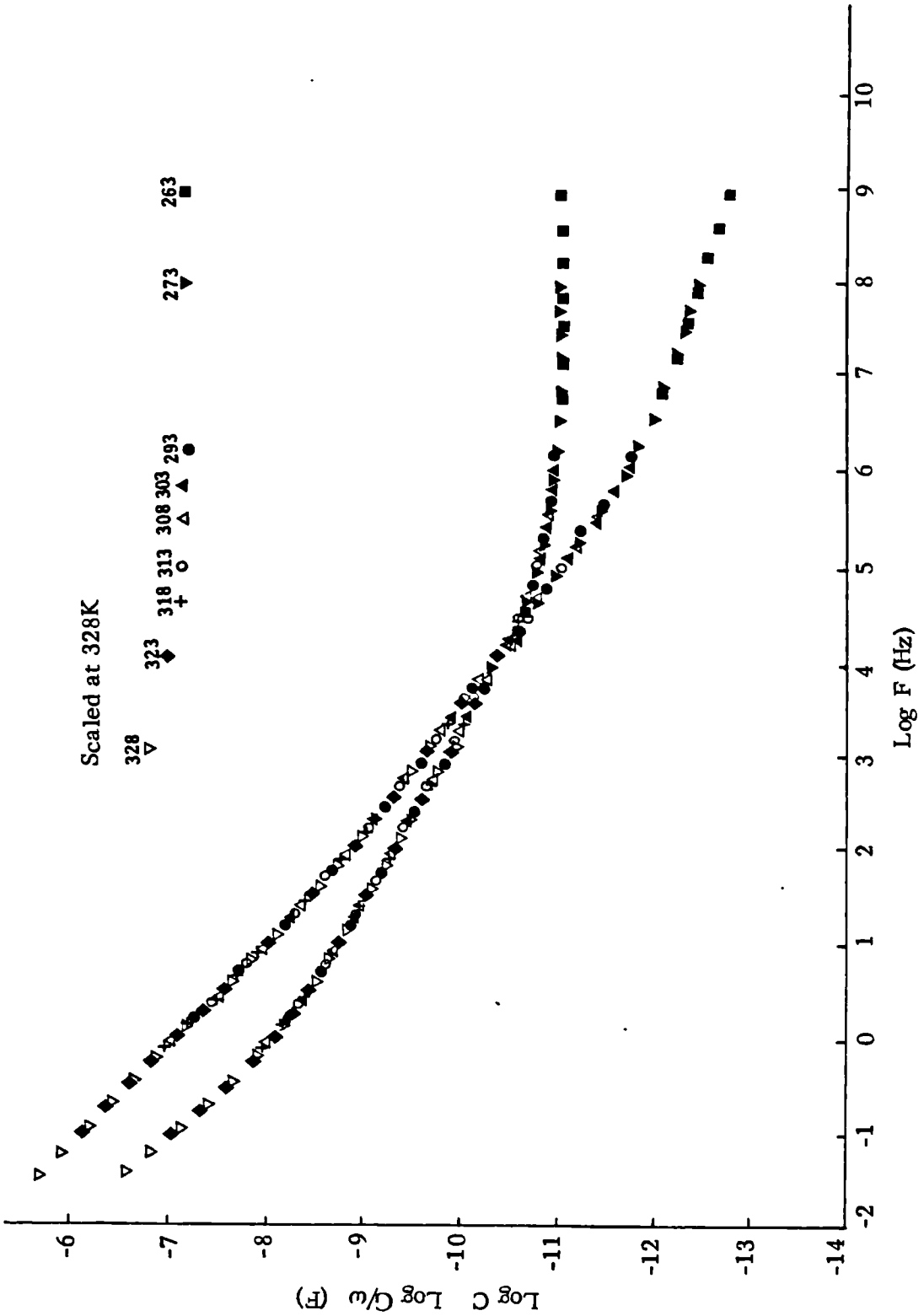

Fig. 4.37. Normalised curve of frequency response for PEG 4000 and 10%^{w}/w trimethoprim solid dispersion

a. On cooling cycle

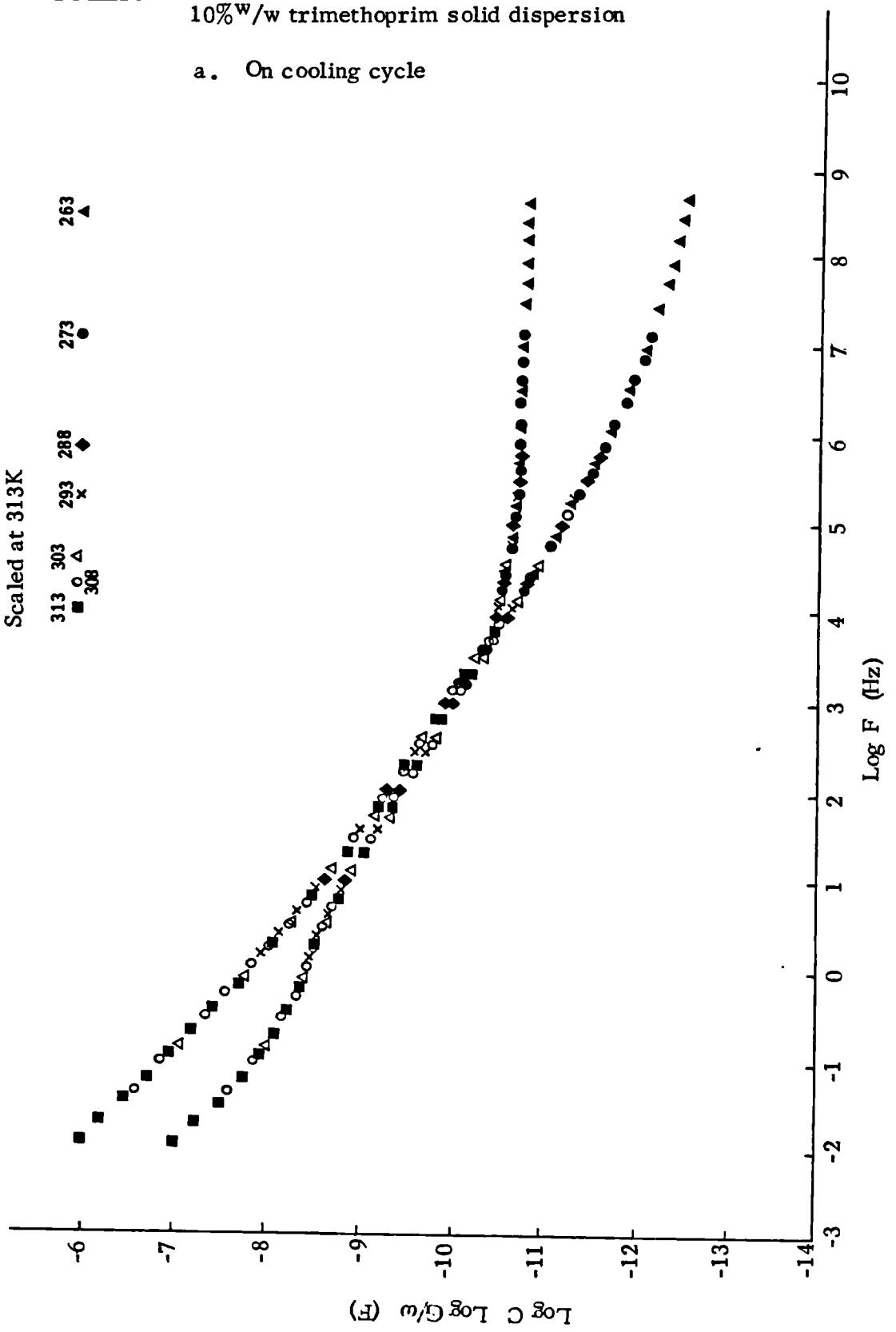

Fig. 4.37. b. On heating cycle

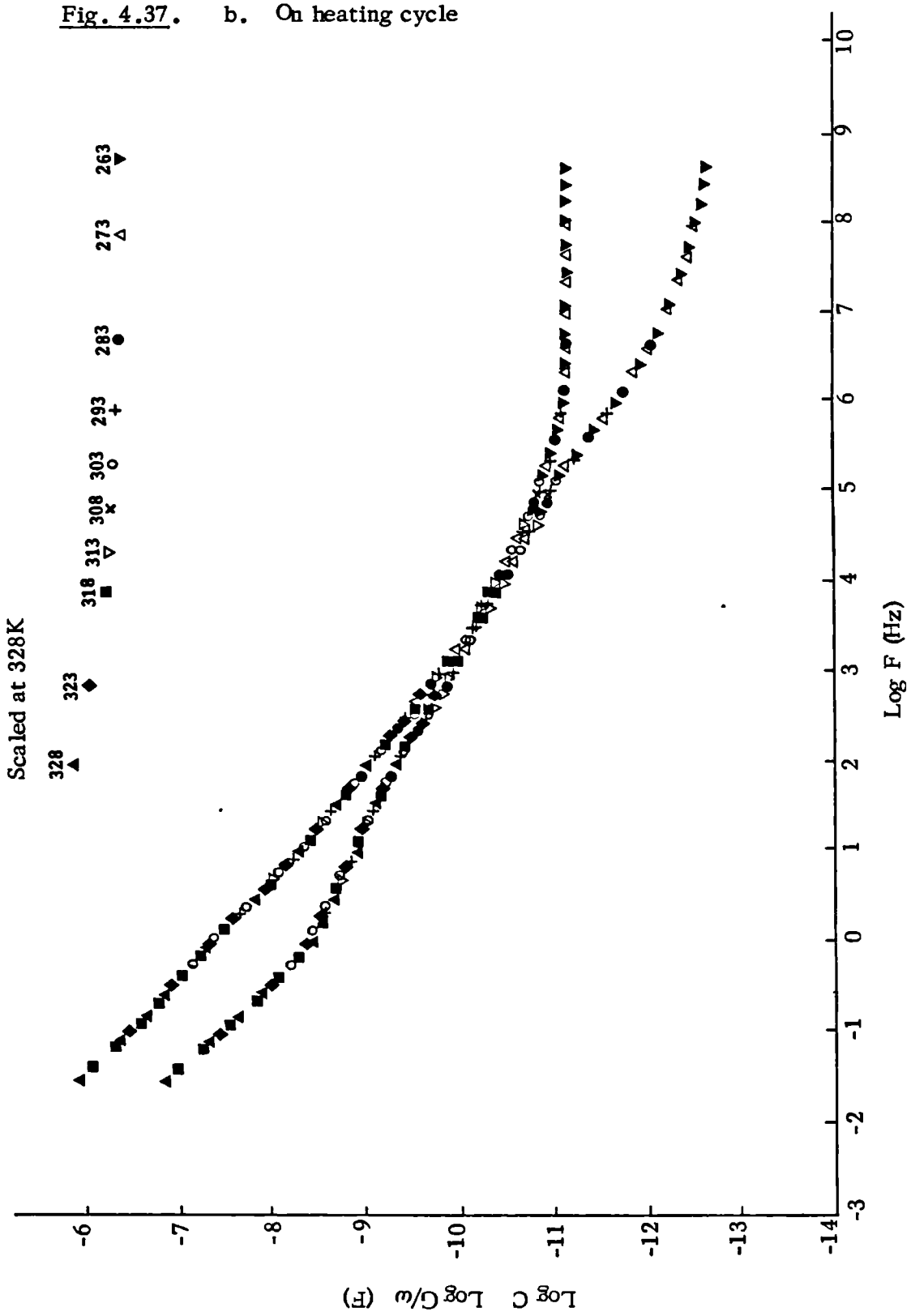

Fig. 4.38. Normalised curve of frequency response for PEG 4000 and 50%^{w}/w trimethoprim solid dispersions

a. On cooling cycle

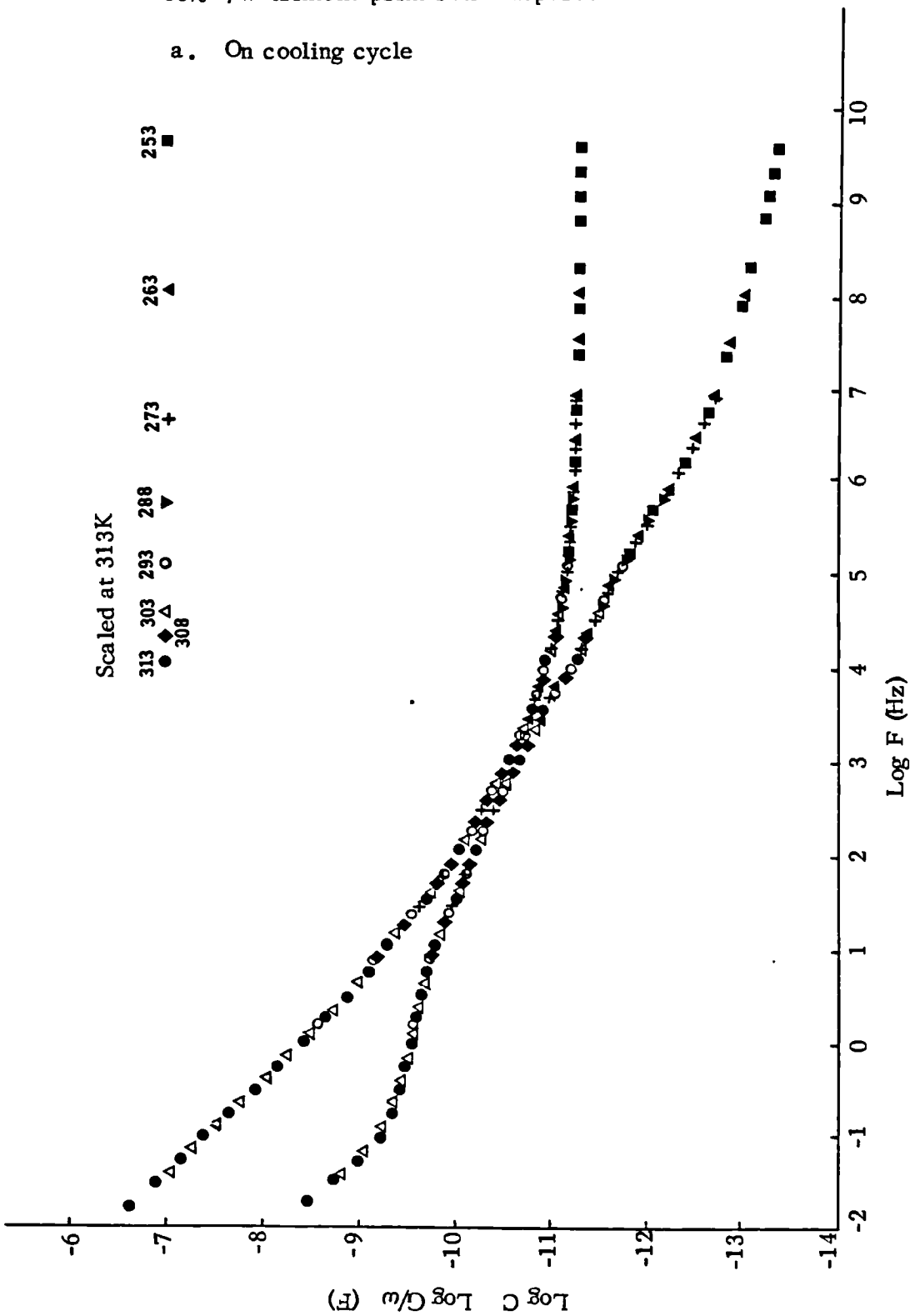

Fig. 4.38. b. On heating cycle

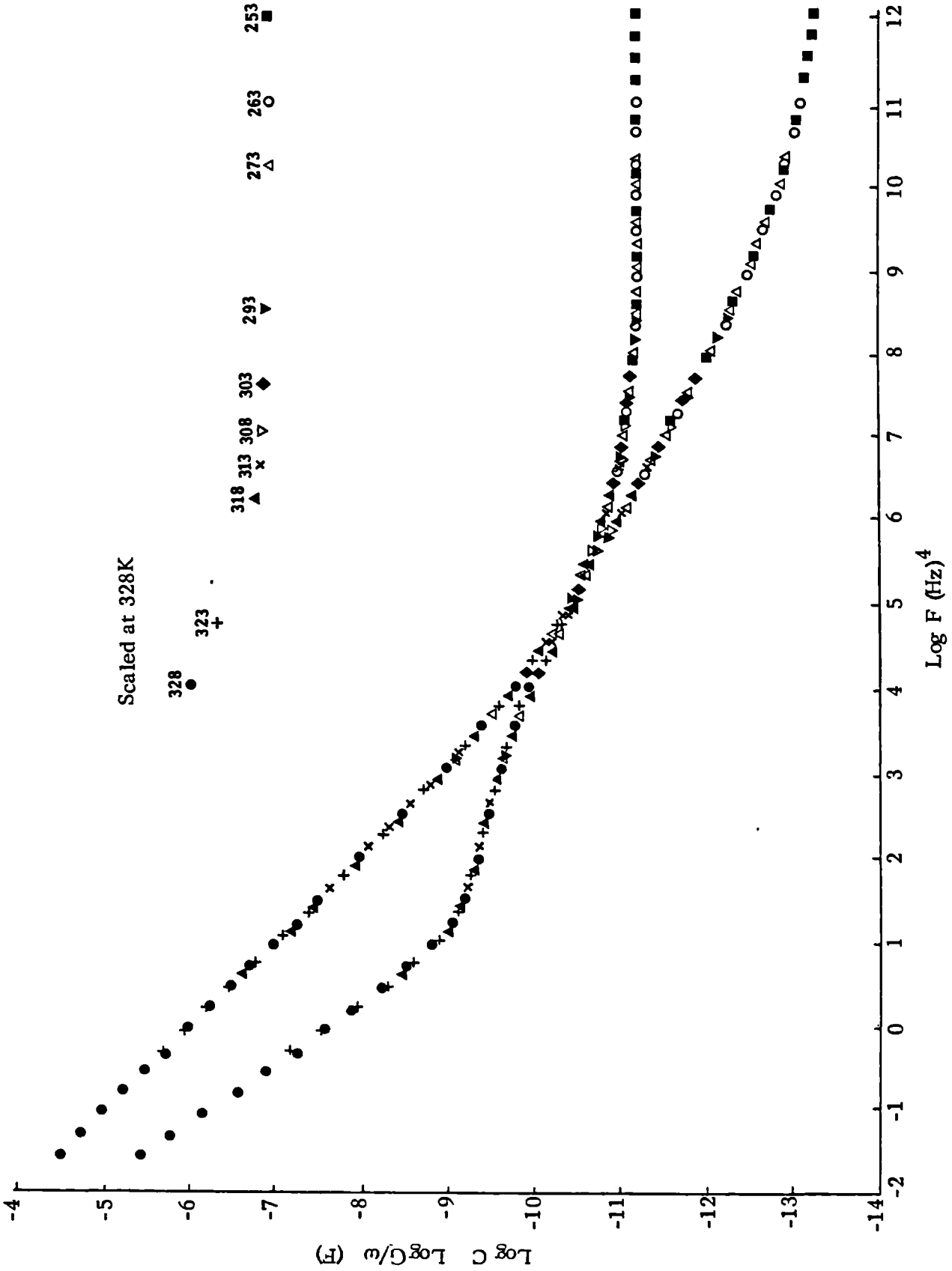

Table 4.9. Characteristic dielectric circuit parameters of PEG 4000 and 2%^{w}/w trimethoprim solid dispersions, at different temperatures on the cooling cycle

Temperature (K)	Dissado-Hill parameters				Barrier ω_{p1} (Hz) x 10^9	Bulk ω_{p2} (Hz) x 10^3	Barrier $C_{(0)1}$ (F) x 10^9	Bulk $C_{(0)2}$ (F) x 10^9	Bulk G_{02} (Ω^{-1}) x 10^{10}	$C_{\infty TOTAL}$ (F) x 10^{11}
	Barrier		Bulk							
	m	n	m	n						
313	-	0.2	0.4	0.45	7,500	7,500	7.1	7.1	3,200	1.8
308	-	0.2	0.4	0.45	5,000	5,000	7.1	7.1	1,900	1.8
303	-	0.2	0.4	0.45	2,800	2,800	7.1	7.1	970	1.8
293	-	0.2	0.4	0.45	560	560	7.5	7.5	240	1.9
288	-	0.2	0.4	0.45	300	300	7.5	7.5	120	1.9
273	-	0.2	0.4	0.45	29	29	7.5	7.5	20	1.9
263	-	0.2	0.4	0.45	9.7	9.7	7.5	7.5	4.3	1.9

Table 4.10. Characteristic dielectric circuit parameters of PEG 4000 and 2%^{w}/w trimethoprim solid dispersions, at different temperatures on the heating cycle

Temperature (K)	Dissado-Hill parameters				Barrier ω_{p1} (Hz) x 10^9	Bulk ω_{p2} (Hz) x 10^3	Barrier $C_{(0)1}$ (F) x 10^3	Bulk $C_{(0)2}$ (F) x 10^9	Bulk G_{02} (Ω^{-1}) x 10^{10}	$C_{\infty TOTAL}$ (F) x 10^{12}
	Barrier		Bulk							
	m	n	m	n						
328	-	0.2	0.4	0.45	72,000	72,000	1.2	1.2	15,000	3
323	-	0.2	0.4	0.45	55,000	55,000	4	4	11,000	10
318	-	0.2	0.4	0.45	4,000	4,000	7.5	7.5	2,400	19
313	-	0.2	0.4	0.45	2,800	2,800	7.5	7.5	1,600	19
308	-	0.2	0.4	0.45	1,800	1,800	7.5	7.5	850	19
303	-	0.2	0.4	0.45	1,100	1,100	7.5	7.5	650	19
293	-	0.2	0.4	0.45	220	220	7.5	7.5	130	19
273	-	0.2	0.4	0.45	20	20	7.5	7.5	11	19
263	-	0.2	0.4	0.45	4	4	7.5	7.5	2.5	19

Table 4.11. Characteristic dielectric circuit parameters of PEG 4000 and 10%^{w}/w trimethoprim solid dispersions, at different temperatures on the cooling cycle

Temperature (K)	Dissado-Hill parameters				Barrier ω_{p1} (Hz) x 10^{10}	Bulk ω_{p2} (Hz) x 10^{4}	Barrier $C_{(0)1}$ (F) x 10^{3}	Bulk $C_{(0)2}$ (F) x 10^{9}	Bulk G_{02} (Ω^{-1}) x 10^{11}	C_{∞}TOTAL (F) x 10^{11}
	Barrier		Bulk							
	m	n	m	n						
313	-	0.2	0.4	0.45	32,000	32,000	4.5	4.5	11,000	1.1
308	-	0.2	0.4	0.45	10,000	10,000	5	5	6,400	1.3
303	-	0.2	0.4	0.45	7,300	7,300	5	5	1,300	1.3
293	-	0.2	0.4	0.45	790	790	5	5	400	1.3
288	-	0.2	0.4	0.45	310	310	5	5	150	1.3
273	-	0.2	0.4	0.45	30	30	5	5	6.1	1.3
263	-	0.2	0.4	0.45	2.5	2.5	5	5	1.1	1.3

Table 4.12. Characteristic dielectric circuit parameters of PEG 4000 and 10%w/w trimethoprim solid dispersions, at different temperatures on the heating cycle

Temperature (K)	Dissado-Hill parameters				Barrier ω_{p1} (Hz) x 10^{11}	Bulk ω_{p2} (Hz) x 10^{5}	Barrier $C_{(0)1}$ (F) x 10^{4}	Bulk $C_{(0)2}$ (F) x 10^{10}	Bulk G_{02} (Ω^{-1}) x 10^{12}	$C_{\infty TOTAL}$ (F) x 10^{12}
	Barrier		Bulk							
	m	n	m	n						
328	-	0.2	0.4	0.45	2.5×10^{6}	2.5×10^{6}	7.1	7.1	650,000	1.8
323	-	0.2	0.4	0.45	1.9×10^{6}	1.9×10^{6}	45	45	350,000	11
318	-	0.2	0.4	0.45	260,000	260,000	50	50	70,000	13
313	-	0.2	0.4	0.45	120,000	120,000	50	50	26,000	13
308	-	0.2	0.4	0.45	45,000	45,000	40	40	11,000	10
303	-	0.2	0.4	0.45	20,000	20,000	50	50	7,900	13
293	-	0.2	0.4	0.45	3,800	3,800	50	50	1,500	11
273	-	0.2	0.4	0.45	68	68	45	45	34	13
263	-	0.2	0.4	0.45	7.5	7.5	50	50	3	13

Table 4.13. Characteristic dielectric circuit parameters of PEG 4000 and 50%w/w trimethoprim solid dispersions, at different temperatures on the cooling cycle

Temperature (K)	Dissado-Hill parameters				Barrier ω_{p1} (Hz) x 10^9	Bulk ω_{p2} (Hz) x 10^3	Barrier $C_{(0)1}$ (F) x 10^4	Bulk $C_{(0)2}$ (F) x 10^{10}	Bulk $G_{02}(\Omega^{-1})$ x 10^{12}	$C_{\infty TOTAL}$ (F) x 10^{12}
	Barrier		Bulk							
	m	n	m	n						
313	-	0.2	0.4	0.45	90,000	90,000	2.5	2.5	85,000	3.8
308	-	0.2	0.4	0.45	30,000	30,000	3	3	21,000	4.5
303	-	0.2	0.4	0.45	11,000	11,000	3	3	63,000	4.5
293	-	0.2	0.4	0.45	1,700	1,700	3	3	3,100	4.5
288	-	0.2	0.4	0.45	700	700	3	3	600	4.5
273	-	0.2	0.4	0.45	40	40	3	3	40	4.5
263	-	0.2	0.4	0.45	3.2	3.2	3	3	3.2	4.5

Table 4.14. Characteristic dielectric circuit parameters of PEG 4000 and 50%^{w}/w trimethoprim solid dispersions, at different temperatures on the heating cycle

Temperature (K)	Dissado-Hill parameters				Barrier ω_{p1} (Hz) x 10^{10}	Bulk ω_{p2} (Hz) x 10^{4}	Barrier $C_{(0)1}$ (F) x 10^{5}	Bulk $C_{(0)2}$ (F) x 10^{11}	Bulk G_{02} (Ω^{-1}) x 10^{13}	C_{∞}TOTAL (F) x 10^{13}
	Barrier		Bulk							
	m	n	m	n						
328	-	0.2	0.4	0.45	1.6×10^{7}	1.6×10^{7}	4.2	4.2	7.5×10^{6}	6.3
323	-	0.2	0.4	0.45	7.9×10^{6}	7.9×10^{6}	13	13	3.1×10^{6}	19
318	-	0.2	0.4	0.45	620,000	620,000	25	25	460,000	38
313	-	0.2	0.4	0.45	360,000	360,000	25	25	280,000	38
308	-	0.2	0.4	0.45	81,000	81,000	30	30	110,000	45
303	-	0.2	0.4	0.45	23,000	23,000	30	30	19,000	45
293	-	0.2	0.4	0.45	5,600	5,600	30	30	4,200	45
273	-	0.2	0.4	0.45	81	81	30	30	160	45
263	-	0.2	0.4	0.45	6	6	30	30	9.7	45

dipole relaxations but with some local correlated motion. As with PEG 4000, the loss peak frequencies of the bulk and barrier responses and the bulk conductance displayed temperature dependent behaviour. Arrhenius plots constructed for these parameters (Figs. 4.39. to 4.44.) revealed that the activation energies for the heating and cooling cycles and for all three components were the same for any given concentration of drug. However, the amount of trimethoprim in the solid dispersion did appear to influence the activation energy. At 2% w/w, the calculated activation energy at ~0.93 eV was slightly lower than that of the polymer which was ~1.1 eV. Conversely, at the other two concentrations of trimethoprim, namely 10% w/w and 50% w/w, higher activation energies of ~1.3 eV and ~1.4 eV respectively were observed. In all cases, an anomalous increase in the values obtained for these parameters on the heating curve above 318K was seen, which was mirrored by a corresponding decrease in the previously temperature independent loss peak amplitudes of the bulk and barrier processes. This behaviour is again similar to that observed for PEG 4000 in the absence of any drug.

As the conductance and loss peak frequencies exhibit the same temperature dependence for both heating and cooling data, it can be assumed that the same molecular motion is involved. Furthermore, since the same circuit elements are involved here as for PEG 4000, it is not unreasonable to assume that the observed relaxation process and conductance arise from the same molecular motion as for the polymer. Thus the α_c relaxation seen in the polymer appears to be present in these solid dispersions also, although the activation energies associated with it are slightly different. At high concentrations of trimethoprim, that is both 10% and 50% w/w, the increased activation energy

Fig. 4.39. Arrhenius plots for barrier and bulk loss peak frequencies on heating and cooling cycles for PEG 4000 and 2%w/w trimethoprim solid dispersions

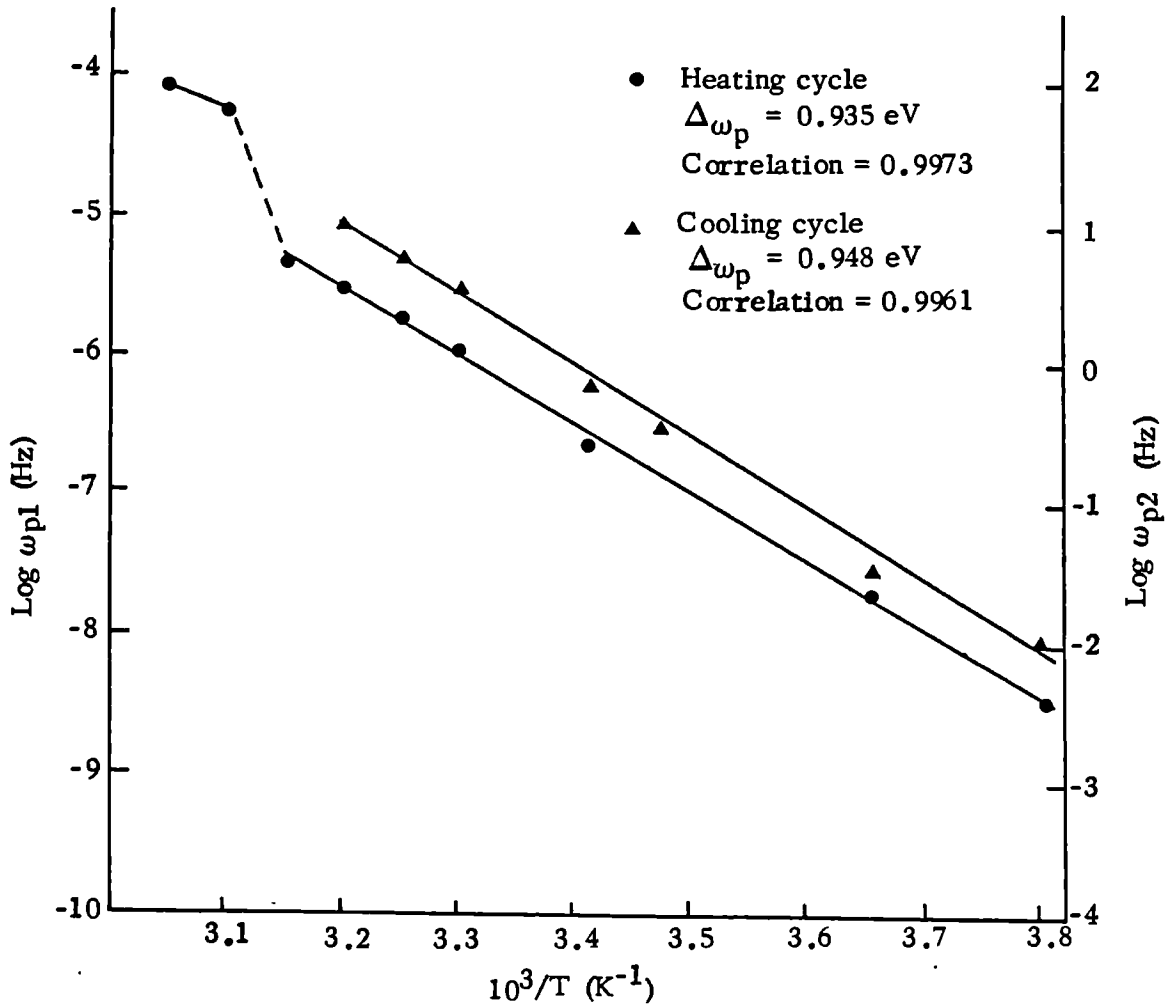

Fig. 4.40. Arrhenius plots for bulk conductance on heating and cooling cycles for PEG 4000 and 2%w/w trimethoprim solid dispersions

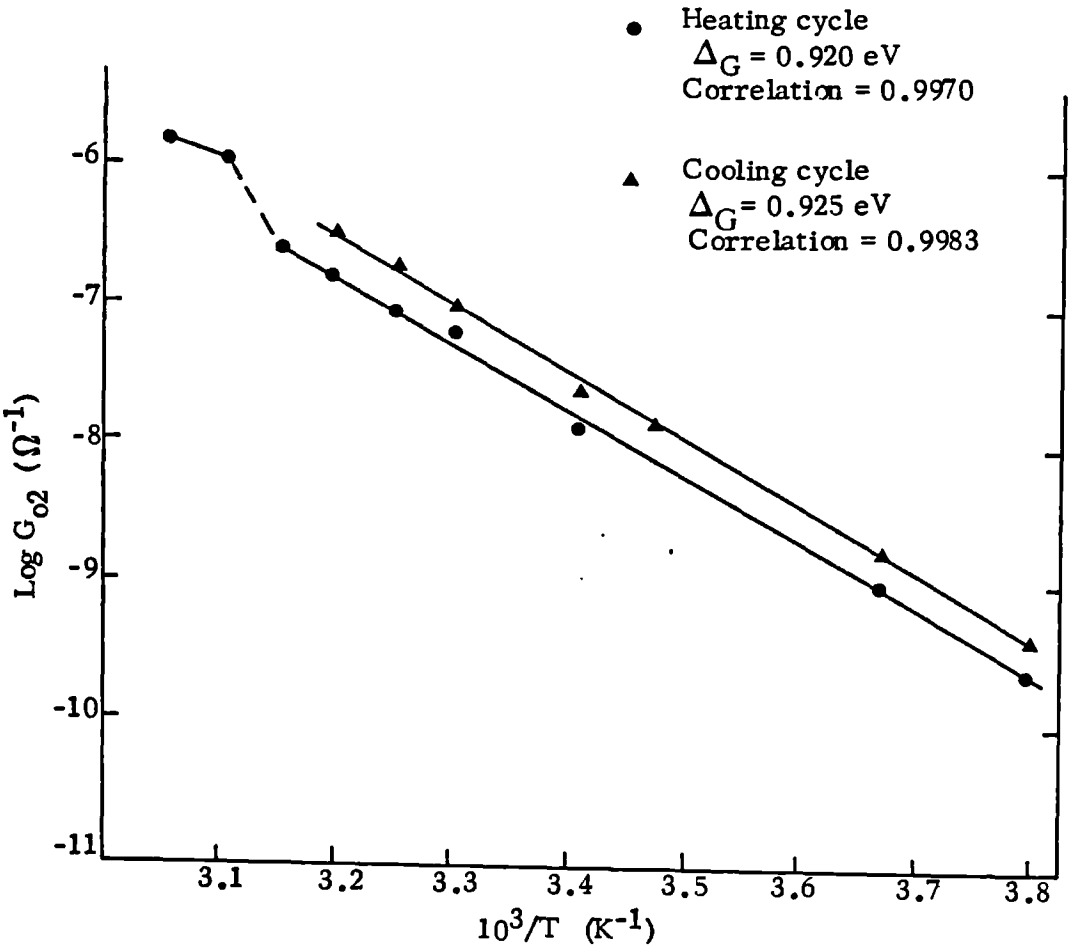

Fig. 4.41. Arrhenius plots for bulk and barrier loss peak frequencies on heating and cooling cycles for PEG 4000 and 10%^{w}/w trimethoprim solid dispersions

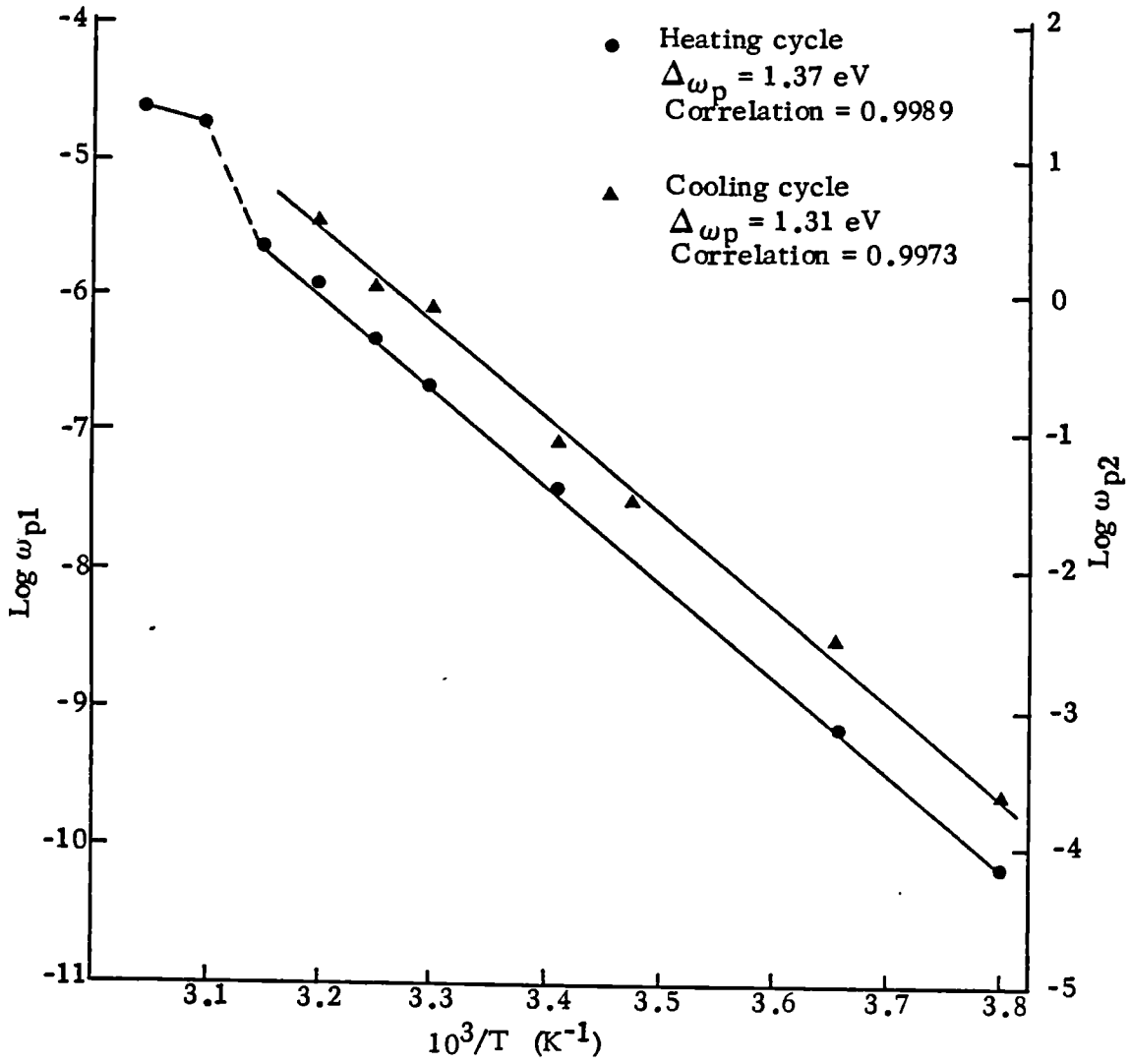

Fig. 4.42. Arrhenius plots for bulk conductance on heating and cooling cycles for PEG 4000 and 10%^{w}/w trimethoprim solid dispersions

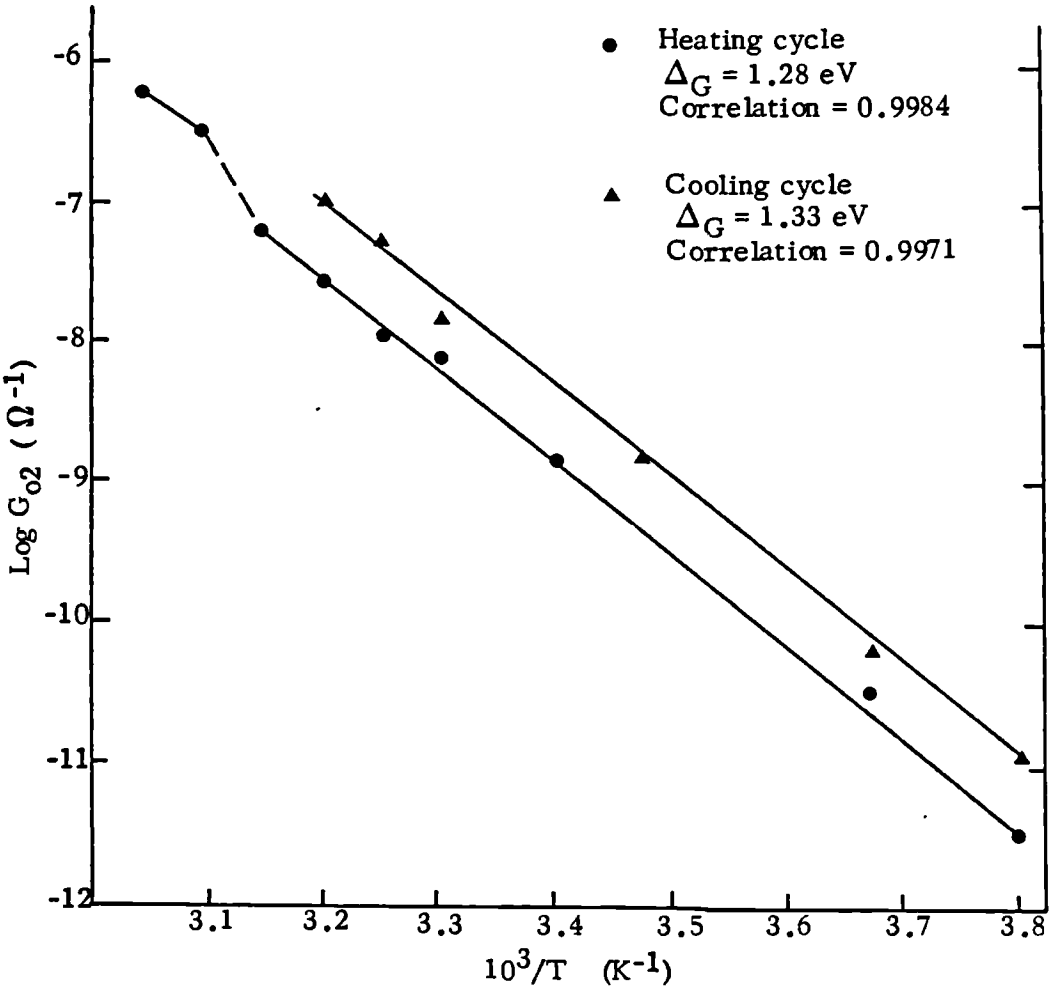

Fig. 4.43. Arrhenius plots for bulk and barrier loss peak frequencies on heating and cooling cycles for PEG 4000 and 50%^{w}/w trimethoprim solid dispersions

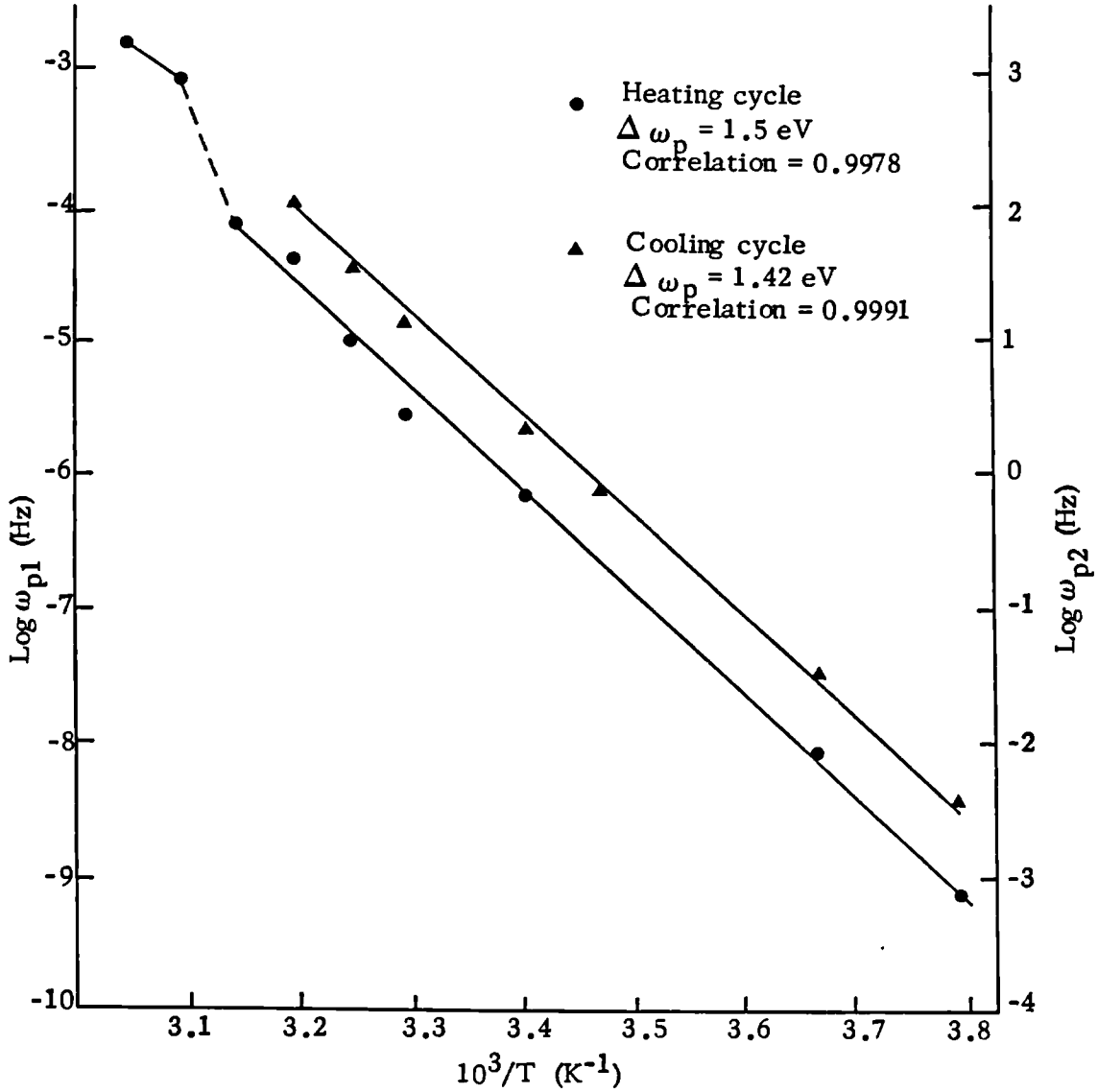

Fig. 4.44. Arrhenius plots for bulk conductance on heating and cooling cycles for PEG 4000 and 50%^{w}/w trimethoprim solid dispersions

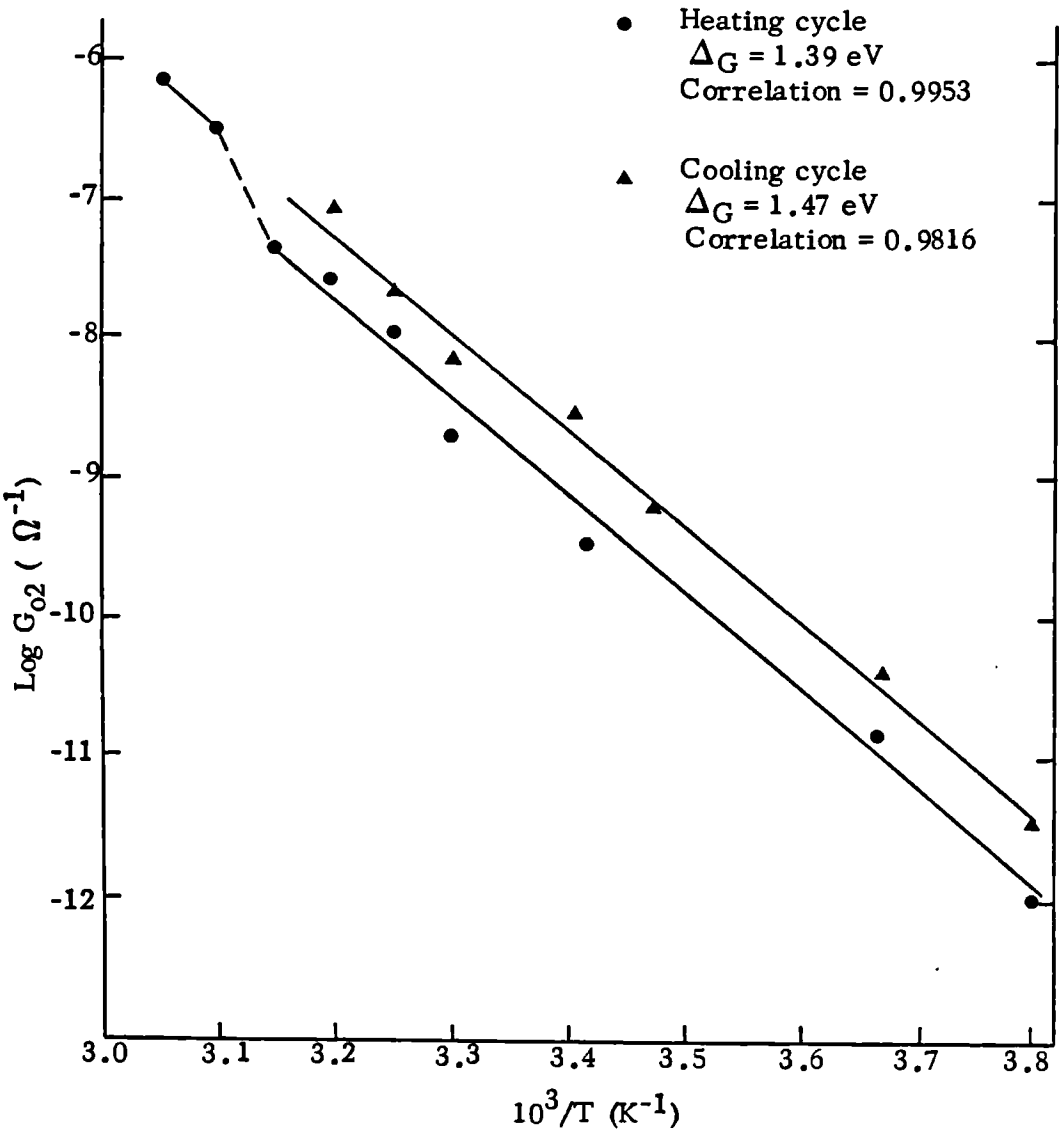

implies that the relaxation route, which also gives rise to the d.c. charge transport process, is more difficult than in the polymer alone. Since the αc relaxation process takes place on the surface of the crystalline lamella and involves mainly the chain ends and folds with only a limited degree of main chain distortion inside the lamella, it seems reasonable to assume that the drug molecules are also outside the crystal itself. This again tends to confirm the results from DSC and X-ray diffraction studies in Chapter 3 which suggest that negligible eutectic or solid solution formation occurs with this system. If a eutectic or solid solution were present, then it would be expected that a totally different dielectric response to that of the polymer alone would be observed, due to the disruption of its structure. However, this is not found here. Thus the presence of the drug does not prevent the relaxation and charge transport processes present in the polymer but does alter the ease with which they occur. The high concentrations of drug obviously hinder these processes, since a high concentration of drug molecules and or crystals would be expected at the lamellae interfaces. It should be remembered that impurities, which would include the drug here, tend to be rejected during the primary crystallisation process and are not incorporated into the crystal. The slight decrease in the activation energy observed when 2%^{w}/w trimethoprim is added to the polymer seems to indicate that at this low concentration of drug the relaxation route in PEG 4000 is facilitated by its presence.

Further evidence for the drug and polymer behaving as separately crystallising entities comes from the anomolous behaviour observed above 318K on the heating cycle. For PEG 4000, this was attributed to the lamella thickening process which resulted in chain extension of folded chain crystals

to their fully extended form. Since this mechanism appears able to occur in the presence of even high concentrations of trimethoprim, and at the same temperatures as for the polymer alone, it suggests that the presence of the drug doe not hinder chain unfolding. Again, this correlates well with the drug molecules being outside of the actual polymer lamellae.

No enhancement of the low temperature β_a relaxation process or reduction of the α_c process, which was observed after quenching PEG 4000 to a more amorphous form was apparent for any of the solid dispersions. Thus it appears that the addition of drug molecules does not result in a significantly higher proportion of amorphous material, and hence has not markedly hindered the polymer crystallisation.

4.3.3.3. Crystallisation behaviour

The temperature and time dependence of the crystallisation of solid dispersions of PEG 4000 and trimethoprim was investigated as for the polymer alone (Chapter 4.3.1.3.). For the solid dispersions crystallised at 318 and 313K, sigmoidal shaped graphs of capacitance as a function of time were observed, which was in contrast to the behaviour at 308K where these graphs displayed a maximum. These results follow a similar pattern to those obtained for the polymer alone (see Figs. 4.28. and 4.29.) which suggests that the same mechanism of crystallisation can occur even if high concentrations of drug are present. The rise and fall in capacitance at 308K therefore probably results from the composite effects of the changes in the bulk conductance and capacitance suggested for PEG 4000.

Crystallisation half times are presented in Table 4.15. for all concentrations of trimethoprim in PEG 4000 studied. There does not appear to be any significant difference between the crystallisation half times of the

Table 4.15. Crystallisation half times ($t_{c\frac{1}{2}}$) for PEG 4000 and trimethoprim solid dispersions

Concentration of trimethoprim (%w/w)	$t_{c\frac{1}{2}}$ at crystallisation temperature of (K) 318	313	308
2	43	28	16
10	49	25	12
50	52	30	18

Table 4.16. Avrami exponents for the crystallisation of PEG 4000 and trimethoprim solid dispersions

Concentration of trimethoprim (%w/w)	Avrami exponent n_a at Crystallisation temperature (K) 318	313
2	2.1	2.3
10	2.3	2.2
50	1.9	1.8

polymer alone or in the presence of trimethoprim, except for a slight increase at high temperatures for 50%^{w}/w solid dispersions. Since drug particles are known to be present at this concentration, this may reflect the additional time required for orientation of the polymer chains during nucleation and growth, which may be hindered by the presence of these particles. No evidence of the drug particles acting as nucleating agents for crystallisation of the polymer could be detected, since the crystallisation times increased slightly instead of being reduced. Thus it seems that the polymer crystallisation process is essentially independent of the concentration of trimethoprim added.

The values of the Avrami exponent were found to range between 1.9 and 2.3 at a crystallisation temperature of 318K and 1.8 and 2.3 at 313K (Table 4.16.). Values of n_a could not be calculated from data at 308K, where the graphs of capacitance as a function of time displayed peaks, for the reasons outlined in Chapter 4.3.1.3. No significant differences were noticeable between solid dispersions containing different concentrations of trimethoprim, or between the two crystallisation temperatures. Furthermore, all these values of n_a are in the same range as those calculated for PEG 4000 alone. Thus it appears that the presence of the drug does not alter the fundamental crystallisation kinetics of the polymer.

This crystallisation behaviour of PEG 4000 and trimethoprim solid dispersions tends to corroborate the results obtained by DSC and X-ray diffraction methods (Chapter 3.3.2.), which suggest that no eutectic or solid solution formation occurs to any detectable extent for this system.

4.3.3.4. Melting behaviour

Investigations of the temperature and time dependence of the melting transition of solid dispersions of PEG 4000 and trimethoprim at 1778 Hz were performed as for PEG 4000 alone. No melting transitions were apparent in samples equilibrated at 328K which is similar to the behaviour observed for the polymer alone. This suggests that the presence of the drug does not significantly depress the melting point of the polymer from 330K, as would be expected if a eutectic or solid solution system were formed, and corroborates the results obtained in Chapter 3.3.2. For temperatures from 333 to 343K, graphs of capacitance as a function of time exhibited maxima, which is again similar to the behaviour determined for PEG 4000 alone.

Melting half times ($t_{m\frac{1}{2}}$) are presented in Table 4.17. and decrease as the temperature of melting is raised. These values are in good agreement with those obtained for PEG 4000, suggesting that the melting behaviour of the polymer is independent of the concentration of drug present. The presence of the drug neither decreases the melting half time of the polymer as would be expected for a eutectic, nor does it increase this parameter as might be expected for a more highly crystalline sample or one which contained a higher proportion of extended chain crystal lamellae. This latter effect is illustrated by annealed PEG 4000 which showed that the melting half time was double that of the unannealed polymer. Small reductions in polymer crystallinity however do not seem to affect the melting half time, in the range studied. As can be seen from Chapter 4.3.1.4., quenched PEG 4000 showed little reduction in this parameter compared to crystalline samples. Thus solid dispersions which DSC results (Chapter 3.3.2.) suggest may

Table 4.17. Melting half times for PEG 4000 and trimethoprim solid dispersions

Temperature (K)	Melting half time in minutes for Concentration of trimethoprim (% w/w) 2	10	50
333	16.0	14.0	17.5
338	6.0	5.0	4.5
343	6.5	4.0	5.0

contain a higher percentage of amorphous material e.g. 50%w/w dispersions, cannot be distinguished from more crystalline solid dispersions by melting half times.

Avrami plots could not be constructed from this data owing to the shape of the graphs of capacitance as a function of time, for the reasons explained previously (Chapter 4.3.1.3.).

CHAPTER 5

CHAPTER 5 Dissolution behaviour

5.1. Introduction

In spite of the number of dissolution studies which have been performed on PEG-drug solid dispersions, the precise mechanisms involved in enhancing the drug release often have not been elucidated. At present, no definite correlation between physical structure and drug release exists in most cases. Furthermore, changes in dissolution rate on ageing have not been related to alterations in structure of the solid dispersion. Various explanations of the drug dissolution enhancement have been postulated, which are summarised below.

(i) Particle size reduction of the drug was suggested by Sekiguchi and Obi (1961) to explain the increased dissolution rate of a eutectic mixture of sulphathiazole and urea compared to that of the drug alone, since the carrier did not exert a solubilising action on the drug nor did it enhance its physiological absorption. The soluble carrier dissolves rapidly releasing a micro-crystalline suspension of the drug with an increased surface area and hence usually a higher rate of dissolution relative to the pure drug. Similarly, for solid solutions where the drug is crystallised as single drug molecules, the maximum surface area is available, which should result in an increase in dissolution (Goldberg et al, 1966). Evidence has been presented by Corrigan et al (1979) from their studies on the dissolution rates of both drug and polymer in support of molecular dispersion as an important factor in enhancing the drug dissolution. McGinity et al (1984) noted that flash cooled solid dispersions of tolbutamide in PEG 6000 had a signficantly faster dissolution rate than slow cooled solid dispersions.

This was attributed mainly to a particle size effect since smaller particles of drug would be expected in the rapidly cooled dispersions.

(ii) Microenvironmental solubilisation of the drug by the carrier may occur in the diffusion layer surrounding the drug particle (Chiou and Riegelman, 1971). PEGS have been shown to increase the aqueous solubility of many drugs (Hargreaves, 1982; Chiou, 1977; Salib and Ebian, 1978; Kaur et al, 1980b) but generally concentrations of more than 10%^{w}/v of polymer are required before any appreciable solubilisation is observed. As a result, many workers have discounted the possibility of microenvironmental solubilisation. Corrigan et al (1979) calculated that the theoretical maximum for enhanced drug dissolution due solely to the solubility enhancing effect of the dissolving polymer was below that of the experimentally observed enhancement. However, Hargreaves (1982) suggested that higher concentrations of PEG may exist in the diffusion layer than had previously been thought and consequently this mechanism cannot be excluded.

(iii) An increase in the actual solubility of the drug may be observed if the crystallites are very small (Chiou and Riegelman, 1971). Alternatively, a metastable polymorph or the amorphous form of the drug may be present in the solid dispersion. Both of these forms would be expected to exhibit a higher solubility than the original crystal form due to their increased surface free energy (Hajratwala, 1974).

(iv) Increased wettability of the drug particles resulting from their intimate contact with the hydrophilic polymer molecules has been proposed by many workers as an important mechanism in the enhanced dissolution rate (Ho and Hajratwala, 1974; Salib et al, 1976; Chiou and Riegelman, 1971). Kim and Jarowski (1977) have demonstrated that lowering the surface

tension resulted in an increase in the dissolution rate of hydrocortisone from solid dispersions. Moreover, studies performed by Hoelgaard and Møller (1975) on the dissolution rate of sparingly soluble drugs formulated as solid dispersions in PEG 6000 or as optimally dispersed and wetted suspensions showed little difference between the two dosage forms. Thus wetting of the drug by the polymer may contribute significantly to the dissolution enhancement.

(v) Decreased aggregation and agglomeration between the particles of the drug (Chiou and Riegelman, 1971). Fine hydrophobic powders often form aggregates (particles which are held together by strong inter or intra molecular cohesive forces) and agglomerates (particles which are held together by weaker cohesive forces) as a result of their increased surface energy. This decreases the surface area available for dissolution. Since in solid dispersion systems, the drug particles are surrounded by hydrophilic polymer, this problem should be removed.

The observed dissolution enhancement of the drug may well result from a combination of the above mechanisms and the relative importance of individual factors may vary from system to system. Changes in the structure of drug-polymer dispersions which arise from differences in the manufacturing conditions or as a result of ageing may or may not have a significant effect on the dissolution rate depending on the mechanisms involved. For example, if particle size reduction is the most important factor in the observed enhancement of dissolution rate, then changes in the manufacturing conditions, such as cooling rate may have a marked influence. Conversely, if microenvironmental solubilisation or improved wetting predominate as the mechanisms of dissolution enhancement of the drug,

these would be expected to be influenced less by changes in the structure of the dispersion.

5.2. Methods

5.2.1. Intrinsic dissolution rate determination

The dissolution apparatus consisted of 1 litre round bottomed flasks containing 1 litre of distilled water as the dissolution medium, maintained at 37°C ± 0.1°C in a water bath (Dissolution system 2000, Copley Instruments Ltd., Nottingham). The constant surface area discs, prepared as described in Chapter 3, were coated with molten paraffin wax such that only the flat surface was available for dissolution. Care was taken to ensure that no localised fusion occurred on the disc surface whilst carrying out this procedure since this might alter the characteristics of the dissolution surface. Subsequently, discs were attached centrally to the lower surface of the rotating shaft and held 6 cm from the bottom of the flask. Several agitation intensities were investigated to determine if the system was diffusion controlled. Two ml samples were withdrawn through a 0.45 μm filter at suitable intervals from a point halfway between the disc and the flask wall, level with the surface of the disc. Duplicate determinations were performed in all cases and the results averaged.

5.2.2. Assay method for PEG 4000

PEG 4000 was assayed using the method of Childs (1975) where a coloured barium iodide complex is produced which can be determined quantitatively at 535 nm.

The procedure adopted was as follows: 1 ml of 5%^{w}/v Barium chloride in 1M Hydrochloric acid and 0.5 ml 0.05M iodine solution were added to 4 ml of PEG solution, which was then mixed thoroughly by shaking. After

standing for 15 minutes, the optical density was read at 535 nm using a UV/visible spectrophotometer (CE292, Cecil Instruments, Cambridge). Blank solutions consisting of distilled water treated similarly were assayed and duplicate determinations were performed in all cases. The influence of trimethoprim on the assay was investigated by using saturated solutions of the drug instead of water, and was found not to affect the results.

5.2.3. Assay method for Trimethoprim

Assay of this drug was carried out by UV spectrophotometry (CE292, Cecil Instruments Ltd., Cambridge) at 270.5 nm. The effect on the assay of adding PEG 4000 was also determined, and was found not to influence the results at the concentrations present.

5.2.4. Solubility determination

The solubility of trimethoprim was determined in distilled water and aqueous PEG 4000 solutions at concentrations of 0.5-60%^{w}/w as follows. Approximately 1 g of trimethoprim together with 10 ml of solvent were placed in a tightly stoppered tube, secured with parafilm, shaken vigorously by hand periodically and equilibrated for 24 hours in a constant temperature oven at 37^{o}C. Preliminary studies indicated that equilibrium solubility was attained within this period of time. After equilibration, the tube contents were filtered through a 0.45 μm millipore filter. The first 4 ml of filtrate were rejected to preclude any filter adsorption effects and the remainder was diluted and assayed by UV spectroscopy as described in 5.2.3. Each solubility determination was carried out in duplicate.

5.3. Results and Discussion

5.3.1. PEG 4000

5.3.1.1. Effect of thermal history

The dissolution behaviour of PEG 4000 prepared under a variety of heating and cooling conditions, and studied at stirring rate of 80 rpm, displayed in all cases a dissolution profile similar to that illustrated in Fig. 5.1. Intrinsic dissolution rates ($mgcm^{-2}min^{-1}$) were calculated from the gradients of the linear portion of the graphs and correlation coefficients were always better than 0.98. All dissolution profiles exhibited a positive curvature initially, confirmed by the negative intercept of the graph, which has been attributed to swelling of the polymer (Heyd et al, 1969). Calorimetric studies of the heat of solution of PEGS showed that two distinct processes occurred in immersing the polymer in water - an initial endothermic process, rapidly followed by a second exothermic reaction (Ikeda et al, 1975). Further studies indicated that if the dissolution was into a saturated solution of PEG, then the latter reaction was not observed. Thus it was concluded that the first process observed related to the swelling and the second to the dissolution of the polymer. These processes are thought to occur simultaneously where the volume of dissolution fluid is large, as in the conditions used in this study.

N.M.R. studies (Liu and Parsons, 1969) on the behaviour of PEGS in aqueous solution suggest that each ethylene oxide unit is hydrated by three water molecules and that much of the trans-gauche-trans sequence and helical conformation associated with the crystalline solid is retained, a conclusion confirmed by I.R. data (Koenig and Angood, 1970).

Fig. 5.1. Representative example of intrinsic dissolution profile of PEG 4000 (sample had been quenched in liquid nitrogen after melting at 100°C for 1 hour)

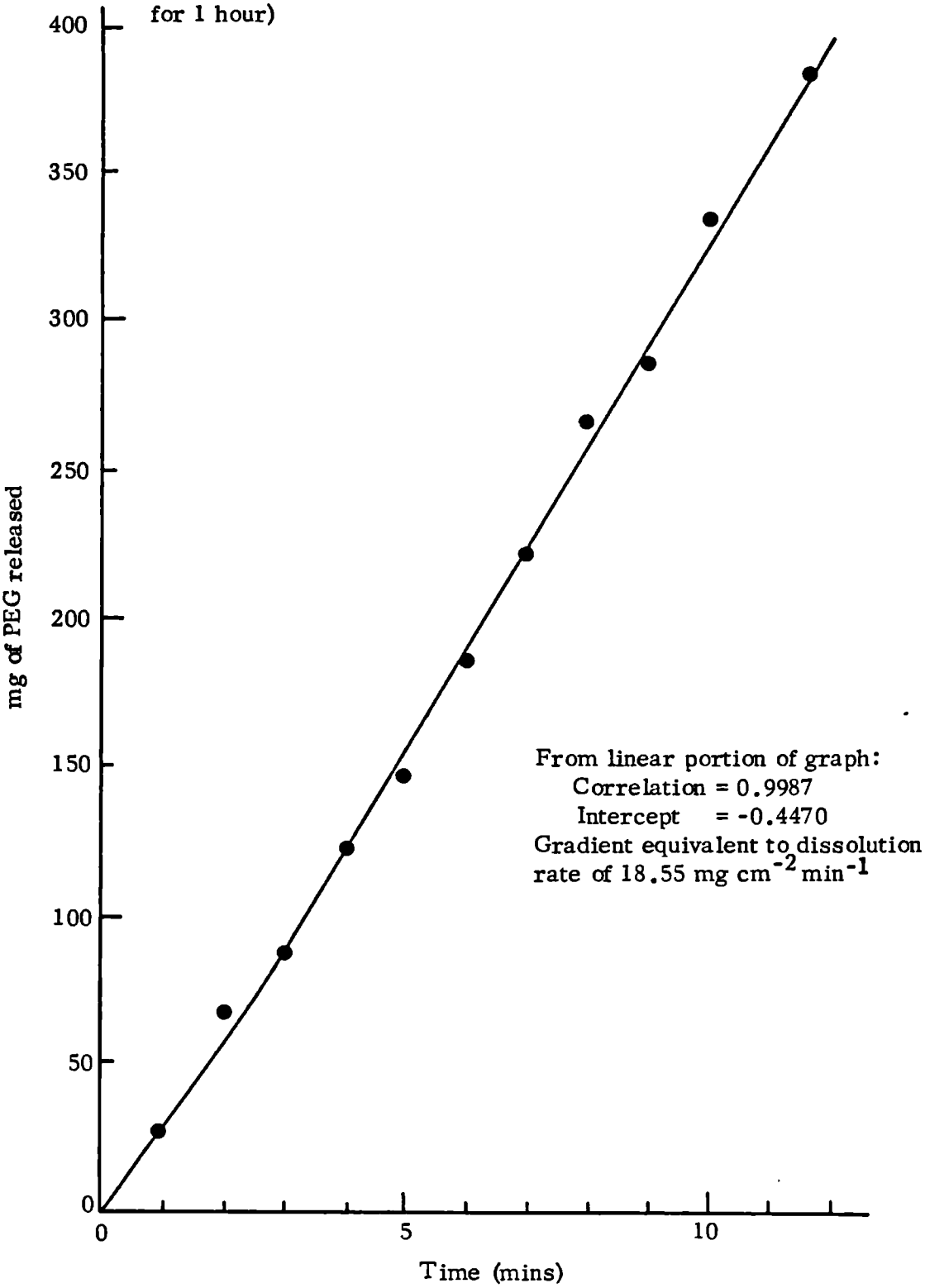

As can be seen from Table 5.1., the temperature of melting and time in the molten state exerted little influence on the dissolution rate of PEG 4000, except when the polymer had been melted at 200°C for 10 hours, where a slight increase in dissolution rate was observed. The information about the structure of PEG 4000 obtained by DSC and X-ray diffraction which is presented in Chapter 3.3.1. showed a corresponding decrease in the heat of fusion for that sample. Thus, the increase in dissolution rate can be attributed to the break-up of polymer chains into shorter molecular weight fragments and to a decrease in the overall crystallinity. It has been reported (Corrigan et al, 1979) that a decrease in the molecular weight of PEGS results in an increase in the dissolution rate. Although differences in the morphology of PEG 4000 melted at different temperatures for various periods of time could be detected by DSC, it appears that these changes are not reflected by differences between the intrinsic dissolution rates observed.

However, changes in the cooling rate were found to influence the subsequent dissolution rate of the polymer (Table 5.2.). A significant increase in the dissolution rate of PEG 4000 quenched in liquid nitrogen was noticeable compared to more slowly cooled samples, although the effect on the dissolution rate of less dramatic differences in the cooling rate i.e. between $20^{\circ}C\,hr^{-1}$ and $5^{\circ}C\,hr^{-1}$, was negligible. This increase in dissolution rate can be attributed to the higher percentage of amorphous material present in the quenched specimens, as can be seen from the data obtained by DSC in Chapter 3.3.1. The heat of solution of the amorphous form of the polymer is much less endothermic than that of its crystalline counterpart (Ikeda et al, 1975) and therefore it is expected that the dissolution of the more amorphous sample of PEG 4000 would be more rapid.

Table 5.1. Effect of temperature of melting and time in the molten state on the intrinsic dissolution rate of PEG 4000

(Cooling rate of samples = $20^{o}Chr^{-1}$)

Time in molten state	Intrinsic dissolution rate after melting at ($mgcm^{-2}min^{-1}$)		
	60°C	100°C	200°C
10 minutes	16.68	16.75	16.66
1 hour	17.15	17.12	17.15
10 hours	16.91	16.68	17.48

Table 5.2. Effect of cooling rate on the intrinsic dissolution rate of PEG 4000

Cooling rate after melting at 100°C for 1 hour	Intrinsic dissolution rate ($mgcm^{-2}min^{-1}$)
Quenching in liquid nitrogen	18.55
$20^{o}Chr^{-1}$	17.12
$5^{o}Chr^{-1}$	16.65

These results suggest that the crystal morphology present - either folded or extended chain type - does not exert a great influence on the dissolution rate of the polymer but that changes in the degree of crystallinity do have a marked effect. Nevertheless, substantial differences in the thermal history of PEG 4000 are necessary before changes in the dissolution behaviour are apparent.

5.3.1.2. Effect of ageing

The effect of ageing on the dissolution behaviour of PEG 4000 was investigated using samples of polymer which had been cooled at different rates, since these displayed the widest initial range of dissolution rates (see previous section). After ageing at 25, 37 or 45°C for 6 months, all samples exhibited decreased dissolution rates relative to their initial profiles. Furthermore, although the different batches had widely differing initial dissolution rates, after 6 months, all the dissolution rates had fallen to approximately the same level of $\sim 16 mg\, cm^{-2} min^{-1}$ (Fig. 5.2a., b., c.). The most rapid decrease in dissolution rate was observed during the first month and in most cases, the majority of the decrease occurred in the first two months. As would be expected, increasing the temperature of storage accelerated the rate of change in the samples but no significant difference between dissolution rates after six months at any of the storage conditions was apparent.

The changes in the dissolution profile of PEG 4000 correlate well with the changes in the structure of the polymer observed under similar ageing conditions by DSC and X-ray diffraction in Chapter 3. An increase in the overall crystallinity of the polymer and conversion of folded chain crystals to the thermodynamically stable extended chain form seem to be mirrored

Fig. 5.2. Effect of ageing on intrinsic dissolution rate of PEG 4000 at various temperatures

a. 25°C

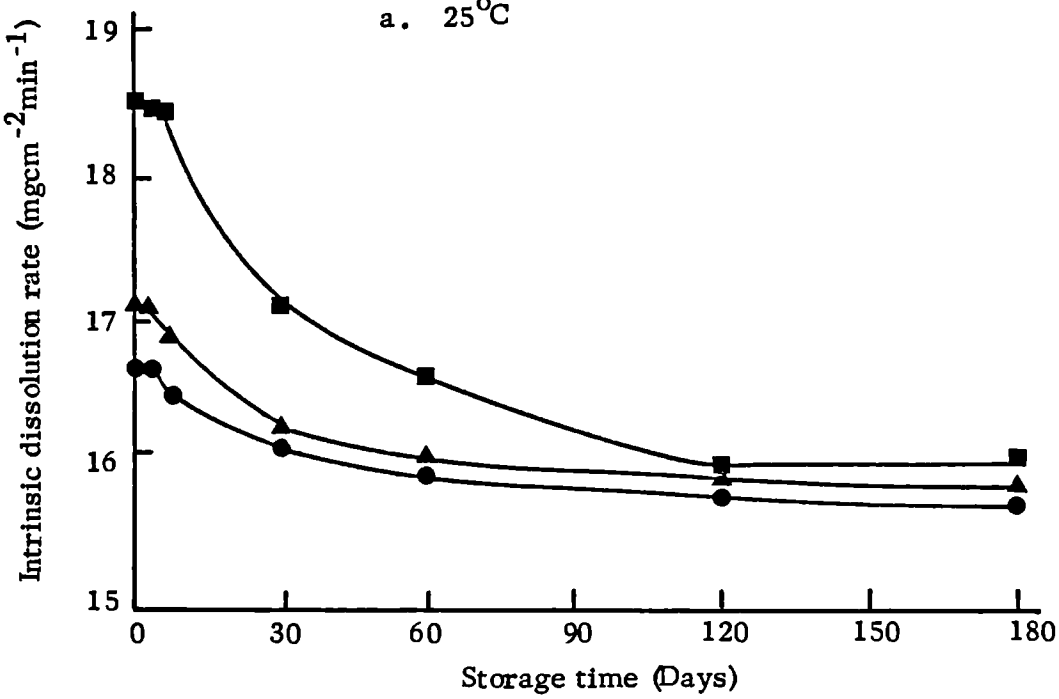

b. 37°C

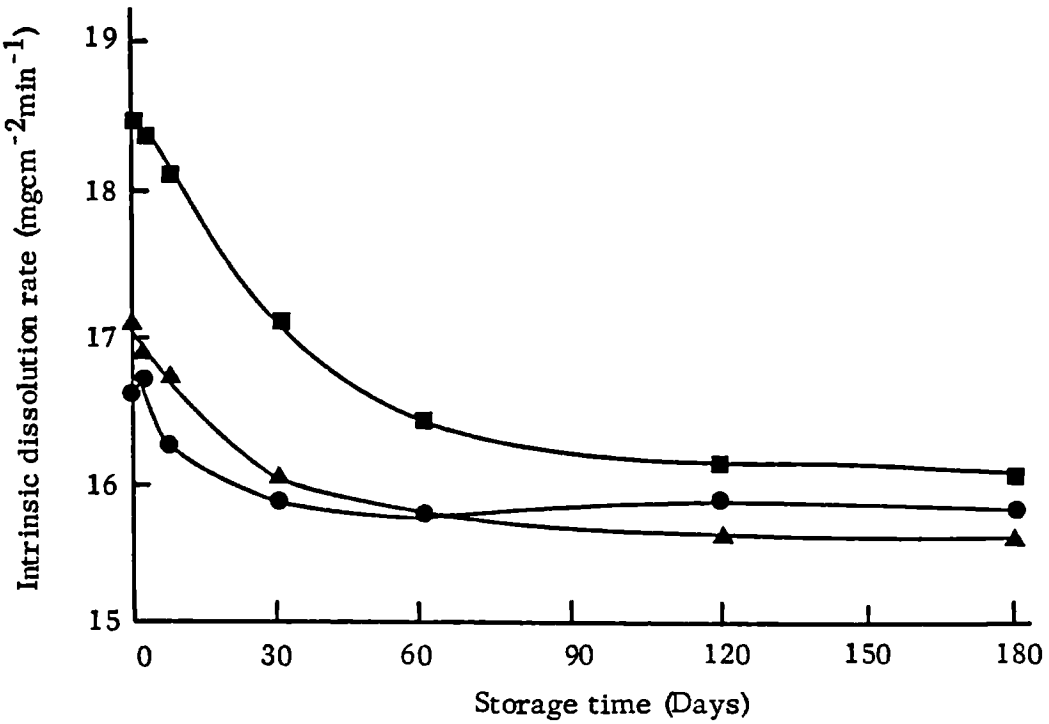

Fig. 5.2. c. 45°C

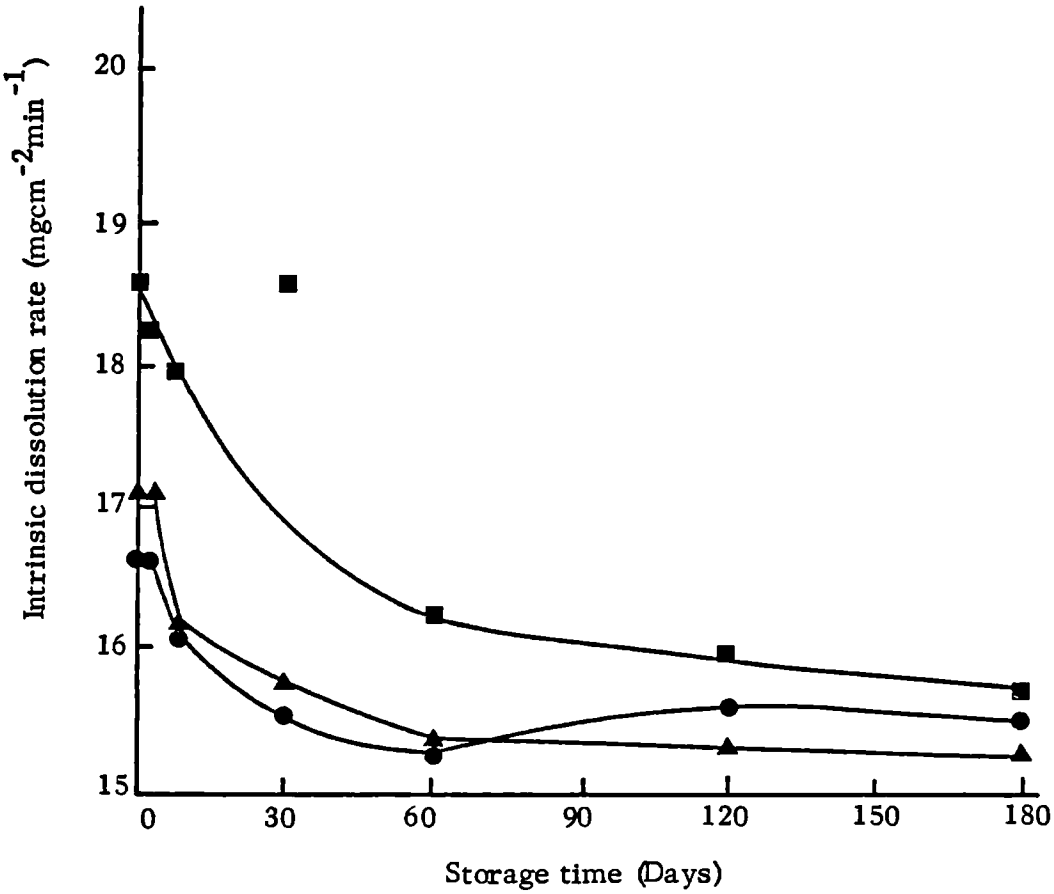

Key

PEG 4000 melted at 100°C for 1 hour and

■ Quenched in liquid nitrogen

▲ Cooled at 20°C hr^{-1}

● Cooled at 5°C hr^{-1}

by a corresponding decrease in the dissolution rate. The quenched samples of PEG 4000, which were the least crystalline initially, displayed the largest subsequent decrease in dissolution rate as recrystallisation occurred, whereas the slowest cooled polymer samples showed only a small decrease in dissolution rate on ageing, since they were highly crystalline to begin with. Presumably, the decrease in dissolution rate is halted once the polymer has achieved its maximum crystallinity, as the results here suggest. Increasing the storage temperature will facilitate the annealing and secondary crystallisation processes but will not alter the final level of crystallinity.

5.3.1.3. Effect of agitation intensity of dissolution rate

The dissolution behaviour of the two batches of PEG 4000 representing the extremes of dissolution rate obtained, namely those samples which had been melted at 100°C for 1 hour and then either quenched in liquid nitrogen or cooled at $5^{\circ}C\,hr^{-1}$, was investigated further. Intrinsic dissolution rates were obtained at various stirring rate conditions between 50 and 120 rpm and the results are presented in Table 5.3. Below 50 rpm, the dissolution profile became erratic because of inadequate mixing of the bulk dissolution fluid and above 120 rpm, adequate sampling proved difficult due to the speed of dissolution of the polymer. As expected for a diffusion controlled system, the dissolution rate increased linearly as the stirring rate increased (Fig. 5.3.). Quenched PEG 4000 displayed a higher dissolution rate than the more crystalline samples at all agitation intensities studied.

Cooper and Kingery (1962) related the diffusion controlled rate of dissolution from the surface of a rotating disc to the stirring rate by the following expression:

Table 5.3. Intrinsic dissolution rates of PEG 4000 with different thermal histories at various agitation intensities

Agitation intensity (rpm)	Dissolution rate ($mgcm^{-2}min^{-1}$) for PEG 4000 melted at 100°C for 1 hr then Quenched in liquid nitrogen	Cooled at $5°Chr^{-1}$
50	14.97	13.78
80	18.55	16.65
100	20.19	18.02
120	21.77	20.32

Table 5.4. Estimated values of the diffusion layer thickness and diffusion coefficients for PEG 4000 under various conditions

Agitation intensity (rpm)	Diffusion layer thickness (cm)	Diffusion coefficients (cm^2sec^{-1}) after melting at 100°C for 1 hour and Quenching x 10^5	Cooling at $5°Chr^{-1}$ x 10^5
50	0.110	3.66	3.37
80	0.087	3.59	3.22
100	0.077	3.45	3.08
120	0.071	3.43	3.21

Fig. 5.3. Intrinsic dissolution rate of two batches of PEG 4000 prepared under different conditions as a function of agitation intensity

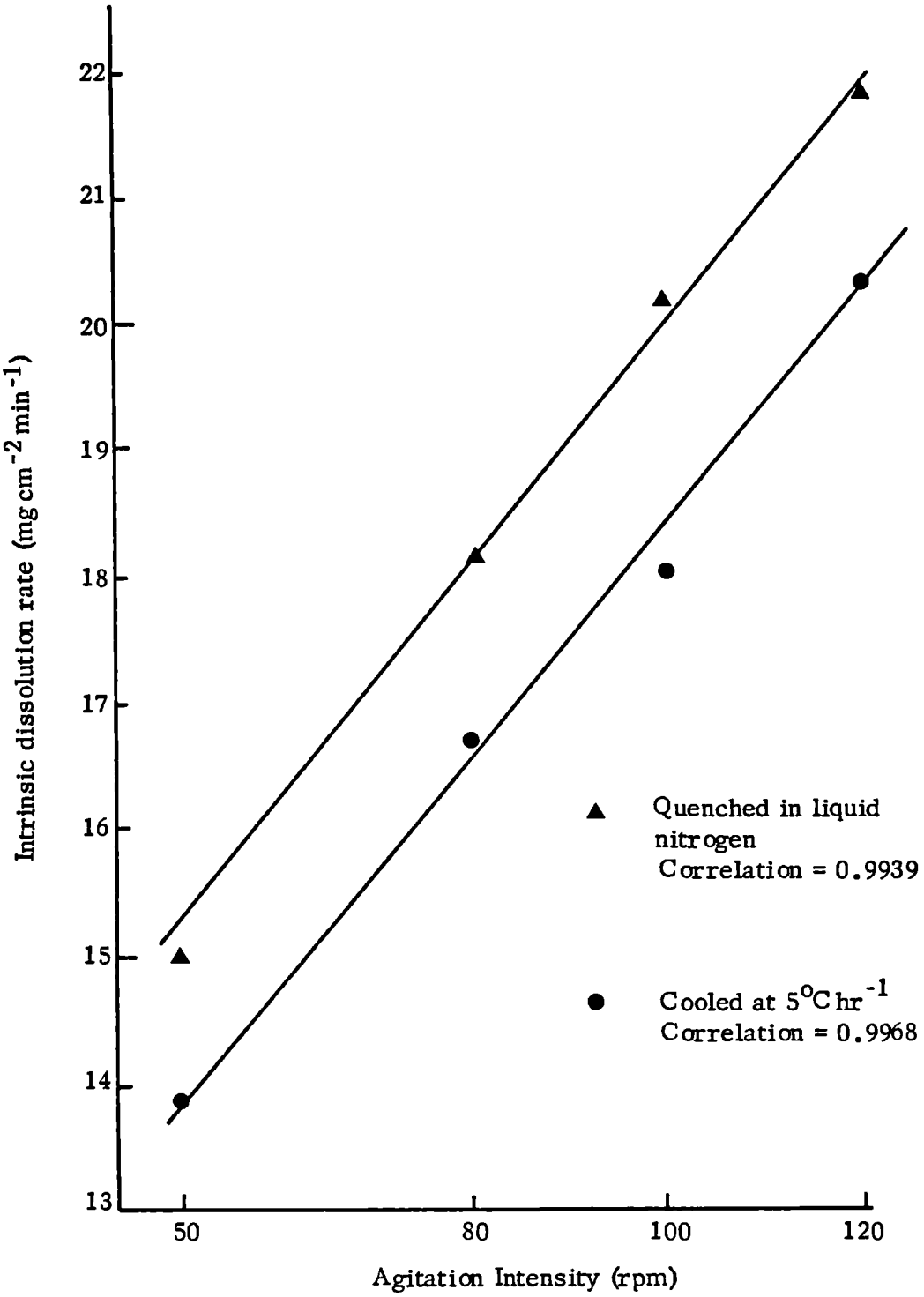

$$H = b(SR)^{0.5} \quad \ldots 5.1.$$

where H = dissolution rate ($mg\,cm^{-2}\,min^{-1}$)

b = constant

SR = rate of stirring (rpm)

Thus:

$$\text{Log } H = \log b + 0.5 \log SR \quad \ldots 5.2.$$

and a graph of log H as a function of log SR should have a slope of 0.5 with intercept log b. The graphs contructed from the data above (Fig. 5.4.) gave the relationship between stirring rate and intrinsic dissolution rate as:

$$H = 2.82(SR)^{0.428}$$

for quenched PEG 4000 and

$$H = 2.56(SR)^{0.429}$$

for PEG 4000 cooled at $5^{o}C\,hr^{-1}$

In both cases, the value of the exponent is less than the predicted 0.5, as has been found for other systems (Muhammed, 1980). Nevertheless, the results can be described by the more general equation postulated by Levy (1963b).

$$H = b(SR)^{a} \quad \ldots 5.3.$$

5.3.1.4. Estimation of the diffusion layer thickness and diffusion coefficients

The diffusion layer thickness for a solvent flowing over a dissolving solid may be estimated from (Nelson, 1957):

$$h = \frac{\eta}{\rho(rps)} \quad \ldots 5.4.$$

where h = the thickness of the diffusion layer (cm)

η = viscosity of the dissolution medium (poise)

Fig. 5.4. Relationship between log stirring rate and log dissolution rate for PEG 4000 prepared under different conditions

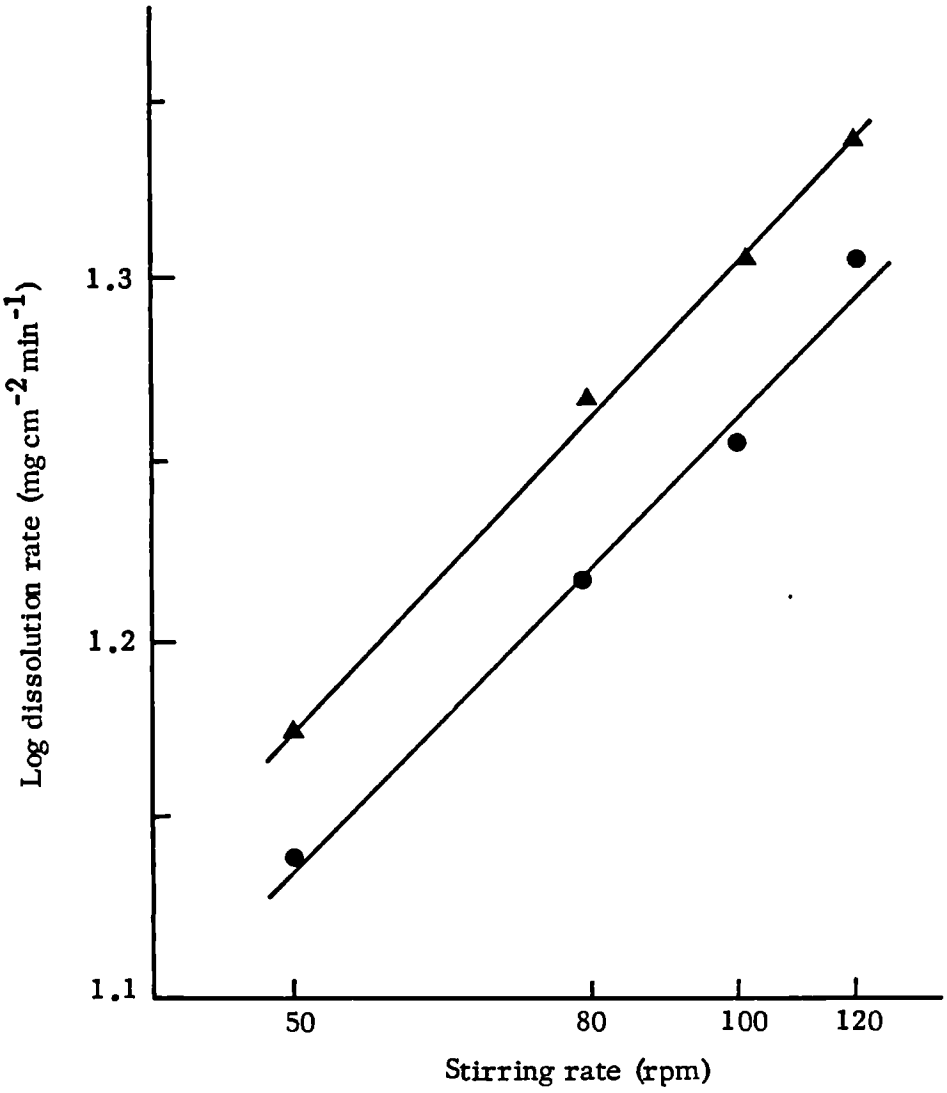

▲ Quenched in liquid nitrogen
Correlation = 0.9992

● Cooled at 5°C hr^{-1}
Correlation = 0.9939

ρ = density of the medium (gml^{-1})

rps = stirring rate in revolutions per second

The maximum concentration of PEG 4000 that could be achieved in the bulk dissolution fluid during the period of dissolution was calculated as less than 0.05%^{w}/w, even at the fastest stirring rate. Therefore, the values for the viscosity and density of the dissolution medium substituted into the above equation were those for water at 37^{o}C, since the error introduced by this assumption was estimated to be minimal. The values of the thickness of the diffusion layer for PEG 4000 under different agitation intensities are listed in Table 5.4. Its thickness was found to be inversely proportional to the stirring rate and as anticipated, the diffusion layer became thinner as the stirring rate rose.

The equation derived by Nernst and Brunner (1904) was used to estimate the diffusion coefficients:

$$H = \frac{D}{h} (C_s^* - C^*) \qquad \ldots 5.5.$$

where H = dissolution rate per unit area ($mg\,cm^{-2}\,sec^{-1}$)

C^*= equilibrium solubility of solute ($mg\,ml^{-1}$)

C_s^* = concentration of solute in dissolution medium ($mg\,ml^{-1}$)

h = diffusion layer thickness (cm)

D = diffusion coefficient of solute (gm^2sec^{-1})

Under sink conditions, C^*can be considered negligible in comparison to C_s^* and thus equation 5.5. may be simplified to:

$$H = \frac{D}{h} .C_s^* \qquad \ldots 5.6.$$

which can be rearranged in terms of the diffusion coefficient as:

$$D = \frac{H.h}{C_s^*} \qquad \ldots 5.7.$$

The equilibrium solubility of PEG 4000 was estimated as 750 $mg\,ml^{-1}$, which is slightly higher than the value of 706 $mg\,ml^{-1}$ obtained by Corrigan et al (1979). As can be seen from Table 5.4., the value of the diffusion coefficient generally decreases as the agitation intensity increases for both batches of PEG 4000 investigated. As these two samples delineate the range of dissolution rates observed for PEG 4000 before ageing, all other values can be expected to lie between the range of diffusion coefficients calculated here. The values of the diffusion coefficient calculated here are approximately an order of magnitude higher than that measured for PEG 4000 by Corrigan et al (1979). However, their value of $3.1 \times 10^{-6}\,cm^2\,sec^{-1}$ was obtained by the method of Goldberg and Higuchi (1968) which utilises a stirring rate dependent barrier and thus the hydrodynamics are unlikely to be equivalent to those here. Moreover, it should be stressed that the values calculated here are purely estimates, although they demonstrate the qualitative behaviour of the system.

5.3.2. PEG 4000 and trimethoprim solid dispersions

5.3.2.1. Aqueous solubility of trimethoprim

The solubility of trimethoprim in aqueous PEG 4000 solutions increases rapidly at high concentrations of polymer, being about twenty six times more soluble in 60%^{w}/v PEG 4000 than in water (Fig. 5.5.). However, relatively little increase in solubility of drug is observed below 10%^{w}/v PEG 4000. Since PEG is a hydrophilic polymer, with no lipophilic moiety as is present in a surfactant, it is not regarded as having potential as a solubilising agent. Recently though, Patel et al (1981) have shown for a variety of hydrophobic drugs that the site of solubilisation within a polyoxyethylene (20) glycol monohexadecyl ether micelle was not the hydrocarbon core as expected, but the hydrophilic PEG mantle, especially the dehydrated PEG region next to the core. Thus, a solubility enhancing effect by PEG 4000 would appear to be feasible, where solubilisation is defined in its most general terms as "the preparation of a thermodynamically stable isotropic solution of a substance normally insoluble or very slightly soluble in a given solvent by the introduction of an additional component or components" (Elworthy et al, 1968).

Many workers have investigated the effect of PEGs on aqueous drug solubility, but in general using polymer concentrations below 10%^{w}/v (e.g. El-Gamal et al, 1978; El-Gindy et al, 1983; Kaur et al, 1980b; Khalil and Mortada, 1978). As here, little solubilising effect is observed and therefore microenvironmental solubilisation has been discounted as an important factor in the enhancement of drug dissolution. However, the diffusion layer would be expected to contain a much greater concentration of PEG than the bulk fluid. Furthermore, swelling of the polymer on initial

Fig. 5.5. Solubility of trimethoprim in aqueous PEG 4000 at 37°C

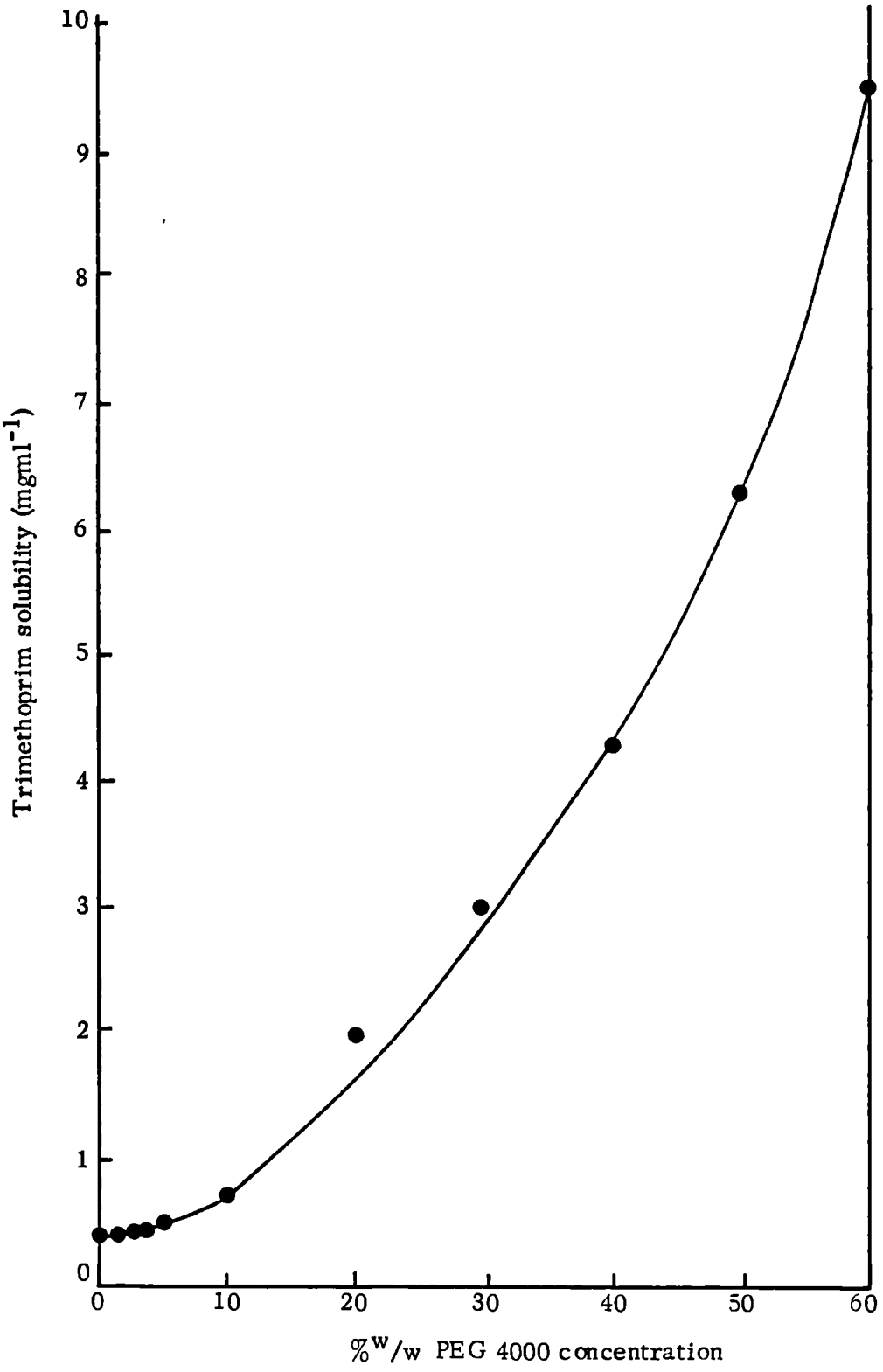

contact with water prior to dissolution may contribute to produce a very dehydrated layer adjacent to the dissolution surface. Where studies of drug solubility in aqueous solutions containing high concentrations of PEGS have been performed (e.g. Hargreaves (1982) for betamethasone alcohol in PEG 6000, Elworthy and Lipscomb (1968) for griseofulvin in PEG 1000), a similar rapid increase in solubility at higher aqueous PEG concentrations to that obtained in this work is reported. Microenvironmental solubilisation may therefore play a more important role than previously thought in enhanced drug dissolution from PEG solid dispersions.

5.3.2.2. Effect of thermal history

To elucidate both the effect of different thermal histories and the probable mechanisms of enhanced drug release from PEG 4000-trimethoprim solid dispersions, data on the dissolution of both components is required. The intrinsic dissolution rate of trimethoprim alone was assessed as 0.054 $mgcm^{-2}min^{-1}$ at 80 rpm from fused discs of drug.

For dispersions previously heated at 100°C for 10 minutes and cooled at $20^{\circ}C\,hr^{-1}$, the dissolution rate of trimethoprim increased linearly as a function of composition up to 10%w/w, with a gradient of 0.217 $mgmin^{-1}\%^{-1}$, then remained steady to 20%w/w before decreasing dramatically at higher drug concentrations (Fig. 5.6.). As sink conditions prevailed throughout dissolution, this decrease cannot be attributed to a saturation solubility effect. Despite the relatively poor dissolution performance at high concentrations of trimethoprim, its formulation as a solid dispersion resulted in a marked enhancement of dissolution rate compared to that of the drug alone.

Investigations of the dissolution behaviour of the polymer from 2, 10 and

Fig. 5.6. Release rate of trimethoprim from dispersions previously melted at 100°C for 10 mins and cooled at $20^{\circ}Chr^{-1}$

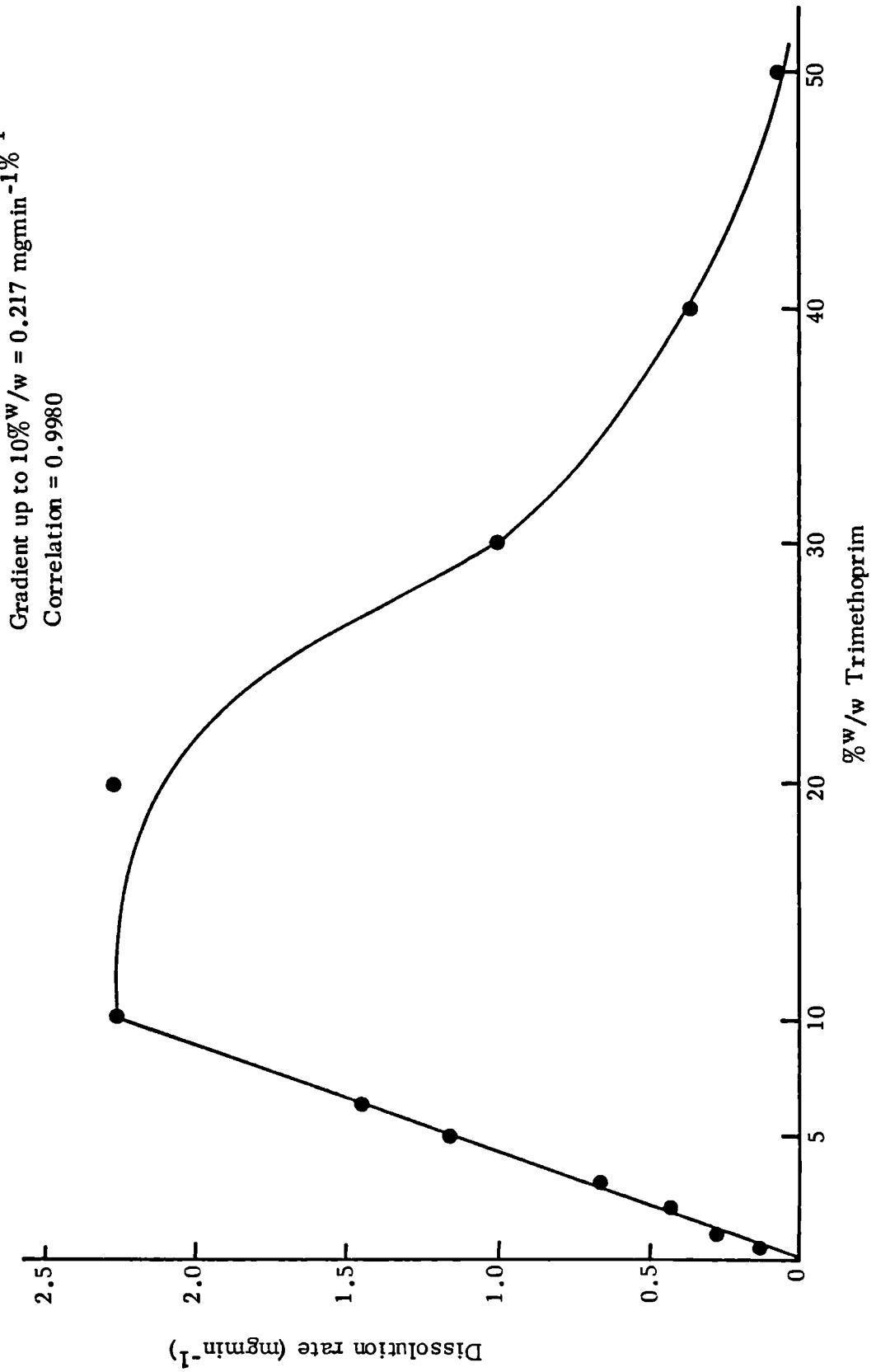

50%w/w trimethoprim dispersions revealed that the release rate of PEG 4000 was slower than for the pure polymer and that it decreased with increasing drug concentration (Table 5.5.). Since small amounts of hydrophobic materials can markedly alter the hydrophilic characteristics of a material, then the overall wettability of the dispersion may be expected to decrease as the proportion of the hydrophobic constituent rises. Hargreaves (1982) reported a sharp increase in the contact angle measured for water on solid dispersions of PEG 6000 and betamethasone alcohol above 10%w/w, indicating a reduction in their hydrophilic nature, which correlated well with the point at which their dissolution performance deteriorated.

As the data was obtained using rotating discs of constant surface area, the actual amount of drug or polymer available for dissolution will depend on the composition of the dispersion. To account for this, relative release rates were calculated from the experimentally observed release rate divided by the weight fraction of the component. This assumes that the same fraction is available at the dissolution surface . The relative release rate of trimethoprim derived as above remained virtually constant up to a composition of 10%w/w drug, before declining rapidly at higher drug concentrations (Fig. 5.7.). The apparent increase in relative dissolution rate at 1%w/w trimethoprim may simply be an anomalous result, but alternatively may be due to the formation of a higher energy amorphous form of the drug with an increased dissolution rate. X-ray diffraction studies had previously demonstrated the absence of trimethoprim diffraction peaks for these dispersions (Chapter 3.3.2.1.).

Table 5.5. Dissolution data from solid dispersions previously melted at 100°C for 10 mins and cooled at $20^{\circ}Chr^{-1}$

%w/w Trimethoprim	Dissolution rate ($mgmin^{-1}$) PEG	Drug	Relative dissolution rate ($mgcm^{-2}min^{-1}$) PEG (X_p)	Drug (X_d)	$\frac{X_p}{X_d}$
2	27.03	0.44	15.58	12.43	1.25
10	22.37	2.23	14.04	12.60	1.11
50	1.09	0.1	1.23	0.15	8.20

Fig. 5.7. Relative release rate of trimethoprim from dispersions previously melted at 100°C for 10 mins and cooled at 20°Chr^{-1}

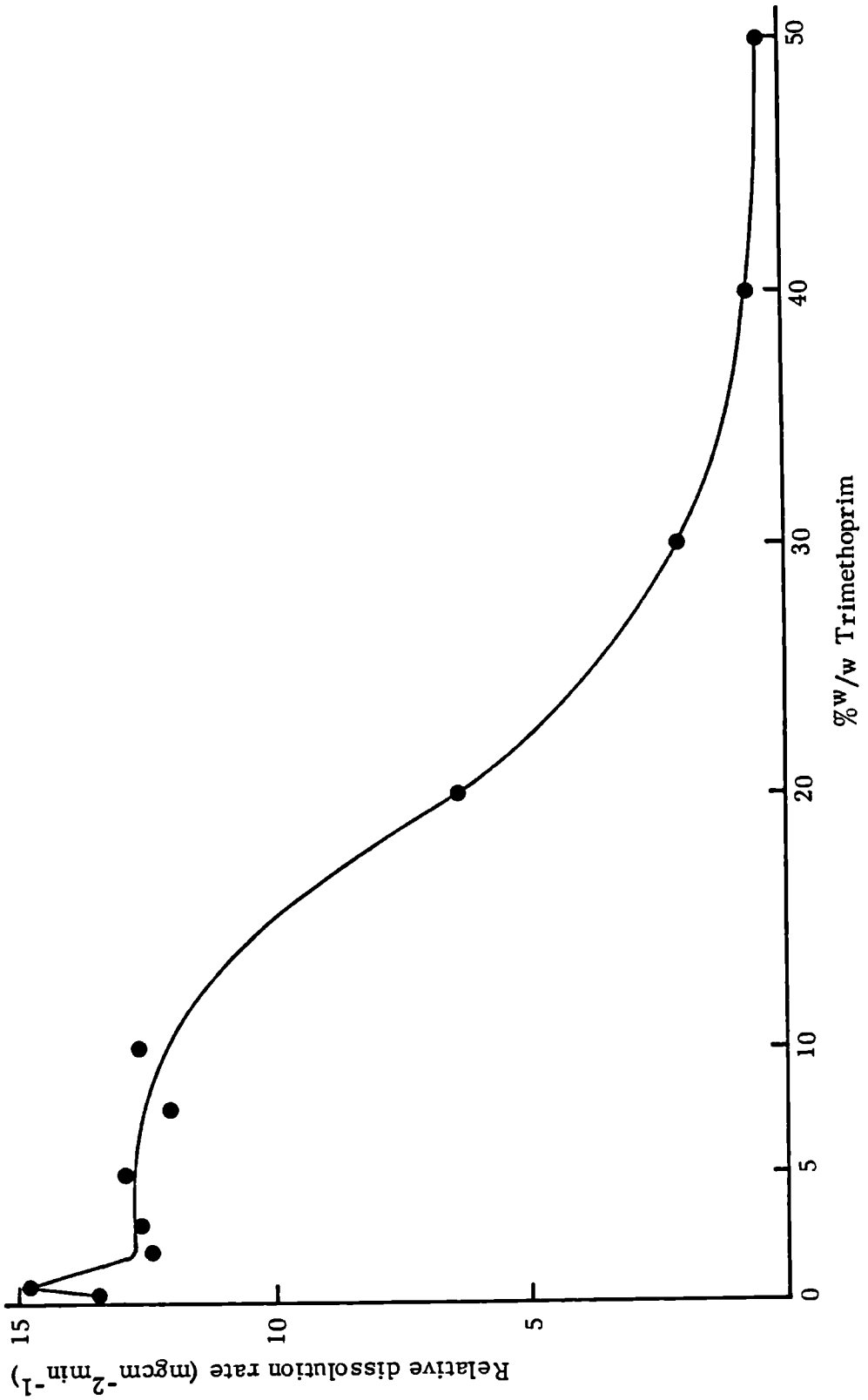

The identity of the controlling layer for dissolution for any composition of solid dispersion can be determined by comparison of the relative dissolution rates of each component. The ratios at 2%^{w}/w and 10%^{w}/w trimethoprim are approximately one, (Table 5.5.), which suggests that both components are being released simultaneously. These results are in agreement with those reported for PEG 4000 and hydroflumethiazide or bendrofluazide solid dispersions by Corrigan et al (1979). Conversely, for 50%^{w}/w trimethoprim dispersions, the relative release rate of the polymer is much faster than that of the drug, resulting in controlling trimethoprim boundary layer as has been reported for sulphathiazole - PVP systems (Simonelli et al, 1969). The positive curvature of the dissolution profiles noted with PEG 4000 alone was also evident in the drug dissolution profiles especially at high polymer weight fractions. This curvature was attributed to the swelling of the polymer prior to dissolution and may therefore lend weight to the suggestion that the two components are released simultaneously at low drug concentrations.

Since the dissolution of trimethoprim in molten PEG 4000 was known to be incomplete for concentrations above 1%^{w}/w, such factors as a reduction in particle size and solid solution formation cannot be invoked as explanations of the observed enhancement in drug dissolution. Consequently, micro-environmental solubilisation or improved wetting and dispersibility seem to be implicated. The simultaneous release of both components at low concentrations of drug may be indicative of the formation of soluble complexes, as has been postulated by Corrigan et al (1979).

Comparison of the dissolution profiles of the above dispersions with those of dispersions which had previously been molten totally at 200^{o}C for 10 mins, prior to cooling at 60^{o}C hr^{-1} revealed only a few differences in the pattern

of behaviour. However, the dissolution rate of trimethoprim as a function of composition appeared to exhibit two regions of linearity, up to 5%^{w}/w and up to 10%^{w}/w (Fig. 5.8.). The gradient of the linear region up to 5%^{w}/w drug was calculated to be 0.264 mgmin^{-1}%$^{-1}$, which is greater than that obtained with the previous dispersion systems investigated. Moreover, dissolution rates were in general higher by 10-20% from this set of completely fused dispersions. Relative release rates from these dispersions reflected this behaviour, but again displayed a marked decline in dissolution performance above 10%^{w}/w trimethoprim (Fig. 5.9.). This improvement in dissolution behaviour, especially at low concentrations of drug, is consistent with the formation of an amorphous form of trimethoprim suggested as an explanation for the absence of X-ray diffraction peaks for the drug in dispersions containing less than 5%^{w}/w trimethoprim (Chapter 3.2.). Comparison of the relative release rate of the two components again suggested that simultaneous dissolution occurred with 2%^{w}/w and 10%^{w}/w trimethoprim, but not for 50%^{w}/w dispersions (Table 5.6.). This relative lack of difference in dissolution performance between dispersions which previously had and had not been fused totally provides further support for the role of microenvironmental solubilisation and wetting in the release mechanism. However, the presence of a small amount of amorphous drug whose recrystallisation had been inhibited by the polymer, possibly together with some reduction in drug crystal size contributed to the greater dissolution rates of totally fused dispersions compared to those in which incomplete dissolution of drug in the polymer melt had occurred.

Quenching in liquid nitrogen of dispersions previously molten at 200^{o}C for 10 minutes enhanced the release rate of both components at all three

Fig. 5.8. Release rate of trimethoprim from dispersions previously melted at 200°C for 10 mins and cooled at 60°C hr^{-1} or quenched in liquid nitrogen

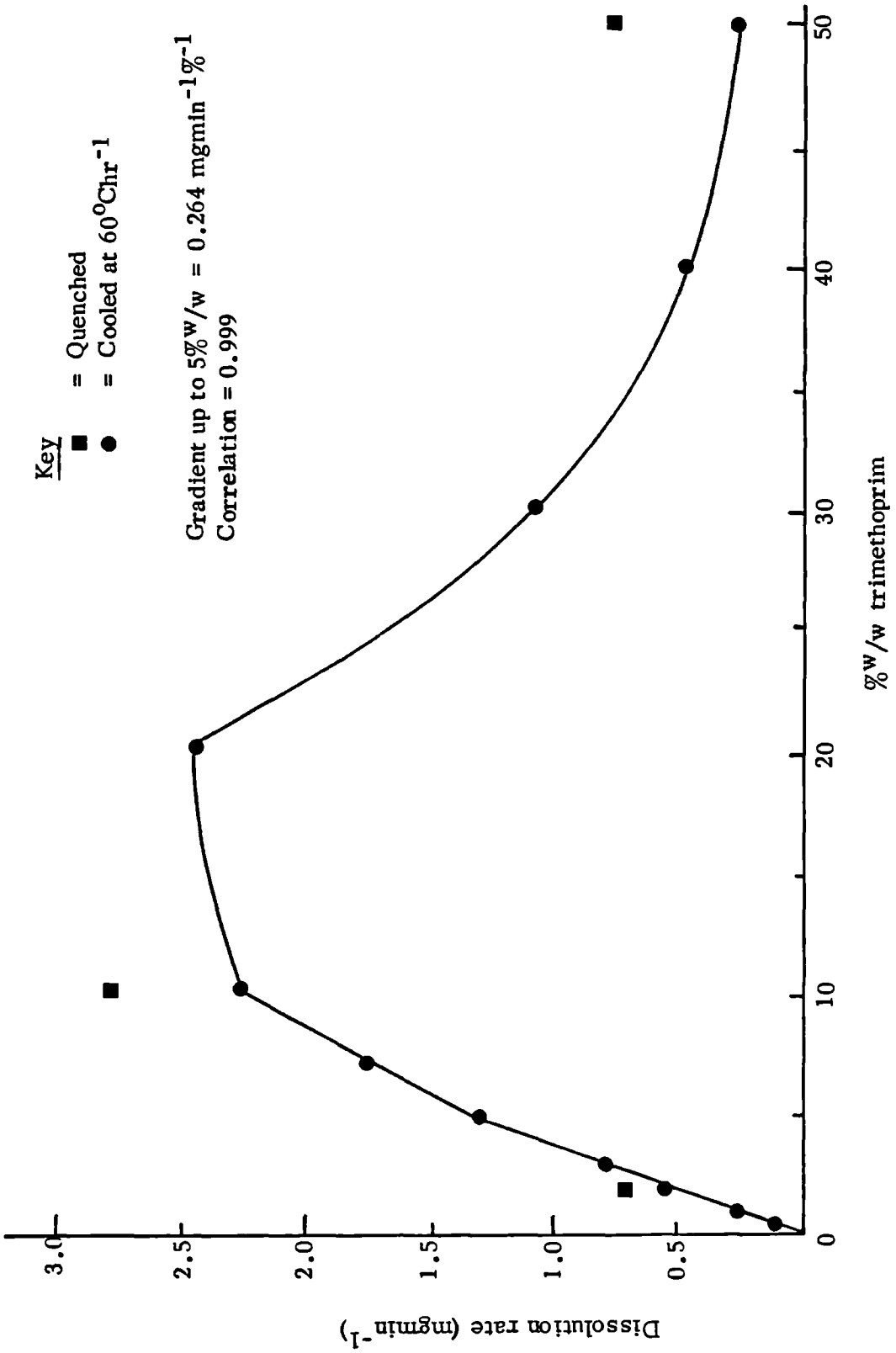

Fig. 5.9. Relative release rate of trimethoprim from dispersions previously melted at 200°C for 10 mins and cooled at 60°C hr^{-1} or quenched in liquid nitrogen

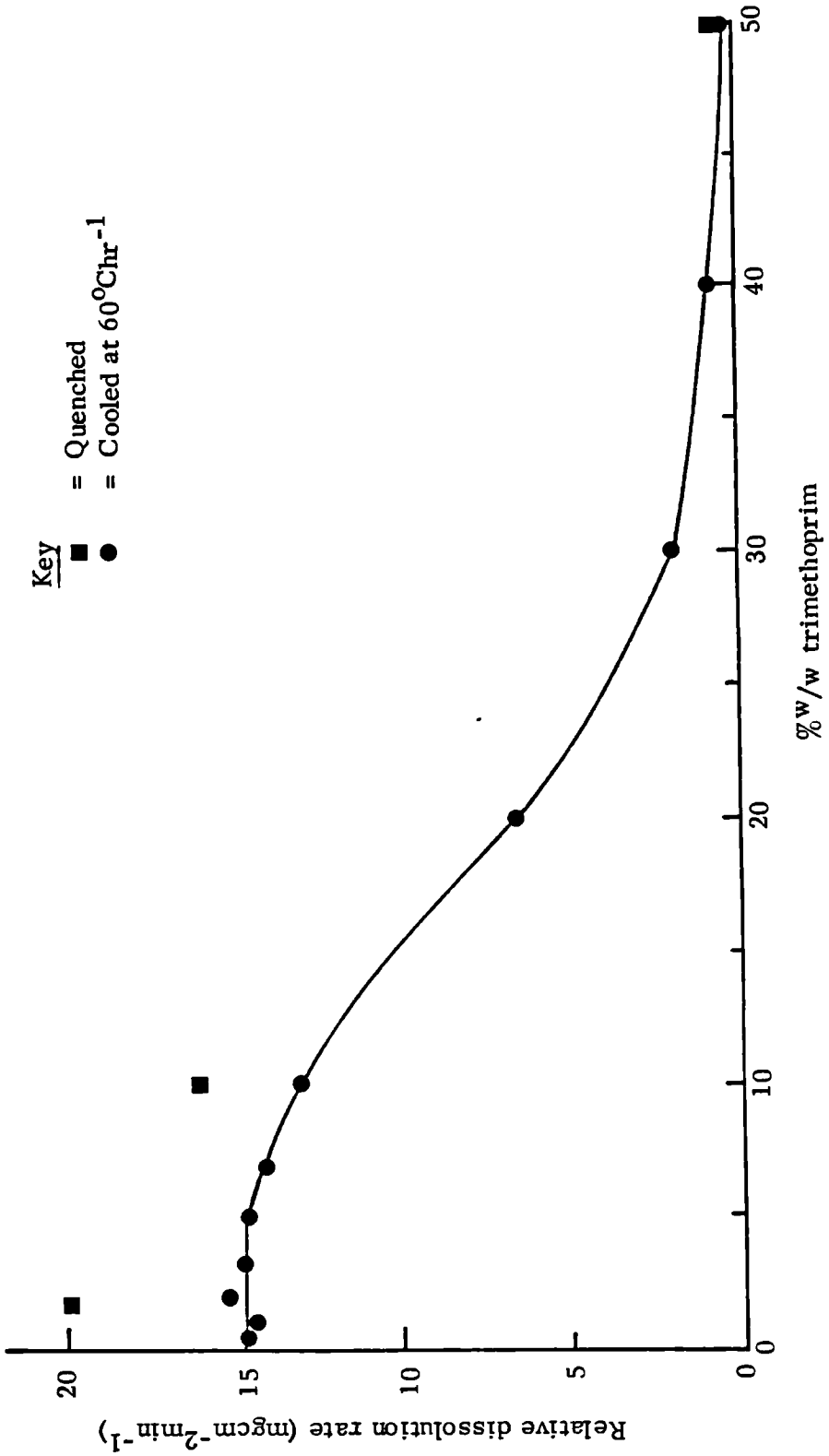

Table 5.6. Dissolution data from solid dispersions previously melted at 200°C for 10 mins and cooled at $60^{\circ}Chr^{-1}$

%w/w Trimethoprim	Dissolution rate ($mgmin^{-1}$) PEG	Drug	Relative dissolution rate ($mgcm^{-2}min^{-1}$) PEG	Drug	$\frac{X_p}{X_d}$
2	26.23	0.54	15.12	15.21	0.99
10	23.16	2.32	14.54	13.10	1.11
50	1.23	0.30	1.39	0.27	5.15

concentrations studied (Table 5.7.), due to the formation of more amorphous material. Since the drug existed in an amorphous state in low concentrations of dispersions which had been fused totally during preparation, this additional increase in the dissolution rate of the drug may be related to the decrease in crystallinity and hence increase in dissolution rate of the PEG 4000. Thus the degree of crystallinity of the polymer may influence the dissolution rate of the drug. Even at 50%^{w}/w, a threefold increase in dissolution rate of the drug is observed compared to the two ranges of dispersion systems prepared under other conditions. Both McGinity et al (1984) and Hargreaves (1982) have reported similar enhancement in the dissolution rates of drugs from rapidly cooled dispersions with PEGS compared to more slowly cooled systems, but the dissolution rate of the polymer was not studied in either instance. Comparison of the relative release rate of the two components from quenched dispersions (Table 5.7.) reveals the same pattern of behaviour as for the more slowly cooled dispersions, with simultaneous release of the two components at high polymer weight fractions.

Overall it appears that changes in the crystallinity of both components may influence the dissolution rate, but that other factors such as micro-environmental solubilisation and improved wettability and dispersibility may contribute strongly to the enhanced dissolution rate of the drug. It is interesting to note that recently Dubois and Ford (1985) produced dissolution data for a wide variety of drugs formulated as solid dispersions with PEG 6000, using a fusion technique, which demonstrated a remarkable similarity in the gradients of the linear portion of the dissolution rate/% drug composition graphs. This followed a suggestion from Corrigan (1984) that dissolution rate from solid dispersions at high carrier levels is independent of the drug

Table 5.7. Dissolution data from solid dispersions previously melted at 200°C for 10 mins and quenched in liquid nitrogen

%w/w Trimethoprim	Dissolution rate ($mgmin^{-1}$) PEG	Drug	Relative dissolution rate ($mgcm^{-2}min^{-1}$) PEG	Drug	$\frac{X_p}{X_d}$
2	32.35	0.70	18.65	19.77	0.94
10	27.26	2.78	17.11	15.73	1.09
50	7.87	0.78	8.90	0.88	10.10

they contain. Further elucidation of the mechanisms of drug dissolution enhancement from PEG dispersions is obviously necessary.

5.3.2.3. Effect of ageing

The effect of ageing on the dissolution rate of both polymer and drug for dispersions containing 2, 10 and 50%^{w}/w trimethoprim was investigated for systems prepared by three different methods. Dispersions were either melted at 100°C for 10 mins and cooled at 20°C hr^{-1} or melted at 200°C for 10 mins and either cooled at 60°C hr^{-1} or quenched in liquid nitrogen. The dissolution performance of all solid dispersions deteriorated to some extent on storage, with the degree of change being dependent on both the concentration of drug and the method of preparation. The deterioration was accelerated at the higher storage temperatures of 37°C and 45°C, which is in agreement with the data reported by Ford and Rubinstein (1979) for the indomethacin-PEG 6000 system, where ageing processes occurred more rapidly at 35°C than 4°C. Conversely, Anastasiadou et al (1983) and Henry et al (1983) observed a greater decline in dissolution rate for 10%^{w}/w diazepam-PEG 4000 dispersions stored at 4°C than at 37°C. This latter finding is somewhat unexpected since higher storage temperatures would facilitate the secondary crystallisation and lamella thickening processes in the polymer, resulting in a higher degree of crystallinity which previous studies have shown tends to decrease the dissolution performance (see preceding section).

Dispersions where complete fusion of the two components was not effected prior to cooling (i.e. those melted at 100°C) were known to exist as a physical dispersion of drug particles in a crystalline polymer matrix (see Chapter 3.3.2.1.). Thus, they would not be expected to manifest large scale changes on ageing, since there is little potential for crystal growth of the drug and a

high percentage of the polymer initially existed in its most stable extended chain crystal form. The changes in dissolution behaviour for all the systems are illustrated in terms of the percentage decrease in the relative dissolution rate, at the highest (45°C) and lowest (25°C) storage temperatures. Changes at 37°C were essentially similar to those at 45°C. As can be seen from the data presented in Fig. 5.10a. and b., a maximum decrease of ~10% in dissolution rate occurred with these dispersions, with approximately equivalent change in both components.

The amorphous form of the drug present in 2%^{w}/w dispersions previously fused at 200°C and cooled at 60°C hr^{-1} appeared to be relatively stable to storage (Fig. 5.11a. and b.) with no evidence of recrystallisation of the drug (Chapter 3.3.2.5.) and only a small decrease in the dissolution rate of both components. Frömming et al (1978) noted similar stability in 5%^{w}/w salicylic acid-PEG 6000 dispersions stored at room temperature where the drug was thought to exist in the amorphous state, which was in contrast to the behaviour of dispersions containing crystalline drug where a large drop in dissolution performance occurred. Similarly, Ravis and Chen (1981) reported that the dissolution performance of a 10%^{w}/w dicoumarol-PEG 4000 was unchanged after a year's storage at room temperature. Again, the drug was postulated to exist in a "high energy" amorphous form. In a study of factors affecting the extent of recrystallisation from an indomethacin-PEG 6000 system, Saboe and Dempski (1976) demonstrated negligible recrystallisation below a "critical supersaturation concentration", estimated at 3.7%^{w}/w for their system. Thus it appears that recrystallisation of small amounts of amorphous drug in crystalline PEGS will be inhibited, possibly indefinitely due to the extreme difficulty of nucleation and crystal growth of the drug in the polymer matrix.

Fig. 5.10. Effect of ageing on the relative dissolution on rate of solid dispersions previously melted at 100°C for 10 mins prior to cooling at 20°C hr^{-1} and stored at:
(a) 25°C

Key to Figs. 5.10-5.12

- ● 2%^{w}/w dispersions - Dissolution rate of PEG 4000
- ○ 2%^{w}/w dispersions - Dissolution rate of trimethoprim
- ■ 10%^{w}/w dispersions - Dissolution rate of PEG 4000
- ◆ 10%^{w}/w dispersions - Dissolution rate of trimethoprim
- ▲ 50%^{w}/w dispersions - Dissolution rate of PEG 4000
- × 50%^{w}/w dispersions - Dissolution rate of trimethoprim

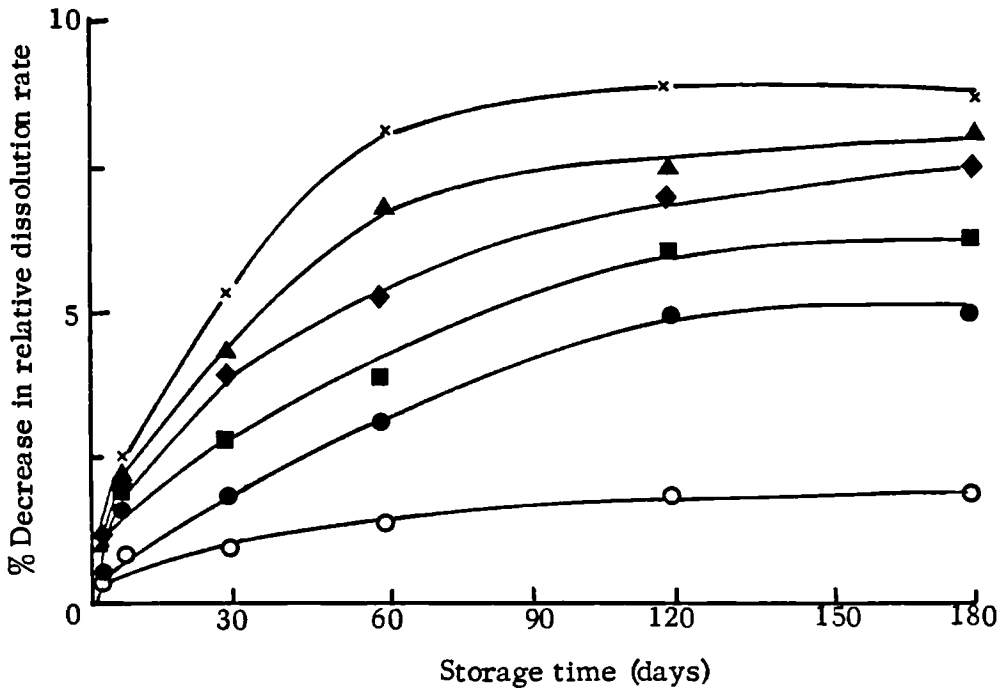

Fig. 5.10. (b) 45°C

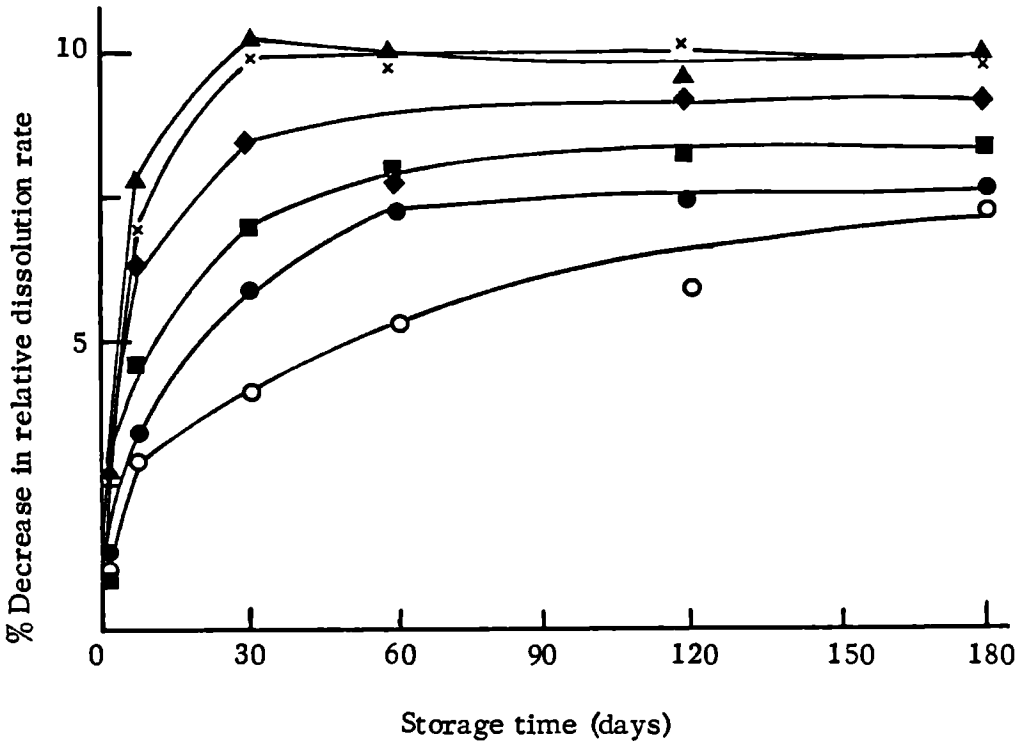
10
5
0
30
60
90
120
150
180
% Decrease in relative dissolution rate
Storage time (days)

Fig. 5.11. Effect of ageing on the relative dissolution rate of solid dispersions previously melted at 200°C for 10 mins and cooled at 60°C hr^{-1}, stored at

(a) 25°C

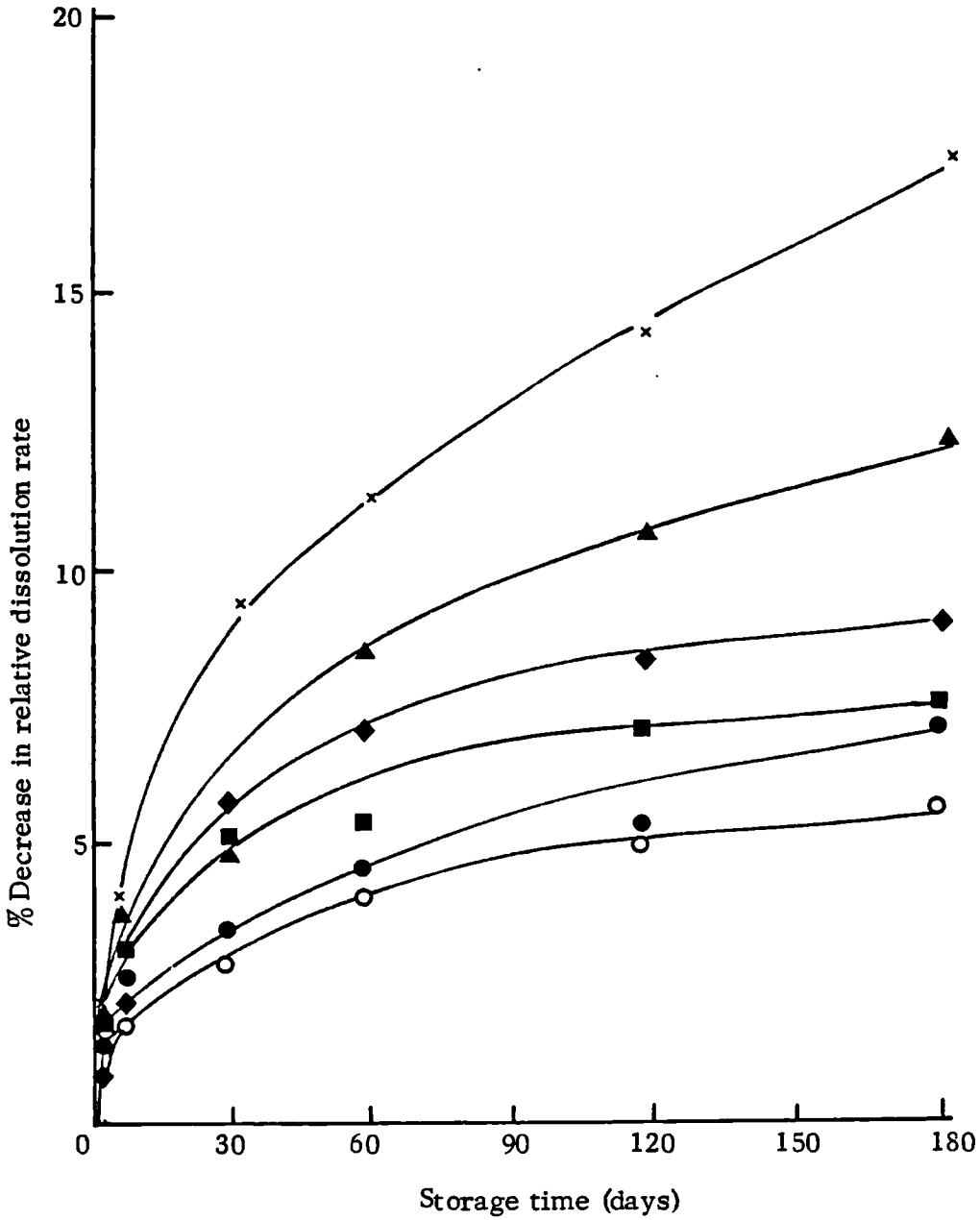

Fig. 5.11. (b) 45°C

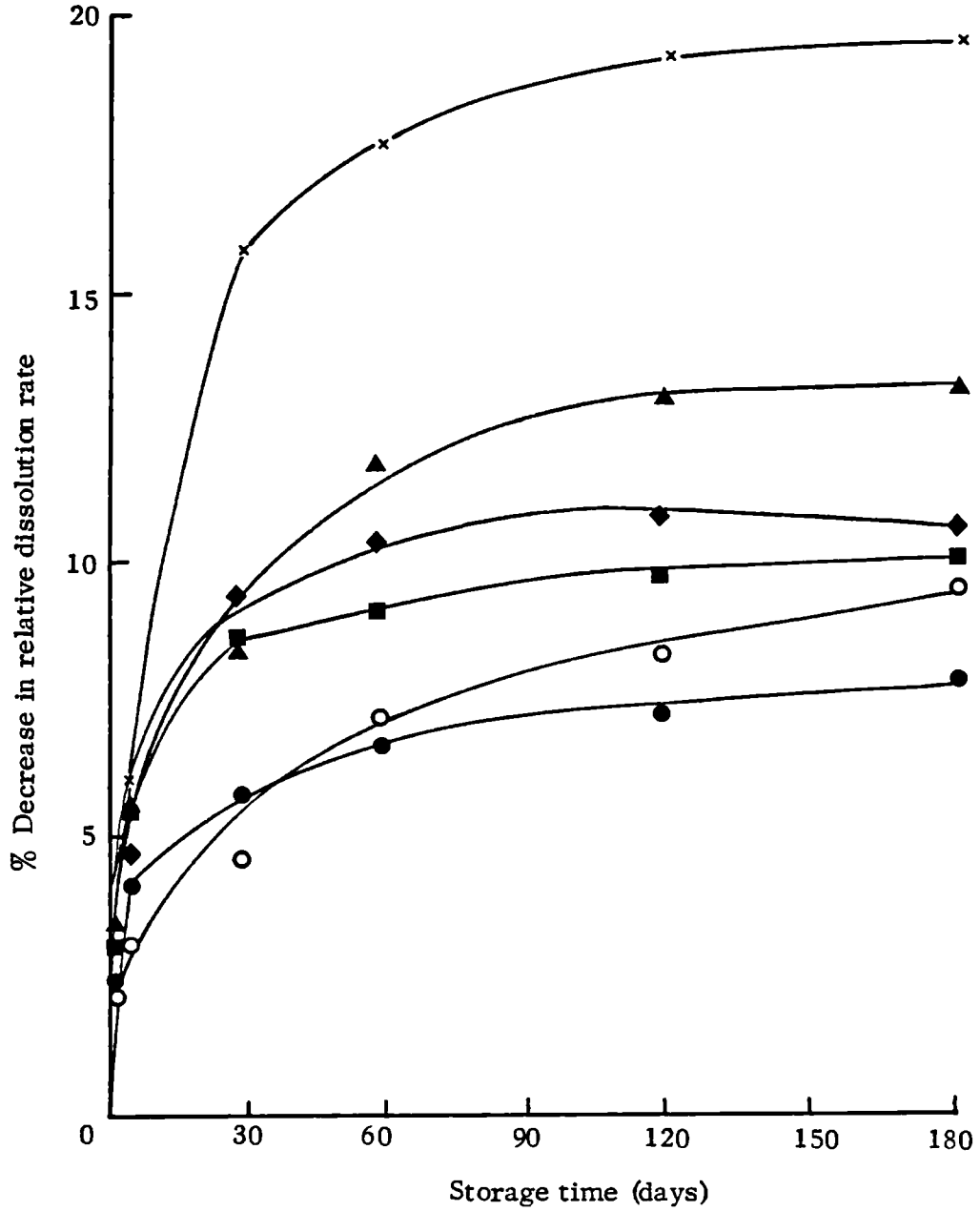
20
15
10
5
0
% Decrease in relative dissolution rate
30
60
90
120
150
180
Storage time (days)

Fig. 5.12. Effect of ageing on the relative dissolution rate of dispersions previously melted at 200°C for 10 mins and quenched in liquid nitrogen

(a) 25°C

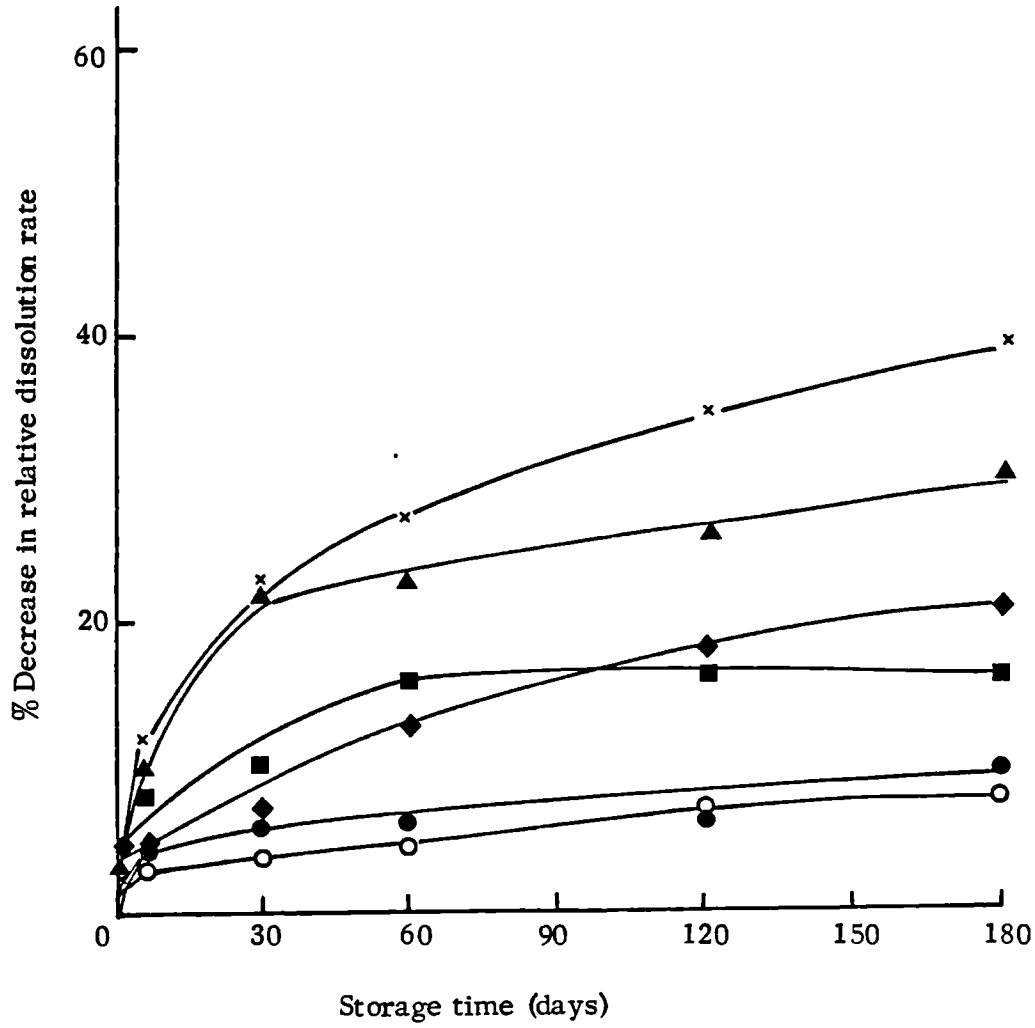

Fig. 5.12. (b) 45°C

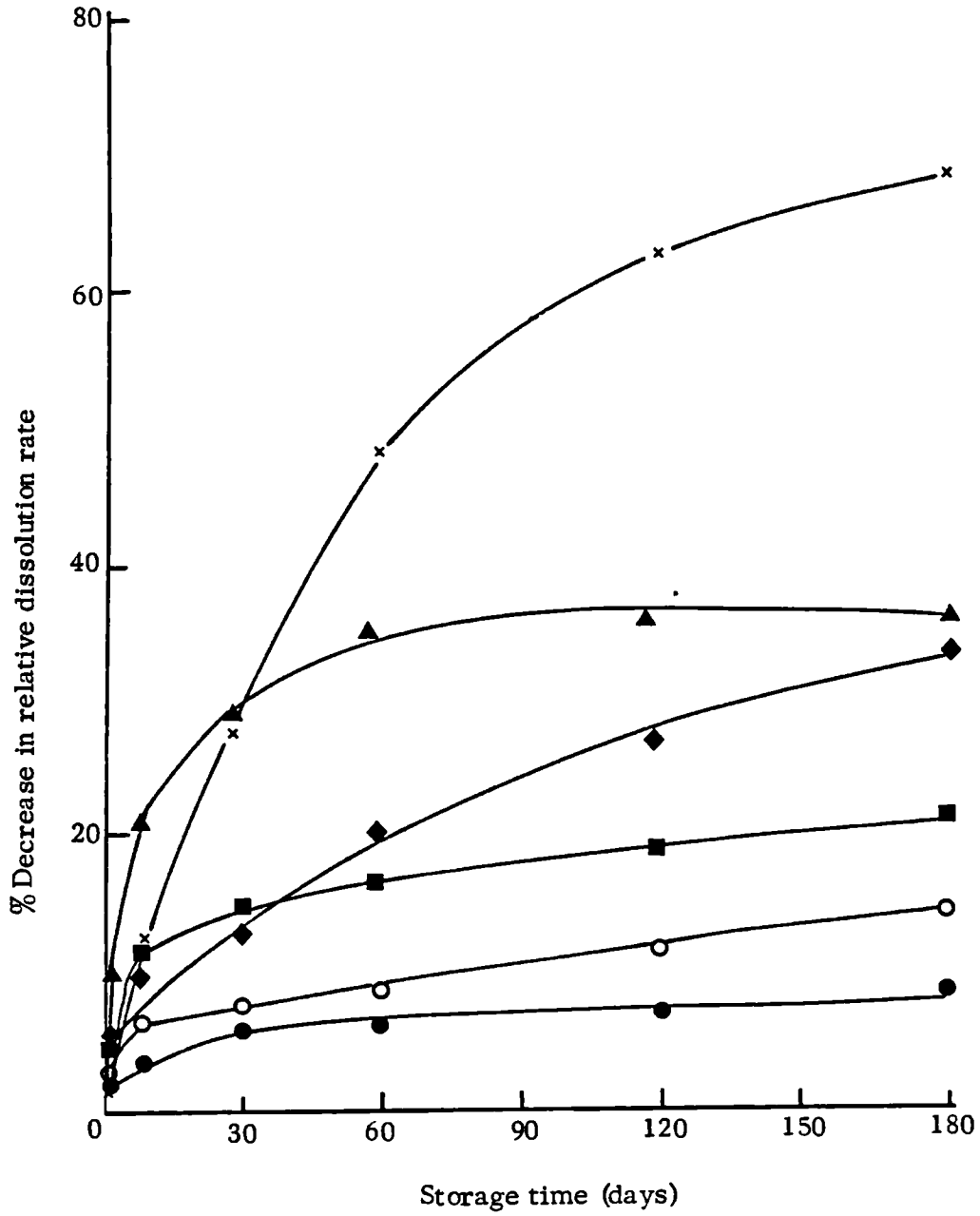
80
60
40
20
0
30
60
90
120
150
180
% Decrease in relative dissolution rate
Storage time (days)

However, 10%^{w}/w and 50%^{w}/w dispersions prepared similarly displayed a greater decrease in dissolution rate than those containing 2%^{w}/w trimethoprim. Presumably, the fine crystallites of drug present tend to encourage further crystal growth. Additionally, for 50%^{w}/w dispersions, a fairly high proportion of PEG 4000 existed as metastable folded chain crystals or had not crystallised due to the hindering effect of the drug crystals, resulting in a significant decrease in dissolution rate on ageing as reversion to the most stable form and an increase in crystallinity occurred.

Hoelgaard and Møller (1975b) reported the largest decrease in dissolution rate on storage with testosterone dispersions formulated with PEGS 4000 or 6000, compared to those with PEGS 1000 or 20,000. This may well be related to the inherent instability of the folded chain crystals of PEG likely to be found in the 4000-6000 molecular weight range, which as they convert to the extended chain form tend to destabilise the entire dispersion. PEG 1000 can only exist as extended chain crystals and for PEG 20,000, the most stable conformation is as folded chain crystals, thus these systems would be expected to exhibit greater resistance to the effects of ageing.

Quenched dispersions displayed the greatest decrease in drug dissolution performance on ageing (Fig. 5.12a. and b.), which appeared at the lower concentrations of drug to be related to the recrystallisation of the polymer. No evidence for the recrystallisation of the drug at 2%^{w}/w or 10%^{w}/w, except after 6 months in the latter case, could be detected from X-ray diffraction studies (Chapter 3.3.2.5.). This seems to support the contention that the crystallinity of the carrier may exert an influence on the dissolution rate of the drug. Dispersions containing 50%^{w}/w trimethoprim aged more rapidly than the lower concentration dispersions, since presumably as before, once

recrystallisation commenced, then the crystallites encouraged further growth.

In conclusion, the greatest stability of solid dispersions to ageing was displayed by samples which either contained low concentrations of drug or where incomplete fusion of the two components occurred before cooling. Furthermore, low storage temperatures and a slow rate of cooling contributed to enhance the resistance to changes on ageing.

CHAPTER 6

CHAPTER 6 Conclusions

Knowledge of the influence of thermal history on the morphology of PEG 4000 and its solid dispersions is obviously important if these materials are to be formulated as molten filled hard gelatin capsules. Characterisation of the structure of solid dispersions has typically been performed by the construction of a temperature-composition phase diagram, often from DSC data, as was carried out here for the PEG 4000-trimethoprim system. An unambiguous interpretation of such data can be difficult in the absence of a melting transition for the drug at low concentrations, especially as it is in this region that solid solution and eutectic formation has been postulated by many workers (Chiou and Riegelman, 1971; Hargreaves, 1982; Hoelgaard and Møller, 1975a). Furthermore, depression of the melting point of the polymer is not necessarily indicative of the presence of a eutectic. Additional information can be gained about the structure of solid dispersions from the relationship between composition and the enthalpies of melting or crystallisation of the components as measured by DSC, but again may be difficult to interpret for systems containing low concentrations of drug.

Likewise, X-ray diffraction studies provided much information about the structure of these systems, but cannot be used to distinguish between low concentrations of drug in the amorphous form or a solid solution of drug in a semi-crystalline carrier. Thus although DSC and X-ray diffraction are very useful techniques, limitations exist in that analysis of the data is sometimes open to several interpretations. Therefore a definite description of the structure of such systems is not always possible.

The technique of dielectric spectroscopy, which had not previously been applied to the study of pharmaceutical solid dispersions, was found to provide a good description of their structure when modelled in terms of the Dissado-Hill theory, which corroborated that inferred by DSC and X-ray diffraction studies. A particular advantage of this method was that it allowed investigations over a wide range of temperatures in the liquid and solid and during temperature cycling, thus providing information which was not readily accessible from the other techniques. Measurements of dielectric response may have considerable potential in the evaluation of other pharmaceutical systems. Preliminary work on the characterisation of emulsions and powders from their dielectric behaviour has already provided encouraging results.

All the above techniques indicated that PEG 4000 and trimethoprim did not form a solid solution or eutectic to any detectable extent, under any of the preparative conditions investigated. Moreover, considerations of the mechanism of crystallisation and crystal structure of PEG 4000 suggest that the formation of solid solutions with drugs is probably much less widespread than originally postulated. Crystallisation of the trimethoprim was inhibited to some extent in the presence of the polymer, resulting in the formation of amorphous drug. Thus solid dispersions of PEG 4000 and trimethoprim existed mainly as a physical dispersion of the drug crystals in the semi-crystalline polymer matrix. The proportion of amorphous drug and polymer formed varied, depending on the previous thermal profile.

The thermal history of PEG 4000 was found to influence its resultant morphology in terms of both the degree of crystallinity and the extent of each crystal type - either extended or thermodynamically metastable, folded chain lamellae. The temperature of melting and time in the molten state however,

exerted a lesser influence on the subsequent morphology of the polymer than did variations in the cooling rate. A similar pattern of behaviour was observed for the solid dispersions with trimethoprim.On ageing, reversion of the folded chain crystals of PEG 4000 to the extended chain form invariably occurred, by a process of chain unfolding and lamellar thickening.

As has often been demonstrated in the past, the formulation of sparingly soluble drugs such as trimethoprim as solid dispersions greatly improves their dissolution performance. The properties of solid dispersions can be influenced by thermal history, especially by quenching samples in liquid nitrogen to produce a more amorphous form of the drug and polymer. Quenched dispersions exhibited faster dissolution rates of both drug and polymer and may offer a method by which the carrying capacity of such systems can be extended. The carrying capacity of solid dispersions has always limited their use to the formulation of low dosage drugs, since the enhancement of dissolution rate is only usually apparent up to concentrations of approximately 10%^{w}/w drug in carrier. Quenched dispersions displayed an improved dissolution performance at higher concentrations of trimethoprim than the more slowly cooled solid dispersions.

Since solid solution and eutectic formation is negligible here, this cannot be the reason for the improvement in the dissolution profile of trimethoprim. The enhanced dissolution rate of the drug probably results from a combination of different mechanisms such as microenvironmental solubilisation, improved wetting, some reduction of particle size and the formation of amorphous drug. The quenched dispersions displayed the fastest dissolution rate due mainly to the formation of amorphous drug, but the faster dissolution rate of the more amorphous PEG 4000 may also be influential in this improvement.

Simultaneous release of drug and polymer appears to occur up to concentrations of ~10%^{w}/w trimethoprim, beyond which the dissolution of the polymer is increasingly more rapid than that of the drug.

Further elucidation of the mechanisms of enhanced dissolution rate and their relative importance is fundamental to the understanding of these systems. One problem with the formulation of drugs as solid dispersions is the decrease in dissolution performance on ageing, which appears to be at least partly related to the increase in crystallinity and conversion to extended chain crystals of the PEG 4000. Hoelgaard and Møller (1975b) reported a greater deterioration in dissolution performance with drugs formulated in PEGS 4000 and 6000 than with those in PEGS 1000 or 20,000. Thus selection of a PEG with a molecular weight outside of the 4000-6000 range, where the greatest degree of chain unfolding would be expected to occur might reduce the effects of ageing.

The importance of characterising the molecular weight distribution of the polymer has in the past been overlooked. It is,however,important because of its influence on the stability of the various crystal forms present and hence, their rate of conversion to a thermodynamically more stable form. This is especially important in the m.wt range 4000-6000, since for example, the rate of conversion of folded to extended chain crystals has been reported to be 50 times greater for PEG 4000 than PEG 6000 (Buckley and Kovacs, 1976). The influence of molecular weight on formulation and dissolution properties could be utilised in that blends of low and high molecular weight PEGS may be used to achieve the desired dissolution profile, but maintain good handling properties.

To confirm the improved dissolution performance of trimethoprim solid dispersions, in vivo studies are of course necessary to establish whether

improvements in drug absorption are possible, as improved bioavailability will only occur for those drugs whose absorption is dissolution rate controlled.

The variations in thermal profile that might be encountered during the molten filling process are unlikely to influence significantly the properties of the final product in terms of dissolution performance. However, it would be advisable to keep the temperature of the melt as low as possible to minimise thermal degradation of the product. For this reason also, the period of time in the molten state should be minimised. The susceptibility of a particular formation to thermal decomposition will obvicusly vary with the stability of the drug, however suspensions of particles of drug in the polymer melt in comparison to full solution melts, may be expected to exhibit greater thermal stability at elevated temperatures. In view of the practically equivalent dissolution performances of solid dispersions where the two components were and were not totally fused during preparation, the latter type may well be preferred on stability grounds. Darkening of the polymer melt on prolonged storage at high temperatures may affect the appearance of the resultant product, but its influence on drug stability is probably minimal. Although cooling rate does influence the dissolution rate of the product, within the range of cooling rates experienced by molten filled capsules, there should be a negligible effect on dissolution performance. The application of stricter thermal controls than currently employed during molten filling is likely therefore to prove unnecessary.

REFERENCES

REFERENCES

Allen, D. J. and Kwan, K. C. (1969) J. Pharm. Sci., 58, 1190-1193

Allen, R. C. and Mandelkern, L. (1982) J. Polym. Sci., Polym. Phys. Ed. 20, 1465-1484

Allen (Jr.), L. V.; Yanchick, V. A. and Maness, D. D. (1977) J. Pharm. Sci., 66, 494-497

Anastasiadou, C.; Henry, S., Legendre, B.; Souleau, C. and Duchene, D. (1983) Drug. Dev. Ind. Pharm., 9, 103-115

Arlie, J. P.; Spegt, P. and Skoulios, A. (1966) Makromol. Chem., 99, 160-174

Arlie, J. P.; Spegt, P. and Skoulios, A. (1967), 104, 212-229

Armstrong, R. D. and Edmondson, K. (1973) Electrochim. Acta., 18, 937-943

Avrami, M. J. (1939) J. Chem. Phys., 7, 1103-1112

Avrami, M. J. (1940) J. Chem. Phys., 8, 212-224

Avrami, M. J. (1941) J. Chem. Phys., 9, 177-184

Bailey (Jr.), F. E. and Koleske, J. V. (1973) J. Chem. Ed., 50, 761-763

Bailey, F. E. and Koleske, J. V. (1976) "Polyethylene Oxide", Academic Press, New York

Bajpai, M. and Varma, K. C. (1981) East. Pharm., 24, 187-188

Banks, W. and Sharples, A. (1963) Makromol. Chem., 67, 42-48

Barnes, W. S.; Luetzel, W. G. and Price, F. P. (1961) J. Phys. Chem., 65, 1742-1748

Bartel, E.; Hodorowicz, S. and Lamot, R. (1979) Makromol. Chem., 180, 2491-2498

Beech, D. R.; Booth, C.; Dodgson, D. V.; Sharpe, R. R. and Waring, J. R. S. (1972a) Polymer, 13, 73-77

Beech, D. R.; Booth, C.; Dodgson, D. V. and Hillier, I. H. (1972b) J. Polym. Sci., Part A-2, 10, 1555-1564

Bettinetti, G. P.; Giordano, F.; La Manna, A. and Guiseppetti, G. (1976) J. Pharm. Pharmacol., 28, 87-88

References

Beyene, T. (1981) "The effect of process variables on the mechanical strength of moulded polyethylene glycol tablets", Msc thesis, Chelsea Department of Pharmacy, University of London

Binks, A. E. and Sharples, A. (1968) J. Polym. Sci., Part A-2, 6, 407-420

Blythe, A. R. (1979) "Electrical properties of polymers", Ed. Cahn, R. W.; Thompson, M. W. and Ward, I. M., Cambridge University Press, Cambridge

Booth, C.; Bruce, M. J. and Buggy, M. (1972) Polymer, 13, 475-478

Brown, N. H. (1978) Drug. Dev. Ind. Pharm., 4, 427-439

Buckley, C. P. and Kovacs, A. J. (1976) Colloid. Polym. Sci., 254, 695-715

Carter, S. J. (1972) "Tutorial Pharmacy", Cooper, J. W. and Gunn, C., 6th Edition, Pitman, London, p. 183-192

Chang, B. L., Nuessle, N. O. and Haney (Jr.), W. G. (1975) J. Pharm. Sci., 64, 1787-1797

Chatterjee, A. M.; Price, F. P. and Newman, S. (1975a) J. Polym. Sci., Polym. Phys. Ed., 13, 2369-2383

Chatterjee, A. M.; Price, F. P. and Newman, S. (1975b) J. Polym. Sci., Polym. Phys. Ed., 13, 2384-2390

Childs, C. E. (1975) Microchem. J., 20, 190-192

Chiou, W. L. and Niazi, S. (1976) J. Pharm. Sci., 65, 1212-1214

Chiou, W. L. and Riegelman, S. (1969) J. Pharm. Sci., 58, 1505-1509

Chiou, W. L. and Riegelman, S. (1970) J. Pharm. Sci., 59, 937-941

Chiou, W. L. and Riegelman, S. (1971) J. Pharm. Sci., 60, 1281-1302

Chiou, W. L. and Smith, L. D. (1971) J. Pharm. Sci., 60, 125-127

Cole, K. S. and Cole, R. H. (1941) J. Chem. Phys., 9, 341-351

Connor, T. M.; Read, B. E. and Williams, G. (1964) J. Appl. Chem., 14, 74-80

Cook, M.; Watts, D. C. and Williams, G. (1970) Trans. Farad. Soc., 66, 2503-2511

References

Cooper (Jr.), A. R. and Kingery, W. D. (1962) J. Phys. Chem., 66, 665-669

Corrigan, O. I. (1984) Proc. 4th. Pharm. Tech. Conf. Edinburgh, 3, 6-37, through Dubois and Ford (1985)

Corrigan, O. I.; Murphy, C. A. and Timoney, R. F. (1979) Int. J. Pharm., 4, 67-74

Daabis, N. A. and Mortada, L. M. (1980) Sci. Pharm., 48, 16-23

Davidson, D. W. and Cole, R. H. (1951) J. Chem. Phys., 19, 1484-1490

Debye, P. (1912) Physik. Z., 13, 97

Debye, P. (1945) "Polar molecules", Dover Press, New York

Decossas, F.; Moliton, A. and Marchal, E. (1982) Eur. Polym. J., 18, 1073-1084

Dissado, L. A. (1984) J. Chem. Phys. (in press)

Dissado, L. A. and Hill, R. M. (1979) Nature, 279, 685-689

Dissado, L. A. and Hill, R. M. (1983) Proc. Roy. Soc., A390, 131-180

Dissado, L. A. and Hill, R. M. (1984a) J. Chem. Soc., Farad. Trans. 2, 80, 291-319

Dissado, L. A. and Hill, R. M. (1984b) Proc. Gordon. Conf. Dielectric. Phenomena. (In press)

Dubois, J. L. and Ford, J. L. (1985) J. Pharm. Pharmacol., 37, 494-496

El-Banna, H. M. and Abdullah, O. (1980) Pharm. Acta. Helv., 55, 256-260

El-Gamal, S.; Borie, N. and Hammouda, Y. (1978) Pharm. Ind., 40, 1373-1376

El-Gindy, N. A.; Karara, A. H. and Abdel-Khalek, M. M. (1976) Sci. Pharm., 44, 283-288

El-Gindy, N. A.; Shalaby, A. A. and Abd El-Khalek, M. M. (1983) Drug. Dev. Ind. Pharm., 9, 1031-1045

Elworthy, P. H. and Lipscomb, F. J. (1968) J. Pharm. Pharmacol., 20, 817-824

Elworthy, P. H.; Florence, A. T. and Macfarlane, C. B. (1968) "Solubilisation by Surface-active agents", Chapman and Hall, London, p. 61

References

Ferry, J. D. (1970) "Viscoelastic properties of polymers", Wiley, New York

Ford, J. L. (1980) "Physical, dissolution and formulation properties of solid dispersions", Ph.D. Thesis, Liverpool Polytechnic

Ford, J. L. (1983) Pharm. Acta. Helv., 58, 101-108

Ford, J. L. and Rubinstein, M. H. (1978a) J. Pharm. Pharmacol., 30, 512-513

Ford, J. L. and Rubinstein, M. H. (1978b) Pharm. Acta. Helv., 53, 93-98

Ford, J. L. and Rubinstein, M. H. (1979) Pharm. Acta. Helv., 54, 353-358

Ford, J. L. and Rubinstein, M. H. (1980) Pharm. Acta. Helv., 55, 1-7

François, D.; Denmat, A.; Waugh, A. and Woodage, T. (1982) Pharm. Ind., 44, 86-89

Frömming, K. H.; Simons, B.; Haase, J. and Hoseman, R. (1978) Pharm. Ind., 40, 967-970

Geneidi, A. S. and Hamacher, H. (1980) Pharm. Ind., 42, 401-404

Geneidi, A. S.; Adel, M. S. and Shehata, E. (1981) Can. J. Pharm. Sci.. 15, 78-80

de Gennes, P. G. (1982) J. Chem. Phys., 76, 3313-3321

Ghanem, A.; Meshali, M. and Ibraheem, Y. (1980) J. Pharm. Pharmacol., 32, 675-677

Godovsky, Yu. K.; Slonimsky, G. L. and Garbar, N. M. (1972) J. Polym. Sci., Part C, 38, 1-21

Goldberg, A. H. and Higuchi, W. I. (1968) J. Pharm. Sci., 57, 1583-1585

Goldberg, A. H.: Gibaldi, M. and Kanig, J. L. (1965) J. Pharm. Sci., 54, 1145-1148

Goldberg, A. H.; Gibaldi, M. and Kanig, J. L. (1966) J. Pharm. Sci., 55, 482-487

Gryte, C. C.; Berghmans, H. and Smets, G. (1979) J. Polym. Sci., Polym. Phys. Ed., 17, 1295-1305

Guven, O. and Senvar, S. (1978) Chim. Acta. Turk., 6, 27-33

Hager, S. L. and Macrury, T. B. (1980) J. Appl. Polym. Sci., 25, 1559-1571

References

Hajratwala, B. R. (1974) Aust. J. Pharm. Sci., NS3, 101-109

Hajratwala, B. R. and Ho, D. S. S. (1984) J. Pharm. Sci., 73, 1539-1541

Hargreaves, B. J. (1982) "A study of betamethasone alcohol-polyethylene glycol solid dispersions", Ph.D. Thesis, Sunderland Polytechnic

Harrison, I. R. and Runt, J. (1980) J. Polym. Sci., Polym. Phys. Ed., 18, 2257-2261

Hartmann, B. (1972) Polymer, 13, 460

Havriliak, S. and Negami, S. (1966) J. Polym. Sci., Part C, 14, 99-103

Hay, J. N.; Sabir, M. and Stevens, R. L. T. (1969) Polymer, 10, 187-202

Henry, S.; Legendre, B.; Souleau, C.; Puisieux, F. and Duchene, D. (1983) Pharm. Acta. Helv., 58, 9-13

Heyd, A.; Kildsig, D. O. and Bankev, G. S. (1969) J. Pharm. Sci., 58, 586-588

Higuchi, W. I. (1967) J. Pharm. Sci., 56, 315-324

Hikichi, K. and Furuichi, J. (1965) J. Polym. Sci., Part A, 3, 3003-3013

Hill, R. M. (1978) Nature, 275, 96-99

Hill, R. M. and Dissado, L. A. (1982) J. Phys.,C., Solid State Phys., 15, 5171-5193

Hill, R. M. and Jonscher, A. K. (1983) Contemp. Phys., 24, 75-110

Hill, R. M.; Dissado, L. A. and Jackson, R. (1981) J. Phys. C., 14, 3915-3926

Hillier, I. H. (1966) J. Polym. Sci., Part A-2, 4, 1-16

Ho, D. S. S. and Hajratwala, B. R. (1981) Aust. J. Pharm. Sci., 10, 65-69

Hoechst (1977) "Polyglycols: properties and uses of polyethylene glycols", Hoechst U.K.

Hoelgaard, A. and Møller, N. (1975a) Arch. Pharm. Chemi. Sci. Ed., 3, 65-72

Hoelgaard, A. and Møller, N. (1975b) Arch. Pharm. Chemi. Sci. Ed., 3, 34-47

References

Hoffman, J. D. and Lauritzen, J. I. (1961) J. Res. NBS., 65A, 297-336

Ikeda, M.; Suga, H. and Seki, S. (1975) Polymer, 16, 634-640

Jonscher, A. K. (1977) Nature, 267, 673-679

Jonscher, A. K. (1978) Phil. Mag. B., 38, 587

Kambe, Y. (1980) Polymer, 21, 352-355

Kassem, A. A.; Ghanem, A.; Meshali, M. and Fahaem, M. (1978) J. Pharm. Pharmacol., 30, 85P

Kassem, A. A.; Zaki, S. A.; Mursi, N. M. and Tayel, S. A. (1979a) Pharm. Ind., 41, 390-393

Kassem, A. A.; Zaki, S. A.; Mursi, N. M. and Tayel, S. A. (1979b) Pharm. Ind., 41, 1220-1223

Kassem, A. A.; Zaki, S. A.; Mursi, N. M. and Tayel, S. A. (1980) Pharm. Ind., 42, 202-205

Kaur, R.; Grant, D. J. W. and Eaves, T. (1980a) J. Pharm. Sci., 69, 1317-1321

Kaur, R.; Grant, D. J. W. and Eaves, T. (1980b) J. Pharm. Sci., 69 1321-1326

Khalil, S. A. H. and Mortada, L. M. (1978) J. Drug. Res. (Egypt), 10, 141-150

Kim, K. H. amd Jarowski, C. I. (1977) J. Pharm. Sci., 66, 1536-1540

Kim, K. H.; Frank, M. J. and Henderson, N. L. (1985) J. Pharm. Sci., 74, 283-289

Kimmich, R. and Schmauder, Kh. (1977) Polymer, 18, 239-243

Klymko, P. W. and Kopelman, R. (1983) J. Phys. Chem., 87, 4565-4567

Koenig, J. L. and Angood, A. C. (1970) J. Polym. Sci., Part A-2, 8, 1787-1796

Koetzle, T. F. and Williams, G. J. B. (1976) J. Am. Chem. Soc., 98, 2074-2078

Kornblum, S. S. and Hirschorn, J. O. (1970) J. Pharm. Sci., 59, 606-609

References

Kovacs, A. J. and Gonthier, A. (1972) Kolloid. Z. Z. Polym., 250, 530-551

Kovacs, A. J.; Gonthier, A. and Straupe, C. (1975) J. Polym. Sci., Part C, 50, 283-325

Kovacs, A. J.; Straupe, C. and Gonthier, A. (1977) J. Polym. Sci., Polym. Symp., 59, 31-54

Krüm, F. and Muller, F. H. (1959) Kolloid. Z. , 164, 8 in McCrum, N. G.; Read, B. E. and Williams, G. (1967) "Anelastic and dielectric effects in polymeric solids", Wiley, London

Lang, M. C.; Noel, C. and Legrand, P. (1977a) J. Polym. Sci., Polym. Phys. Ed., 15, 1319-1327

Lang, M. C.; Noel, C. and Legrand, P. (1977b) J. Polym. Sci., Polym. Phys. Ed., 15, 1328-1338

Larson, A. B. and Banker, G. S. (1976) J. Pharm. Sci., 65, 838-843

Levy, G. (1963a) Am. J. Pharm., 135, 78-92

Levy, G. (1963b) J. Pharm. Sci., 52, 1039-1046

Lin, S. L.; Menig, J. and Lachman, L. (1968) J. Pharm. Sci., 57, 2143-2148

Lui, K. J. and Parsons, J. L. (1969) Macromolecules, 2, 529-533

Lovinger, A.; Lau, C. and Gryte, C. C. (1976) Polymer, 17, 581-586

Malone, M. H.; Hochman, H. I. and Nieforth, K. A. (1966) J. Pharm. Sci., 55, 972-974

Martin, A. N.; Swarbrick, J. and Cammarata, A. (1969) "Physical Pharmacy", 2nd Ed., Lea and Febiger, Philadelphia, p. 313

Matsuura, H. and Miyazawa, T. (1969) J. Polym. Sci., Part A-2, 7, 1735-1744

Matsuzaki, K. and Ito, H. (1974) J. Polym. Sci., Polym. Phys. Ed., 12, 2507-2520

Maulding, H. V. (1978) J. Pharm. Sci., 67, 391-394

Maxfield, J. and Shepherd, I. W. (1975) Polymer, 16, 505-509

Mayersohn, M. and Gibaldi, M. (1966) J. Pharm. Sci., 55, 1323-1324

References

McGinity, J. W.; Maness, D. D. and Yakatan, G. J. (1974-1975) Drug. Dev. Comm., 1, 369-387

McGinity, J. W.; Maincent, P. and Steinfink, H. (1984) J. Pharm. Sci., 10, 1441-1444

McCrum, N. G.; Read, B. E. and Williams, G. (1967) "Anelastic and dielectric effects in polmeric solids", Wiley, London

Meares, P. (1965) "Polymers - structure and bulk properties", van Nostrand, London

Meshali, M.; Ghanem, M. and Ibraheem, Y. (1983) Pharm. Acta. Helv., 58, 62-64

Mikhailov, M.; Nedhov, E. and Goshev, I. (1978) J. Macromol. Sci. Phys., B15, 313-328

Morgan, L. B. (1954) Phil. Trans. A., 247, 13-22

Morse, C. T. (1974) J. Physics. E., Sci. Instrum., 7, 657-662

Muhammed, N. A. H. (1980) "The influence of dissolution fluid on the in vitro drug release from hard gelatin capsules", Ph.D. thesis, University of Nottingham

Mullins, J. D. and Macek, T. J. (1960) J. Pharm. Sci., 49, 245-248

Nelson, E. (1957) J. Am. Pharm. Ass., Sci. Ed., 46, 607-614

Nernst, W. and Brunner, E. (1904) Z. Physik. Chem., 47, 56-102

Patel, M. S.; Elworthy, P. H. and Dewsnup, A. K. (1981) J. Pharm. Pharmacol., 33, 64P

Point, J. J. and Kovacs, A. J. (1980) Macromolecules, 13, 399-409

Price, C.; Evans, K. A. and Booth, C. (1975) Polymer, 16, 196-200

Prud'homme, R. E. (1982) J. Polym. Sci., Polym. Phys. Ed., 20, 307-317

Ravis, W. R. and Chen, C. Y. (1981) J. Pharm. Sci., 70, 1353-1357

Read, B. E. (1962) Polymer, 3, 529-542

Reddy, R. K.; Khalil, S. A. and Govda, M. W. (1976) J. Pharm. Sci., 65, 1753-1758

References

Reed-Hill, R. E. (1964) "Physical metallurgy principles", van Nostrand, New Jersey

Reisman, A. (1970) "Phase equilibria: Basic principles, applications, experimental techniques", Vol. 19 in Physical Chemistry: A series of monographs, Ed. Loebl, E. M., Academic Press, New York

Saboe, J. C. and Dempski, R. E. (1976) Drug. Dev. C., 2, 359-376

Said, S. A.; El-Fatatry, H. M. and Geneidi, A. S. (1974a) Aust. J. Pharm. Sci., 3, 42-45

Said, S. A.; El-Fatatry, H. M. and El-Samaligy, M. S. (1974b) Aust. J. Pharm. Sci., 3, 123-126

Salib, N. N. and Ebian, A. R. (1978) Pharm. Ind., 40, 262-265

Salib, N. N.; El-Gamal, S. A. and Ismail, A. A. (1976) Pharm. Ind., 38, 918-921

Scheikh, M. A.; Price, J. C. and Gerraughty, R. J. (1966) J. Pharm. Sci., 55, 1048-1050

Sekiguchi, K. and Obi, N. (1961) Chem. Pharm. Bull., 9, 866-872

Shablakh, M. (1982) "Dielectric properties of plastic crystals and small organic glasses", Ph.D. Thesis, Chelsea College, University of London

Shablakh, M.; Hill, R. M. and Dissado, L. A. (1982) J. Chem. Soc., Farad. Trans. 2, 78, 625-638

Shablakh, M.; Dissado, L. A. and Hill, R. M. (1983) J. Chem. Soc., Farad. Trans. 2, 79, 369-417

Shapiro, B. and Abrahams, E. (1981) Phys. Rev. B., 24, 4889

Sharples, A. (1966) "Introduction to polymer crystallisation", Arnold, London

Shimada, T.; Okui, N. and Kawai, T. (1980) Makromol. Chem., 181, 2643-2654

Simonelli, A. P.; Mehta, S. C. and Higuchi, W. I. (1969) J. Pharm. Sci., 58, 538-549

Singh, P.; Guillory, J. K.; Sokoloshi, T. D.; Benet, L. Z. and Bhatia, V. N. (1966) J. Pharm. Sci., 55, 63-68

References

Sirenius, I. (1979) J. Pharm. Sci., 68, 791-792

Skauern, D. M. (1967) J. Pharm. Sci., 56, 1373-1387

Slater, L. J. (1960) "Confluent hypergeometric functions", Cambridge University Press, Cambridge

Slater, L. J. (1966) "Generalised hypergeometric functions", Cambridge University Press, Cambridge

Smith, P. and Pennings, A. J. (1977) J. Polym. Sci., Polym. Phys. Ed., 15, 523-540

Tachibana, T. and Nakamura, A. (1965) Kolloid. Z. Z. Polym., 203, 130-133

Takahashi, Y. and Tadokoro, H. (1973) Acta. Chem. Scand., 27, 1430-1432

Tsuji, T.; Fueki, K. and Makaibo, T. (1969) Bull. Chem. Soc. Japan, 42, 2193-2198

Vainshtein, B. K. (1966) "Diffraction of X-rays by chain molecules", Elsevier, Holland

Walker, S. E.; Ganley, J. A.; Bedford, K. and Eaves, T. (1980) J. Pharm. Pharmacol., 32, 389-393

Wells, J.; Rubinstein, M. and Walter, V. (1975) J. Pharm. Pharmacol., 27, 56P

Wendlandt, W. W. (1974) "Thermal methods of analysis", 2nd Ed., Wiley-Interscience, New York, p.260

Williams, R. L.; Blume, C. D.; Lin, E. T.; Holford, N. H. G. and Benet, L. Z. (1982) J. Pharm. Sci., 71, 533-535